Modelling liquid crystalline ordering in anisotropic and inhomogeneous fluids: From simple models of rod- and disc-like particles to polypeptides

A thesis submitted in partial fulfilment of the requirements of the degree of Doctor of Philosophy of Imperial College London

by

LIANG WU

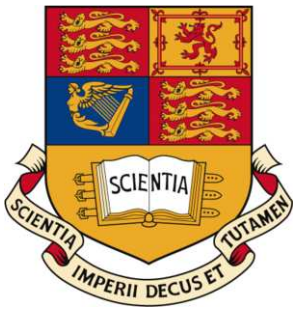

Department of Chemical Engineering
Imperial College London
London SW7 2AZ, United Kingdom

• July 2013 •

Declaration of Originality

This dissertation contains work done between October 2009 and July 2013 in the Department of Chemical Engineering, Imperial College London. I hereby declare that all the material in this dissertation is the result of my own work and that all else is appropriately referenced.

Liang WU

July 2013

Copyright Declaration

Abstract

A liquid crystal (LC) is a substance that exhibits phases intermediate between a crystal and a disordered liquid state. LCs have attracted longstanding research interest because of their potential commercial applications in opto-electronics, pharmaceuticals and surfactants but also because ordered soft matter is prevalent in bio-molecular systems such as DNA and lipid cell membranes. In liquid-crystalline systems, both molecular shape and asymmetric attractive interactions contribute to the formation and ultimate stability of anisotropic phases. The research outlined in this thesis provides a fundamental understanding of these systems by developing theoretical models and undertaking detailed molecular simulation studies.

In the first part of this thesis, prototype oblate models for LCs are studied: cut spheres and cylindrical discs. Coupled with a scaled Onsager approach, a general equation of state (EoS) for hard-core discotic LCs is developed that allows for an accurate description of the isotropic and nematic phases of oblate discs by introducing a correction to incorporate the negative contributions from high-order virial coefficients. Combining the above mentioned approach with an extended cell approach, the isotropic-nematic-columnar phase diagram of cut spheres is determined. The accuracy of the EoS is assessed by comparison with the more traditional Parsons-Lee description and existing simulation data.

Although the anisotropic athermal hard-body fluid is a reasonable representation of lyotropic or colloidal LCs, for thermotropic LC systems temperature plays a key role. In the second part of this thesis a model of hard-core particles incorporating additional anisotropic attractive interactions is proposed to describe thermotropic LCs. Based on a perturbation theory and the Onsager-Parsons-Lee approach, a van der Waals-type (mean-field level) theory of attractive hard-core particles is formulated in a compact algebraic form. The phase diagrams of model attractive prolate (spherocylinder) and oblate (cylindrical disc) molecules are calculated in order to examine the separate effects of molecular shape and anisotropic attractive interactions. As a practical example, a coarse-grained model comprising an attractive spherocylinder is employed to describe phase behaviour of solutions of the polypeptide poly-(γ-benzyl-L-glutamate) (PBLG) in dimethylformamide

(DMF). Quantitative agreement between the results obtained from the EoS and experimental data is obtained.

In the final part of the thesis, a detailed Monte Carlo (MC) simulation study of athermal mixtures of hard spherocylinders and hard spheres between two well separated parallel hard walls is performed. A combination of constant volume (canonical ensemble) and constant (normal) pressure (isobaric-isothermal ensemble) simulations are carried out. With these simulations, the bulk phase behaviour as well as surface-induced LC ordering are explored. The phase diagram of binary mixtures of hard spherocylinders and hard spheres is presented and is compared with the predictions of the one-fluid Parsons-Lee and many-fluid theories. Rich phase behaviour is exhibited on the surface of the walls: drying (de-wetting), isotropic wetting, and nematic wetting are all observed. A previously unreported entropy-driven transition from a bulk nematic state to a homeotropic smectic surface ordering (with particles arranged in a perpendicular orientation relative to the surface plane) is seen in for both the pure hard rod system and the mixture of hard rods and hard spheres as the density is increased (high pressure states).

Contents

List of Figures

List of Tables

Acknowledgements

It is a great pleasure to be able to acknowledge the people who have helped me during my studies at Imperial College, either with academic matters or personal affairs, and their support has been invaluable over the past three years.

First, I would like to express my gratitude to my supervisors, Prof. George Jackson and Prof. Erich A. Müller for their restless guidance and generous support throughout the duration of this work. I am grateful for their wisdom, encouragement, patience, and interdisciplinary expertise in a broad range of thermodynamics. I would particularly thank Prof. George Jackson for giving me the opportunity to join such an amazing research group.

I must thank Dr. Carlos Avendaño for sharing his experience and knowledge of molecular simulation and conversations and meetings about my research. I wish to thank Dr. Rik Wensink and Dr. Alexandr Malijevský for their insightful advice and indispensable efforts on shaping my work. I give thanks to Dr. Paul Brumby for providing his simulation results for my study and helpful advice on my simulation.

I would like to thank the other MSE group supervisors: Prof. Amparo Galindo, Prof. Claire Adjiman and Dr. Andrew Haslam for the excellent seminars and social events they organised. To following MSE members, past and present, I would like to thank for all the good times we shared: Andrei, Apostolos, Charles, Eirini, Esther, Francis, Heiko, Hendrik, Jens, Lara, Manolis, Niall, Nina, Olga, Roochi, Simon, Tom, Vasileios, and Zara.

I must acknowledge Simon Burbidge for providing the amazing High Performance Computing Service at Imperial College. To Susi Underwood I give thanks for her help with administrative issues throughout my Ph. D. in the Department of Chemical Engineering.

I also would like to thank Prof. Jun Cai at East China University of Science and Technology for his generous help and support.

I would like to recognise the financial support from the programme, Scholarship for Excellence which is jointly funded by the Department for Business, Innovation and Skills, United Kingdom and China Scholarship Council.

Finally, I thank my parents for their love and support.

Chapter 1

General introduction

Liquid crystals [1–3] are intermediate (meso) phases that share some, but not all, of the characteristics of a fully positionally and orientationally ordered crystal and those of disordered liquid states. Since their discovery by Reinitzer in 1883 [4], liquid crystals (LCs) have attracted a longstanding research interest because of their unique of thermodynamic, structural, optical, and electronic properties. The thermodynamics and structure of liquid crystals in bulk and on a surface plays a critical role in technological advances and applications of LCs. In this thesis, our objective is to explore the liquid crystalline ordering exhibited in various systems ranging from idealized modelled LC particles to bio-macromolecules, and enhance the understanding of LC ordering induced by a surface. In the introductory chapter, we briefly describe LC molecules and the characteristics of LC phase behaviour. In order to lay the foundations of subsequent chapters, the Onsager approach for theoretically modelling LCs is introduced in this chapter.

1.1 Liquid crystals

A LC phase is a state of matter which is intermediate between a crystal and a liquid state [1]. In a crystal, the constituent molecules are constrained in specific sites of crystal lattice and the order in a crystal is both orientational and positional. By contrast, the particles in molecular liquids diffuse randomly in space, have short-range positional and orientational order but no long-range order. What makes a LC so fascinating is that it combines the properties of both liquid and crystalline phases. As an example, a substance in LC state may show anisotropy in some of its properties, while maintaining some degree of fluidity and other characteristics of a disordered liquid [2]. The short- and long-range ordered structure of LCs leads to a uniqueness of physical and chemical properties that make them

suitable for various applications such as cosmetics, pharmaceuticals and surfactants. One important commercial use of LCs is in liquid crystal displays (LCD) which are ubiquitous in consumer electronic products from high-definition flat screen TV to computers. Solutions of thermotropic chiral liquid crystals whose pitch is strongly temperature-dependent are used as thermometers. Beside these commercial applications, some natural substances like DNA and the lipids in cell membranes can exhibit liquid crystalline states. This certainly motivates research into a better understanding and description of liquid crystals using a whole range of experimental, theoretical and computer simulation techniques.

When a liquid crystal state is formed by changing the temperature of the system, we refer to it as a thermotropic liquid crystal. The first discovery of a liquid crystal material, cholesteryl benzoate was made by Reinitzer as early as 1888 [4]. This substance is a thermotropic liquid crystal which has two melting points: at 145.5°C it melts into a cloudy liquid, and at 178.5°C it melts again and the cloudy liquid becomes clear. In today's jargon, we would describe the first formation as the solid-LC transition and the latter as the LC-isotropic liquid transition. One can also consider the dissolution of anisometric colloidal or macroscopic particles or amphiphilic molecules in a solvent: for certain(high) concentrations, orientationally and positionallly ordered stated are observed, which are commonly known as lyotropic liquid crystals. Solutions of soap and detergents are well known examples [2]. Many biomacromolecular systems such as protein fibers [5, 6] and tobacco mosaic virus [7, 8], *fd*-virus [9–14], and DNA chains [15, 16] also exhibits rich liquid crystal phase. Depending on the details of the molecular structure and of the intermolecular interactions, some systems such as polypeptide solutions exhibit liquid crystal state over a range of concentrations and temperatures [17–24]. Colloidal particles have also been extensively studied in recent years, including nickel hydroxide theophrastite (nickel II hydroxide sheets), aluminium hydroxide gibbsite platelets, and nontronite or laponite mineral clays [25–33].

Although in some cases (as cholesteryl benzoate) LC molecules may exhibit rich and complex phase behaviour such as chiral nematic (cholesteric), in this work we concentrate on the following LC phases: nematic, (rod) smectic, and (disc) columnar phases.

Isotropic phase. At low densities and high temperatures, LC molecules exhibit an isotropic fluid phase which is either a disordered gas or liquid phase. The isotropic state is characterised by short-range positional and no orientational order.

Nematic phase. The isotropic-nematic transition appears at intermediate to high densities. In the nematic phase there is orientational order but no positional order, the

molecules align along the nematic director.

Smectic phase. The smectic mesophase formed by rod-like LCs is more positionally ordered state than nematic phase. In figure 1.4, the layered structure of the smectic phase is clearly seen showing not only orientational but positional order. Within each layer, the rod-like LC molecules still retain fluidity.

Columnar phase. In the columnar state, disc molecules stack into columns and the columns are arranged into a two-dimensional hexagonal lattice perpendicular to the preferred orientational direction. Whithin the columns, the disc-like molecules show orientation order but their positional arrangement is disordered.

The characteristics of these LC phases are summarised in Figure 1.1

	Rod-like LC	Disc-like LC	Orientational order	Positional order
Isotropic		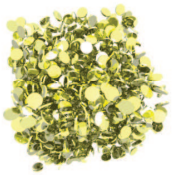	No	No
Nematic		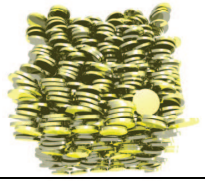	Yes	No
Smectic	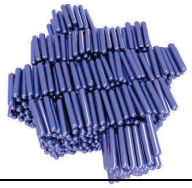		Yes	Yes
Columnar			Yes	Yes

Figure 1.1: Liquid crystalline phases exhibited in rod-like and disc-like LCs.

1.2 Modelling liquid crystals

It is well understood that the highly anisotropic geometry of the molecules can give rise to liquid crystalline states over the intermediate to high-density region [1,3]. Hence much

of the fundamental modelling both in theory and computer simulation has focussed on two classes of systems: rod-like and disc-like particles. A well-known approach to the liquid crystal transition is the Landau-de Gennes phenomenological model [34] using a free energy which is expanded as a series in the order parameters characterising the degree of orientational and positional order for a certain anisotropic phase [1, 3]. The prefactors of each term are assumed to be system and state dependent and treated as adjustable parameters obtained by comparison with experimental data. The Landau-de Gennes approach, being a macroscopic theory, fails to predict the transition quantitatively or bridge the link between the parameters used in the theory and the molecular properties.

The first attempt to understanding LCs at the molecular level was made by Born [35, 36] who suggested that the polar interactions between molecules are responsible for the formation of LC phases. Born's idea is further developed in the Maier-Saupe (MS) theory [37–40], which is a mean-field description of nematic LCs. In the MS theory, the intermolecular potential is expressed as an effective single-molecular interaction U as

$$U(\cos\theta) = -\bar{\epsilon_2}\bar{P}_2 P_2(\cos\theta). \tag{1.1}$$

where θ is the angle between the orientation of a LC molecule and the nematic director; $\bar{\epsilon_2}$ is the energetic parameter, and $\bar{P}_2$ is the uniaxial order parameter, and P_2 is the second Legendre polynomial.

A particular strength of the MS theory is the fact that it can be expressed analytically, and as a consequence, the MS theory is widely adopted in correlating experiential results. Although to some extent the MS theory is a successful model, the weak point of the theory is most likely the neglect of the short-ranged repulsive interactions. Another important model for LC transitions is the Lebwohl-Lasher (LL) model [41] which is a lattice method for anisotropic fluids in which the LC molecules are fixed on the specific lattice and the interaction of a particle with its nearest neighbour is of same type as MS approach. In some aspects, the LL model is essentially a discrete extension of MS theory.

It is well understood that an essential requirement for stabilizing liquid crystal phases is that the molecule be of highly anisotropic geometry. In a liquid crystalline molecule, it is sufficient to consider a hard non-spherical core in order to induce orientational and positional order in anisotropic phases. In such a way, calamitic liquid crystals are modelled as rod-like (prolate) particles and the flat disc-shaped (oblate/discotic) particle is the mesogen for discotic liquid crystals [3,42] In Figure 1.2, two examples of LC molecules and corresponding mesogens are depicted. In the case of cyanobiphenyl compounds they can be represented by a hard rod-like shape while the flat core of triphenylene derivatives

is approximated as a disc-shaped particle. These basic physical models (rod- and disc-like

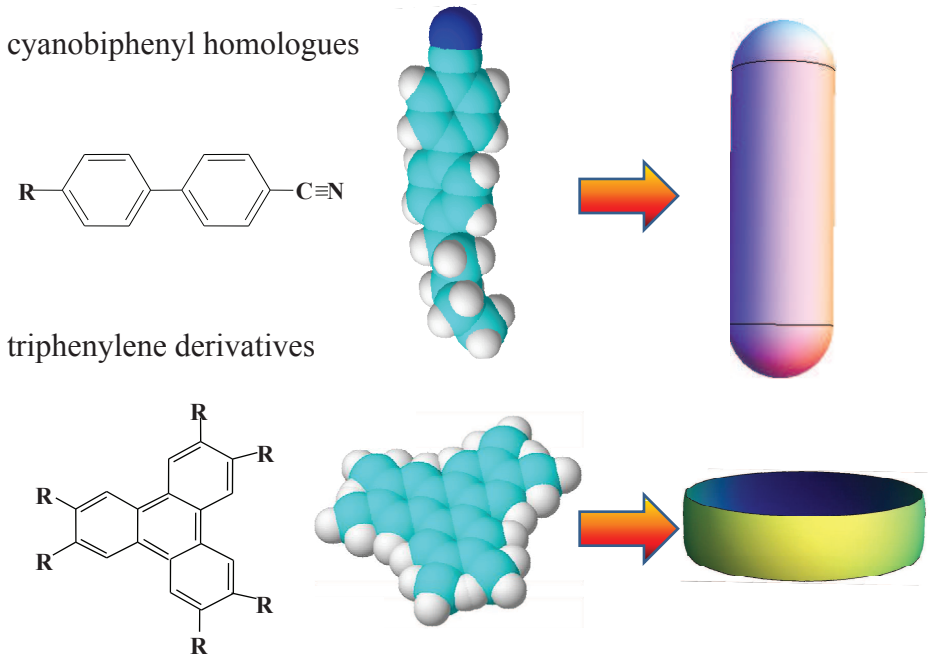

Figure 1.2: Examples of liquid crystal molecules and corresponding model mesogens.

particles) are characterised by aspect ratios which are defined as L/D, L is the thickness of disc particle or the length of rod-like particle and D represents the diameter (cf. Figure 1.3). Although the flexible part of liquid crystalline molecule will also affect the formation of anisotropic phases, it is widely accepted that the specific shape of the hard core is primarily responsible for the appearance of the liquid crystalline phase behavior. At higher densities (packing fractions), the space between a pair of molecules on average reduces, or in other words, the excluded volume of two particles diminishes. Thus, the non-spherical hard-cores of molecules align in more ordered configurations but compensate the entropy because of the increase in free volume of the total system. The results obtained using computer simulation of hard-core particles qualitative confirm the LC phase transformation of rod-like as well as disc-like LCs. As shown in Figure 1.4, the hard spherocylinder [43–45] model exhibit nematic and smectic phases over a certain range of system densities. Due to the difference in geometry as opposed to the rod-like shape, disc-like LCs align along the short axis of the flat discs producing discotic nematic and columnar phases [46–49] with increasing packing fraction (cf. Figure 1.5).

As discussed above the excluded volume between two hard anisometric particles plays an key role in the isotropic-nematic transition of rod- and disc-like hard particles. The

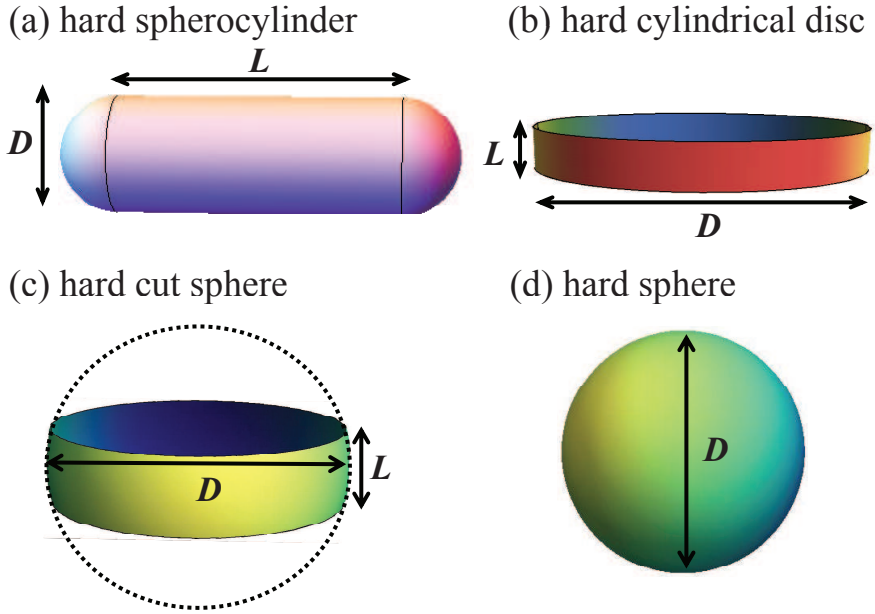

Figure 1.3: Hard-core particles: (a) hard spherocylinder (HSC), (b) hard cylindrical disc, (c) hard cut sphere, and (d) hard sphere (HS) particles.

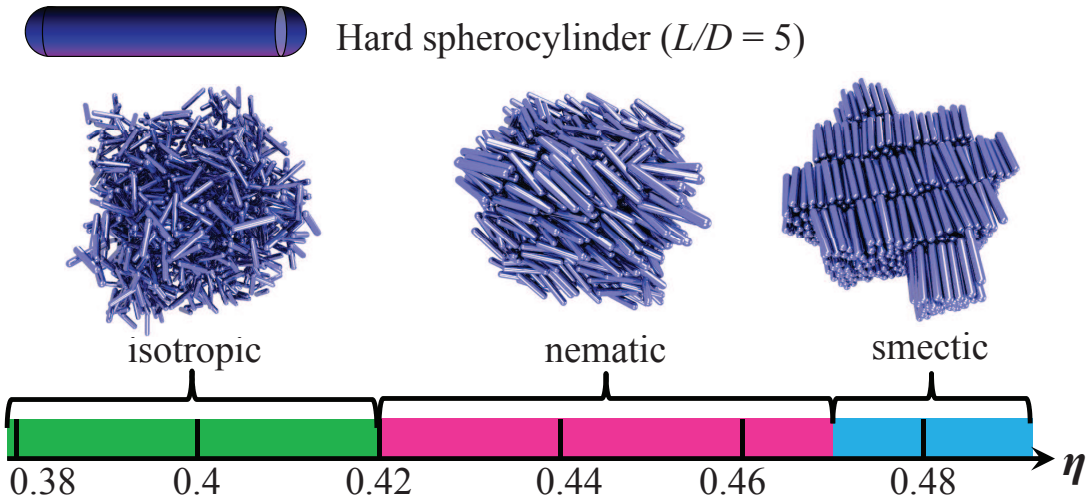

Figure 1.4: The phase transition in system of hard rod-like particles spanning from disordered isotropic liquid to liquid crystalline phases of nematic and smectic states. The packing fraction is defined as $\eta = NV_{\mathrm{m}}/V$ where N is the number of particles, V_{m} molecular volume and V is the total volume.

excluded volume is defined as the space inaccessible to a particle i with fixed orientation, $\vec{\omega}_i$ due to the presence of another particle j with orientation $\vec{\omega}_j$. In figure 1.6, the excluded volumes of two spherocylinders and cylindrical discs at two fixed relative orientations are

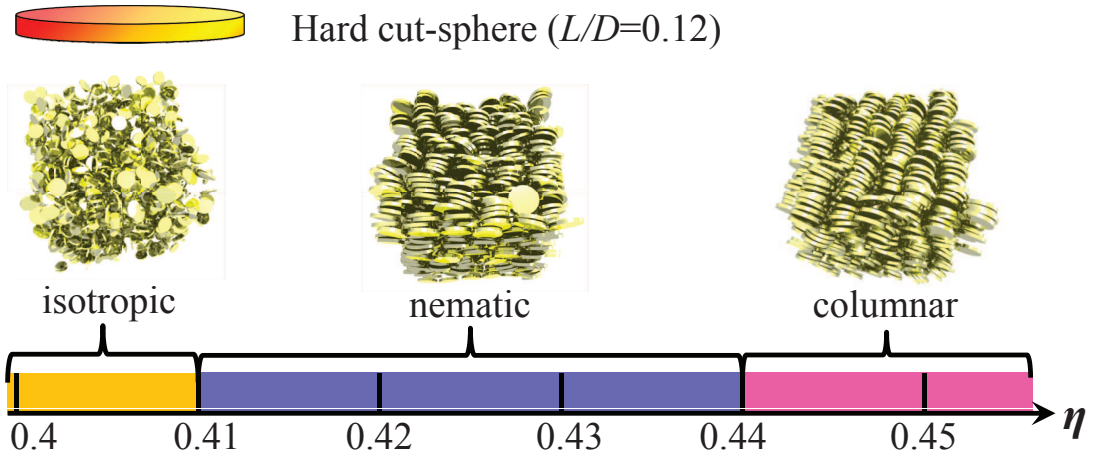

Figure 1.5: The phase transition in system of hard disc-like particles spanning from disordered isotropic liquid to liquid crystalline phases of discotic nematic and columnar states. The packing fraction is defined as $\eta = NV_{\mathrm{m}}/V$ where N is the number of particles, V_{m} molecular volume and V is the total volume.

illustrated. It is apparent that the excluded volume between a pair of anisometric particles depends on the intermolecular orientation.

1.3 Onsager theory

The Onsager theory which was proposed in 1949 [25], was a landmark in the theory of liquid crystals. Using anisometric hard particle models, Onsager showed that the transition between disordered and orientationally-ordered phases can be driven by the entropy of the system alone, which is in apparent stark opposition to the Maier-Saupe approach. The idea of the Onsager approach is adopted and extended in the thesis, thus we briefly outline the main points of Onsager's theory for the isotropic-nematic transition in this chapter.
In his seminal work Onsager [25] presented an expression for a free energy functional of non-spherical molecules which he used to describe the isotropic-nematic phase transition by taking each orientation of the particles as separate components in a mixture. Consider a system of N non-spherical molecules in a volume V at a temperature T. The single-particle density $\rho(\vec{r},\vec{\omega})$ which characterises the inhomogeneous and anisotropic nature of the phase is a function which depends both on the position $\vec{r}$ and the orientation $\vec{\omega}$ of the LC molecule. If the system is homogeneous and only a nematic phase is considered (which is characterised by long-range orientational order but no positional order) the

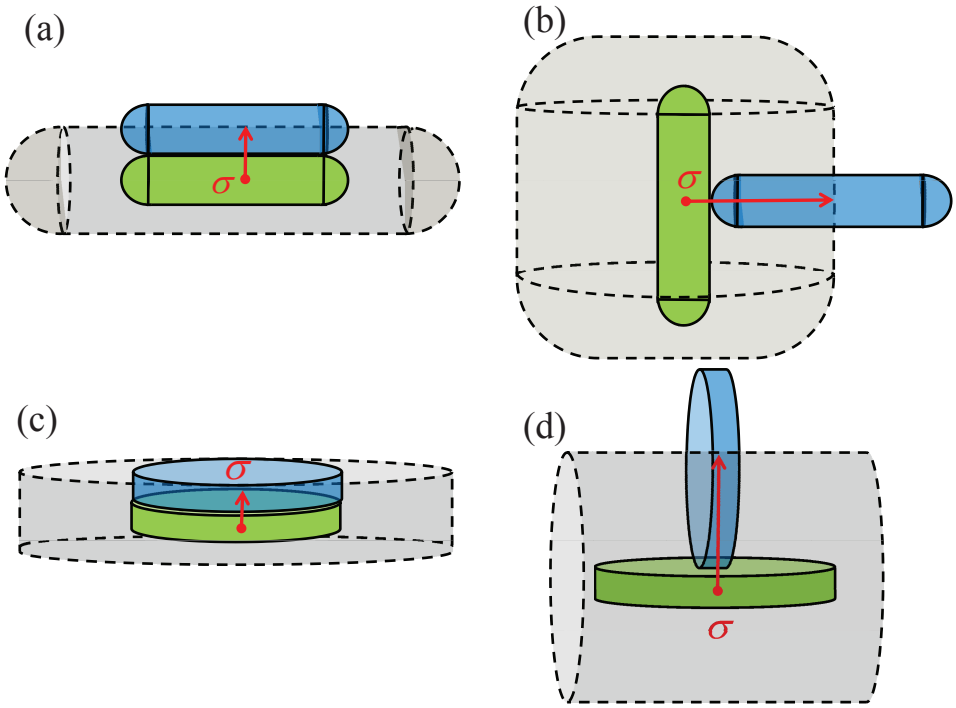

Figure 1.6: The excluded volume of two hard spherocylinders at fixed relative orientations (a) 0° and (b) 90°. The excluded volume of two hard cylindrical discs at fixed relative orientations (c) 0° and (d) 90°. The excluded volume is approximately represented by the shadowed space and the contact distance σ is also shown in each cases.

density $\rho(\vec{r},\vec{\omega})$ can be factorised into a uniform number density $\rho(\vec{r}) = \rho = N/V$ and an orientational distribution function $f(\vec{\omega})$: $\rho(\vec{r},\vec{\omega}) = \rho f(\vec{\omega})$. on the other hand, the total free energy of the system can be written as a sum of an ideal contribution A^{id}, and a residual term A^{res}, which includes the effect of the interparticle interactions:

$$\frac{A}{NkT} = \frac{A^{\mathrm{id}}}{NkT} + \frac{A^{\mathrm{res}}}{NkT}, \tag{1.2}$$

where k is the Boltzmann constant. The ideal contribution to free energy can be written as [50, 51]

$$\frac{A^{\mathrm{id}}}{NkT} = \ln(\mathcal{V}\rho) - 1 + \int f(\vec{\omega}) \ln\{\Omega f(\vec{\omega})\} \mathrm{d}\vec{\omega}, \tag{1.3}$$

where $\mathcal{V}$ is the de Broglie volume (which incorporates the translational and rotational kinetic contributions to the free energy) and for particles of uniaxial symmetry, $\Omega = \int \mathrm{d}\vec{\omega} = 4\pi$. The residual free energy, A^{res}, is written as a virial expansion up to the second virial term:

$$\frac{A^{\mathrm{res}}}{NkT} = \rho B_2 = \frac{\rho}{2} \iint V_{\mathrm{exc}}(\vec{\omega}_1,\vec{\omega}_2) f(\vec{\omega}_1) f(\vec{\omega}_2) \mathrm{d}\vec{\omega}_1 \mathrm{d}\vec{\omega}_2. \tag{1.4}$$

where the second virial coefficient B_2 is calculated as the orientational average of the excluded volume, $V_{\mathrm{exc}}(\vec{\omega}_1, \vec{\omega}_2)$

$$B_2 = \frac{1}{2}\langle V_{\mathrm{exc}}(\vec{\omega}_1, \vec{\omega}_2)\rangle_{\vec{\omega}_1,\vec{\omega}_2} = \frac{1}{2}\iint V_{\mathrm{exc}}(\vec{\omega}_1, \vec{\omega}_2) f(\vec{\omega}_1) f(\vec{\omega}_2) \mathrm{d}\vec{\omega}_1 \mathrm{d}\vec{\omega}_2. \tag{1.5}$$

Here the excluded volume $V_{\mathrm{exc}}(\vec{\omega}_1, \vec{\omega}_2)$ (cf. figure 1.6) is the space inaccessible to a particle with orientation $\vec{\omega}_1$ due to another particle with orientation $\vec{\omega}_2$ and is defined as

$$V_{\mathrm{exc}}(\vec{\omega}_1, \vec{\omega}_2) = \frac{1}{3}\int \sigma^3(\hat{r}_{12}, \vec{\omega}_1, \vec{\omega}_2) \mathrm{d}\hat{r}_{12}. \tag{1.6}$$

where $\sigma^3(\hat{r}_{12}, \vec{\omega}_1, \vec{\omega}_2)$ is the contact distance between the centres of two LC molecules (cf. figure 1.6) and $\hat{r}_{12}$ is the unit vector along that direction ($\vec{r}_{12}$).

The equilibrium state corresponds to the minimum of the total free energy (Equation (1.2)) hence an equilibrium orientational distribution function can be obtained by taking variation of $A[f(\vec{\omega})]$ with respect to the orientational distribution function $f(\vec{\omega})$ under the constraint that $f(\vec{\omega})$ is normalised:

$$\frac{\delta}{\delta f(\vec{\omega})}(A[f(\vec{\omega})] - \lambda_{\mathrm{L}} \int f(\vec{\omega}) \mathrm{d}\vec{\omega}) = 0 \tag{1.7}$$

where λ_{L} is a Lagrange undetermined multiplier defined such that $\int f(\vec{\omega}) \mathrm{d}\vec{\omega} = 1$. The minimum condition leads to a self-consistent integral equation in $f(\vec{\omega})$ which can be solved by various numerical methods [52].

Instead of solving the integral equation, Onsager used a trial function $f_{\mathrm{OTF}}(\vec{\omega})$ (Onsager trial function, OTF) which is written in hyperbolic form:

$$f_{\mathrm{OTF}}(\theta) = \frac{\alpha \cosh(\alpha \cos\theta)}{4\pi \sinh(\alpha)} \tag{1.8}$$

where the polar angle $\theta = \arccos(\vec{\omega} \cdot \vec{\omega}_0)$ and $\vec{\omega}_0$ is the director of the nematic phase. The OTF depends on the variational parameter α which describes the degree of orientational order. It can be shown the OTF is normalised and if $\alpha \to 0$ the OTF reduces to the solution to orientational distribution function in the isotropic phase ($f(\theta) = 1/(4\pi)$). Using the OTF, the functional variation subsequently becomes the derivative of the free energy with respect to the parameter α at a given density.

A simpler form of trial function (Gaussian trial function, GTF) introduced by Odijk and Lekkerkerker [53] is written as

$$f_{\mathrm{GTF}}(\theta) = \begin{cases} \frac{\alpha}{4\pi} \exp[-\frac{\alpha}{2}\theta^2] & 0 \le \theta < \frac{\pi}{2} \\ \frac{\alpha}{4\pi} \exp[-\frac{\alpha}{2}(\pi - \theta)^2] & \frac{\pi}{2} \le \theta \le \pi. \end{cases} \tag{1.9}$$

Compared with OTF, the adoption of GTF renders the orientational average of the excluded volume (second virial coefficient) more tractable and easy to analyse. The shortcoming of the GTF is obvious in that the orientational distribution in the isotropic phase ($f(\theta) = 1/(4\pi)$) cannot be obtained in the limit of $\alpha \to 0$ (cf. figure1.7).

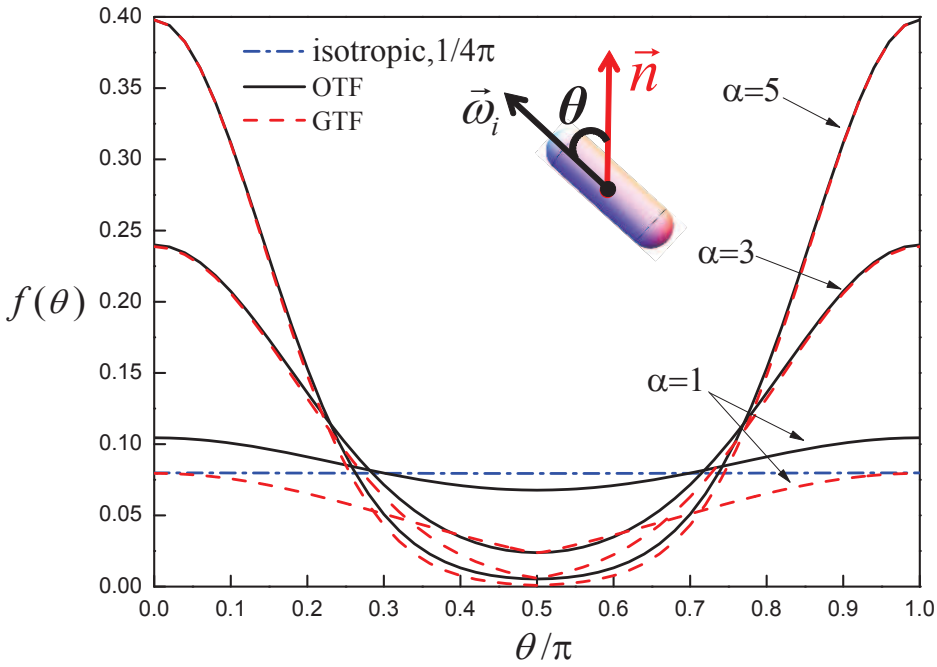

Figure 1.7: Comparison between Onsager trial function (OTF) and Gaussian trial function (GTF) for various values of α.

Using numerical iteration or a trial function (OTF or GTF) to minimize the Onsager free energy (Equation (1.2)), the isotropic-nematic phase behaviour of a system of hard anisometric particles can be qualitatively described. For hard-particle systems, the interplay between the orientational entropy (the orientational integral in Equation (1.3)) and the configuration contribution (Equation (1.4)) determines the degree of orientational order at a given density. One must bear in mind that the Onsager theory is equivalent to the truncation of the virial expansion to second order. As a result, the Onsager theory is exact only for the case of infinitely-long rods ($L/D \to +\infty$) where the isotropic-nematic transition tends to zero density. For most systems of intermediate to small aspect ratios, the Onsager approach does not provide quantitative results. This is a particular issue for systems of oblate disk-like particles, as specified by Onsager in his original paper, the high-body correlations cannot be neglected. In Chapter 2, we focus on the improvement of Onsager second-virial theory for isotropic-nematic phase behaviour of the oblate disc

particles.

1.4 Computer simulation

Complementing theoretical and experimental studies, substantial progress has been achieved in all aspects of computer simulation since the decription of Monte Carlo (MC) simulations by Metropolis et al. in 1953 [54]. The discussion in this section focuses on the simulation work of the LC phase behaviour of hard-core particle systems (hard rods/discs).

The earliest attempts to use computer simulation to study the phase behaviour of non-spherical particles can be traced back to the 1960s. The phase transition of hard discs in two dimensions was first studied by Alder and co-workers [55, 56]. Wood [57] presented a MC simulation study of hard discs in NPT ensemble. Simulation of hard ellipsoids [58] and hard spherocylinders [59] were performed by Vieillard-Baron in 1970s using MC method. However, due to the limitation of the existing computers, these anisotropic particle systems were most likely not equilibrated and definite conclusions could not be drawn with respect to the phase transition between disordered and orientationally-ordered phases. Ten years later, Frenkel and Mulder [60] identified the appearance of the isotropic-nematic transition for hard ellipsoids with a length-breadth ratios larger than 2.75. The smectic state was observed in the hard spherocylinder system [61, 62] which is somewhat different from elongated ellipsoids in terms of geometry. The LC phase diagram of hard spherocylinders with aspect ratio of $5 \geq L/D \geq 3$ was presented by McGrother et al. [45]. Using free energy calculation technique, Bolhuis and Frenkel [63] mapped out the full phase diagram of hard spherocylinder ranging from the hard sphere limit ($L/D = 0$) to the Onsager limit ($L/D \to \infty$).

The Rod-like model for LCs, such as hard spherocylinders, exhibits isotropic, nematic, and smectic phases with increasing system packing fraction (cf. figure 1.4) while the isotropic counterpart, the hard-sphere fluid, undergoes only a fluid-solid transition [64–66]. However, in spite of our understanding of the phase behaviour of the pure bodies, the knowledge of the behaviour of hard-body fluid mixtures is much poorer. In this scenario, apart from the composition dependence of the bulk phases, the complexity of the problem increases as there is a possibility of experiencing phase separation. Mixtures of hard rods and hard spheres are the essential model for studies of liquid crystal mixtures and colloidal suspension mixtures. The phase diagram of the hard rod-sphere mixture remains a open question although some efforts have been directed towards its study [67–71].

Chapters 5-7 of this thesis are devoted to the study of phase behaviour of a binary HSC-HS mixture using MC simulation in the constant normal-pressure ensemble. In a previous study [72], the isotropic-nematic phase transition of HSC-HS mixture has been simulated using MC simulation in the isobaric-isothermal ensemble and compared with the Parsons-Lee descriptions [73]. A shortcoming of using the isobaric-isothermal ensemble to simulate the mixture is that the two coexisting phases are of the same compositions which is clearly not consistent thermodynamically. The study by simulation of this system is plagued by technical problems including a very low interfacial tension (hence a broad interface), low diffusion rates (hence slow mixing) and discontinuous potentials. In this thesis we present a study of the phase behaviour of hard rod-sphere mixture by MC simulation in the constant normal-pressure (stress) ensemble. Two hard walls are placed in the z-axis of the simulation box and normal pressure is applied in the z-direction while the periodic boundary condition is used in xy plane. Due to the presence of the hard walls, the composition of the states in the centre of the simulation cell varies with the imposed pressure. This method enables one to to study the phase behaviour of mixture in a single-box simulation, which is computationally much cheaper than Gibbs ensemble simulation. When the simulation cell is sufficiently large, the state in the centre of the simulation box represents the bulk phase behaviour. However, the external field, i.e., hard walls, induces an ordering in the adjacent fluid driving the neighbouring phase to be an ordered phase. This simulation strategy has proven to be an efficient way of modelling ordered phases [74]. The results of the bulk isotropic-nematic phase behaviour of hard rod-sphere mixture is presented in Chapter 5.

1.5 Outline of the thesis

The layout of the thesis is arranged into two parts. The first part of the thesis concentrates on the theoretical approaches to the description of liquid crystalline phase behaviour. Chapter 2 includes a detailed review of Onsager theory and Parson-Lee scaling approach for the nematic phase and the straightforward application to oblate disc molecules using the Onsager trial function. In addition, a generic equation-of-state for the isotropic-nematic transition of disc-shaped molecules is developed and its adequacy is assessed in detail for the isotropic and nematic phases of systems with varying aspect ratio. Combining this with a cell theory, the complete isotropic-nematic-columnar phase diagram of hard cut spheres is presented.

Hard anisotropic particle systems are reasonable models for lyotropic LCs where the temperature plays a trivial role. However, in the thermotropic LC systems the formation of anisotropic phases is driven by the change of temperature. Thus, the effect temperature plays on the LC phase behaviour should not be neglected. In Chapter 3 and 4, two hard-core attractive particle models are proposed , attractive hard spherocylinders and attractive hard cylindrical discs, to describe the rod- and disc-shaped thermotropic LC systems respectively. Based on the generalised Onsager-van der Waals approach, the free energy for attractive hard particles is developed. To conclude this part, the attractive hard spherocylinder model is applied in the description of the liquid crystalline phase behaviour of poly-(γ-benzyl-L-glutamate) (PBLG) in dimethylformamide (DMF) solutions.
In the second part of the thesis, the liquid crystalline phase behaviour of binary mixtures of hard spheres and hard spherocylinders is studied using Monte Carlo simulation. In Chapter 5, the bulk phase diagram of a binary mixture of hard spheres and hard spherocylinders is reported and compared with the descriptions of Parsons-Lee and many-fluid approaches. We present detailed MC simulation of the surface phase behaviour of HSC-HS mixture of various compositions in Chapters 6 and 7. Our results of HSC-HS mixture in low-density states (low normal pressures) exhibit competing adsorption between the hard rods and hard spheres while in the region of high densities some evidence is shown for the existence of nematic-smectic transition on the surface of the hard wall. We analyse the fluid structure and orientational order profile of the binary mixture and rich surface behaviour including drying, wetting, surface nematization is observed in the simulations. Finally the formation of a smectic monolayer of hard rods (homoetropic alignment) on the surface of a hard wall is discovered for the high-density states a understanding of the behaviour is proposed.

Chapter 2

A generic equation of state for liquid crystalline phases of hard-oblate particles

In his pioneering work [25, 75], Onsager showed the interaction between anisometric hard cores alone can be responsible for the formation of orientationally-ordered phases. We begin the work with a detailed analysis of Onsager theory and its extension: Parsons-Lee approach. In this chapter, we extend the Onsager-Parsons-Lee approach to oblate disc-like fluids and point out some shortcomings of the Parsons-Lee method. In order to improve Parsons-Lee's descriptions, a generic approach for isotropic and nematic phases of oblate disc-shaped particles is thus developed within Vega-Lago scaling relation [76].

2.1 Introduction

As is well known a liquid crystal is the state of matter which is intermediate between crystal and liquid [1, 2, 42]. A substance in its liquid crystal state is highly anisotropic in some of its properties, and maintain some degree of the fluidity of the disordered liquid [2]. The uniqueness of the thermodynamic, structural, optical and electronic properties of liquid crystal materials make them suitable for various applications such as opto-electronics, cosmetics, pharmaceuticals and surfactants.

An essential requirement for stabilising a liquid crystal phase is that the molecule is highly anisotropic in shape. Therefore, the hard-sphere model, which can only form isotropic fluid and crystalline solid states, is not a good representation of liquid crystal molecules

(mesogens). The flat disc-shaped (oblate,discotic, see Figure 2.1) particle is a prototype model for discotic liquid crystals [3, 42]. These models are characterised by aspect ratio which is defined as L/D, L is the thickness of disc particle or length of rod-like particle, and D represents the diameter. Though the flexible part of liquid crystalline molecule will also affect formation of anisotropic phases, it is widely accepted that the specific shape of hard core of the mesogen is primarily responsible for the rich liquid crystalline phase behaviour [46, 47, 62, 77, 78]. At higher densities (packing fractions), the space between a pair of molecules on average become more compact, so that, the excluded volume of the two particles will need to decrease where possible.

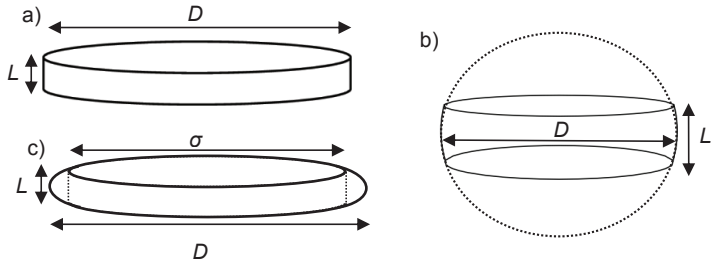

Figure 2.1: Examples of models of oblate mesogens: (a) cylindrical disc (CD), (b) cut sphere (CS), and (c): oblate hard spherocylinder (OHSC). For all of the models, L represents the thickness of disc, D the diameter of disc, and $\sigma = D - L$ in the case of the OHSC model.

Thus, the non-spherical hard cores of molecules align in more ordered configurations which lose the orientational disorder compensating by increasing the translational entropy (free volume) of system. The idea that anisotropic phases are driven by entropic considerations has been examined extensively by computer simulation of hard-body anisometric particles. Discotic nematic and columnar phases have been observed for disc-like particles [46–49] on increasing the packing fraction of the system including a disputed cubatic phase [79]. It is well understood that the highly anisotropic geometry of the molecules can give rise to liquid crystalline states over the intermediate to high-density region [1, 3]. Much of the fundamental understanding has focussed on model rod-like and disc-like particles both in theory and computer simulation. A well known approach to the liquid crystal transition is the Landau-de Gennes phenomenological model [34] using a free energy which is expanded as a series of the order parameters characterising the degree of orientational and positional order for a certain anisotropic phase [1, 3]. The prefactors of each term are assumed to be system and state dependent and treated as adjustable parameters obtained by comparison

with experimental data. Thus, Landau-de Gennes approach, as a macroscopic theory, fails to predict the transition quantitatively or bridge the links between the parameters used in the theory and the molecular features.

As early as 1949, Onsager [25] proposed a free energy functional for the isotropic-nematic transition of prolate and oblate particles by taking a virial expansion up to the second virial coefficient. The truncation of the theory to second order is valid in the limit of long rods where the isotropic-nematic transition tends to zero packing fraction. As specified by Onsager in his original paper, the high-body correlations cannot be neglected in systems of oblate disc-like particles, even for infinitely thin discs, and higher order virial expansion terms have to be included. Much effort have been devoted to improving the Onsager second-virial theory. Density functional theory (DFT) [50, 80] has proved to be an efficient method for the prediction of thermodynamic properties of anisotropic fluids [81, 82]. Successful attempts have involved, amongst other approaches, integral equation theories (e.g., [83, 84]) and fundamental measure theory (FMT) [82, 85]. Integral equation theory is a rigorous method which has a sound basis in statistical mechanics and where the Ornstein-Zernike equation is solved by expanding the radial distribution function $g(\vec{r})$ in terms of spherical harmonic functions. The applicability of integral equation theory is however restricted to the isotopic states with low to intermediate density. Fundamental measure theory, which is a weighted DFT, deconvolutes the Mayer bond between two particles into a series of weighted functions which depend on the geometric shape of the particles. Previous approaches based on FMT fail either to recover the exact second virial coefficient for non-spherical particle or are restricted to specific models, such as 2D discs and needles. Recent progress [86] provides a unified description for arbitrarily shaped convex body and the derived free energy functional captures the isotropic-nematic phase transition for hard spherocylinders, and other rod-like particles. Though both integral equation and fundamental measure theories offer very promising avenues, these theories involves a complicated mathematical treatment which make them difficult to implement for more realistic model systems and practical engineering applications.

An alternative, and perhaps more intuitive, approach to improving the Onsager theory is to include high-body terms in the free energy [79,87,88]. For models of discotic liquid crystals such as cut spheres, the virial expansion has to be taken up to the eighth virial coefficient in both the isotropic and nematic phases so as to provide a good description of the equation of state [79]. However, the poor convergence of virial series means that one is incapable of providing precise predictions for thin discs [79], and the negative values of the higher order

virial coefficients result in a reduction (collapse) of the pressure at high densities [87]. One of the more popular methods used to incorporate high-body contributions is the Parsons-Lee (PL) approximation [89–91]. In this approach the distance between the two particles is scaled by the contact distance σ and the scaled radial distribution function is assumed to be the same as the radial distribution of a reference hard-sphere system at the same packing fraction which can be exactly solved. With the PL method one can treat the particle-particle correlations beyond the pair-level and avoid taking complex details of the structure of the non-spherical fluid into consideration; the expressions for the free energy is thus based simply on that of hard-sphere reference system which incorporates all of the high-order terms. The adequacy of the Onsager-Parsons-Lee free energy for the isotropic-nematic transition has been tested for various hard-body systems, including hard spherocylinders [45,51], hard discs [92] and disc mixtures [93]. Although the PL approach has been applied to hard discotic particles [92], an analytical form of the equation-of-state has not yet been developed. A direct application of the PL approximation gives only positive contributions to the free energy while hard disc-like particles are known to exhibit negative higher-order virial coefficients and more worryingly the theoretical description is not satisfactory when compared with simulation data.

In the current work, the scaled Onsager free energy is extended and an algebraic equation-of-state for oblate particles is developed by using an Onsager trial function to characterise the orientational order of the phase. An accurate novel equation-of-state is developed for the isotropic fluid by introducing an extra parameter to incorporate the negative contributions that are important at high density. This closed-form expression for the free energy of the isotropic phase is then used to construct an extended Onsager free energy of the nematic phase which includes the higher virial contributions using the reference fluid approach of Vega and Lago [76]. Using virial coefficient mapping, the proposed equation of state can be extended to other oblate disc-like particles. In order to investigate the complete phase diagram of discotic particles, an extended Lennard-Jones-Devonshire cell theory [92, 94] is also used to describe the columnar phase. The results predicted with our newly developed parametric equation-of-state are tested against available Monte Carlo simulation data.

2.2 Onsager theory of hard-core liquid crystals

2.2.1 Onsager-Parsons-Lee molecular theory

In his seminal work Onsager [25] presented an expression for a free energy functional of non-spherical molecules which he used to describe the isotropic-nematic phase transition by taking each orientation of particles as separate components in a mixture. Let us consider a system of N non-spherical molecules in a volume V at a temperature T. The single particle density $\rho(\vec{r},\vec{\omega})$ which characterises the inhomogeneous and anisotropic nature of the phase is a function which depends both on the position $\vec{r}$ and the orientation $\vec{\omega}$. If the system is homogeneous, the single particle density $\rho(\vec{r},\vec{\omega})$ can be factorised into a uniform number density $\rho(\vec{r}) = \rho = N/V$ and an orientational distribution function $f(\vec{\omega})$: $\rho(\vec{r},\vec{\omega}) = \rho f(\vec{\omega})$. The Onsager free energy functional for the nematic liquid crystalline state of hard-core particles is obtain combining the ideal and residual contributions as

$$\frac{A}{NkT} = \ln(\mathcal{V}\rho) - 1 + \int f(\vec{\omega}) \ln\{\Omega f(\vec{\omega})\} \mathrm{d}\vec{\omega} + \rho B_2. \tag{2.1}$$

where k is the Boltzmann constant and $\mathcal{V}$ is the de Broglie volume (which incorporates the translational and rotational kinetic contributions to the free energy), and $\Omega = \int \mathrm{d}\vec{\omega} = 4\pi$ is the solid angle for cylindrically symmetric molecules. The second virial coefficient B_2 is the orientational average of the excluded volume V_{exc} given by

$$B_2 = \frac{1}{2}\langle V_{\mathrm{exc}}(\vec{\omega}_1,\vec{\omega}_2)\rangle_{\vec{\omega}_1,\vec{\omega}_2} = \frac{1}{2}\iint V_{\mathrm{exc}}(\vec{\omega}_1,\vec{\omega}_2) f(\vec{\omega}_1) f(\vec{\omega}_2) \mathrm{d}\vec{\omega}_1 \mathrm{d}\vec{\omega}_2. \tag{2.2}$$

V_{exc} is the space inaccessible to a particle with orientation $\vec{\omega}_1$ due to another particle with orientation $\vec{\omega}_2$ and is defined as

$$V_{\mathrm{exc}} = \frac{1}{3}\int \sigma^3(\vec{r}_{12},\vec{\omega}_1,\vec{\omega}_2) \mathrm{d}\vec{r}_{12}. \tag{2.3}$$

where the contact distance σ depends on the relative orientation and position of a pair of discs (See Figure 2.2).

The Onsager free energy corresponds to truncating the virial expansion of the anisotropic and isotropic state up to second virial coefficient. One would therefore expect the Onsager approach to provide good description of the system only in very low-density limit. This can be explained by following facts: first, the isotropic-nematic transition moves to lower packing fraction as the particles are made more anisotropic; second, in the case of hard particles with prolate geometries, the isotropic-nematic transition is described exactly for infinitely long hard rods because the higher-body contributions can be neglected. As we shall see in subsequent sections this is not the case for oblate geometries, even in the

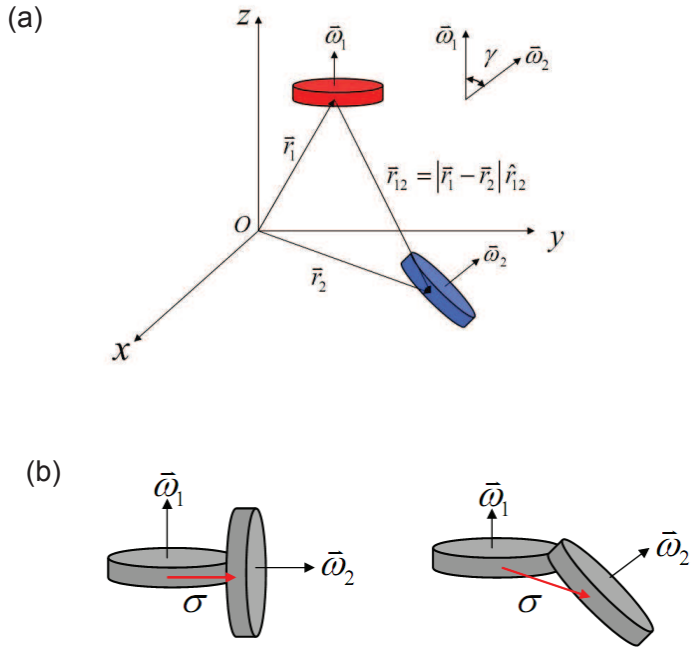

Figure 2.2: (a) The relative separation and orientations of two disc-like particles at positions $\vec{r}_1$ and $\vec{r}_2$ with orientations $\vec{\omega}_1$ and $\vec{\omega}_2$; γ is the angle between two orientational vectors. (b) The dependence of contact distance on the relative orientation and position of the two discs

case of infinitely thin hard discs. For most molecules with moderate aspect ratios, the higher-body contributions are dominant and must be incorporated in the formulation of the free energy. The improvement of the description of the system by incorporating the higher-body contributions can be achieved in an approximate manner for prolate particles by use of the PL scaling approach [89–91].

The PL approach involves a mapping of radial distribution (RDF) function of the non-spherical particles onto an equivalent hard-sphere RDF via the virial (pressure) equation. In this approximation, the volume of the molecule V_{m} is assumed to be the same as that of the hard sphere system and the PL approach is equivalent to the introduction of the following approximation for all of the higher virial coefficients of the non-spherical particles:

$$\frac{B_{\mathrm{n}}}{B_2} = \frac{B_{\mathrm{n,hs}}}{B_{2,\mathrm{hs}}}. \tag{2.4}$$

where B_{n} and $B_{\mathrm{n,hs}}$ are the nth virial coefficient of the hard-core and equivalent hard-sphere particles, respectively. Using PL scaling, the free energy for nematic phase incor-

porating the higher-body contributions albeit approximately.can then be written as [45,51]

$$\begin{aligned}\frac{A}{NkT} &= \ln(\mathcal{V}\rho) - 1 + \int f(\vec{\omega})\ln\{\Omega f(\vec{\omega})\}\mathrm{d}\vec{\omega} \\ &\quad + \frac{G_{\mathrm{PL}}}{V_{\mathrm{m}}}(\eta)\iint V_{\mathrm{exc}}(\vec{\omega}_1,\vec{\omega}_2)f(\vec{\omega}_1)f(\vec{\omega}_2)\mathrm{d}\vec{\omega}_1\mathrm{d}\vec{\omega}_2, \end{aligned} \tag{2.5}$$

where $G_{\mathrm{PL}}(\eta)$ is a density-dependent function obtained by integrating the residual compressibility factor of hard-sphere system with respect to the packing fraction $\eta = \rho V_{\mathrm{m}}$. Using the Carnahan-Starling equation of state for hard-sphere system [95], one obtains

$$G_{\mathrm{PL}}(\eta) = \frac{4\eta - 3\eta^2}{8(1-\eta)^2}. \tag{2.6}$$

Throughout the subscript PL refers to Parsons-Lee scaling method. If a linear density-dependence $G(\eta) = \eta/2$ is assumed, the original Onsager expression is recovered which is valid in the limit of vanishing packing fraction. There are two important and competing contributions in the expression of the free energy (2.5). The first orientational integral on the right-hand-side of Equation (2.5) refers to orientational entropy and the second double orientational integral to the configurational term. The orientational entropy is maximal in the isotropic state while the configurational entropy is maximized when the particles are perfectly aligned. The equilibrium orientational distribution of molecules in the nematic state is found by minimising the total free energy.

2.2.2 Onsager trial function

Generally, the equilibrium state corresponds to the minimum of the total free energy $A[f(\vec{\omega})]$. We can take the variation of the total free energy with respect to the orientational distribution function under the additional constraint that the orientational distribution function is normalised.

$$\frac{\delta}{\delta f(\vec{\omega})}(A[f(\vec{\omega})] - \lambda\int f(\vec{\omega})\mathrm{d}\vec{\omega}) = 0 \tag{2.7}$$

where λ is Lagrange undetermined multiplier so that $\int f(\vec{\omega})\mathrm{d}\vec{\omega} = 1$. The minimum condition leads to a self-consistent integral equation of $f(\vec{\omega})$ which can be solved by various numerical methods [52, 96] including the use of Monte Carlo annealing techniques [97]. In his seminal publication [25] Onsager proposed a functional form for $f(\vec{\omega})$ including a parameter α which characterises the degree of orientational order. The Onsager trial function(OTF) $f_{\mathrm{OTF}}(\vec{\omega})$ is written in hyperbolic form:

$$f_{\mathrm{OTF}}(\vec{\omega}) = \frac{\alpha\cosh(\alpha\cos\theta)}{4\pi\sinh(\alpha)} \tag{2.8}$$

which depends on the single parameter α and the polar angle $\theta = \arccos(\vec{\omega} \cdot \vec{\omega}_0)$ where $\vec{\omega}_0$ is the director of the nematic phase. It should be noticed that the OTF is not a self-consistent solution of the formal minimum condition Equation (2.7) though the equilibrium free energy for nematic phase obtained using OTF is of high accuracy when compared with full numerical solutions [51]. Noting that if $\alpha \to 0$, the $f_{\mathrm{OTF}}(\vec{\omega})$ naturally reduces to $1/4\pi$ corresponding to the isotropic phase. Large values of $\alpha(> 10)$ correspond to the nematic phase. Integrating the OTF over all orientations, one can show that the OTF is normalised, thus it is not necessary to specify the multiplier λ in Equation (2.7) when incorporating the OTF. By substituting the OTF into the total free energy, Equation (2.5), the functional variation of $A[f(\vec{\omega})]$ with respect to $f(\vec{\omega})$ simplifies to a derivative of the free energy with respect to the parameter α. T he simplification provided by the OTF can make the solution of equilibrium orientational distribution straightforward. The details of calculations of the orientational averages by using the OTF have been discussed in detail by Franco-Melgar et al. [51, 98].

2.2.3 Algebraic equation-of-state for the isotropic and nematic phases of oblate hard cylinders

The general expression for the free energy of the nematic phase of hard cylinders can be expressed in a semi-algebraic from involving Bessel integrals. The Onsager-Parsons-Lee approach is difficult to implement in practical applications because conventional equation-of-states in engineering are often expressed as algebraic functions of the thermodynamics variables. The form of excluded volume depends on the specific geometry of molecules. In this work disc-shaped molecules are considered. A scaled Onsager approach of the type outlined in previous section can be applied to hard oblate disc particles (e.g, hard cylindrical discs and cut spheres) depicted in Figure 2.1. The PL free energy for disc-like mesogen:

$$\frac{A}{NkT} = \frac{A^{\mathrm{id}}_{\mathrm{iso}}}{NkT} + \int f(\vec{\omega}) \ln\{\Omega f(\vec{\omega})\} \mathrm{d}\vec{\omega} + G_{\mathrm{PL}}(\eta) \left\langle \frac{V_{\mathrm{exc}}(\sin\gamma)}{V_{\mathrm{m}}} \right\rangle_{\vec{\omega}_1, \vec{\omega}_2}, \tag{2.9}$$

where $A^{\mathrm{id}}_{\mathrm{iso}}/NkT = \ln(\mathcal{V}\rho) - 1$. Using the OTF, the orientational entropy can be approximated as $\int f_{\mathrm{OTF}}(\theta) \ln\{\Omega f_{\mathrm{OTF}}(\theta)\} \mathrm{d}\vec{\omega} \approx \ln\alpha - 1$ [25, 51, 98]. The molecular volume of hard oblate cylindrical particle of length L and diameter D is $V_{\mathrm{m}} = (\pi/4)LD^2$. The closed form of excluded volume of hard cylinders was first presented by Onsager [25]:

$$V^*_{\mathrm{exc,O}} = \frac{V_{\mathrm{exc}}(\gamma)}{V_{\mathrm{m}}} = 2 + (\frac{2D}{L} + \frac{8L}{\pi D}) \sin\gamma + 2|\cos\gamma| + \frac{8}{\pi} E(\sin\gamma), \tag{2.10}$$

where $E(\sin\gamma) = \int_0^{\pi/2}(1-\sin^2\gamma\sin^2\phi)^{1/2}\mathrm{d}\phi$ is the elliptic integral of second kind. It has been shown by Ibarra-Avalos et al. [99] that the expression reported by Onsager is not exact in that it treats the end-to-end contributions in an approximate manner; for highly anisometric cylinders of either prolate or oblate geometry, this contribution becomes negligible. An approximate but highly accurate (within 0.1%) parametric form of the excluded volume of hard cylinders was proposed by Ibarra-Avalos et al [99]:

$$\begin{aligned} V^*_{\mathrm{exc,IA}} = \frac{V_{\mathrm{exc}}(\gamma)}{V_{\mathrm{m}}} &= 2 + \frac{8}{\pi} + \left(2\frac{D}{L} + \frac{8}{\pi}\frac{L}{D}\right)\sin\gamma \\ &+ 2\left[\left(\frac{3\pi}{4}-1\right)|\cos\gamma| + \left(3-\frac{4}{\pi}\right)\left(1-\frac{\pi}{4}\right)\cos^2\gamma\right]. \end{aligned} \tag{2.11}$$

By using the identity $\cos^2\gamma = 1-\sin 2\gamma$, and the expansions of $|\cos\gamma| = \sqrt{1-\sin^2\gamma} = 1-\frac{1}{2}\sin^2\gamma-\frac{1}{8}\sin^4\gamma+\cdots$ and of the elliptical integral $E(\sin\gamma) = \frac{\pi}{2}(1-\frac{1}{4}\sin^2\gamma-\frac{3}{64}\sin^4\gamma-\frac{5}{256}\sin^6\gamma)$, we can express the Onsager and the parametric excluded volume of Ibarra-Avalos et al. as a series in $\sin\gamma$ is truncated at the fourth order term in $\sin^4\gamma$:

$$V^*_{\mathrm{exc,O4}} = \frac{V_{\mathrm{exc}}(\gamma)}{V_{\mathrm{m}}} = 8 + (2\frac{D}{L} + \frac{8}{\pi}\frac{L}{D})\sin\gamma - 2\sin^2\gamma - \frac{7}{16}\sin^4\gamma, \tag{2.12}$$

$$V^*_{\mathrm{exc,IA4}} = \frac{V_{\mathrm{exc}}(\gamma)}{V_{\mathrm{m}}} = C_0^* + C_1^*\sin\gamma + C_2^*\sin^2\gamma + C_4^*\sin^4\gamma. \tag{2.13}$$

Here, the coefficients are $C_0^* = 8$, $C_1^* = (2D/L + 8L/\pi D)$, $C_2^* = (3\pi/4 + 8/\pi - 7)$ and $C_4^* = (4-3\pi)/16$. The differences between the Onsager, the Ibarra-Avalos et al. [99], and the exact numerical values obtained for the second virial coefficient of the isotropic phase of hard cylinders of varying aspect ratio are given in Table 2.1 and Figure 2.3. Using the results of orientational averages of $\sin^i\gamma$ $(i = 1,2,3,4)$ [51, 98], the Onsager-Parsons-Lee free energy for nematic phase of the oblate cylindrical particles can be represented as

$$\frac{A}{NkT} = \frac{A^{\mathrm{id}}_{\mathrm{iso}}}{NkT} + \ln\alpha - 1 + G_{\mathrm{PL}}(\eta)\left[C_0^* + C_1^*\sqrt{\pi}\left(\frac{1}{\alpha^{1/2}} - \frac{15}{16\alpha^{3/2}}\right) + \frac{4}{\alpha}C_2^*\right]. \tag{2.14}$$

The orientational order of the equilibrium nematic phase is characterised by the Onsager trial function with the value of α_{eq} which is determined by minimising the total free energy with respect to the orientational parameter α. The solution of α_{eq} which minimising the free energy can be expressed in trigonometric form as [51, 100]:

$$\alpha_j = 9\left\{\zeta_2 - 2\sqrt{\zeta_2^2 - 3\zeta_1}\cos\left(\frac{2j\pi}{3} + \frac{1}{3}\arccos\frac{-27\left[\zeta_0 - \frac{1}{3}\zeta_1\zeta_2 + \frac{2}{27}\zeta_2^3\right]}{2\left[\zeta_2^2 - 3\zeta_1\right]^{3/2}}\right)\right\}^{-2}, \tag{2.15}$$

$j = 0, 1, 2$ represent three roots and the coefficients

$$\zeta_0 = \frac{32}{45}(\sqrt{\pi}C_1^* G_{\mathrm{PL}}(\eta))^{-1}, \quad \zeta_1 = -\frac{16}{45}, \quad \zeta_2 = -\frac{128}{45\sqrt{\pi}}\frac{C_2^*}{C_1^*}. \tag{2.16}$$

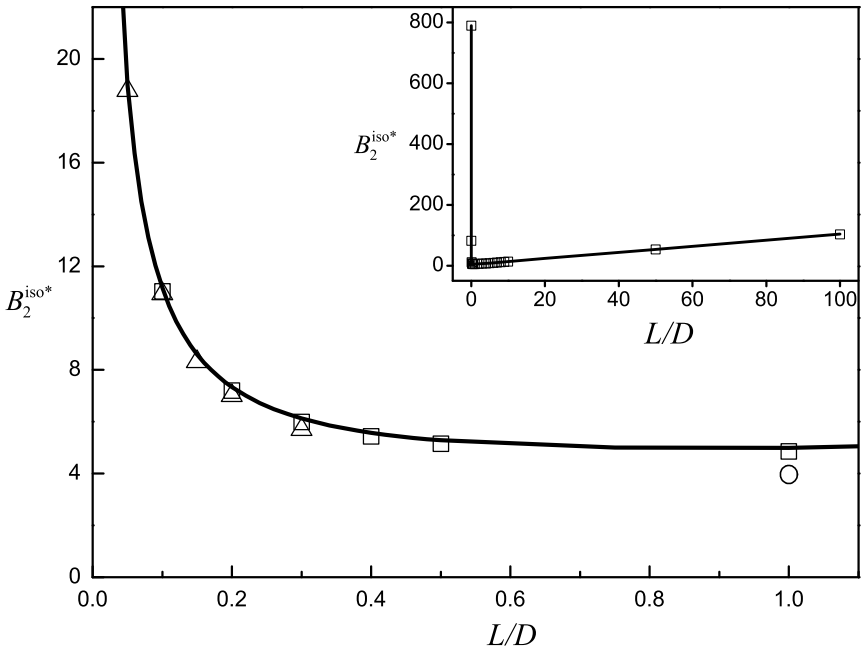

Figure 2.3: The reduced second virial coefficient $B_2^{\mathrm{iso}*} = B_2^{\mathrm{iso}}/V_m = V_{\mathrm{exc}}^* = V_{\mathrm{exc}}/2V_m$ for the isotropic phase of hard right cylinders with different aspect ratio L/D. The continuous curve is the fourth-order expansion (Equation (2.13)), squares are the corresponding MC data for cylinders [99], and the triangles represent the MC data for cut-spheres [87], the circle is the second virial coefficient for hard spheres. The inset shows the comparison of $B_2^{\mathrm{iso}*}$ between fourth-order expansion (Equation (2.13)) and MC data in the whole range of aspect ratios from $L/D = 0.001$ to $L/D = 100$.

The largest root of the cubic equation corresponds to the equilibrium value of the orientational parameter $\alpha_{\mathrm{eq}} = \alpha_2$ for the stable nematic phase. The expressions for the chemical potential and compressibility can then be obtained from the standard thermodynamic relation $\mu/(kT) = PV/(NkT) + A/(NkT)$:

$$\begin{aligned}\frac{\mu^{\mathrm{nem}}}{kT} &= \frac{1}{kT}\left(\frac{\partial A}{\partial N}\right)_{VT} = \frac{\mu^0}{kT} + \ln\eta + \ln\alpha - 1 \\ &+ G'_{\mathrm{PL}}(\eta)\left[C_0^* + C_1^*\sqrt{\pi}\left(\frac{1}{\alpha_{\mathrm{eq}}^{1/2}} - \frac{15}{16\alpha_{\mathrm{eq}}^{3/2}}\right) + \frac{4}{\alpha_{\mathrm{eq}}}C_2^*\right] \qquad (2.17)\end{aligned}$$

$$Z^{\mathrm{nem}} = \frac{PV}{NkT} = 1 + \frac{Z_{\mathrm{hs}}^{\mathrm{res}}}{8}\left[C_0^* + C_1^*\sqrt{\pi}\left(\frac{1}{\alpha_{\mathrm{eq}}^{1/2}} - \frac{15}{16\alpha_{\mathrm{eq}}^{3/2}}\right) + \frac{4}{\alpha_{\mathrm{eq}}}C_2^*\right], \qquad (2.18)$$

Table 2.1: Isotropic second virial coefficient $B_2^{\mathrm{iso}*} = B_2^{\mathrm{iso}}/V_{\mathrm{m}} = V_{\mathrm{exc}}^{\mathrm{iso}}/2$ of hard cylinders of several aspect ratios L/D. Comparisons are made with the data obtained by MC quadrature $B_{2,\mathrm{MC}}^{\mathrm{iso}*}$ [99], the original Onsager expression $B_{2,\mathrm{O}}^{\mathrm{iso}*}$ (Equation (2.10)), the truncated fourth-order Onsager expression $B_{2,\mathrm{O4}}^{\mathrm{iso}*}$ (Equation (2.12)), the parametric Ibarra-Avalos et al. expression $B_{2,\mathrm{IA}}^{\mathrm{iso}*}$ (Equation (2.11)) and the corresponding fourth-order truncated expression $B_{2,\mathrm{IA4}}^{\mathrm{iso}*}$ (Equation (2.13)), and MC quadrature data for cut spheres $B_{2,\mathrm{cs}}^{\mathrm{iso}*}$ [87].

L/D	$B_{2,\mathrm{MC}}^{\mathrm{iso}*}$ [99]	$B_{2,\mathrm{O}}^{\mathrm{iso}*}$	$B_{2,\mathrm{O4}}^{\mathrm{iso}*}$	$B_{2,\mathrm{IA}}^{\mathrm{iso}*}$	$B_{2,\mathrm{IA4}}^{\mathrm{iso}*}$	$B_{2,\mathrm{cs}}^{\mathrm{iso}}$ [87]
1/1000	788.5	788.5	788.616	788.474	788.610	-
1/100	81.62	81.62	81.766	81.625	81.760	-
1/20	-	18.83	18.975	18.833	18.968	18.782
1/15	-	14.92	15.064	14.922	15.058	-
1/10	11.03	11.02	11.171	11.029	11.164	10.929
1/5	7.202	7.198	7.344	7.202	7.337	7.0020
3/10	5.993	5.989	6.135	5.993	6.128	5.6903
1	4.860	4.856	5.002	4.860	4.996	4.000
2	5.468	5.463	5.609	5.468	5.603	
5	8.232	8.228	8.374	8.232	8.368	
10	13.15	13.15	13.295	13.153	13.289	
50	53.09	53.09	53.232	53.091	53.226	
100	103.1	103.1	103.225	103.083	103.218	

where μ^0 is the chemical potential of the reference state, and the density-dependent functions $G'_{\mathrm{PL}}(\eta)$ and $Z_{\mathrm{hs}}^{\mathrm{res}}$ take their usual PL form as

$$G'_{\mathrm{PL}}(\eta) = \mu_{\mathrm{hs}}^{\mathrm{res}} = \left(3\eta^3 - 9\eta^2 + 8\eta\right)/[8(1-\eta)^3] \tag{2.19}$$

$$Z_{\mathrm{hs}}^{\mathrm{res}} = Z_{\mathrm{hs}} - 1 = (4\eta - 2\eta^2)/(1-\eta)^3 \tag{2.20}$$

Carrying out the orientational average of excluded volume for isotropic phase where $f(\vec{\omega}) = 1/(4\pi)$, the corresponding chemical potential μ^{iso} and compressibility factor $Z^{\mathrm{iso}}$of isotropic phase of hard cylinders can then be expressed as

$$\frac{\mu^{\mathrm{iso}}}{kT} = \frac{\mu^0}{kT} + \ln\eta + G'_{\mathrm{PL}}(\eta)\left(C_0^* + \frac{\pi}{4}C_1^* + \frac{2}{3}C_2^* + \frac{8}{15}C_4^*\right) \tag{2.21}$$

$$Z^{\mathrm{iso}} = 1 + \frac{Z_{\mathrm{hs}}^{\mathrm{res}}}{8}(\eta)\left(C_0^* + \frac{\pi}{4}C_1^* + \frac{2}{3}C_2^* + \frac{8}{15}C_4^*\right) \tag{2.22}$$

The PL approach developed here for hard cylindrical discs (CD) can be extended to other disc-like particles by assuming that the second virial coefficients in the nematic and isotropic phases scale. In the case of hard cut spheres (CS) this would correspond to:

$$\frac{B_{2,\mathrm{cs}}^{\mathrm{nem}}}{B_{2,\mathrm{cs}}^{\mathrm{iso}}} = \frac{B_{2,\mathrm{cd}}^{\mathrm{nem}}}{B_{2,\mathrm{cd}}^{\mathrm{iso}}} \tag{2.23}$$

This means that a PL treatment of the nematic phase of cut spheres will only require the second virial coefficient of the nematic phase of the CD (which is known algebraically) and the CS and CD second virial coefficients of the isotropic state (which are also known). Therefore, it is convenient to insert the ratios $B_{2,\mathrm{cs}}^{\mathrm{iso}}/B_{2,\mathrm{cd}}^{\mathrm{iso}}$ into expression of free energy for the isotropic and nematic phases of the CD particles, Equation (2.9). The Helmholtz free energy of the CS system can thus be written as

$$\begin{aligned} \frac{A_{\mathrm{cs}}}{NkT} &= \frac{A_{\mathrm{iso}}^{\mathrm{id}}}{NkT} + \ln\alpha - 1 + G_{PL}(\eta)\left\langle V_{\mathrm{exc,cs}}^{*}\right\rangle_{\vec{\omega}_1,\vec{\omega}_2} \\ &= \frac{A_{\mathrm{iso}}^{\mathrm{id}}}{NkT} + \ln\alpha - 1 + G_{PL}(\eta)\frac{B_{2,\mathrm{cs}}^{\mathrm{iso}}}{B_{2,\mathrm{cd}}^{\mathrm{iso}}}\left\langle V_{\mathrm{exc,cd}}^{*}\right\rangle_{\vec{\omega}_1,\vec{\omega}_2}, \end{aligned} \tag{2.24}$$

where $\left\langle V_{\mathrm{exc,cs}}^{*}\right\rangle_{\vec{\omega}_1,\vec{\omega}_2} = 2B_{2,\mathrm{cs}}/V_{\mathrm{m,cs}}$ and $\left\langle V_{\mathrm{exc,cd}}^{*}\right\rangle_{\vec{\omega}_1,\vec{\omega}_2} = 2B_{2,\mathrm{cd}}/V_{\mathrm{m,cd}}$ are orientational averages of the excluded volume of the CS and CD systems reduced by the molecular volume. Substituting Equation (2.13), the expression for nematic excluded volume of the CD, into Equation (2.24), the equilibrium free energy for nematic phase of the CS system can then be obtained. The corresponding free energy for isotropic phase is readily derived when the orientational distribution function takes a constant in isotropic phase: $f(\vec{\omega}) = 1/(4\pi)$

The orientational order parameter S_n is used to characterise the degree of orientational order of the phase and is defined by

$$S_n = \int P_n(\cos(\theta)) f(\theta)\mathrm{d}\vec{\omega}, \tag{2.25}$$

where $P_n(\cos(\theta))$ is the nth Legendre polynomial. If $n = 2$, S_2 represent the nematic order parameter. A value of $S_2 = 0$ characterises the isotropic state, and $S_2 = 1$ corresponds to the perfect ordered nematic phase. Using the orientational integral in Ref. [51, 98], we obtain

$$S_2 = 1 - \frac{3\coth\alpha_{\mathrm{eq}}}{\alpha_{\mathrm{eq}}} + \frac{3}{\alpha_{eq}^2}. \tag{2.26}$$

One of the main deficiencies of the PL approach as applied to hard-oblate particles is its inadequacy in describing the isotropic state for particles with moderate to large anisotropy. In the Figure 2.4, the deviation of the PL representation of the equation of state for cut

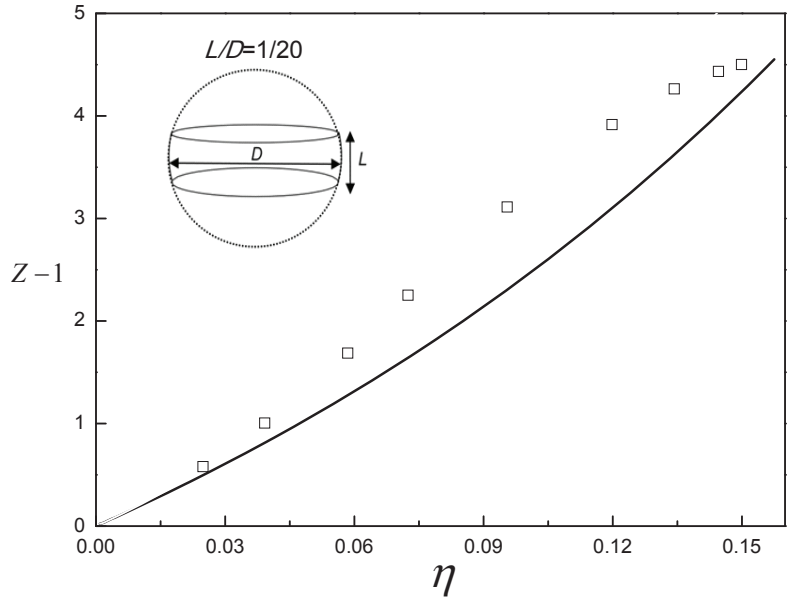

Figure 2.4: Equation-of-state (the compressibility factor $Z-1 = PV/NkT-1$ as function of packing fraction $\eta = \rho V_{\mathrm{m}}$) for the isotropic phase of cut-sphere particles with aspect ratio $L/D = 1/20$. The continuous curve represents Parsons-Lee approach with corresponding second virial coefficient for the isotropic phase of cut sphere of $L/D = 1/20$ [87] (cf. Equation (2.23))

spheres with an aspect ratio of $L/D = 1/20$ from the simulation data is clearly apparent. In the next section, an new accurate equation-of-state for oblate disc-like particles is proposed to accurately describe the isotropic phase of generic oblate particles including cut spheres and right cylindrical discs. This allows for an improved description of the isotropic-nematic transition, and the higher density nematic and columnar states of these systems.

2.3 Generic equation of state for the isotropic and nematic phases of hard-oblate particles

As we have seen the Onsager-Parsons-Lee approach can be readily extended to systems of hard disc-like particles such as cylinders or cut spheres (CS). The CS model has attracted much attention as it is asymptotically similar to the hard oblate cylindrical disc model in the limit of large anisotropies (cf. Figure 2.3 and Table 2.1); in contrast to the hard cylinder model, cut spheres reduce to the hard-sphere limit for aspect ratios of unity $D/L = 1$. The cut-sphere model has been investigated extensively by MC simulation [46,47,79,101], so it

is an ideal choice for assessing the adequacy of an equation of state of hard-oblate particles. The differences in the excluded volume between hard cut spheres or hard cylinders are also less than 1% for moderate values of the aspect ratio, $L/D < 1/5$. In keeping with the notation in previous section, the aspect ratio L/D is used to characterise the cut-sphere molecules of thickness L and diameter D, and in this case the molecular volume is given by

$$\frac{V_{\mathrm{m,cs}}}{D^3} = \frac{\pi}{4}\frac{L}{D} - \frac{\pi}{12}\left(\frac{L}{D}\right)^3. \tag{2.27}$$

Since there is only a negligible difference between the excluded volumes of cut spheres and the cylindrical disc for the aspect ratios of relevance to discotic nematic phases, it is reasonable to develop a theory for isotropic and nematic phases based on CD model for which there are algebraic expressions of the excluded volume. The approximation adopted here should be valid in low to intermediate density range where isotropic and nematic phases are located while recent simulation results [102] indicate that the shape of particle rim play a role in determining the packing pattern at very high densities.

Here, we develop a free energy of the Onsager form employing both the PL [89–91] decoupling approximation and a convenient scaling approach of the Vega-Lago [76] type that we adapt for oblate particles. In the Vega-Lago approach, the virial coefficient in the nematic phase is approximated as the value in the corresponding isotropic phase scaled by the appropriate ratio of the nematic and isotropic second virial coefficients [76, 103]:

$$B_n^{\mathrm{nem}} = \frac{B_n^{\mathrm{iso}}}{B_2^{\mathrm{iso}}} B_2^{\mathrm{nem}}. \tag{2.28}$$

It then follows that the equation of state for nematic phase of hard particles is

$$Z^{\mathrm{nem}} - 1 = \frac{B_2^{\mathrm{nem}}}{B_2^{\mathrm{iso}}}\left(Z^{\mathrm{iso}} - 1\right) \tag{2.29}$$

One can thus express the nth virial coefficient of hard cut spheres in the nematic phase in terms of its second virial coefficient in the nematic phase, and the second and nth virial coefficients in the isotropic phase. The equation of state for the isotropic phase is used to provide information about the isotropic virial coefficients. A prerequisite for using a Vega-Lago approach is an equation of state for the isotropic phase. Unfortunately, the anisotropic virial coefficient of cut spheres is not known algebraically in the nematic phase. In this case we can use the same approximation as we did with the PL approach and assume that the second virial coefficients of the anisotropic states of cut spheres can be obtained from the corresponding values for the cylindrical discs (cf. the scaling relation(2.23)):

$$B_{2,\mathrm{cs}}^{\mathrm{nem}} = \frac{B_{2,\mathrm{cs}}^{\mathrm{iso}}}{B_{2,\mathrm{cd}}^{\mathrm{iso}}} B_{2,\mathrm{cd}}^{\mathrm{nem}} \tag{2.30}$$

The equation of state for the nematic phase of the hard cut-sphere system is expressed in terms of the second virial coefficient and the equation of state of the isotropic phase together with the corresponding isotropic and nematic second virial coefficients of the cylindrical-disc system. Combining Equation (2.29) and Equation (2.30), the equation of state for the nematic phase of the hard cut-sphere particles is then obtained as

$$Z_{\rm cs}^{\rm nem} \;=\; 1+\frac{B_{2,\rm cs}^{\rm nem}}{B_{2,\rm cs}^{\rm iso}}\left(Z_{\rm cs}^{\rm iso}-1\right)=1+\frac{B_{2,\rm cd}^{\rm nem}}{B_{2,\rm cd}^{\rm iso}}\left(Z_{\rm cs}^{\rm iso}-1\right) \tag{2.31}$$

The form of approximation, Equation (2.28) is similar to Equation (2.4) using in the PL approach, but now the virial coefficients of the reference isotropic phase of the particles are employed rather than those of the reference hard-sphere system. The representation of the equation of state (compressibility factor) for the isotropic liquid phase of cut-sphere particles with different aspect ratios is presented in Figure 2.5.

The description obtained with the PL scaling are in reasonable agreement with the simulation data in the very low density region, but as we indicated in the previous section a marked underestimate the compressibility factor is seen at intermediate densities. The percentage absolute deviation (AAD% = $|(\mathrm{Z}-\mathrm{Z_{MC}})/\mathrm{Z_{MC}}|\times 100$) of the theoretical description from the simulated data is also shown in the insets of Figure 2.5. The PL approach leads to an AAD% in the compressibility factor of the fluid of between 20% and 50% for aspects ratios in the range D/L=1/20 to 1/5. Any deviation of theoretical description for the isotropic phase will lead to a poor description of the coexisting densities and pressure of isotropic-nematic transition, which is exhibited by the system at higher densities. It is crucial to have an accurate representation of the isotropic phase of the system over the entire fluid range in order to be confident of the description of the isotropic-nematic transition with a scaled Onsager approach. It is clear from the deficiencies of the PL approach that the scaling to an equivalent hard-sphere system and the subsequent use of the residual part of Carnahan-Starling [50, 95] equation-of-state does not capture the thermodynamic properties of these hard disc-like particles in the isotropic phase.

The virial coefficients of the hard-sphere fluid are always found to be positive [104] as can be seen from an expansion of the Carnahan and Starling [95] expression. The virial coefficients obtained for hard cut spheres obtained by MC integration are compared with the corresponding hard-sphere values in Figure 2.6, it is evident that for the very thin discs ($L/D < 0.2$) the higher-order virial terms of the hard-disc particles exhibit both positive and negative contributions of comparable magnitude.

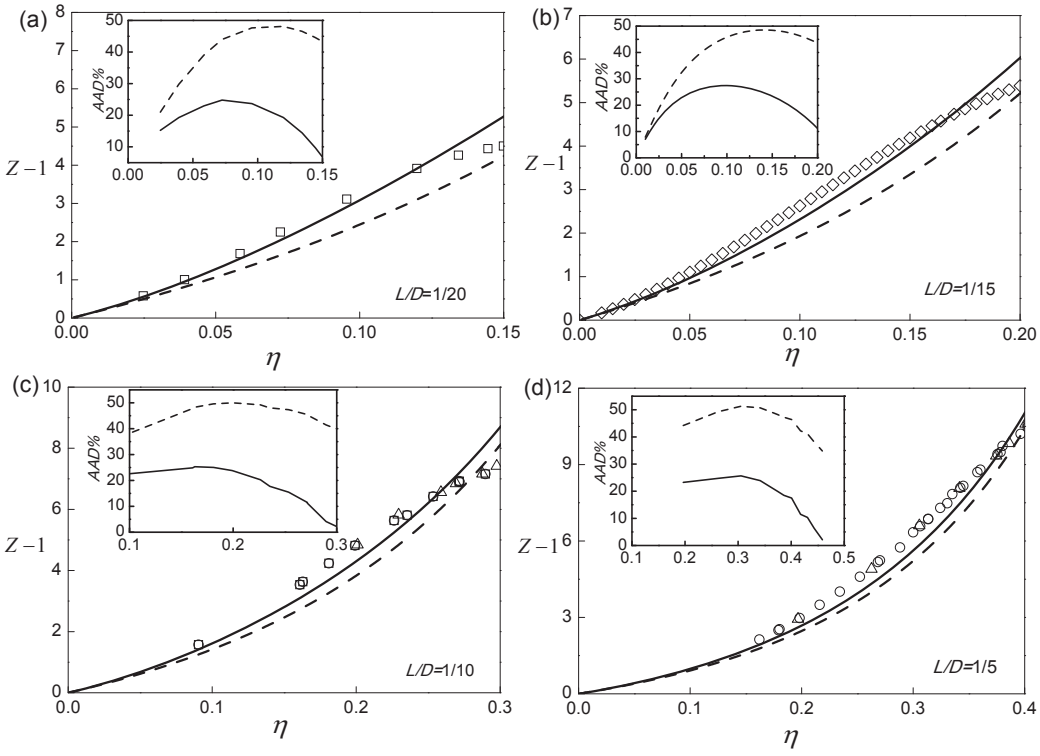

Figure 2.5: Equation-of-state (compressibility factor, $Z = PV/NkT$, as a function of packing fraction, $\eta = NV_m/V$) of cut-spheres (CS) with different aspect ratios in isotropic liquid phase. The percentage absolute average deviations, $\mathrm{AAD\%} = |(\mathrm{Z}-\mathrm{Z_{MC}})/\mathrm{Z_{MC}}|\times 100$ of the theoretical description from the simulated data are shown in the insets respectively. The dashed curve represents the Parsons-Lee scaling approach, and the continuous curve the new algebraic expression developed in this work. The theoretical expressions are compared with the exact simulation data: Squares [101], triangles [79], circles [47]; the diamonds to correlated simulation data [48].

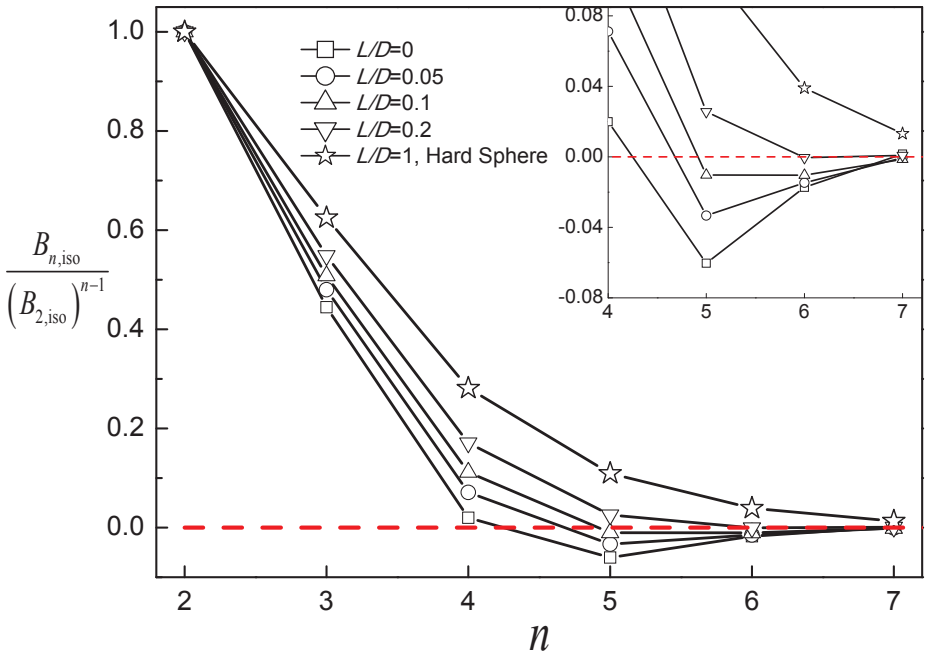

Figure 2.6: Virial coefficients of hard cut spheres for different aspect ratios, L/D, for a thickness L and diameter D [87]. The negative virial coefficients for the very thin disc particles are highlighted in the inset.

One approach proposed by Masters and co-workers [79, 88] is to incorporate the actual contributions from each of the higher-order virial terms of the isotropic and nematic phases explicitly, where the virial coefficients of nematic states can be expressed as functions of the orientational parameter α with an Onsager trial function (OTF). The series is truncated at a certain order (usually up to the eighth virial coefficient) and the Helmholtz free energy for the nematic phase can then be minimised with respect to α at a given density. In this way one avoids the scaling approximation for the virial coefficients such as the one that is commonly used with the PL approach (see Equation (2.4)). Unfortunately, the convergence of the virial series for the isotropic and nematic phases remains problematic and this approach is computational very demanding.

In our current work, we opt to develop an algebraic equation of state (EoS) for isotropic oblate disc-shaped particles. As well as providing an improved description of the isotropic liquid state, it will also enable us to represent the nematic phase in algebraic form using a Vega-Lago type treatment as discussed earlier. The equation of state for the isotropic phase of generic hard particles is formally expressed as

$$Z^{\mathrm{iso}} = 1 + B_2^{\mathrm{iso}*}\eta + B_3^{\mathrm{iso}*}\eta^2 + B_4^{\mathrm{iso}*}\eta^3 + \cdots + B_n^{\mathrm{iso}*}\eta^{n-1} + \cdots . \tag{2.32}$$

where the dimensionaless virial coefficients are defined as $B_n^{\mathrm{iso}*} = B_n^{\mathrm{iso}}/V_{\mathrm{m}}^{n-1}$. Although some data for higher virial coefficients of the isotropic cut-sphere fluid are available [87], the description with the virial equation of state at higher densities is poor as the negative virial coefficients leads to negative pressures in the region close to the isotropic-nematic transition [87, 88]. In order to construct an equation of state that is more robust, the higher-order virial coefficients for isotropic phase of the cut-sphere fluid can be scaled with respect to the corresponding hard-sphere values and a correction can be introduced in the following way:

$$B_{n,\mathrm{cs}}^{\mathrm{iso}*} = \frac{B_{2,\mathrm{cs}}^{\mathrm{iso}*}}{B_{2,\mathrm{hs}}^{*}} B_{n,\mathrm{hs}}^{*} + \Delta B_{n,\mathrm{cs}}^{\mathrm{iso}*} \qquad n = 4, 5, 6, \cdots \tag{2.33}$$

This relation allows us to re-express equation (2.32) as

$$\begin{aligned} Z_{\mathrm{cs}}^{\mathrm{iso}} &= 1 + B_{2,\mathrm{cs}}^{\mathrm{iso}*}\eta + B_{3,\mathrm{cs}}^{\mathrm{iso}*}\eta^2 + \frac{B_{2,\mathrm{cs}}^{\mathrm{iso}*}}{B_{2,\mathrm{hs}}^{*}}\left(B_{4,\mathrm{hs}}^{*}\eta^3 + B_{5,\mathrm{hs}}^{*}\eta^4 + \cdots + B_{n,\mathrm{hs}}^{*}\eta^{n-1} + \cdots\right) \\ &+ \left(\Delta B_{4,\mathrm{cs}}^{\mathrm{iso}*}\eta^3 + \Delta B_{5,\mathrm{cs}}^{\mathrm{iso}*}\eta^4 + \cdots + \Delta B_{n,\mathrm{cs}}^{\mathrm{iso}*}\eta^{n-1} + \cdots\right) \\ &= \frac{4\eta - 2\eta^2}{(1-\eta)^3}\frac{B_{2,\mathrm{cs}}^{\mathrm{iso}*}}{B_{2,\mathrm{hs}}^{*}} + \left(B_{3,\mathrm{cs}}^{\mathrm{iso}*} - \frac{B_{2,\mathrm{cs}}^{\mathrm{iso}*}}{B_{2,\mathrm{hs}}^{*}}B_{3,\mathrm{hs}}^{*}\right)\eta^2 + \sum_{i=4}^{\infty}\Delta B_{i,\mathrm{cs}}^{\mathrm{iso}*}\eta^{i-1}. \end{aligned} \tag{2.34}$$

The last sum in equation (2.34) which is unknown represents the deviation from PL approach where the virial coefficients are scaled with respect to a hard-sphere reference. Considering that both positive and negative higher-order virial coefficients are found for cut spheres of moderate to high anisotropy in the isotropic phase, we propose the following form for the correction term:

$$\begin{aligned} \sum_{i=4}^{\infty}\Delta B_{i,\mathrm{cs}}^{\mathrm{iso}*}\eta^{i-1} &= a\frac{\eta^3\left(1-\eta/2\right)}{\left(1+\eta\right)^3} \\ &= a\left(1-\frac{\eta}{2}\right)\sum_{i=2}^{\infty}(-1)^i\frac{i(i-1)}{2}\eta^{i+1}. \end{aligned} \tag{2.35}$$

The parameter a is introduced to incorporate the contributions from the both positive and negative contributions to the virial series stemming from the prefactor $(-1)^i$. The equation of state for the isotropic cut-sphere fluid is then expressed in compact form as

$$Z_{\mathrm{cs}}^{\mathrm{iso}} = 1 + \frac{4\eta - 2\eta^2}{4(1-\eta)^3}B_{2,\mathrm{cs}}^{\mathrm{iso}*} + (B_{3,\mathrm{cs}}^{\mathrm{iso}*} - \frac{10}{4}B_{2,\mathrm{cs}}^{\mathrm{iso}*})\eta^2 + a\frac{\eta^3(1-\eta/2)}{\left(1+\eta\right)^3}, \tag{2.36}$$

where the reduced virial coefficients of hard cut spheres $B_{2,\mathrm{cs}}^{\mathrm{iso}*} = B_{2,\mathrm{cs}}^{\mathrm{iso}}/V_{\mathrm{m,cs}}$ and $B_{3,\mathrm{cs}}^{\mathrm{iso}*} = B_{3,\mathrm{cs}}^{\mathrm{iso}}/V_{\mathrm{m,cs}}^2$, and the reduced hard-sphere values of $B_{2,\mathrm{hs}}^{*} = B_{2,\mathrm{hs}}/V_{\mathrm{m,hs}} = 4$ and $B_{2,\mathrm{hs}}^{*} = B_{3,\mathrm{hs}}/V_{\mathrm{m,hs}}^2 = 10$. The corresponding virial series is obtained by expanding Equation

(2.36) as a power series in density,

$$\begin{aligned} Z_{\rm cs}^{\rm iso} &= 1 + B_{2,\rm cs}^{\rm iso*}\eta + B_{3,\rm cs}^{\rm iso*}\eta^2 + \left(a + \widetilde{B}_{4,\rm hs}B_{2,\rm cs}^{\rm iso*}\right)\eta^3 \\ &- \left(\frac{7}{2}a - \widetilde{B}_{5,\rm hs}B_{2,\rm cs}^{\rm iso*}\right)\eta^4 + \left(\frac{15}{2}a + \widetilde{B}_{6,\rm hs}B_{2,\rm cs}^{\rm iso*}\right)\eta^5 \\ &- \left(13a - \widetilde{B}_{7,\rm hs}B_{2,\rm cs}^{\rm iso*}\right)\eta^6 + \left(20a + \widetilde{B}_{8,\rm hs}B_{2,\rm cs}^{\rm iso*}\right)\eta^7 \cdots , \end{aligned} \tag{2.37}$$

where $\widetilde{B}_{\rm n,hs} = B_{\rm n,hs}^{*}/B_{2,\rm hs}^{*}$. It is clear that the second and third virial coefficients of isotropic cut-sphere fluid are retained to provide an exact descriptions of phase behaviour of cut spheres at lower densities. The sum of higher order terms ($\eta^i, i > 3$) is seen to contain the parameter a introduced to correct deviations of the higher order virial coefficients of oblate particles from the scaled hard-sphere values.

The exact values for the second and third virial coefficients in isotropic state of hard cut spheres with aspect ratios in the range $0 < L/D < 1$ are available [87]. The value of a is obtained by correlating the existing simulation data for cut spheres with $L/D = 1/20, 1/15, 1/10, 1/5$ to our new parametric EoS (Equation (2.36)). The reduced correction parameter $\tilde{a}V_{\rm m,cs} = aV_{\rm m,cs}/B_{2,\rm cs}^{\rm iso*}$ is then found to be a simple linear function of aspect ratio L/D:

$$\tilde{a}V_{\rm m,cs} = \frac{a}{B_{2,\rm cs}^{\rm iso*}}V_{\rm m,cs} = -2.08252 + 7.034162\left(\frac{L}{D}\right). \tag{2.38}$$

Since the values of virial coefficients increases very rapidly when the virial coefficients are expressed in units of the molecular volume of the cut spheres ($V_{\rm m,cs}$) with increasing anisotropy $L/D \to 0$ (see Figure 2.3), it is convenient to scale the second and third virial coefficients as $B_{2,\rm cs}^{\rm iso*}V_{\rm m,cs}$ and $B_{3,\rm cs}^{\rm iso*}V_{\rm m,cs}^2$ which are more smoothly varying functions of the aspect ratio:

$$B_{2,\rm cs}^{\rm iso*}V_{\rm m,cs} = 0.61896 + 2.34326\left(\frac{L}{D}\right) \tag{2.39}$$

$$B_{3,\rm cs}^{\rm iso*}V_{\rm m,cs}^2 = 0.15204 + 1.67822\left(\frac{L}{D}\right) + 3.2991\left(\frac{L}{D}\right)^2. \tag{2.40}$$

In order to use a Vega-Lago [76] approach, we can express the compressibility factor in the form:

$$Z_{\rm cs}^{\rm iso} = 1 + B_{2,\rm cs}^{\rm iso*}\left[\frac{4\eta - 2\eta^2}{4\left(1-\eta\right)^3} + \left(\widetilde{B}_{3,\rm cs}^{\rm iso} - \frac{10}{4}\right)\eta^2 + \widetilde{a}\frac{\eta^3(1-\eta/2)}{(1+\eta)^3}\right], \tag{2.41}$$

with reduced parameters $\widetilde{B}_{3,\rm cs}^{\rm iso} = B_{3,\rm cs}^{\rm iso*}/B_{2,\rm cs}^{\rm iso*}$ and $\widetilde{a} = a/B_{2,\rm cs}^{\rm iso*}$.

Adopting the new equation of state with the correction parameter a for hard cut spheres (Equation (2.41)), the description of the isotropic phase of hard cut spheres with aspect

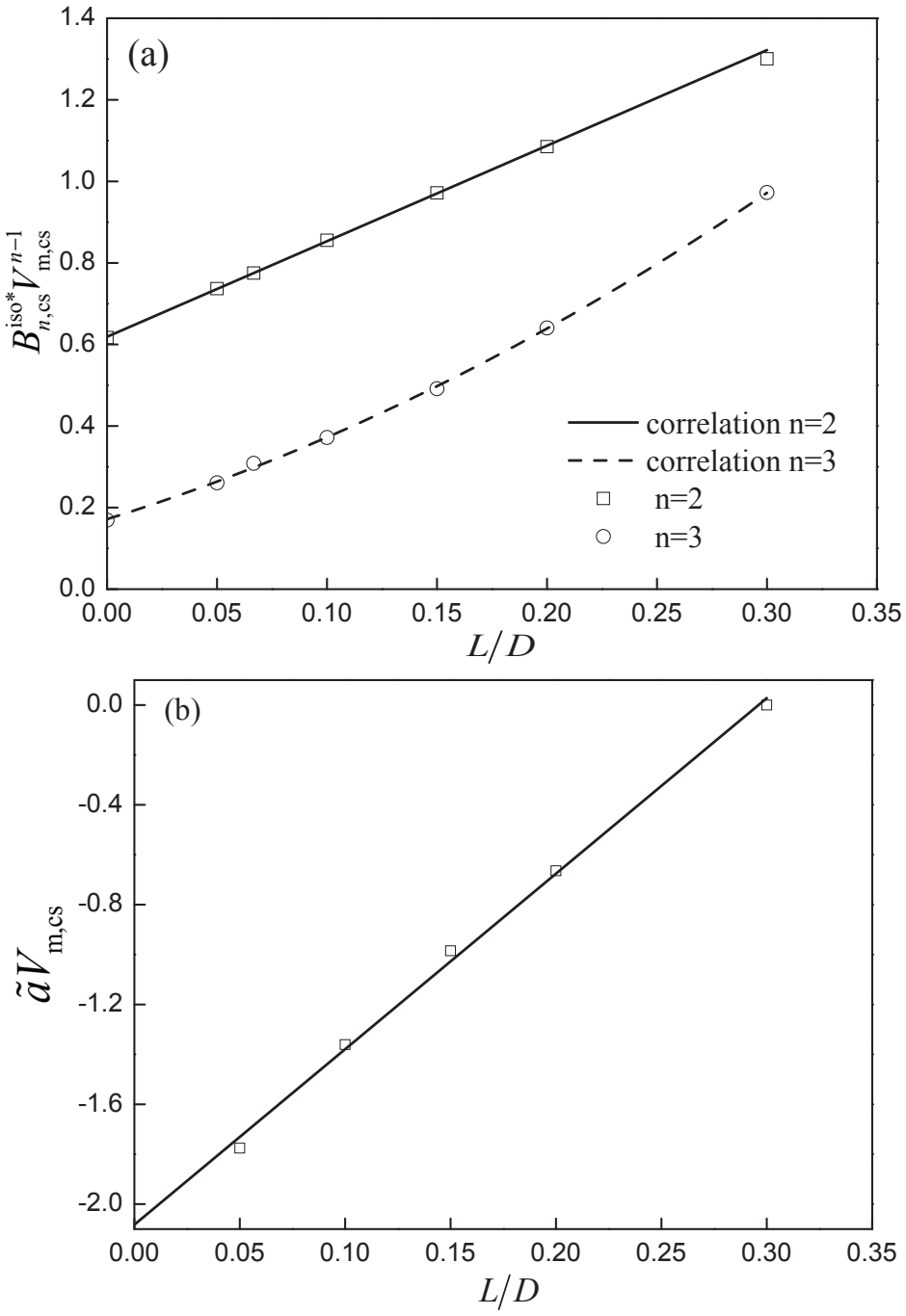

Figure 2.7: (a): The dependence of the reduced isotropic second ($n = 2$) and third ($n = 3$) virial coefficients of cut spheres $B^{\mathrm{iso}*}_{n,\mathrm{cs}}V^{n-1}_{\mathrm{m,cs}}$, and with the aspect ratio L/D. The squares and circles denote the exact values obtained by numerical integration [87]. The continuous and dashed curves are obtained from correlations of the data with Equations (2.39) and (2.40). (b): The linear dependence of reduced correction parameter $\tilde{a}V_{\mathrm{m,cs}} = \left(a/B^{\mathrm{iso}*}_{2,\mathrm{cs}}\right)V_{\mathrm{m,cs}}$ with L/D. the squares are obtained by correlating Equation (2.36) to the simulation data and the continuous line is obtained from Equation (2.38)

ratios $L/D = 1/20, 1/15, 1/10, 1/5$ is compared with the PL description in Figure 2.5. It is clear that the results of new equation of state are in good agreement with simulation data in both lower and intermediate density region. In particular, it can be seen that in the region close to isotropic-nematic transition, the new parametric equation of state provides a description which deviate from the simulation data by less than AAD% $< 10\%$. The accurate representation of the isotropic state of hard cut-sphere particles is expected to improved the prediction of the isotropic-nematic transition point and nematic state of the system.

Recall that the second virial coefficient of cut spheres in the nematic phase can be approximated as

$$B_{2,\mathrm{cs}}^{\mathrm{nem}*} = \frac{B_{2,\mathrm{cs}}^{\mathrm{iso}*}}{B_{2,\mathrm{cd}}^{\mathrm{iso}*}} B_{2,\mathrm{cd}}^{\mathrm{nem}*} = \frac{B_{2,\mathrm{cs}}^{\mathrm{iso}*}}{B_{2,\mathrm{cd}}^{\mathrm{iso}*}} \frac{1}{2} \left[C_0^* + C_1^* \sqrt{\pi} \left(\frac{1}{\alpha^{1/2}} - \frac{15}{16\alpha^{3/2}} \right) + \frac{4}{\alpha} C_2^* \right]. \tag{2.42}$$

Here, we have used the expansion of the cylindrical excluded volume (cf. Equation (2.13)) up to forth order in the $\sin\gamma$ where γ now is the relative orientation between two cut spheres. Introducing $B_{2,\mathrm{cs}}^{\mathrm{nem}*}$ for $B_{2,\mathrm{cs}}^{\mathrm{iso}*}$ in Equation (2.41), the EoS for hard cut-sphere particles in the nematic phase can be expressed in compact form as

$$\begin{aligned} Z_{\mathrm{cs}}^{\mathrm{nem}} &= 1 + B_{2,\mathrm{cd}}^{\mathrm{nem}*} \frac{B_{2,\mathrm{cs}}^{\mathrm{iso}*}}{B_{2,\mathrm{cd}}^{\mathrm{iso}*}} \left[\frac{4\eta - 2\eta^2}{4\left(1-\eta\right)^3} + \left(\widetilde{B}_{3,\mathrm{cs}}^{\mathrm{iso}} - \frac{10}{4} \right) \eta^2 + \widetilde{a} \frac{\eta^3 (1 - \eta/2)}{(1+\eta)^3} \right] \\ &= 1 + \left[\frac{4\eta - 2\eta^2}{4\left(1-\eta\right)^3} + \left(\widetilde{B}_{3,\mathrm{cs}}^{\mathrm{iso}} - \frac{10}{4} \right) \eta^2 + \widetilde{a} \frac{\eta^3 (1 - \eta/2)}{(1+\eta)^3} \right] \\ &\times \frac{B_{2,\mathrm{cs}}^{\mathrm{iso}*}}{2B_{2,\mathrm{cd}}^{\mathrm{iso}*}} \left[C_0^* + C_1^* \sqrt{\pi} \left(\frac{1}{\alpha^{1/2}} - \frac{15}{16\alpha^{3/2}} \right) + \frac{4}{\alpha} C_2^* \right]. \end{aligned} \tag{2.43}$$

By integrating the residual part of compressibility factor of Equation (2.43), the free energy is can be then obtained as

$$\begin{aligned} \frac{A_{\mathrm{cs}}^{\mathrm{nem}}}{NkT} &= \frac{A_{\mathrm{id}}^{\mathrm{iso}}}{NkT} + \ln(\alpha) - 1 + \frac{A_{\mathrm{res}}^{\mathrm{nem}}}{NkT} \\ &= \ln(\mathcal{V}\rho) - 1 + \ln(\alpha) - 1 + G(\eta) \\ &\times \left\{ C_0^* + C_1^* \sqrt{\pi} \left(\frac{1}{\alpha^{1/2}} - \frac{15}{16\alpha^{3/2}} \right) + \frac{4}{\alpha} C_2^* \right\}, \end{aligned} \tag{2.44}$$

where the density dependence is collected in the function

$$\begin{aligned} G(\eta) &= \frac{B_{2,\mathrm{cs}}^{\mathrm{iso}*}}{2B_{2,\mathrm{cd}}^{\mathrm{iso}*}} \int_0^\eta \frac{Z(\eta') - 1}{\eta'} \mathrm{d}\eta' \\ &= \frac{B_{2,\mathrm{cs}}^{\mathrm{iso}}}{2B_{2,\mathrm{cd}}^{\mathrm{iso}}} \left\{ \frac{4\eta - 3\eta^2}{4\left(1-\eta\right)^2} + \frac{1}{2} \left(\widetilde{B}_{3,\mathrm{cs}}^{\mathrm{iso}} - \frac{10}{4} \right) \eta^2 \right. \\ &+ \left. \widetilde{a} \left[-\frac{10\eta + 15\eta^2 + 2\eta^3}{4(1+\eta)^2} + \frac{5}{2} \ln(1+\eta) \right] \right\}. \end{aligned} \tag{2.45}$$

By introducing this modified density-dependent function $G(\eta)$ instead of the PL function $G_{PL}(\eta)$, the expression for the nematic free energy is expressed in a form which is similar to Equation (2.14), so that an equivalent cubic equation can be derived to determine the equilibrium value of the orientational parameter $\alpha_{\rm eq}$ of Onsager trial function (cf. the coefficient ζ_0 of Equation (2.16)). Using standard thermodynamic relation, the compressibility factor and the chemical potential of the nematic phase thus expressed as

$$\begin{aligned} Z_{\rm cs}^{\rm nem} &= 1 + \left[\frac{4\eta - 2\eta^2}{4\left(1-\eta\right)^3} + \left(\widetilde{B}_{3,\rm cs}^{\rm iso} - \frac{10}{4}\right)\eta^2 + \frac{\widetilde{a}\eta^3(1-\eta/2)}{(1+\eta)^3}\right] \\ &\times \frac{B_{2,\rm cs}^{\rm iso*}}{2B_{2,\rm cd}^{\rm iso*}}\left[C_0^* + C_1^*\sqrt{\pi}\left(\frac{1}{\alpha^{1/2}} - \frac{15}{16\alpha^{3/2}}\right) + \frac{4}{\alpha}C_2^*\right] \qquad (2.46) \\ \frac{\mu_{\rm cs}^{\rm nem}}{kT} &= \frac{\mu_{\rm cs}^0}{kT} + \ln\eta + \ln\alpha - 1 + G'(\eta) \\ &\times \left[C_0^* + C_1^*\sqrt{\pi}\left(\frac{1}{\alpha^{1/2}} - \frac{15}{16\alpha^{3/2}}\right) + \frac{4}{\alpha}C_2^*\right], \qquad (2.47) \end{aligned}$$

where the density dependent factor $G'(\eta)$ is

$$\begin{aligned} G'(\eta) &= \frac{B_{2,\rm cs}^{\rm iso*}}{2B_{2,\rm cd}^{\rm iso*}}\left\{\frac{8\eta - 9\eta^2 + 3\eta^3}{4\left(1-\eta\right)^3} + \frac{3}{2}\left(\widetilde{B}_{3,\rm cs}^{\rm iso} - \frac{10}{4}\right)\eta^2\right. \\ &+ \left.\tilde{a}\left[-\frac{10\eta + 25\eta^2 + 13\eta^3 + 4\eta^4}{4\left(1+\eta\right)^3} + \frac{5}{2}\ln(1+\eta)\right]\right\} \qquad (2.48) \end{aligned}$$

For the isotropic phase, the corresponding free energy is simply

$$\frac{A_{\rm cs}^{\rm iso}}{NkT} = \frac{A_{\rm id}^{\rm iso}}{NkT} + \frac{A_{\rm res}^{\rm iso}}{NkT} = \ln(\mathcal{V}\rho) - 1 + G(\eta)B_{2,\rm cs}^{\rm iso*}. \qquad (2.49)$$

where one can use either the exact numerical value for the second virial coefficient in the isotropic phase [87], or the correlation given by Equation (2.39). The corresponding compressibility factor and chemical potential for the isotropic state of hard cut spheres is then obtained as

$$\begin{aligned} Z_{\rm cs}^{\rm iso} &= 1 + B_{2,\rm cs}^{\rm iso*}\left[\frac{4\eta - 2\eta^2}{4(1-\eta)^3} + (\widetilde{B}_{3,\rm cs}^{\rm iso} - \frac{10}{4})\eta^2 + \tilde{a}\frac{\eta^3(1-\eta/2)}{\left(1+\eta\right)^3}\right] \qquad (2.50) \\ \frac{\mu_{\rm cs}^{\rm iso}}{kT} &= \frac{\mu_{\rm cs}^0}{kT} + \ln\eta + 2G'(\eta)B_{2,\rm cs}^{\rm iso*} \qquad (2.51) \end{aligned}$$

The phase coexistence between isotropic and nematic states is established by ensuring the equality of pressure and chemical potential in both phases:

$$\begin{aligned} P^{\rm nem} &= P^{\rm iso} \\ \mu^{\rm nem} &= \mu^{\rm iso}. \qquad (2.52) \end{aligned}$$

The set of nonlinear equations can readily be solved numerically [105].

Our new approach is generic and can be applied in a flexible manner to other oblate particle systems. The proposed EoS is expected to give a good descriptions of cylindrical discs since both positive and negative higher-body correlations have been included. Another oblate disc fluid model which has recently studied by Cuetos and co-workers [102,106–108] is the oblate hard spherocylinder (OHSC) shown in Figure 2.1c;

The PL approach has been applied to the OHSC model [109]. The description suffers from the same inadequacies as with the cut-sphere system, as there is a negligible difference between the properties of the OHSC and the hard cut-sphere and hard cylindrical-disc particles in the limit of large anisotropies ($L/D \to 0$). We use the isotropic second virial coefficient of OHSC particle derived in [109] by following the geometric approach of Mulder [110] ,

$$B_{2,\mathrm{ohsc}}^{\mathrm{iso}} = \frac{\pi^2}{16}\sigma^3 + \frac{\pi}{2}\sigma^2 L + \frac{\pi^2}{2}\sigma L^2 + \frac{2}{3}\pi L^3 + \frac{\pi^3}{16}\sigma^2 L, \tag{2.53}$$

and the molecular volume of an OHSC particle is

$$V_{\mathrm{m,ohsc}} = \frac{\pi}{6}L^3 + \frac{\pi^2}{8}\sigma L^2 + \frac{\pi}{4}\sigma^2 L \tag{2.54}$$

where $\sigma = D - L$. The corresponding the expression for excluded volume of OHSC particles in nematic phase can be expressed in algebraic form by using Legendre polynomials [109, 110]. The form of the anisotropic second virial coefficient makes it difficult to develop an explicit algebraic EoS for nematic phase of the OHSC fluid. Here we treat the OHSC system in the same way as the hard cut-sphere system by mapping the virial coefficients onto the algebraic forms for the cylindrical-disc model. In order to obtain the nth virial coefficient for both the isotropic and nematic phases of the OHSC model, an approximation similar to Equation (2.23) and (2.42) is used:

$$\frac{B_{n,\mathrm{ohsc}}^{\mathrm{iso}}}{B_{2,\mathrm{ohsc}}^{\mathrm{iso}}} = \frac{B_{n,\mathrm{cd}}^{\mathrm{iso}}}{B_{2,\mathrm{cd}}^{\mathrm{iso}}} \quad \frac{B_{n,\mathrm{ohsc}}^{\mathrm{nem}}}{B_{2,\mathrm{ohsc}}^{\mathrm{nem}}} = \frac{B_{n,\mathrm{cd}}^{\mathrm{nem}}}{B_{2,\mathrm{cd}}^{\mathrm{nem}}}. \tag{2.55}$$

The Helmholtz free energy for isotropic and nematic phases of OHSC can then be obtained in the similar way to that of CS particles.

2.4 Results and discussion

By modifying the density-dependent function $G(\eta)$ in the PL approach and introducing an extra parameter a to correct the high-body contributions, we have developed a novel parametric EoS for the isotropic and nematic phases of hard-oblate particles. Combined with the approximate free energy for the columnar phase reviewed in Reference [92], one

can investigate the complete phase diagram of hard disc-like system. In Figure 2.5, we compared the equation of state for the isotropic fluid obtained by molecular simulation for hard cut spheres for various aspect ratios with the theoretical description obtained using the PL scaling approach and with our new parametric EoS. It was clear from this analysis that the negative higher-body terms can not be neglected for systems of thin disc-like particles; this leads to a poor description of the isotropic phase with a PL approach. In our equation of state these contributions are incorporated in an effective manner through the correction parameter is described by the parameter a which was found to obey a simple linear dependence with L/D (see Equation (2.38) and Figure 2.7). This leads to a much improved description of the isotropic phase for a wide range of aspect ratios.

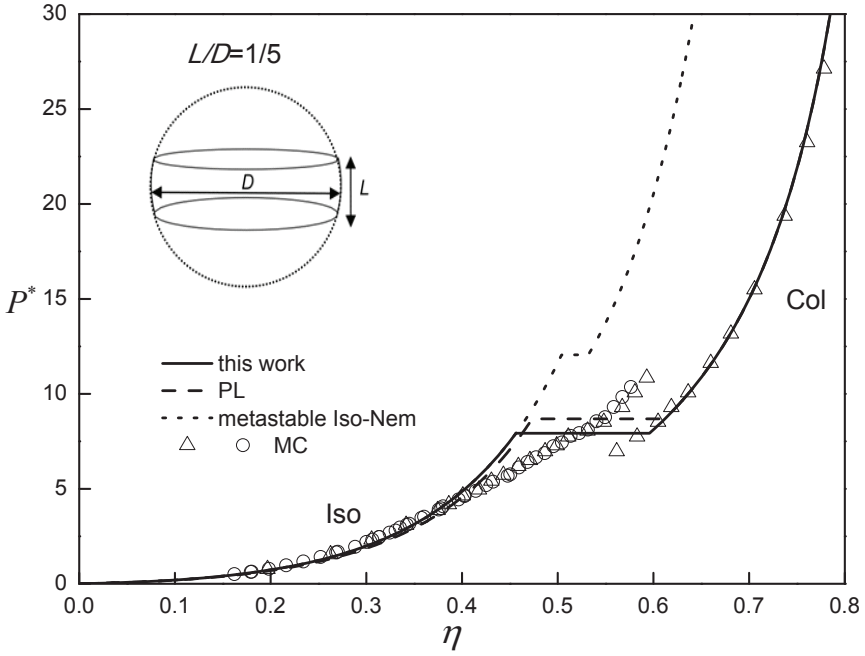

Figure 2.8: The equation of state for cut spheres with an aspect ratio of $L/D = 1/5$ represented as the reduced pressure $P^* = \frac{PV_\mathrm{m}}{kT}$ as a function of the packing fraction $\eta = \rho V_\mathrm{m}$. The isotropic and columnar branches can clearly be identified. The continuous curves correspond to the predictions with our new algebraic scaled Onsager approach, the dashed curves the corresponding results of the Parson-Lee (PL) theory, and the symbols the Monte Carlo simulation data (triangles [79] and circles [47]). The coexistence pressure corresponding to isotropic-columnar transition $P^*_{\mathrm{Iso-Col}} = 5.43$ is determined by simulation [79]. The metastable isotropic-nematic transition is also denoted on the figure (dotted curve).

We start by assessing the capabilities of our new equation of state for the hard cut-sphere

system with $L/D = 1/5 = 0.2$. The algebraic expression provides an adequate description of the isotropic phase of this system for packing fractions up to about $\eta \sim 0.4$. For this aspect ratio the nematic phase is found to be metastable relative to the columnar phase. This can be seen in Figure 2.8 where the compressibility factor is plotted as a function of the packing fraction. There is a clear transition from the isotropic to the columnar phase at $\eta \sim 0.45$. A stable nematic branch is exhibited for the CS systems with $L/D = 1/10, 1/15$ and $1/20$. The equation of state for the isotropic, nematic and columnar phases of these systems displayed in Figures 2.12-2.9 indicate the predictive capability of our algebraic approach for these thin discs. The new EoS provides a reasonable description of the simulation data in both the isotropic and nematic phases, and in most cases is superior to that obtained with the PL scaling. Estimates for the isotropic-nematic transition are also in good agreement with simulation data, with the predicted coexistence pressure and densities deviating from the MC results only by a few percent. As the approach provides a good description of the I-N transition densities, the predicted density dependence of the nematic order parameter is also expected to be in good agreement with the simulation data, as we show for the hard cut-sphere system with $L/D = 1/10$ in Figure 2.10. The description obtained using the novel EoS with Onsager trial function $f_{\mathrm{OTF}}(\vec{\omega})$ are compared with that using a full numerical solution of the equilibrium orientational distribution function (ODF) $f(\vec{\omega})$; details of the determination of the exact equilibrium ODF without the constraint of a particular functional form are given in an earlier publication [45]. The numerical predictions of isotropic-nematic transition are improved slightly which suggests that algebraic EoS leads to a small overestimation of the first-order nature of isotropic-nematic transition.

A nematic-columnar phase transition is exhibited in the systems of hard cut spheres with aspect ratios $L/D < 0.15$. The representation of the nematic-columnar (Nem-Col) transition region is again improved with our novel EoS which is seen to provide a more accurate coexisting pressure, when compared with the PL calculations. Although our approach leads to a better description of the phase behaviour of the system than the PL scaling (particularly for the isotropic liquid) we should acknowledge that there is still a discrepancy in the representation of the nematic phase for the systems with an intermediate aspect ratio.

There are two main sources to the deterioration of the representation of the nematic phase. Firstly, the estimates of the higher-body contributions in nematic phase provided by the Vega-Lago scaling, especially for the dense discotic nematic states close to columnar

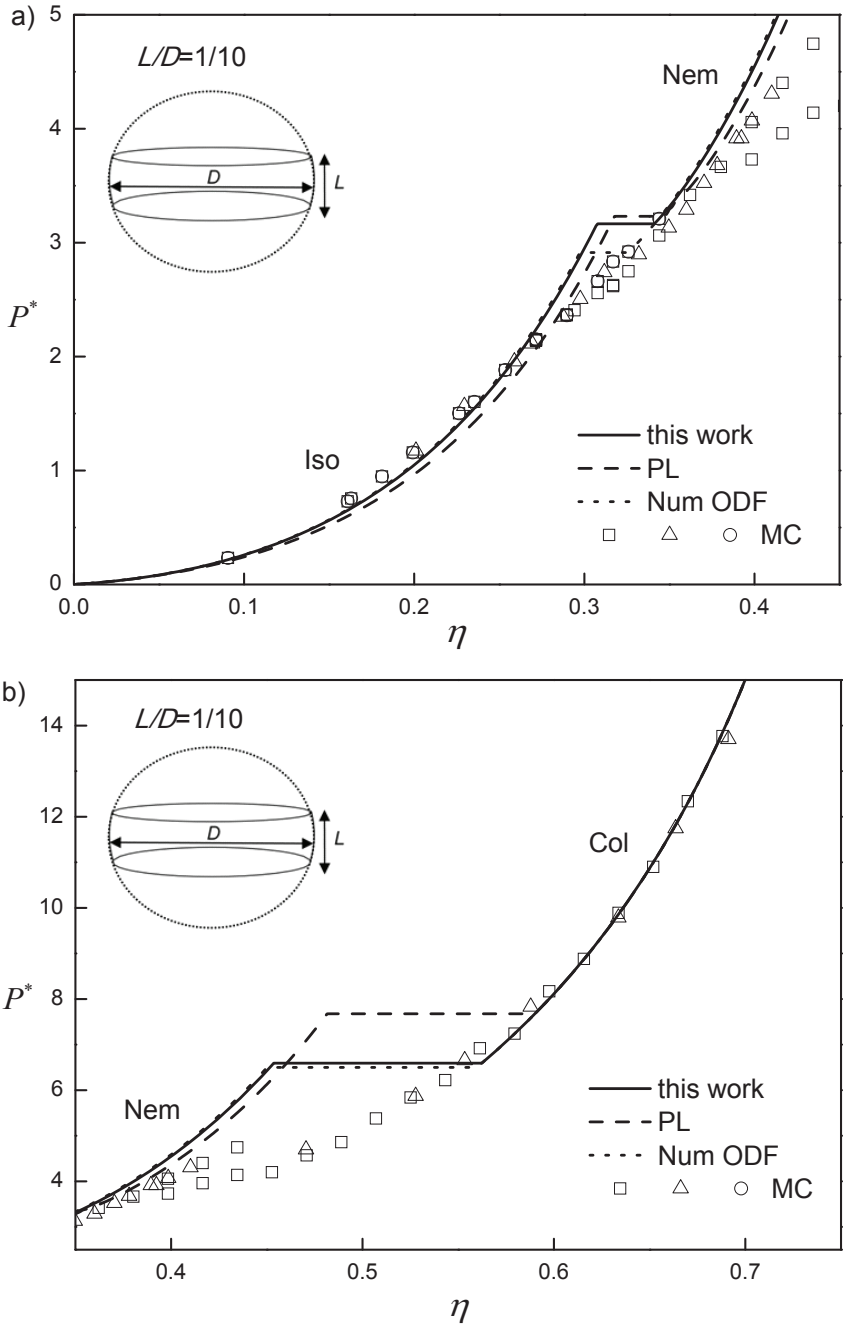

Figure 2.9: The equation of state for cut spheres with an aspect ratio of $L/D = 1/10$ represented as the reduced pressure $P^* = \frac{PV_\mathrm{m}}{kT}$ as a function of the packing fraction $\eta = \rho V_\mathrm{m}$. (a): the isotropic-nematic (Iso-Nem) transition; (b): the nematic-columnar (Nem-Col) transition. In all cases the continuous curves correspond to the predictions of our new algebraic scaled Onsager approach, the dashed curves the corresponding results of the Parson-Lee (PL) theory, the dotted curves represent the numerical solution (Num ODF) and the symbols the Monte Carlo simulation data (squares [101], triangles [79], and circles [47]). The coexistence pressure corresponding to isotropic-nematic transition $P^*_{\mathrm{Iso-Nem}} = 2.74$ and nematic-columnar transition $P^*_{\mathrm{Nem-Col}} = 4.15$ are determined by simulation [79].

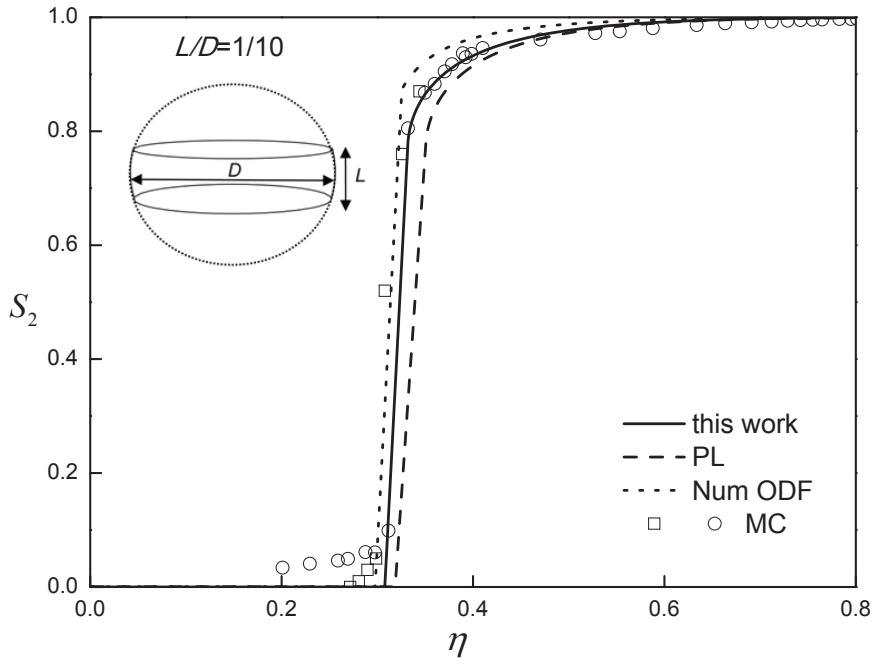

Figure 2.10: The density-dependence of the nematic order parameter $S_2 = \int P_2(\cos(\theta))f(\theta)\mathrm{d}\vec{\omega}$ for cut spheres with an aspect ratio of $L/D = 1/10$. The continuous curve corresponds to the predictions of our new algebraic scaled Onsager approach, the dotted curve represents the numerical solution(Num ODF) and the symbols to the Monte Carlo data (triangles [79] and circles [47]).

phase, is expected to be inaccurate. Second, the problem in representing the position of the isotropic-columnar transition is an approximate theory is used to describe the columnar phase based on a hexagonal 2D lattice of columns and 1D fluid along each column which possibly exaggerates the ordering in the lower-density columnar states; the approximate free energy provides a near exact description of the columnar phase at higher densities. A detailed study of the columnar phase has been undertaken by Cuetos and Martinez-Haya [106]; in their simulations, they observe three types of structures in the columnar phase: a hexatic disordered phase, a hexatic ordered phase and hexatic interdigitated phase. The contributions from the less ordered structures may be important at the lower densities close to nematic phase. At high density the system will adopt the more ordered configurations which will conform with the assumptions made in the development of the cell theory. A comparison of the simulation data for isotropic-nematic and nematic-columnar phase transitions between simulation data and theoretical predictions is provided in Table 2.2.

Next we examine the adequacy of our equation of state in describing the phase behaviour of the system of infinitely thin discs corresponding to $L/D = 0$. The compressibility factor and order parameter are plotted against a reduced density $\tilde{\rho} = \rho D^3$ in Figure 2.13; note that in this limiting case the packing fraction is not a useful variable as it is always zero because the molecules do not have a volume. The description can be compared with that of the PL approach which for infinitely thin discs is identical to Onsager second-virial theory. The new parametric EoS is seen to provide a much better representation of the simulation data for isotropic phase, but still deviates considerably from the data along the nematic branch. In the limit $L/D \to 0$, the packing fraction vanishes, but even at very low packing fraction, the number density can be very high; as a consequence the density-dependent function $G(\eta)$ is not expected to provide a good description. We should mention, however, that infinitely thin discs with $L/D = 0$ correspond to a highly idealized model, and it is more instructive to assess the theory for discs with finite aspect ratios which are more realistic. For real liquid crystal molecules of disc-like shape with small aspect ratios, other factors as surface charges and flexibility are expected to affect the phase behaviour.

The global phase diagram of hard cut-sphere particles is plotted as a function of the aspect ratios L/D in Figure 2.14, where the results of our scaled-Onsager/cell theory are compared with available simulation data [47,48,79,101]. It is clear that as expected the packing fractions of coexisting isotropic and nematic phases increase when the molecules become less anisometric; our novel scaled Onsager theory (with a trial function to represent the

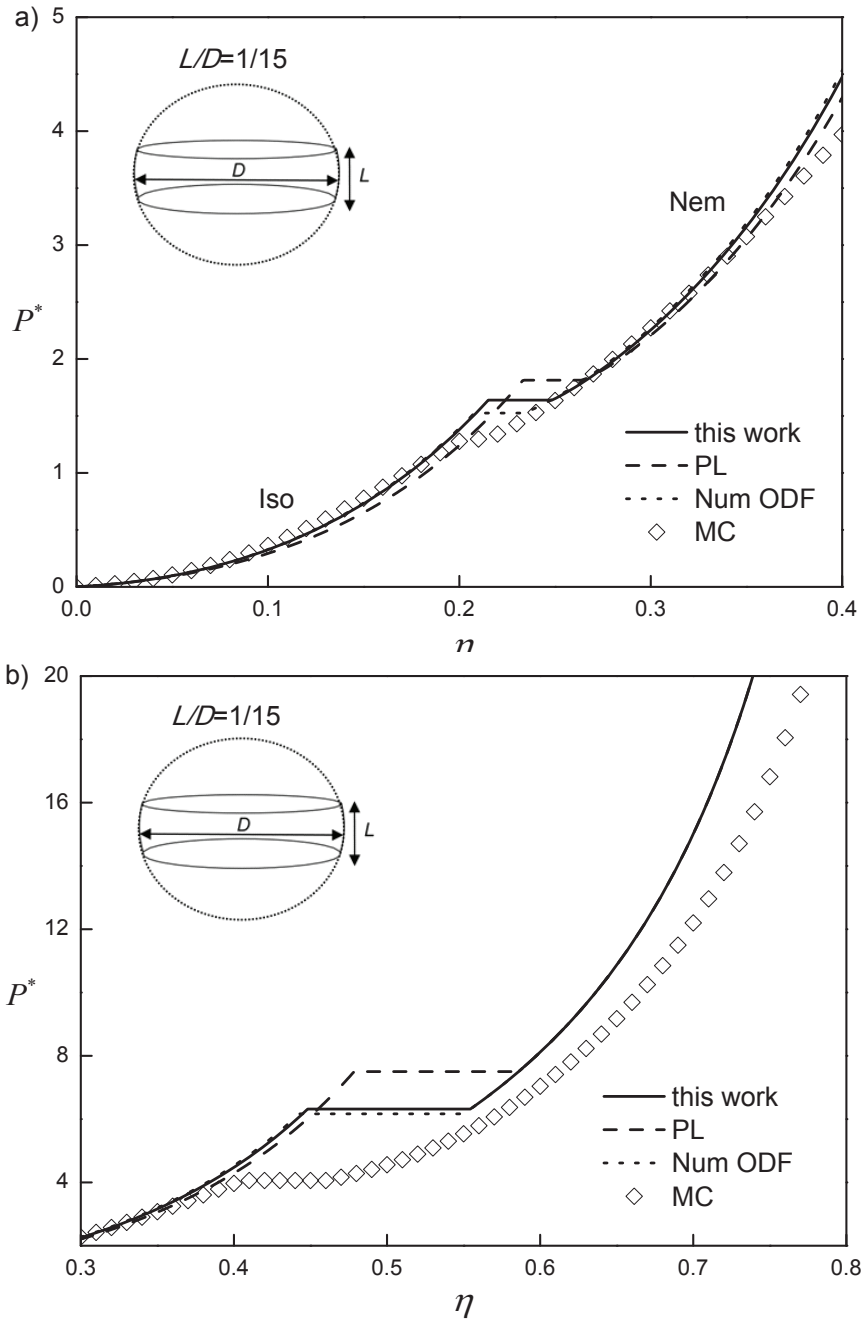

Figure 2.11: The equation of state for cut spheres with an aspect ratio of $L/D = 1/15$ represented as the reduced pressure $P^* = \frac{PV_\mathrm{m}}{kT}$ as a function of the packing fraction $\eta = \rho V_\mathrm{m}$. (a): the isotropic-nematic (Iso-Nem) transition; (b): the nematic-columnar (Nem-Col) transition. In all cases the continuous curves correspond to the predictions of our new algebraic scaled Onsager approach, the dashed curves the corresponding results of the Parson-Lee (PL) theory, the dotted curves represent the numerical solution (Num ODF) and the symbols the Monte Carlo simulation data [48]

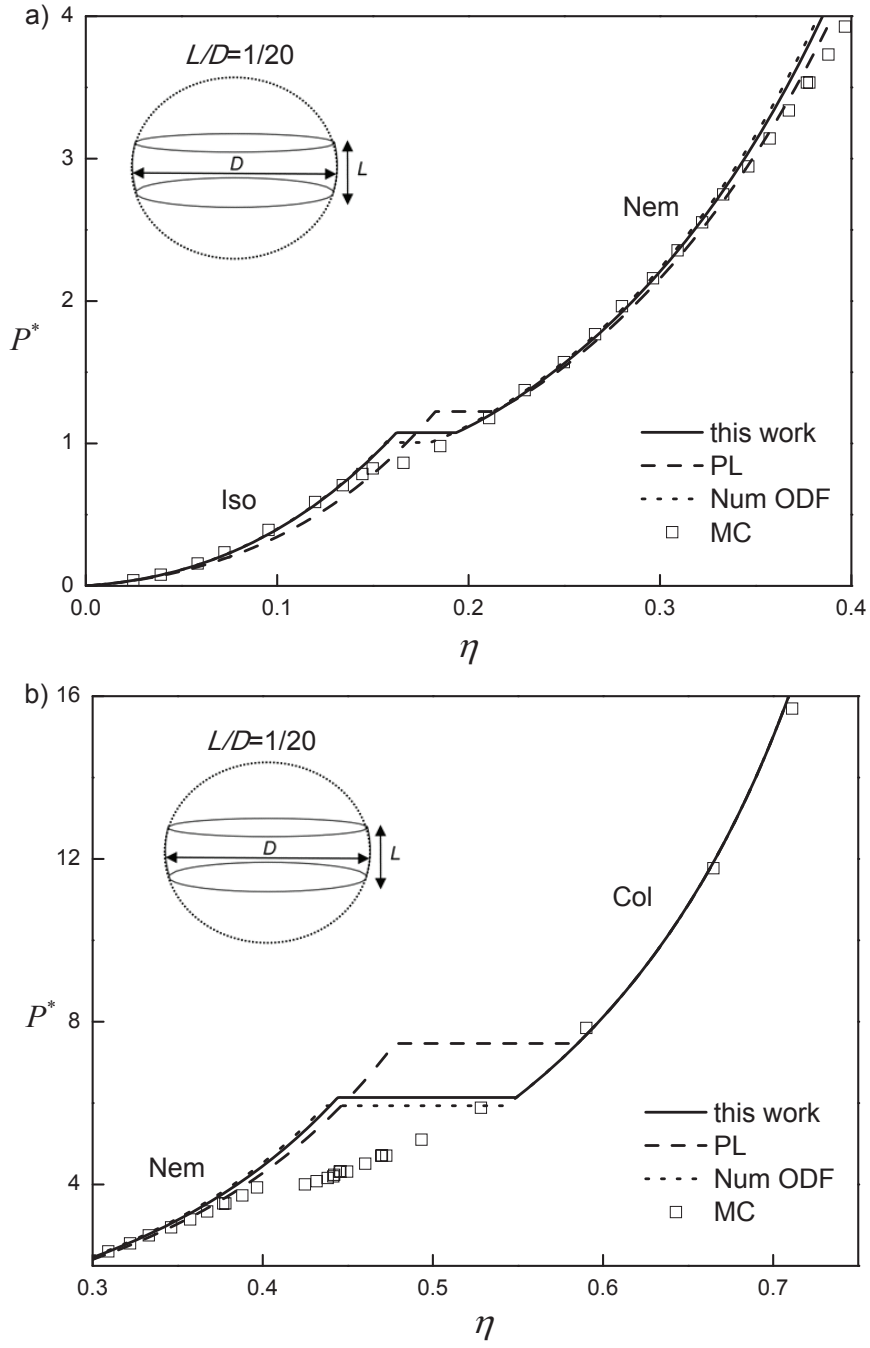

Figure 2.12: The equation of state for cut spheres with an aspect ratio of $L/D = 1/20$ represented as the reduced pressure $P^* = \frac{PV_\mathrm{m}}{kT}$ as a function of the packing fraction $\eta = \rho V_\mathrm{m}$. (a): the isotropic-nematic (Iso-Nem) transition; (b): the nematic-columnar (Nem-Col) transition. In all cases the continuous curves correspond to the predictions of our new algebraic scaled Onsager approach, the dashed curves the corresponding results of the Parson-Lee (PL) theory, the dotted curves represent the numerical solution (Num ODF) and the symbols the Monte Carlo simulation data [101].

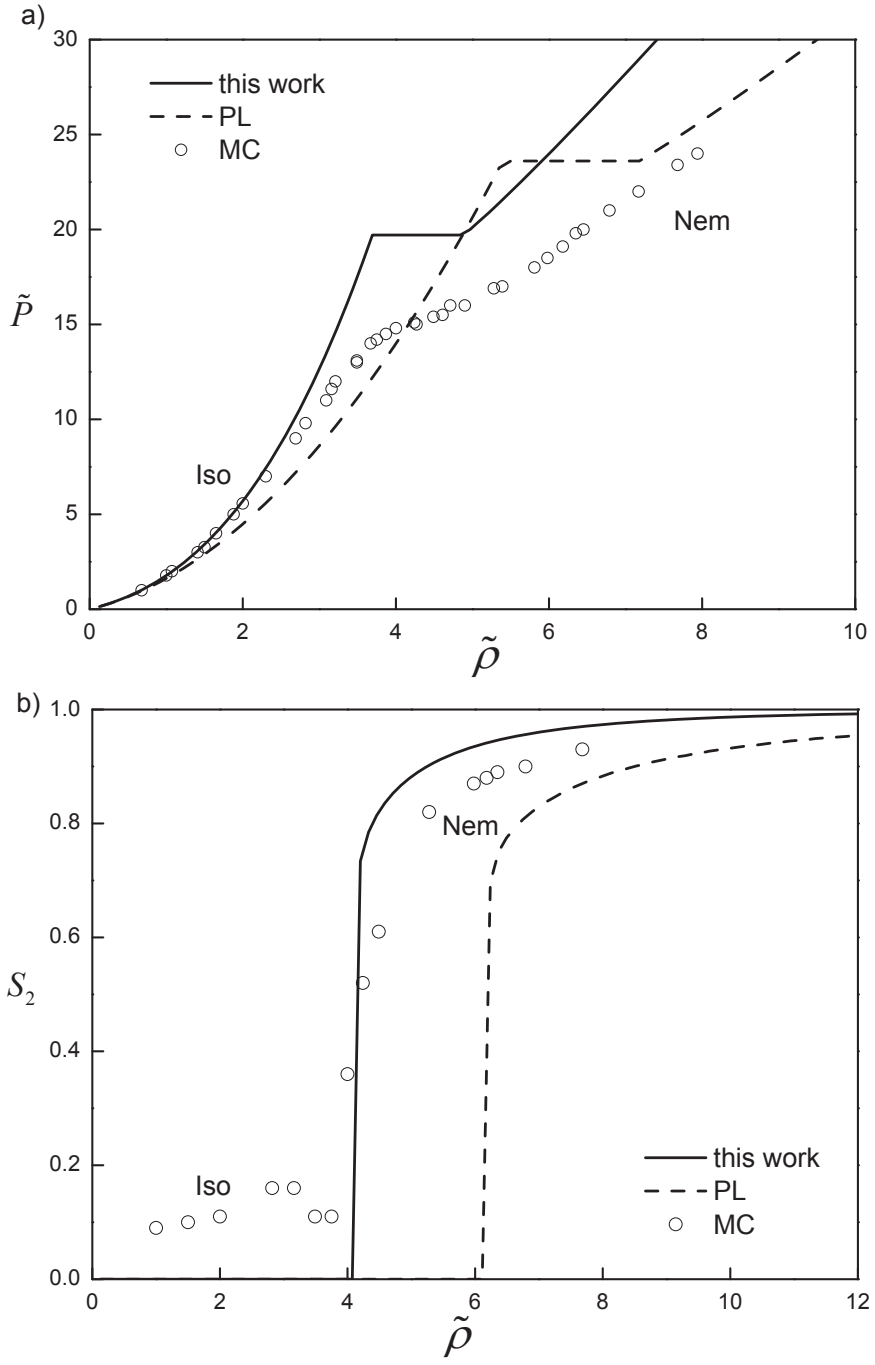

Figure 2.13: (a): The equation of state for infinitely thin hard discs represented in terms of the reduced pressure $\tilde{P} = PD^3/kT$ versus the reduced density $\tilde{\rho} = \rho D^3$. The isotropic (Iso) and nematic (Nem) branches are seen at low and high densities respectively. The continuous curves correspond to our new algebraic scaled Onsager appraoch, the dashed curves the Parson-Lee (PL) theory, and the symbols the Monte Carlo data [46]. (b): The dependence of the nematic order parameter $S_2 = \int P_2(\cos(\theta))f(\theta)\mathrm{d}\vec{\omega}$ of the system as a function of reduced density$\tilde{\rho}$

Table 2.2: Coexistence data for the isotropic-nematic and nematic-columnar phase transitions of hard cut spheres. $P^*_{\rm IN}(P^*_{\rm NC})$ is the pressure at isotropic-nematic (nematic-columnar) phase transition, and $\eta_{\rm iso}$, $\eta_{\rm nem}$ and $\eta_{\rm col}$ are the densities of isotropic, nematic, and columnar phases, respectively. PL, Algebraic EoS and Num ODF represent the results are obtained with Parsons-Lee approach, new algebraic equation of state, and numerical solution of the orientational distribution function.

L/D		$\eta_{\rm iso}$	$\eta_{\rm nem}$	$P^*_{\rm IN}$	$\eta_{\rm nem}$	$\eta_{\rm col}$	$P^*_{\rm NC}$
1/20	Simulation [101]	0.153	0.164	0.844	0.405	0.432	4.084
	PL	0.182	0.211	1.224	0.478	0.585	7.464
	Algebraic EoS	0.163	0.194	1.076	0.445	0.549	6.137
	Num ODF	0.158	0.180	1.007	0.438	0.543	5.936
1/15	Simulation [48]	0.202	0.215	1.296	0.405	0.433	4.067
	PL	0.234	0.264	1.814	0.479	0.586	7.501
	Algebraic EoS	0.215	0.248	1.639	0.448	0.554	6.318
	Num ODF	0.208	0.234	1.526	0.443	0.549	6.167
1/10	Simulation [47]	0.299	0.303	2.528	0.450	0.494	5.129
	Simulation [101]	0.316	0.326	2.795	0.405	0.435	4.202
	Simulation [79]	0.312	0.336	2.741	0.437	0.482	4.15
	PL	0.318	0.346	3.231	0.482	0.589	7.676
	Algebraic EoS	0.308	0.341	3.166	0.454	0.562	6.592
	Num ODF	0.298	0.326	2.913	0.450	0.559	6.499

single particle orientational distribution) is seen to provide a good representation of the Iso-Nem transition densities for the entire range of aspect ratios, albeit with a slightly broader density gap than is found from simulation. By comparison the nematic-columnar transition densities are seen to be relatively insensitive to the particle anisotropy over a large range $0.01 < L/D < 0.15$. In this case the scaled Onsager/cell theory only provides a qualitative description of the Nem-Col transition; the coexisting nematic and columnar densities are overestimated by the theory, most probably due to the improper treatment of the orientational degrees of freedom of the discs for the lower-density columnar states. The aspect ratio at the triple point predicted with our theory is $L/D = 0.154$ which is slightly larger than the previous estimate with Parsons-Lee approach where $L/D = 0.125$ [92]. The larger

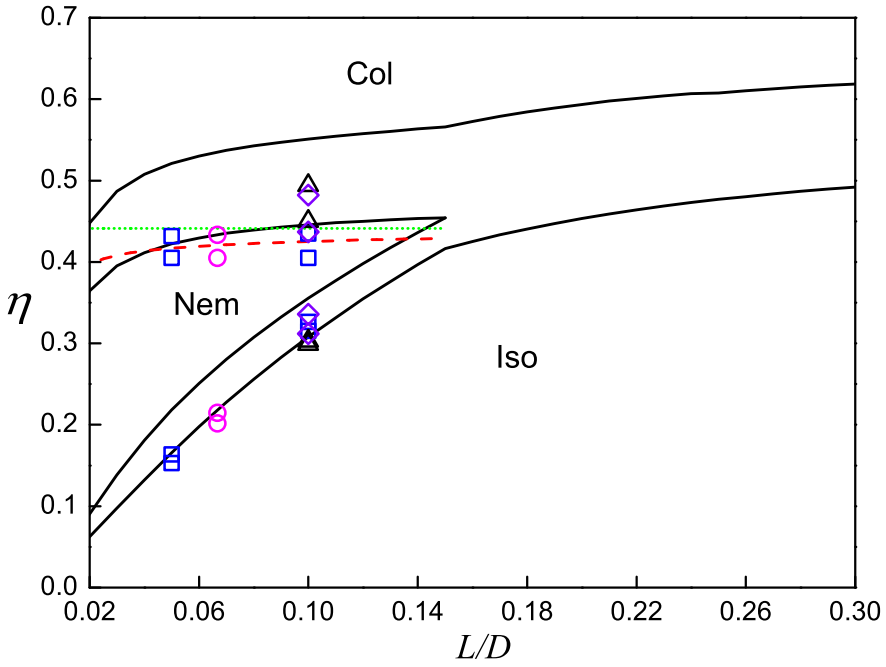

Figure 2.14: Global phase diagram of the hard cut-sphere system of variable aspect ratio L/D. The predictions (continuous curves) of the boundaries between the isotropic (Iso), nematic (Nem) and columnar (Col) phases are obtained with our new scaled-Onsager/cell theory. The theoretical predictions are compared with the available simulation data: Squares [101], diamonds [48], triangles [79], and circles [47]. The dotted and dash curves are the results obtained with a bifurcation analysis using the Parsons-Lee scaling and Vega-Lago scaling approximations.

value of the aspect ratio at the triple point could be due to the incorporation of the negative contributions of higher-body virial coefficients. The simulation data for the infinitely thin discs suggests that the Nem-Col transition densities remain finite and are insensitive to the molecular anisotropy in the limit $L/D \to 0$; the theoretical description of the Nem-Col transition breaks down in this limit due to an inadequate treatment of the higher virial coefficients. For infinitely thin disc, the packing fractions of the nematic-columnar transition obtained from simulations are $\eta_{\rm nem} = 0.490$ and $\eta_{\rm col} = 0.521$ [49], while low values of $\eta_{\rm nem} = 0.0452$ and $\eta_{\rm col} = 0.0935$ are predicted with our scaled-Onsager/cell theory We attribute the failure of the theory in limit $L/D \to 0$ to the vanishing volume of the infinitely thin discs ($\lim_{L/D\to 0} V_{\rm m} = 0$) which leads to an inadequate representation of the

density-dependent factor $G(\eta)$ in Equation (2.45). The results obtained using bifurcation analysis are also presented (see Appendix A). Using a simple density modulation, we find that the bifurcation point predicted is in a reasonable agreement with the simulation data. The bifurcation point gives an accurate estimate of the coexisting densities of nematic and columnar phases.

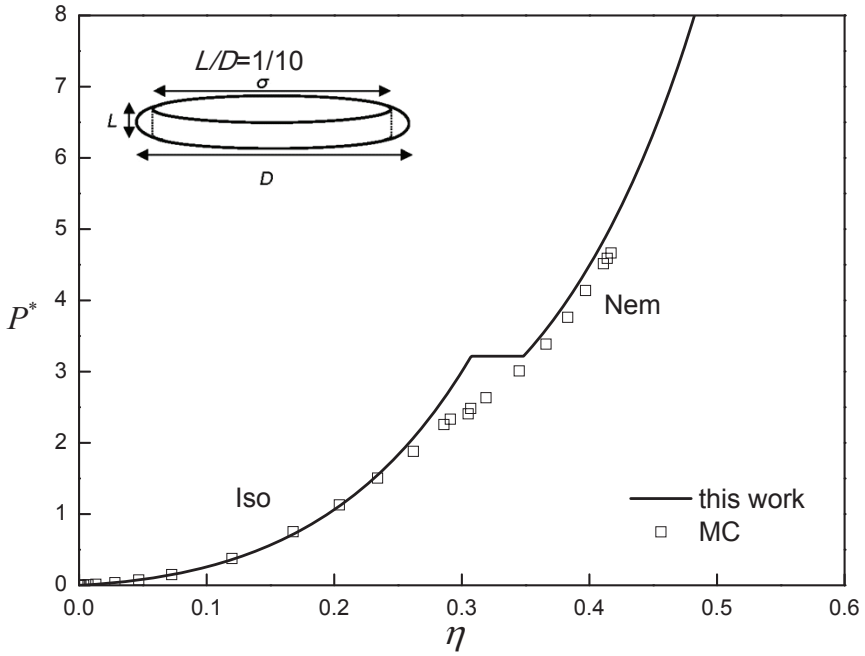

Figure 2.15: The equation of state for oblate hard spherocylinders with an aspect ratio of $L/D = 1/10$ represented as the reduced pressure $P^* = \frac{PV_m}{kT}$ as a function of the packing fraction $\eta = \rho V_m$. The isotropic-nematic (Iso-Nem) transition. The continuous curves correspond to the predictions of our new algebraic scaled Onsager approach, and the symbols the Monte Carlo simulation data (squares [106])

In order to demonstrate the generality and versatility of our novel generic EoS, the isotropic and nematic branches of the equation of state of the OHSC system with an aspect ratio of $L/D = 1/10$ are also determined. The results of the theory are compared with existing simulation data in Figure 2.15. The new EoS is seen to accurately represent the isotropic and nematic branches but the transition pressure are seen to be somewhat overestimated. The predictions of isotropic-nematic coexistence densities of the OHSC particles of variable aspect ratios are presented in Figure 2.16. Although the first-order nature of the isotropic-nematic transition of OHSC is seen to be exaggerated our EoS is seen to provide a good representation of existing MC simulation data.

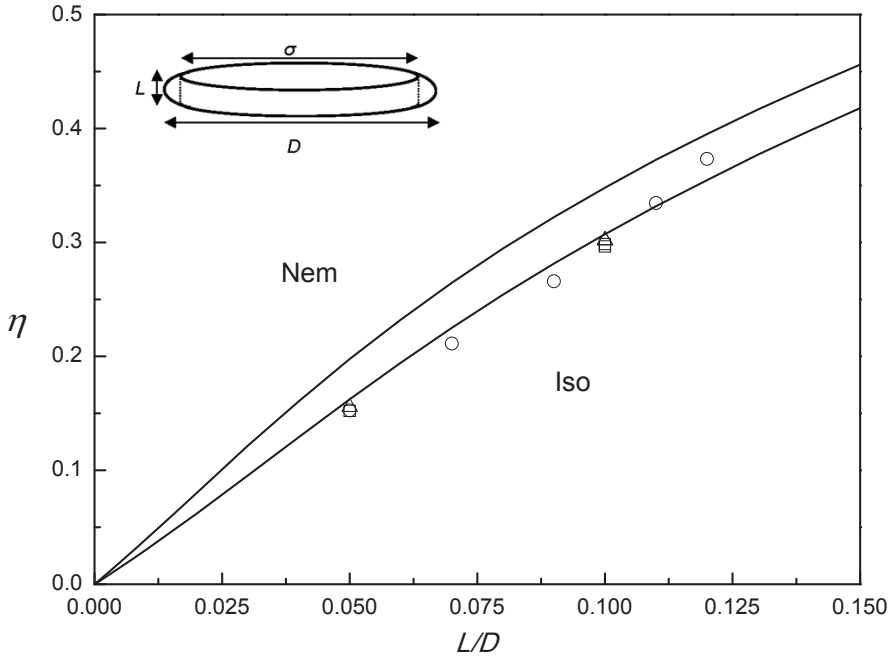

Figure 2.16: Isotropic-nematic (Iso-Nem) coexisting densities of the oblate hard spherocylinder as a function of the aspect ratio L/D. The continuous curve represents the description of the new algebraic scaled Onsager approach and the points are the Monte Carlo simulation data(circles [106] and triangles [102]).

2.5 Conclusions

A generic algebraic equation of state for isotropic and nematic phases of oblate disc particle is developed in this work. The extra term is introduced to incorporate the negative contributions from high-order virial terms and the description of isotropic phase of hard cut spheres is much improved. The Vega-Lago scaling approximation is then applied to extend our approach to the nematic phase and the isotropic-nematic transition is predicted accurately, especially with a numerical solutions of orientational distribution function. We should note that a similar scaling approach has been proposed for fluids comprising molecules of arbitrary shape using a phenomenological procedure [111]. Combining the new EoS with an extended cell theory, we investigate the global phase diagram of hard cut spheres. Our approach provides a better representation of the nematic-columnar transition than with the PL approach. By mapping the virial coefficients of hard cylindrical discs to other oblate disc particle, the new EoS can be used to describe the isotropic and nematic phases of a wide range of disc-like particles. We have been applied this approach to OHSC and assessed the accuracy of descriptions by comparison with MC simulation data.

An accurate and fully algebraic representation of the thermodynamic properties and orientational order of hard-oblate particles of generic shape is a starting point for the extension of the description to mixtures and to systems with more realistic interactions. In his original paper, Onsager [25] already presented a generalisation of his second virial theory for anisotropic phases of mixtures of hard particles (see the excellent review of Vroege and Lekkerkerker [52]). The extension of the Parsons-Lee (or the related Vega-Lago) treatment to mixtures is also relatively straightforward, and there are a number of one- and two-fluid options that can be followed in this case [112]. Mixtures comprising both oblate and prolate particles have attracted much attention owing to the rich fluid phase behaviour that can be exhibited, including the coexistence between anisotropic phases and states with biaxial order [77, 113–117]. An improved equation of state for oblate particles is a prerequisite for an accurate description of such mixtures and an assessment of the stability of the various phases. The intermolecular interactions between real thermotropic (and in some cases lyotropic) mesogens will also include attractive contributions. An Onsager-like treatment of the repulsive core can be used within perturbation theories to represent the properties of particles with both repulsive and attractive interactions (see reference [118] for a recent review). The presence of attractive forces, such as dipolar interactions, can play an important role in determining the relative stability of anisotropic phases [119–123], and can be engineered to promote the formation of biaxial phases [106, 124]. In the next chapter, we incorporate the reference equation of state for hard-oblate particles with attractive interactions to propose an attractive disc model for thermotropic LC molecules and study the temperature effect on the LC phase behaviour of attractive discs.

Chapter 3

Liquid crystal phase behaviour of attractive disc-like particles

In this chapter, we propose an attractive disc model for thermotropic LCs based on the hard disc model. The attractive interaction is introduced in terms of an anisotropic square-well potential which is located on the centre of the hard disc. In the framework of perturbation theory, the reference free energy for hard discs is coupled with attractive free energy contribution which is treated at a mean-field level of description. For the attractive discs model, we study the fluid phase equilibria: vapour-liquid, isotropic-nematic, nematic-nematic. The effects of isotropic/ansitropic attractive interaction, the range of attractions and molecular shapes (aspect ratios) are examined in detail.

3.1 Introduction

Liquid crystals [1–3] are intermediate (meso) phases with characteristics which lie between the fully positionally and orientationally ordered crystal and the disordered liquid states. Since their discovery by Reinitzer in 1883 [4], liquid crystals (LCs) have attracted a long-standing research interest because of their uniqueness of the thermodynamic, structural, optical, and electronic properties. An essential requirement for the stabilization of a LC phase is that molecules be highly anisometric in shape. A wide variety of oblate disc-shaped LC particles with length scales ranging from tens of Ångström (molecular dimensions) to hundreds of nanometers (macromolecular/colloidal dimensions) have been observed to exhibit rich phase behaviour including isotropic, nematic, and columnar phases. Discotic LCs tend to comprise poly-aromatic cores of oblate geometry, e.g., hexa-alkanoyloxy

benzenes, or metal organic complexes of phenyl pyridines, porphyrazines, phthalocyanines, triphenylenes, etc. [2, 3, 125–127]. These relatively low molecular weight compounds are commonly referred to as thermotropic liquid crystals owing to the leading role temperature plays in the phase transformations between the various states. Colloidal particles of discotic geometry have also been extensively studied in recent years, including nickel hydroxide theophrastite sheets, aluminium hydroxide gibbsite platelets, and nontronite or laponite mineral clays [25–33]. The stability of the colloidal anisotropic phases are commonly governed by the solute concentration, a characteristic that leads to the classification of such systems as lyotropic LCs. An interesting intermediate class of naturally occurring discotic particles include asphaltenes, polyaromatic compounds of intermediate molecular weight (500 to 10,000 g/mol) found in heavy crude oils which aggregate and precipitate from solution over particular ranges of composition, temperature and pressure [128]. As a result of their oblate rigid cores these asphaltenic systems exhibit anisotropic LC phases with both thermotropic and lyotropic characteristics [129–133].

In computer simulation studies [46,47,49,60,79,101,102,106–108,134–137] and theoretical treatments [84, 87, 88, 92, 94, 109, 138–141], simple disc-like particles are often taken as prototypical models of the oblate LC molecules; the particles are usually characterised by their aspect ratio D/L, where L is the thickness of disc and D is its diameter. Hard disc-like particles have proven to be appropriate models for lyotropic colloidal LCs.

The theoretical treatment of hard non-spherical fluids dates back to the 1940s [25]. The Onsager view that repulsive (excluded volume) interactions are of key importance in the formation of orientationally ordered phases is now widely accepted. In his pioneering work on nematic LCs [25], Onsager proposed the now well-accepted free energy functional for nematic states and demonstrated that the isotropic-nematic phase transition can be driven by entropy alone. Entropy driven phase transitions have now been studied extensively by computer simulation of hard-body anisometric particles, where both nematic (discotic) and columnar ordering has been identified in hard disc models on increasing the density of the system [46, 47, 49, 60, 79, 101, 102, 107, 108, 142].

For a proper description of the temperature dependence of the thermodynamic properties of a system both repulsive and attractive inter-molecular interactions have to be considered on an equal footing. This is in line with a van der Waals description of fluids where the hard core is treated as reference in determining the fluid structure [50, 143], and a mean-field attraction is included to account for the cohesive interactions and fluid phase equilibria. A simple hard-core model which incorporates the attractive interactions therefore offers

promise in representing the phase behaviour of thermotropic LCs. A number of studies have extended the early work of Kimura [144] who combined Onsager's hard rod model with anisotropic dispersion forces [145–154]. Some progress has been made in treating generalised attractive potentials [154–158] and dipolar [119, 121, 159–162] or chiral [163–165] interactions between LC molecules.

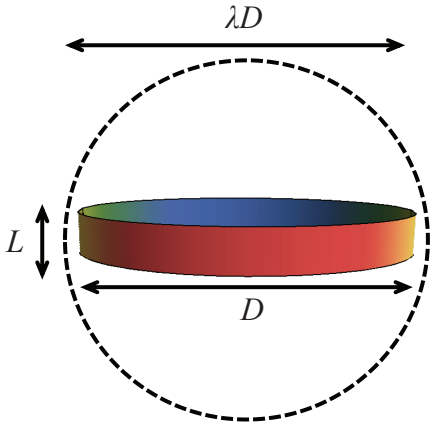

Figure 3.1: The attractive cylindrical disc (ACD) model. The model is characterised by the thickness L and diameter D of the hard core. A spherical attractive interaction of range λD is represented as the dashed sphere.

Of particular to our current work is the closed-form of algebraic equation-of-state developed for attractive hard spherocylinders [98, 118], where the attractive potential is expanded in spherical harmonics representing different contributions to the anisotropic attractions [166]. We develop a model for attractive oblate (cylindrical disc) mesogens by adding an anisotropic square-well (SW) potential representing intermolecular interactions to a hard-cylindrical disc. The model of attractive discs is depicted in Figure 3.1 where the parameter λ is introduced to quantify the attractive range. A perturbation approach is applied to develop a free energy functional for the attractive disc system. By using the Onsager trial function to describe the degree of orientational order in the nematic phase, the free energy and equation of state for the nematic state is expressed in closed algebraic form which also allows a straightforward superimposition of contributions from other intermolecular interactions such as chiral, dipolar, and associating interactions, or the extension to other types of dispersive inter-molecular potentials (e.g., Lennard-Jones, Mie, Yukawa).

3.2 Theory

3.2.1 Generalised van der Waals-Onsager free energy functional

In this section we describe the perturbation theory [50,167] employed to construct the free energy for the nematic and isotropic phases of attractive non-spherical particles. A system of N particles in a volume V at a temperature T is considered where the total Helmholtz free energy A is divided into two contributions, a reference term and a perturbation term. The former is assumed to be known precisely and the latter represents the contribution from the attractive potential perturbation:

$$\frac{A}{NkT} = \frac{A^{\mathrm{ref}}}{NkT} + \frac{A^{\mathrm{att}}}{NkT}. \tag{3.1}$$

Here k is the Boltzmann constant and the reference contribution A^{ref} is taken from an expression for the hard-core particles. Following the Parsons-Lee approach (PL) [89–91], the reference repulsive term can be expressed in compact form as

$$\begin{aligned} \frac{A^{\mathrm{ref}}}{NkT} &= \frac{A^{\mathrm{id}}_{\mathrm{iso}}}{NkT} + \int f(\vec{\omega}) \ln\{4\pi f(\vec{\omega})\} \mathrm{d}\vec{\omega} \\ &+ \frac{G(\eta)}{V_{\mathrm{m}}} \iint V_{\mathrm{exc}}(\vec{\omega}_1, \vec{\omega}_2) f(\vec{\omega}_1) f(\vec{\omega}_2) \mathrm{d}\vec{\omega}_1 \mathrm{d}\vec{\omega}_2, \end{aligned} \tag{3.2}$$

where $A^{\mathrm{id}}_{\mathrm{iso}}$ is the ideal contribution to the free energy of the isotropic state (incorporating the translational and rotational kinetic terms), $\vec{\omega}$ is the orientation vector of a particle, V_{m} is the molecular volume, and $f(\vec{\omega})$ is the single-particle orientational distribution function. In the Parsons-Lee approach, the contributions from the high-order virial terms are incorporated in an effective manner by scaling the corresponding hard-sphere equation of state [95,168]. The density-dependent function $G(\eta)$ represents the residual free energy of the equivalent hard-sphere system,

$$G(\eta) = \frac{4\eta - 3\eta^2}{8V_{\mathrm{m}}(1-\eta)^2}, \tag{3.3}$$

where the packing fraction $\eta = \rho V_{\mathrm{m}}$, ρ is the single-particle density. Alternatively, a improved generic equation of state for hard disc-like particles developed in Ref. [141] can be chosen to describe the reference system.

In the high-temperature limit, the attractive free energy can be approximated at first order [50,118,167] by

$$A^{\mathrm{att}} = \left\langle U^{\mathrm{att}} \right\rangle_{\mathrm{ref}} \tag{3.4}$$

where $< \cdots >_{\text{ref}}$ represents an ensemble average over all configurations of the reference system. In the canonical ensemble, the mean attractive energy is formally written as:

$$\begin{aligned} A^{\text{att}} &\approx \left\langle U^{\text{att}} \right\rangle_{\text{ref}} \\ &= \frac{1}{Z_{NVT}} \iint \mathrm{d}\vec{r}^N \mathrm{d}\vec{\omega}^N U^{\text{att}}(\vec{r}^N, \vec{\omega}^N) \exp\left(-\frac{U^{\text{ref}}(\vec{r}^N, \vec{\omega}^N)}{kT}\right), \end{aligned} \tag{3.5}$$

with the configurational integral defined as

$$Z_{NVT} = \iint \mathrm{d}\vec{r}^N \mathrm{d}\vec{\omega}^N \exp\left(-\frac{U^{\text{ref}}(\vec{r}^N, \vec{\omega}^N)}{kT}\right), \tag{3.6}$$

which is a function of the positions $\vec{r}^N$ and orientations $\vec{\omega}^N$ of all N particles. Further simplification is achieved by assuming pairwise additive interactions such that $U^{\text{att}}(\vec{r}^N, \vec{\omega}^N) = \sum_{i=1}^{N} \sum_{j>i}^{N} u_{ij}^{\text{att}}(\vec{r}_{ij}, \vec{\omega}_i, \vec{\omega}_j)$, where the vector $\vec{r}_{ij} = \vec{r}_i - \vec{r}_j$, and introducing the pair distribution function of reference system $g^{\text{ref}}(\vec{r}_{12}, \vec{\omega}_1, \vec{\omega}_2)$ defined as

$$\begin{aligned} g^{\text{ref}}(\vec{r}_{12}, \vec{\omega}_1, \vec{\omega}_2) &= \frac{\rho_{12}^{\text{ref}}(\vec{r}_{12}, \vec{\omega}_1, \vec{\omega}_2)}{\rho_1^{\text{ref}}(\vec{r}_1, \vec{\omega}_1)\rho_1^{\text{ref}}(\vec{r}_2, \vec{\omega}_2)} \\ &= \frac{N(N-1)}{\rho_1^{\text{ref}}(\vec{r}_1, \vec{\omega}_1)\rho_1^{\text{ref}}(\vec{r}_2, \vec{\omega}_2)} \\ &\times \frac{1}{Z_{\text{NVT}}} \int \mathrm{d}\vec{r}^{N-2} \mathrm{d}\vec{\omega}^{N-2} \exp\left[-\frac{U^{\text{ref}}(\vec{r}^N, \vec{\omega}^N)}{kT}\right]. \end{aligned} \tag{3.7}$$

The attractive term can thus be re-written as a sum of pair contributions. When considering a nematic phase where the distribution of particle positions is uniform, the single-particle density of the system can be factorised as $\rho^{\text{ref}}(\vec{r}_i, \vec{\omega}_i) = \rho f(\vec{\omega}_i)$ where the single-particle orientation distribution function $f(\vec{\omega})$ has been introduced. On inserting Equation (3.7) into Equation (3.5) and using the nematic form of the single-particle density, one can write

$$\begin{aligned} A^{\text{att}} &= \frac{1}{2} \iiiint u_{12}^{\text{att}}(\vec{r}_{12}, \vec{\omega}_1, \vec{\omega}_2)\, g^{\text{ref}}(\vec{r}_{12}, \vec{\omega}_1, \vec{\omega}_2) \\ &\times \rho^{\text{ref}}(\vec{r}_1, \vec{\omega}_1)\rho^{\text{ref}}(\vec{r}_2, \vec{\omega}_2)\, \mathrm{d}\vec{r}_1 \mathrm{d}\vec{\omega}_1 \mathrm{d}\vec{r}_2 \mathrm{d}\vec{\omega}_2 \\ &= \frac{\rho^2 V}{2} \iiint u_{12}^{\text{att}}(\vec{r}_{12}, \vec{\omega}_1, \vec{\omega}_2) \\ &\times f(\vec{\omega}_1) f(\vec{\omega}_2) g^{\text{ref}}(\vec{r}_{12}, \vec{\omega}_1, \vec{\omega}_2)\, \mathrm{d}\vec{r}_{12} \mathrm{d}\vec{\omega}_1 \mathrm{d}\vec{\omega}_2. \end{aligned} \tag{3.8}$$

Since the particles of interest are non-spherical, both the attractive interaction and the excluded volume are complicated functions of the relative positions and orientations of particles [166, 169]. It is thus useful to expand the pair potential as a series in spherical harmonics. Here we consider an anisotropic square-well (ASW) potential of the form

[118, 166]:

$$u^{\mathrm{att}}(\vec{r}_{12},\vec{\omega}_1,\vec{\omega}_2) = -s(r_{12})[\epsilon_0+\epsilon_2 P_2(\cos\gamma)] \tag{3.9}$$

$$s(r_{12}) = \begin{cases} 1 & \sigma(\hat{\vec{r}}_{12},\vec{\omega}_1,\vec{\omega}_2) \geq r_{12} < \lambda D \\ 0 & r_{12} \geq \lambda D, \end{cases} \tag{3.10}$$

where λ is the range parameter, D is the reference diameter of the disc, and $P_2(\cos\gamma)$ is the second Legendre polynomial for the relative orientation $\gamma = \arccos(\vec{\omega}_1 \cdot \vec{\omega}_2)$ between the principle axes of the two discs. In order to make the approach tractable, we use the low-density limit to approximate the pair distribution function of the reference system,

$$\lim_{\rho\to 0} g^{\mathrm{ref}}(\vec{r}_{12},\vec{\omega}_1,\vec{\omega}_2) = \exp\left(-\frac{u^{\mathrm{ref}}(\vec{r}_{12},\vec{\omega}_1,\vec{\omega}_2)}{kT}\right) \tag{3.11}$$

where $u^{\mathrm{ref}}(\vec{r}_{12},\vec{\omega}_1,\vec{\omega}_2)$ is the pair interaction of the reference system. Since the reference system corresponds to the hard-core particles, $u^{\mathrm{ref}}(\vec{r}_{12},\vec{\omega}_1,\vec{\omega}_2)$ is a purely repulsive interaction which is infinity when hard cores overlap and zero otherwise. Introducing the ASW attractive potential in Equation (3.8) with the approximation of Equation (3.11), and integrating out the centre-to-centre distance between particle 1 and 2, one can express the free energy perturbation as [98, 118]

$$\begin{aligned} \frac{A^{\mathrm{att}}}{NkT} &= -\frac{\rho\epsilon_0}{2kT}\left[\frac{4\pi}{3}\lambda^3 D^3 - \langle V_{\mathrm{exc}}(\gamma)\rangle_{\vec{\omega}_1,\vec{\omega}_2}\right] \\ &- \frac{\rho\epsilon_2}{2kT}\left[\frac{4\pi}{3}\lambda^3 D^3 \langle P_2(\cos\gamma)\rangle_{\vec{\omega}_1,\vec{\omega}_2} - \langle V_{\mathrm{exc}}(\gamma)P_2(\cos\gamma)\rangle_{\vec{\omega}_1,\vec{\omega}_2}\right]. \end{aligned} \tag{3.12}$$

where the the double orientational average of a quantity $J(\vec{\omega}_1,\vec{\omega}_2)$ is defined as

$$\langle J(\vec{\omega}_1,\vec{\omega}_2)\rangle_{\vec{\omega}_1,\vec{\omega}_2} = \iint J(\vec{\omega}_1,\vec{\omega}_2) f(\vec{\omega}_1) f(\vec{\omega}_2) \mathrm{d}\vec{\omega}_1 \mathrm{d}\vec{\omega}_2. \tag{3.13}$$

Combining the separate contributions, the free energy of the full system is obtained in terms of angle averages of the configurational contributions:

$$\begin{aligned} \frac{A[f(\vec{\omega})]}{NkT} &= \frac{A^{\mathrm{id}}_{\mathrm{iso}}}{NkT} + \int f(\vec{\omega}) \ln\left[\Omega f(\vec{\omega})\right] \mathrm{d}\vec{\omega} + G(\eta)\langle V_{\mathrm{exc}}(\gamma)\rangle_{\vec{\omega}_1,\vec{\omega}_2} \\ &- \frac{\rho\epsilon_0}{2kT}\left[\frac{4\pi}{3}\lambda^3 D^3 - \langle V_{\mathrm{exc}}(\gamma)\rangle_{\vec{\omega}_1,\vec{\omega}_2}\right] \\ &- \frac{\rho\epsilon_2}{2kT}\left[\frac{4\pi}{3}\lambda^3 D^3 \langle P_2(\cos\gamma)\rangle_{\vec{\omega}_1,\vec{\omega}_2} - \langle V_{\mathrm{exc}}(\gamma)P_2(\cos\gamma)\rangle_{\vec{\omega}_1,\vec{\omega}_2}\right], \end{aligned} \tag{3.14}$$

In this expression for the free energy one can recognize the coupling between repulsive and attractive contributions of the pair potential. The excluded volume is seen both in the terms corresponding to the isotropic and anisotropic attractive contributions; the last term in $\langle V_{\mathrm{exc}}(\gamma)P_2(\cos\gamma)\rangle_{\vec{\omega}_1,\vec{\omega}_2}$ also constitutes a direct coupling of the two contributions.

The single-particle orientational distribution function in the isotropic state is constant $f_{\rm iso}(\vec{\omega}) = 1/4\pi$ which simplifies the orientational integrals of Equation (3.14). In the anisotropic phases, the equilibrium orientational distribution of the molecules can be found by minimizing the total free energy functional, $A\left[f(\vec{\omega})\right]$.

3.2.2 Equation of state for hard cylindrical disc particles with an anisotropic square-well potential

We start by examining the angle averages of the purely repulsive contributions, i.e., the excluded volume term. The excluded volume $V_{\rm exc}(\gamma)$ of hard cylinders can be expressed conveniently as a power series in $\sin\gamma$:

$$V_{\rm exc}(\gamma) = \sum_{i=0}^{\infty} C_i \sin^i \gamma, \tag{3.15}$$

where the coefficients C_i depends on the specific geometry of molecules. It had been shown that an approximate expression which is obtained by truncation of the series at the fourth-order term in $\sin^4\gamma$ is sufficient to faithfully reproduce exact numerical results [141]. The excluded volume of two hard cylinders can be accurately represented as [99, 141]

$$\frac{V_{\rm exc}(\gamma)}{V_{\rm m}} = C_0^* + C_1^* \sin\gamma + C_2^* \sin^2\gamma + C_4^* \sin^4\gamma, \tag{3.16}$$

where the coefficients are given by

$$\begin{aligned} C_0^* &= 8, & C_1^* &= 2\frac{D}{L} + \frac{8}{\pi}\frac{L}{D}, \\ C_2^* &= \frac{3\pi}{4} + \frac{8}{\pi} - 7, & C_4^* &= (4-3\pi)/16, \end{aligned} \tag{3.17}$$

and the molecular volume of a cylindrical disc is $V_{\rm m} = \pi L D^2/4$. Using the notation of Equation (3.13), the double orientational average of the excluded volume can be written as

$$\left\langle \frac{V_{\rm exc}(\gamma)}{V_{\rm m}} \right\rangle_{\vec{\omega}_1,\vec{\omega}_2} = C_0^* + C_1^* \left\langle \sin\gamma \right\rangle_{\vec{\omega}_1,\vec{\omega}_2} + C_2^* \left\langle \sin^2\gamma \right\rangle_{\vec{\omega}_1,\vec{\omega}_2} + C_4^* \left\langle \sin^4\gamma \right\rangle_{\vec{\omega}_1,\vec{\omega}_2}. \tag{3.18}$$

The equilibrium state corresponds to the minimum of the total free energy $A[f(\vec{\omega})]$ with respect to the orientational distribution function under the additional constraint that the orientational distribution function is normalised:

$$\frac{\delta}{\delta f(\vec{\omega})}\left(A[f(\vec{\omega})] - \lambda_{\rm L} \int f(\vec{\omega}) {\rm d}\vec{\omega}\right) = 0, \tag{3.19}$$

where $\lambda_{\rm L}$ is a Lagrange undetermined multiplier which ensures that $\int f(\vec{\omega}){\rm d}\vec{\omega} = 1$. The minimum condition leads to a self-consistent integral equation for $f(\vec{\omega})$ which can be solved

by various numerical methods including the expansion of the orientational distribution function as a spherical harmonic series [52,96], or use of Monte Carlo annealing techniques [97]. These approaches do not however provide an analytical solution for the equilibrium orientational distribution function. In his seminal publication [25], Onsager proposed a functional form for $f(\vec{\omega})$ in terms of a parameter α which characterises the degree of orientational order. This so-called Onsager trial function (OTF) $f_{\mathrm{OTF}}(\vec{\omega})$ is written in hyperbolic form,

$$f_{\mathrm{OTF}}(\vec{\omega}) = \frac{\alpha \cosh(\alpha \cos\theta)}{4\pi \sinh(\alpha)}, \tag{3.20}$$

and is seen to depend on a single parameter α and the polar angle $\theta = \arccos(\vec{\omega} \cdot \vec{\omega}_0)$ where $\vec{\omega}_0$ is the director of the nematic phase. One should note that if $\alpha \to 0$, the $f_{\mathrm{OTF}}(\vec{\omega})$ naturally reduces to $1/4\pi$ corresponding to the expected distribution in the isotropic phase. Large values of α (~ 10) correspond to a nematic phase. Integrating the OTF over all possible orientations, one can show that it is correctly normalised, thus it is not necessary to include the term in the multiplier λ_{L} in Equation (3.19) when incorporating the OTF. The details of calculations of the orientational averages using OTF have been discussed in detail in earlier publications [51,98]. The introduction of the OTF to describe the degree of orientational order of the nematic phase allows the orientational averages to be rendered in algebraic form, which is more tractable in practice [51,98,118]:

$$\langle \sin\gamma \rangle_{\vec{\omega}_1,\vec{\omega}_2} \approx \sqrt{\pi}\left(\frac{1}{\alpha^{1/2}} - \frac{15}{16\alpha^{3/2}}\right) + \mathcal{O}(1/\alpha^{5/2}) \tag{3.21}$$

$$\langle \sin^2\gamma \rangle_{\vec{\omega}_1,\vec{\omega}_2} \approx \frac{4}{\alpha} + \mathcal{O}(1/\alpha^2) \tag{3.22}$$

$$\langle \sin^3\gamma \rangle_{\vec{\omega}_1,\vec{\omega}_2} \approx \sqrt{\pi}\frac{6}{\alpha^{3/2}} + \mathcal{O}(1/\alpha^{5/2}) \tag{3.23}$$

$$\langle \sin^4\gamma \rangle_{\vec{\omega}_1,\vec{\omega}_2} \approx 0 + \mathcal{O}(1/\alpha^2), \tag{3.24}$$

Using Equations (3.21)-(3.24) in Equations (3.18) for the excluded volume and $P_2(\sin\gamma) = 1 - 3\sin^2\gamma/2$ for the anisotropic attractive term, the contributions to configurational free energy can be expressed in terms of the OTF parameter α as

$$\langle P_2(\sin\gamma) \rangle_{\vec{\omega}_1,\vec{\omega}_2} \approx 1 - \frac{6}{\alpha} \tag{3.25}$$

$$\left\langle \frac{V_{\mathrm{exc}}(\gamma)}{V_{\mathrm{m}}} \right\rangle_{\vec{\omega}_1,\vec{\omega}_2} \approx C_0^* + C_1^*\sqrt{\pi}\left(\frac{1}{\alpha^{1/2}} - \frac{15}{16\alpha^{3/2}}\right) + C_2^*\frac{4}{\alpha} \tag{3.26}$$

$$\begin{aligned}\left\langle \frac{V_{\mathrm{exc}}(\gamma)}{V_{\mathrm{m}}} P_2(\sin\gamma) \right\rangle_{\vec{\omega}_1,\vec{\omega}_2} &\approx C_0^* + C_1^*\sqrt{\pi}\left(\frac{1}{\alpha^{1/2}} - \frac{15}{16\alpha^{3/2}}\right) \\ &+ \left(C_2^* - \frac{3}{2}C_0^*\right)\frac{4}{\alpha} - \frac{9}{\alpha^{3/2}}C_1^*\sqrt{\pi},\end{aligned} \tag{3.27}$$

Collecting all of the terms, one obtains the Helmholtz free energy for the system of attractive cylinder disc (ACD) in terms of the orientational parameter α:

$$\begin{aligned}\frac{A^{\mathrm{nem}}(\alpha)}{NkT} &= \frac{A^{\mathrm{id}}_{\mathrm{iso}}}{NkT} + \ln\alpha - 1 + G(\eta)\left[C_0^* + C_1^*\sqrt{\pi}\left(\frac{1}{\alpha^{1/2}} - \frac{15}{16\alpha^{3/2}}\right) + C_2^*\frac{4}{\alpha}\right] \\ &- \frac{\rho V_{\mathrm{m}}}{2}\frac{\epsilon_0}{kT}\Bigg\{\left(\frac{4\pi}{3}\frac{D^3}{V_{\mathrm{m}}} - C_0^*\right)\left(1+\frac{\epsilon_2}{\epsilon_0}\right) - C_1^*\sqrt{\pi}\left(1+\frac{\epsilon_2}{\epsilon_0}\right)\alpha^{-1/2} \\ &- \left[4C_2^*\left(1+\frac{\epsilon_2}{\epsilon_0}\right) + 6\frac{\epsilon_2}{\epsilon_0}\left(\frac{4\pi}{3}\frac{D^3}{V_{\mathrm{m}}} - C_0^*\right)\right]\alpha^{-1} \\ &+ \frac{15}{16}C_1^*\sqrt{\pi}\left(1+\frac{53}{5}\frac{\epsilon_2}{\epsilon_0}\right)\alpha^{-3/2}\Bigg\}. \end{aligned} \tag{3.28}$$

Using the OTF to represent the orientational order of the nematic phase, the free energy is expressed in an explicit algebraic form. As a result, the functional variation of $A[f(\vec{\omega})]$ with respect to $f(\vec{\omega})$ can be simplified to a derivative of the free energy (Equation (3.28)) with respect to the orientational parameter α. Taking derivative of the free energy with respect to α results in a cubic expression for $x = \sqrt{\alpha}$:

$$\frac{\partial}{\partial\alpha}\frac{A(\alpha)}{NkT} = \frac{1}{x^5}\left(x^3 + a_2x^2 + a_1x + a_0\right) = 0, \tag{3.29}$$

where the coefficients are given by

$$a_0 = \frac{45}{32}C_1^*\sqrt{\pi}\left[G(\eta) + \frac{\rho V_{\mathrm{m}}}{2}\frac{\epsilon_0}{kT}\left(1+\frac{53}{5}\frac{\epsilon_2}{\epsilon_0}\right)\right] \tag{3.30}$$

$$a_1 = -4C_2^*G(\eta) - \frac{\rho V_{\mathrm{m}}}{2}\frac{\epsilon_0}{kT}\left[4C_2^*\left(1+\frac{\epsilon_2}{\epsilon_0}\right) + 6\frac{\epsilon_2}{\epsilon_0}\left(\frac{4\pi}{3}\frac{D^3}{V_{\mathrm{m}}} - C_0^*\right)\right] \tag{3.31}$$

$$a_2 = -\frac{C_1^*\sqrt{\pi}}{2}\left[G(\eta) + \frac{\rho V_{\mathrm{m}}}{2}\frac{\epsilon_0}{kT}\left(1+\frac{\epsilon_2}{\epsilon_0}\right)\right]. \tag{3.32}$$

The equilibrium value of α is determined by solving the cubic equation the roots of which can be cast in a trigonometric form:

$$\alpha_j = \frac{1}{9}\left\{a_2 - 2\sqrt{a_2^2 - 3a_1}\cos\left(\frac{2j\pi}{3} + \frac{1}{3}\arccos\frac{-27\left[a_0 - \frac{1}{3}a_1a_2 + \frac{2}{27}a_2^3\right]}{2\left[a_2^2 - 3a_1\right]^{3/2}}\right)\right\}^2, \tag{3.33}$$

where $j = 0, 1, 2$ represent three solutions to Equation 3.29. The value of α_j describing the equilibrium orientational distribution of the nematic phase corresponds to the largest root ($j = 0$): $\alpha_{\mathrm{eq}} = \alpha_0$.

The expressions for the chemical potential μ^{nem} and the compressibility factor (equation of state) $Z^{\mathrm{nem}} = PV/(NkT)$ of the nematic phase can be derived from standard thermo-

dynamic relationships, $\mu = (\partial A/\partial N)_{V,T}$ and $P = -(\partial A/\partial V)_{N,T}$:

$$\begin{aligned}
\frac{\mu^{\text{nem}}}{kT} &= \frac{\mu^{\text{id}}_{\text{iso}}}{kT} + \ln\rho + \ln\alpha_{\text{eq}} - 1 + \frac{1}{8}\frac{\mu^{\text{res}}_{\text{hs}}}{kT}\left[C_0^* + C_1^*\sqrt{\pi}\left(\frac{1}{\alpha_{\text{eq}}^{1/2}} - \frac{15}{16\alpha_{\text{eq}}^{3/2}}\right) + C_2^*\frac{4}{\alpha_{\text{eq}}}\right] \\
&- \rho V_{\text{m}}\frac{\epsilon_0}{kT}\Bigg\{\left(\frac{4\pi}{3}\frac{D^3}{V_{\text{m}}} - C_0^*\right)\left(1 + \frac{\epsilon_2}{\epsilon_0}\right) - C_1^*\sqrt{\pi}\left(1 + \frac{\epsilon_2}{\epsilon_0}\right)\alpha_{\text{eq}}^{-1/2} \\
&- \left[4C_2^*\left(1 + \frac{\epsilon_2}{\epsilon_0}\right) + 6\frac{\epsilon_2}{\epsilon_0}\left(\frac{4\pi}{3}\frac{D^3}{V_{\text{m}}} - C_0^*\right)\right]\alpha_{\text{eq}}^{-1} \\
&+ \frac{15}{16}C_1^*\sqrt{\pi}\left(1 + \frac{53}{5}\frac{\epsilon_2}{\epsilon_0}\right)\alpha_{\text{eq}}^{-3/2}\Bigg\}, \qquad (3.34)
\end{aligned}$$

and

$$\begin{aligned}
Z^{\text{nem}} &= 1 + \frac{Z^{\text{res}}_{\text{hs}}}{8}\left[C_0^* + C_1^*\sqrt{\pi}\left(\frac{1}{\alpha_{\text{eq}}^{1/2}} - \frac{15}{16\alpha_{\text{eq}}^{3/2}}\right) + C_2^*\frac{4}{\alpha_{\text{eq}}}\right] \\
&- \frac{\rho V_{\text{m}}}{2}\frac{\epsilon_0}{kT}\Bigg\{\left(\frac{4\pi}{3}\frac{D^3}{V_{\text{m}}} - C_0^*\right)\left(1 + \frac{\epsilon_2}{\epsilon_0}\right) - C_1^*\sqrt{\pi}\left(1 + \frac{\epsilon_2}{\epsilon_0}\right)\alpha_{\text{eq}}^{-1/2} \\
&- \left[4C_2^*\left(1 + \frac{\epsilon_2}{\epsilon_0}\right) + 6\frac{\epsilon_2}{\epsilon_0}\left(\frac{4\pi}{3}\frac{D^3}{V_{\text{m}}} - C_0^*\right)\right]\alpha_{\text{eq}}^{-1} \\
&+ \frac{15}{16}C_1^*\sqrt{\pi}\left(1 + \frac{53}{5}\frac{\epsilon_2}{\epsilon_0}\right)\alpha_{\text{eq}}^{-3/2}\Bigg\}, \qquad (3.35)
\end{aligned}$$

where $\mu^{\text{res}}_{\text{hs}}/kT = \left(3\eta^3 - 9\eta^2 + 8\eta\right)/\left(1-\eta\right)^3$ is the residual chemical potential and $Z^{\text{res}}_{\text{hs}} = (4\eta - 2\eta^2)/(1-\eta)^3$.

An important quantity that is used to characterize the degree of orientational order of the nematic phase is the nematic order parameter S_2, which is commonly defined as the orientational average of the second Legendre polynomial $P_2(\cos(\theta))$:

$$S_2 = \int P_2(\cos(\theta))f(\theta)\mathrm{d}\vec{\omega}. \qquad (3.36)$$

Because the OTF is used to represent the orientational distribution in nematic phase, $f(\theta) = f_{\text{OTF}}(\vec{\omega})$, S_2 can be expressed as a function of the orientational parameter α [51]:

$$S_2 = 1 - \frac{3\coth\alpha_{\text{eq}}}{\alpha_{\text{eq}}} + \frac{3}{\alpha_{\text{eq}}^2} \qquad (3.37)$$

In the case of the isotropic phase, where no orientational order is exhibited, the orientational averages of Equation (3.14) are evaluated using the isotropic value $f(\vec{\omega}) = 1/4\pi$. The Helmholtz free energy expression for the isotropic phase is then given by

$$\begin{aligned}
\frac{A^{\text{iso}}}{NkT} &= \frac{A^{\text{id}}_{\text{iso}}}{NkT} + G(\eta)\left\langle\frac{V_{\text{exc}}(\gamma)}{V_{\text{m}}}\right\rangle^{\text{iso}}_{\vec{\omega}_1,\vec{\omega}_2} - \frac{\rho V_{\text{m}}}{2}\frac{\epsilon_0}{kT}\left[\frac{4\pi}{3}\frac{D^3}{V_{\text{m}}} - \left\langle\frac{V_{\text{exc}}(\gamma)}{V_{\text{m}}}\right\rangle^{\text{iso}}_{\vec{\omega}_1,\vec{\omega}_2}\right] \\
&+ \frac{\rho V_{\text{m}}}{2}\frac{\epsilon_2}{kT}\left\langle\frac{V_{\text{exc}}(\gamma)}{V_{\text{m}}}P_2(\sin\gamma)\right\rangle^{\text{iso}}_{\vec{\omega}_1,\vec{\omega}_2}. \qquad (3.38)
\end{aligned}$$

The orientational averages in the isotropic phase can be evaluated as

$$\left\langle \frac{V_{\rm exc}(\gamma)}{V_{\rm m}} \right\rangle^{\rm iso}_{\vec{\omega}_1,\vec{\omega}_2} \approx C_0^* + \frac{\pi}{4}C_1^* + \frac{2}{3}C_2^* + \frac{8}{15}C_4^* \tag{3.39}$$

$$\left\langle \frac{V_{\rm exc}(\gamma)}{V_{\rm m}} P_2(\sin\gamma) \right\rangle^{\rm iso}_{\vec{\omega}_1,\vec{\omega}_2} \approx -\frac{\pi}{32}C_1^* - \frac{2}{15}C_2^* - \frac{16}{105}C_4^*. \tag{3.40}$$

From the expressions for free energy of the isotropic phase (cf. Equation (3.38)), we obtain the corresponding chemical potential and equation of state:

$$\begin{aligned} \frac{\mu^{\rm iso}}{kT} &= \frac{\mu^{\rm id}_{\rm iso}}{kT} + \ln\rho + \frac{1}{8}\frac{\mu^{\rm res}_{\rm hs}}{kT}\left(C_0^* + \frac{\pi}{4}C_1^* + \frac{2}{3}C_2^* + \frac{8}{15}C_4^*\right) \\ &- \rho V_{\rm m}\frac{\epsilon_0}{kT}\left(\frac{4\pi}{3}\frac{D^3}{V_{\rm m}} - C_0^* - \frac{\pi}{4}C_1^* - \frac{2}{3}C_2^* - \frac{8}{15}C_4^*\right) \\ &+ \rho V_{\rm m}\frac{\epsilon_2}{kT}\left(-\frac{\pi}{32}C_1^* - \frac{2}{15}C_2^* - \frac{16}{105}C_4^*\right) \end{aligned} \tag{3.41}$$

and

$$\begin{aligned} Z^{\rm iso} &= 1 + \frac{Z^{\rm res}_{\rm hs}}{8}\left(C_0^* + \frac{\pi}{4}C_1^* + \frac{2}{3}C_2^* + \frac{8}{15}C_4^*\right) \\ &- \frac{\rho V_{\rm m}}{2}\frac{\epsilon_0}{kT}\left(\frac{4\pi}{3}\frac{D^3}{V_{\rm m}} - C_0^* - \frac{\pi}{4}C_1^* - \frac{2}{3}C_2^* - \frac{8}{15}C_4^*\right) \\ &+ \frac{\rho V_{\rm m}}{2}\frac{\epsilon_2}{kT}\left(-\frac{\pi}{32}C_1^* - \frac{2}{15}C_2^* - \frac{16}{105}C_4^*\right). \end{aligned} \tag{3.42}$$

3.3 Results and Discussion

The fluid phase diagrams of attractive cylindrical discs of various aspect ratios with square-well attractive interaction are calculated by equating the pressure and chemical potential of the coexisting phases at a given temperature. In the present ACD model, the range of the attractive potential is characterised by the parameter λD, which is chosen to be $\lambda \geq 1$ in order to ensure that the resulting integrals into the contributions from repulsive and attractive interactions remain separable. Dimensionless units are adopted throughout: temperature $T^* = kT/\epsilon_0$, pressure $P^* = PV_{\rm m}/\epsilon_0$ and packing fraction $\eta = \rho V_{\rm m}$.

3.3.1 Attractive cylindrical discs with isotropic SW potentials

First, we focus on discs with a spherically symmetric SW potential, so that the orientation-dependent attractive contribution is inactive, i.e., $\epsilon_2 = 0$. Although the attractive interaction is isotropic, the orientation-dependent excluded volume gives rise to an overall interaction between discs which is anisotropic. The fluid phase behaviour of ACDs of aspect ratio $D/L = 5$ and attractive range $\lambda = 1$ is presented in Figure 3.2. It is clear from

the phase diagram that the system exhibits three fluid phases: vapour (V), liquid (L), and nematic (N). The vapour-liquid equilibrium (VLE) seen at relatively low densities, which terminates at the VLE critical point ($T_c^* = 0.37720$, $\eta_c = 0.10362$ and $P_c^* = 0.01383$) is determined by the free energy of the isotropic phase of the ACD particles. Oblate hard-cores with square-well attractive interactions have been studied by Meneses-Juárez et al. [170], but in this case the range of the attractive interaction is smaller than the diameter of the molecule so a direct comparison is not possible. At moderate to high densities, an isotropic liquid-nematic transition is observable. In the low temperature region, the isotropic-nematic coexistence becomes a broad region of vapour-nematic equilibrium (VNE) which is bounded by a vapour-liquid-nematic (V-L-N) triple line. Above the triple temperature, the nematic phase coexists with an isotropic liquid phase. It is worthwhile noting that the width of liquid-nematic equilibrium (LNE) coexistence curve broadens markedly when T approaches the triple point.

The model developed in our current work allows the effect of the anisotropy of underlying hard disc on the phase behaviour of the ACD system. The phase diagram of hard discs of aspect ratio $D/L = 10$ with attractive interactions of range $\lambda = 1$ is shown in Figure 3.3. The system shows a single region of coexistence between isotropic (vapour or liquid) and nematic phases within the temperature range concerned. In the attractive disc systems with aspect ratios $D/L > 5$, the VLE becomes metastable with respect to isotropic-nematic (I-N) coexistence. The region of I-N coexistence is broad at low temperatures, with the difference between the coexisting densities of the isotropic and nematic phases becoming narrow at higher temperatures. The coexisting densities of the two phases is also seen to gradually shift to higher packing fractions when the temperature is increased. The contribution of the attractive interactions stabilises the orientational order in the low-density and low-temperature region. The I-N transition of the attractive disc model approaches the behaviour of the corresponding purely repulsive discs in the high-temperature region.

When the aspect ratio is increased to $D/L = 80$, a different type of phase behaviour is exhibited by the system. As shown in Figure 3.4, the isotropic-nematic coexistence is located at low densities ($\eta \sim 0.1$) while a region of nematic-nematic equilibrium (NNE) appears at moderate to high densities. The N_1-N_2 coexistence is bounded by I-N_1-N_2 triple line and nematic-nematic critical point (T_{NN}^*). An examination of the temperature-dependence of the nematic order parameter is shown in Figure 3.5 that the degree of order of the high-density nematic state (N_2) decreases slightly, while that of low-density nematic

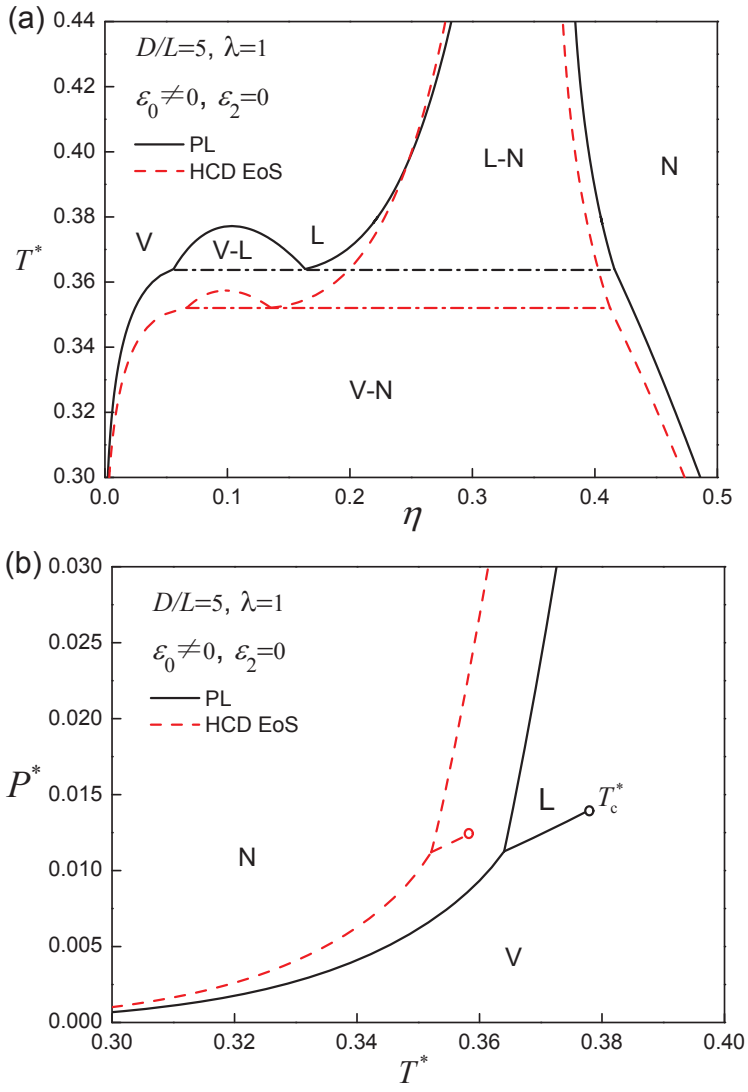

Figure 3.2: (a) The temperature-density and (b) pressure-temperature representations of the fluid phase equilibria for attractive cylindrical discs (ACDs) with an aspect ratio of $D/L = 5$ and an isotropic attractive interaction of range $\lambda = 1$. The generic disc-like molecules are modelled as hard cylinders of length L and diameter D, enveloped by an attractive square well of depth $-(\epsilon_0 + \epsilon_2 P_2(\cos\gamma))$ and range λD; in the case of isotropic attractions $\epsilon_0 \neq 0$ and $\epsilon_2 = 0$. The dimensionless properties are defined in terms of D and ϵ_0 as $T^* = kT/\epsilon_0$ for the temperature, $P^* = PD^3/\epsilon_0$ for the pressure, and $\eta = \rho V_m$ for the packing fraction, where V_m is the volume of the cylindrical core. The stable phases are indicated as vapour (V), isotropic liquid (L), and nematic (N), and T_c^* denotes VLE critical point. The dashed curves represent the results obtained using a generic reference EOS for hard cylindrical discs (HCD) [141]. The dot-dashed line in (a) represents the V-L-N three-phase coexistence line.

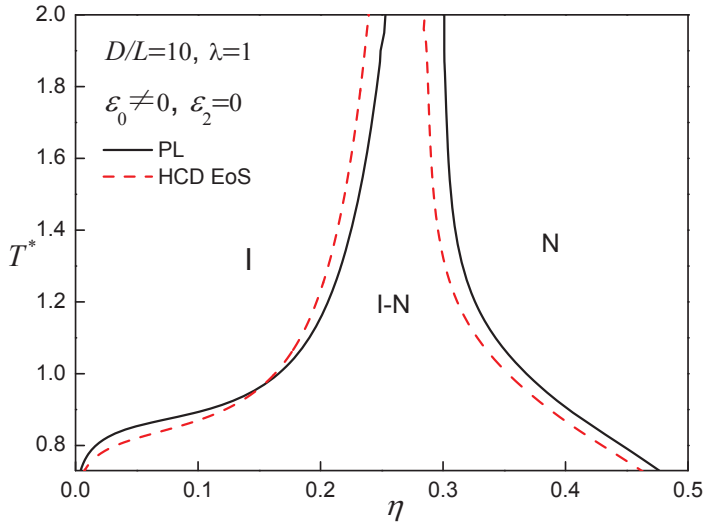

Figure 3.3: Temperature-density representation of the fluid phase equilibria for attractive cylindrical discs (ACDs) with an aspect ratio of $D/L = 10$ and an isotropic attractive interaction of range $\lambda = 1$. The stable phases are indicated as isotropic (I) and nematic (N). See the caption of Figure 3.2 for further details.

state (N_1) though still highly ordered behaves as a monotonically increasing function of temperature up to T^*_{NN}. At T^*_{NN} by definition, the differences in density and orientational order between two nematic phases become indistinguishable. In the experimental study of hexaalkynylbenzene derivatives LC molecules [171], the coexistence between two nematic phases has been observed. A similar progression from V-L-N, through I-N, to I-N_1-N_2 phase behaviour with increasing aspect ratio has been observed for attractive rod-like LC molecules [23, 118, 172–175]. It is also interesting to note that an analogous transition in the vapour-liquid-solid phase equilibria is exhibited by attractive spherical particles as the range of interaction is decreased: the VLE is found to become metastable relative to the isotropic fluid-solid transition, and on further decreasing the attractive range an iso-structural coexistence between two solid phases is observed [176, 177].

Also included in Figures 3.2-3.4 are calculations using an improved representation of reference EOS [141] of the isotropic and nematic states of hard cylindrical discs HCD, rather than the PL approximation. It is clear that the qualitative features of the fluid-phase behaviour are similar to those obtained with the PL approach for the hard-core reference system, so we retain the standard PL treatment for simplicity and the HCD reference EOS is not employed in the subsequent analysis.

By varying the parameter λ, different ranges of the attractive interaction may be explored. The temperature-density projections of the fluid phase equilibria are shown in Figure 3.6 for discs with an aspect ratio of $D/L = 10$ and attractive ranges of $\lambda = 1, 3$,and 5 in a representation where the temperature is reduced by the attractive range, $T^*_{vdw} = T^*/\lambda^3$. As the attractive range is increased, the phase diagrams for the $D/L = 10$ discs with $\lambda = 3$ and 5 exhibit vapour, liquid, and nematic phases and the corresponding triple points, the same features as seen with the less anisotropic discs ($D/L = 5, \lambda = 1$). The fluid phase coexistence of ACDs with $\lambda = 3$ and 5 converge onto a universal van der Waalsian curve. However, it is apparent that the phase coexistence curve for $\lambda = 1$ does not follow this type of corresponding state behaviour. Presumably the VLE coexistence is not observed for attractive discs with the same aspect ratio ($D/L = 10$) but a smaller attractive range ($\lambda = 1$) because the average excluded volume of a pair of discs is of comparable size to the enveloping attractive sphere induced by the isotropic SW interaction.

The fluid phase behaviour of discs characterized by an aspect ratio $D/L = 50$ is shown in Figure 3.7 for various values of the attractive range. It is noted that the large attractive range parameter widens the isotropic-nematic coexistence and shifts the I-N transition to higher densities. Increasing the attractive range is not seen to promote a change in phase

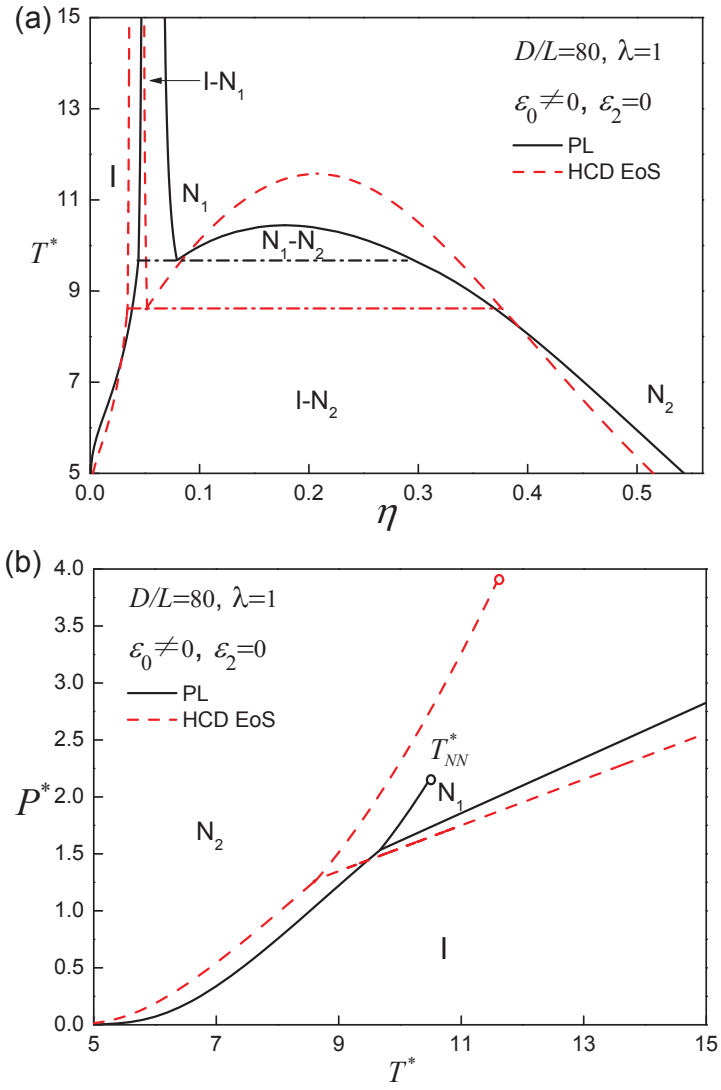

Figure 3.4: a) The temperature-density and (b) pressure-temperature representations of the fluid phase equilibria for attractive cylindrical discs (ACDs) with an aspect ratio of $D/L = 80$ and an isotropic attractive interaction of range $\lambda = 1$. The stable phases are indicated as isotropic liquid (I), low-density nematic (N_1), and high-density nematic (N_2), and T^*_{NN} is the nematic-nematic critical point. The dot-dashed line in (a) represents the I-N_1-N_2 three-phase coexistence line. See the caption of Figure 3.2 for further details.

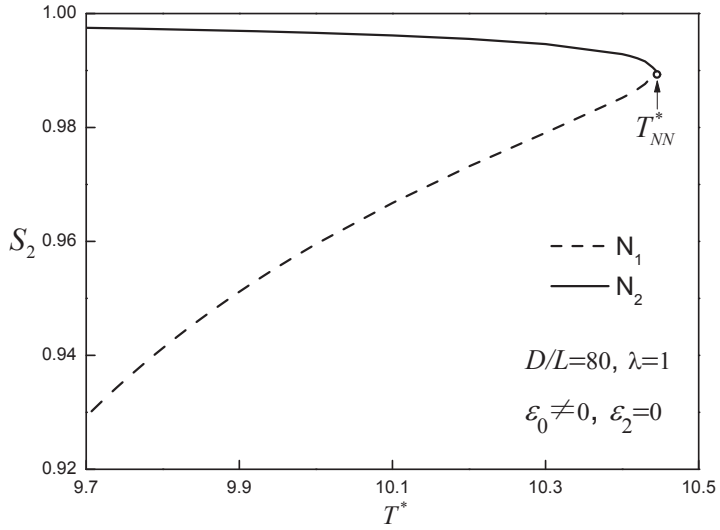

Figure 3.5: The temperature dependence of nematic order parameter S_2 of the coexisting nematic phases for attractive cylindrical discs (ACDs) of aspect ration $D/L = 80$ with an isotropic attractive interaction of range $\lambda = 1$ (cf. Figure 3.4) The nematic-nematic critical point T^*_{NN} is also indicated. See the caption of Figure 3.2 for further details.

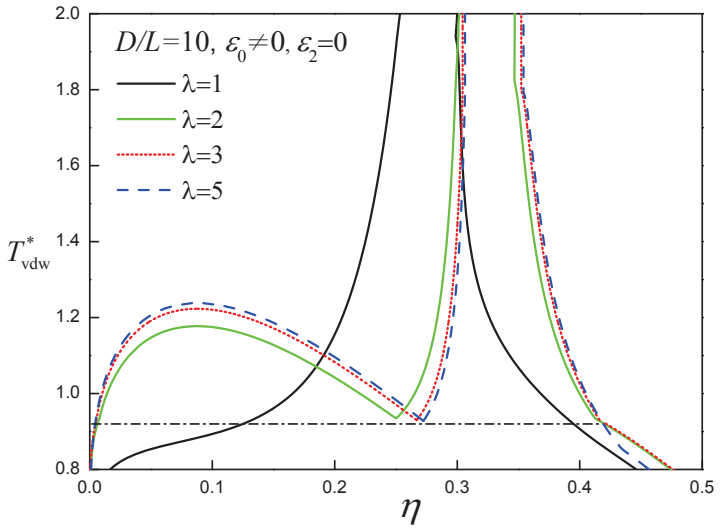

Figure 3.6: Temperature-density representation of the fluid phase equilibria of attractive cylindrical discs (ACDs) with an aspect ratio $D/L = 10$ and isotropic attractive interaction of varying range λ. The dot-dashed line corresponds to V-L-N three-phase coexistence line for the systems with $\lambda = 3$ and 5. The reduced temperature is defined in a van der Waals corresponding states form as $T^*_{\mathrm{vdw}} = T^*/\lambda^3$. See the caption of Figure 3.2 for further details.

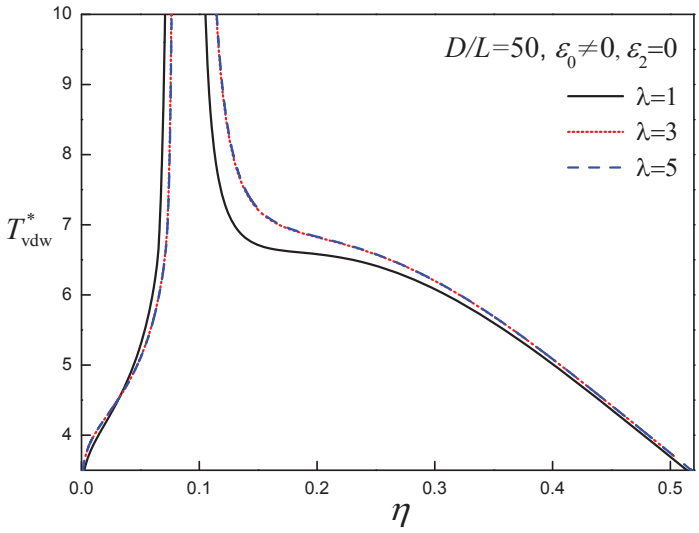

Figure 3.7: Temperature-density representation of the fluid phase equilibria of attractive cylindrical discs (ACDs) with an aspect ratio $D/L = 50$ and isotropic attractive interaction of varying range λ. The reduced temperature is defined in a van der Waals corresponding states form as $T^*_{\text{vdw}} = T^*/\lambda^3$. See the caption of Figure 3.2 for further details.

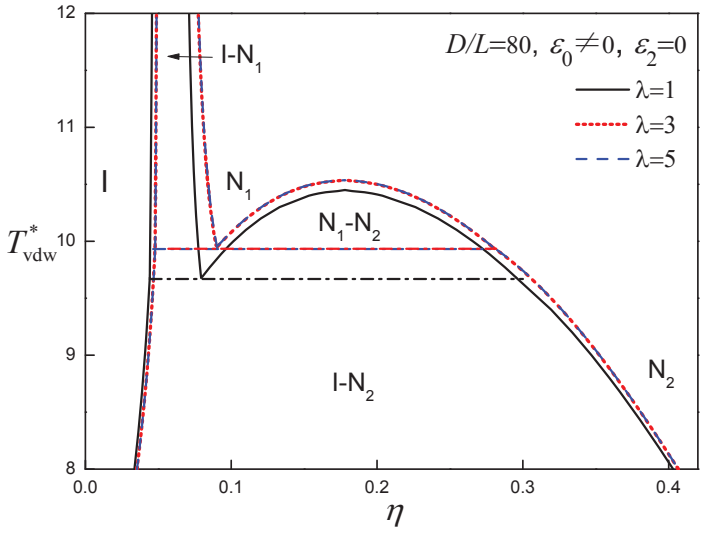

Figure 3.8: Temperature-density representation of the fluid phase equilibria of attractive cylindrical discs (ACDs) with an aspect ratio $D/L = 80$ and isotropic attractive interaction of varying range λ. The reduced temperature is defined in a van der Waals corresponding states form as $T^*_{\rm vdw} = T^*/\lambda^3$. The dot-dashed lines correspond to the I-N_1-N_2 three-phase coexistence lines in each case. See the caption of Figure 3.2 for further details.

behaviour supporting the view that the hard-body interaction (free-volume entropy) is the dominant feature of highly anisometric particles. The coexistence between two nematic phases is maintained in attractive disc systems of even larger aspect ratio, $D/L = 80$. In Figure 3.8, systems of $D/L = 80$ attractive discs of varying attractive range are seen to exhibit the same type of phase diagram and all appear to obey a corresponding state principle in terms of the reduced temperature. Although a larger range of the isotropic attraction does not qualitatively affect the phase behaviour of discs with $D/L = 80$, the degree of orientational order of the coexisting low-density nematic phase (N_1) becomes lower as λ increases, as can be seen in Figure 3.9.

These examples indicate that the long-ranged isotropic SW attraction slightly destabilizes the orientationally ordered phases. In the case of the thicker discs ($D/L = 10$), the long-range attractions ($\lambda = 3$ and 5) promote the coexistence between gas and isotropic liquid phases with no orientational order ($S_2 = 0$), while attractive discs with short-ranged attractive interactions ($\lambda = 1$) exhibit an isotropic-nematic transition. For the systems with large aspect ratios ($D/L = 50$ and 80) where the phase behaviour is dominated by the excluded volume interactions, long-range isotropic attractions do not change the type of phase behaviour, but weaken the degree of orientational order of the coexisting nematic

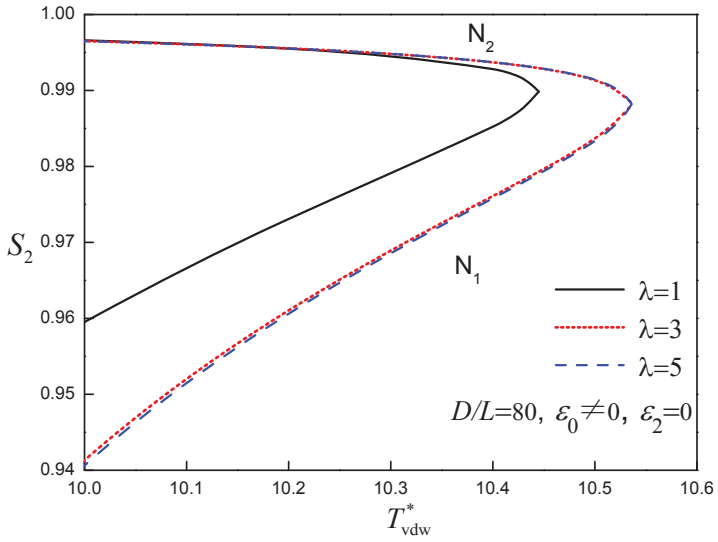

Figure 3.9: The temperature dependence of nematic order parameter S_2 of the coexisting nematic phases for attractive cylindrical discs (ACDs) of aspect ration $D/L = 80$ with an isotropic attractive interaction of varying range $\lambda = 1, 3, 5$ (cf. Figure 3.8) The nematic-nematic critical point T^*_{NN} is also indicated. See the caption of Figure 3.2 for further details.

phases.

3.3.2 Attractive cylindrical discs with anisotropic SW potentials

In real systems the dispersion forces are associated with the functional groups distributed at various points in the molecule. In that sense, the assignment of a central isotropic attraction is but a simplistic first-order approximation. Recognizing the morphological anisotropy of discotic LCs, one can postulate the existence of additional orientation-dependent (anisotropic) attractions. The effect of including anisotropic attractions on the fluid phase diagram of discs with $D/L = 10$ and $\lambda = 1$ is shown in Figure 3.10: increasing the anisotropy of the attractions does not alter the phase behaviour qualitatively but drives the I-N transition to lower densities. The VLE in the low-density region is very sensitive to the incorporation of anisotropic attractive interactions. As shown in Figure 3.11, the VLE is destabilised on increasing the strength of the positive anisotropic attractions; for a sufficient large value of the anisotropy ($\epsilon_2 = 0.3\epsilon_0$), the VLE becomes metastable with respect to the isotropic-nematic coexistence. A similar phenomena was also reported for the systems of attractive spherical and rod-like particles with anisotropic attractions [118].

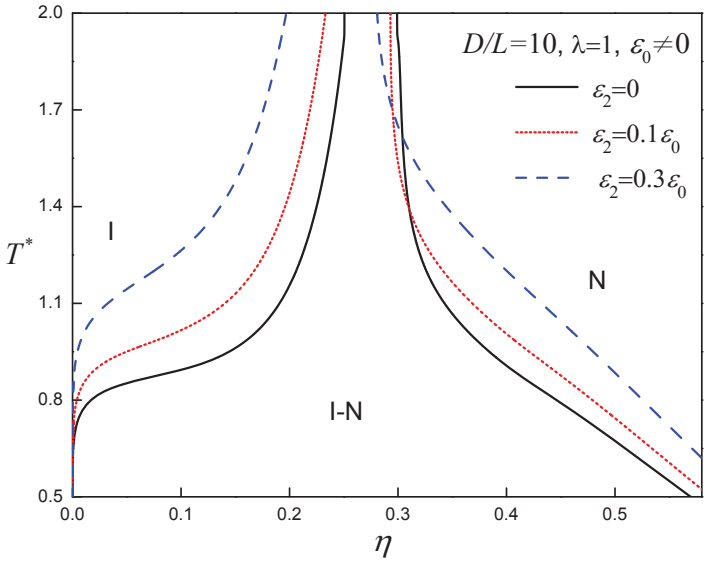

Figure 3.10: Temperature-density representation of the fluid phase equilibria of attractive cylindrical discs (ACDs) with an aspect ratio of $D/L = 10$, and an positive anisotropic attractive interaction range $\lambda = 1$ and varying strength $\epsilon_2 > 0$. See the caption of Figure 3.2 for further details.

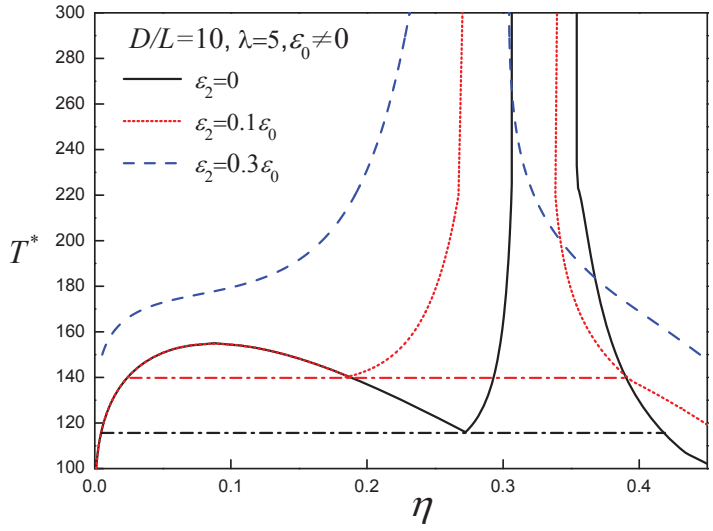

Figure 3.11: Temperature-density representation of the fluid phase equilibria of attractive cylindrical discs (ACDs) with an aspect ratio of $D/L = 10$, and an positive anisotropic attractive interaction range $\lambda = 5$ and varying strength $\epsilon_2 > 0$. The dot-dashed lines corresponds to V-L-N three-phase coexistence line in each case. See the caption of Figure 3.2 for further details.

It is clear that a positive anisotropic attractive interaction stabilises the nematic phase and enhances the propensity of the system to form orientationally ordered states. For a system of discs with a large aspect ratio, e.g., $D/L = 50$ (cf. Figure 3.12), the isotropic-nematic region becomes much broader at lower temperatures as ϵ_2 is increased while the system converges into the hard disc limit in the high-temperature limit. For highly anisometric systems the anisotropic shape and orientation-dependent attractions both contribute to the stabilization of the nematic phases. Hence, for an anisotropic strength of $\epsilon_2 = 0.7\epsilon_0$, which is comparable to the isotropic attraction, the $D/L = 50$ discs with anisotropic attractions exhibit a nematic-nematic coexistence which is equivalent to that seen for $D/L = 80$ discs with isotropic attractions.

In addition to attractive interactions with a positive anisotropy, for some molecules one could expect interactions with a negative anisotropy that would favour a perpendicular configuration. For example, the quadrupolar interactions between aromatic moieties give rise to both parallel (side-by-side) and perpendicular (T-shaped) relative orientations of the cores. These kinds of interactions can be represented in our ACD models using negative values for the parameter ϵ_2. In Figures 3.13 and 3.14, we present the phase behaviour of $D/L = 10, \lambda = 1$ and $D/L = 80, \lambda = 3$ disc systems, respectively. In the case of the $D/L = 10, \lambda = 1$ system, increasing the negative anisotropic attractions leads to a destabilization of the isotropic-nematic region and promotes the appearance of VLE when $\epsilon_2 = -0.3\epsilon_0$. For the discs with the larger aspect ratio of $D/L = 80$, the orientation-dependent attractive interaction is seen to destabilize the nematic-nematic equilibrium and drive the isotropic phase boundary to higher densities. For sufficiently large values of the negative anisotropic attractions, $\epsilon_2 = -0.5\epsilon_0$, the system even exhibits an isotropic-nematic transition in spite of the large value of the aspect ratio ($D/L = 80$).

3.4 Conclusions

In this work, we present a closed-form equation of state for the description of the thermodynamic properties and orientational ordering of attractive hard-core cylindrical disc fluids which serve as a basic model for thermotropic discotic liquid crystals. With the aid of the Onsager trial function to represent the single-particle orientational distribution function in the nematic phase, the free energy is expressed in algebraic form and the functional variation of free energy reduced to a simple derivative with respect to the Onsager orientational parameter α. A cubic solution of α_{eq} is then obtained when higher-order terms

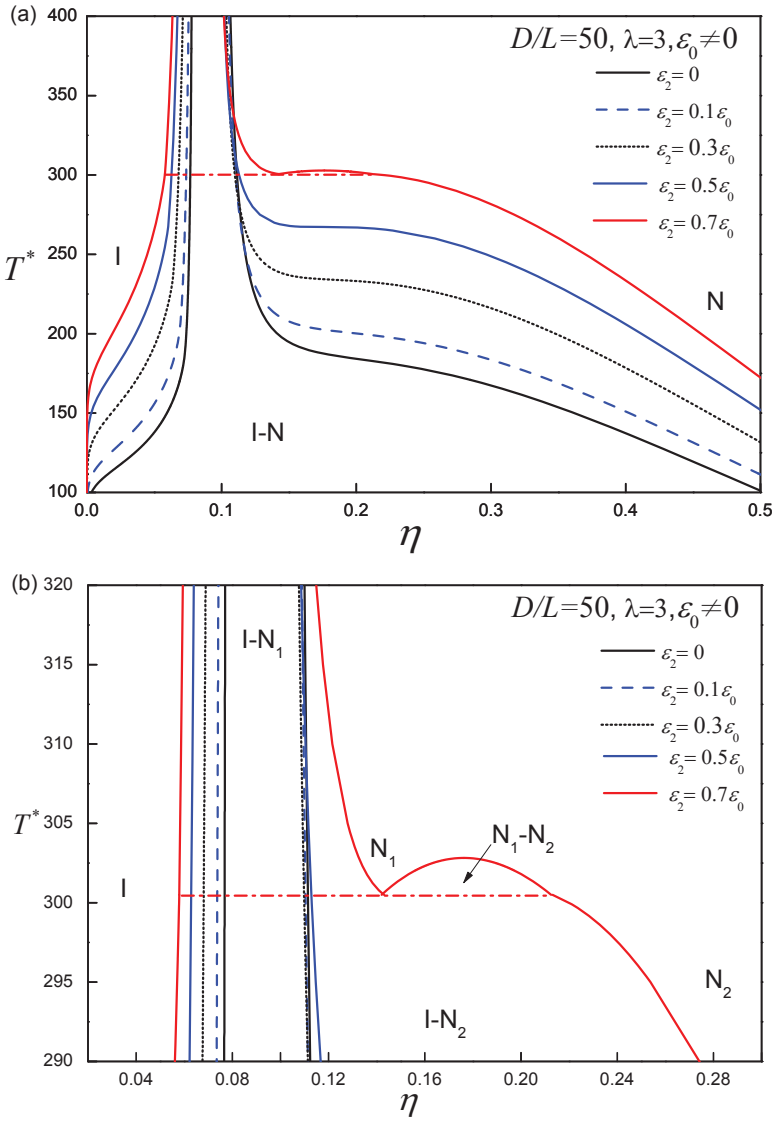

Figure 3.12: (a):Temperature-density phase diagram for ACD with aspect ratio $D/L = 50$, attractive range $\lambda = 3$ and varying anisotropic interaction strength ϵ_2. The dot-dashed line represents I-N_1-N_2 three-phase coexistence line. (b): the nematic-nematic coexistence region for the case of $\epsilon_2 = 0.7\epsilon_0$. See the caption of Figure 3.2 for further details.

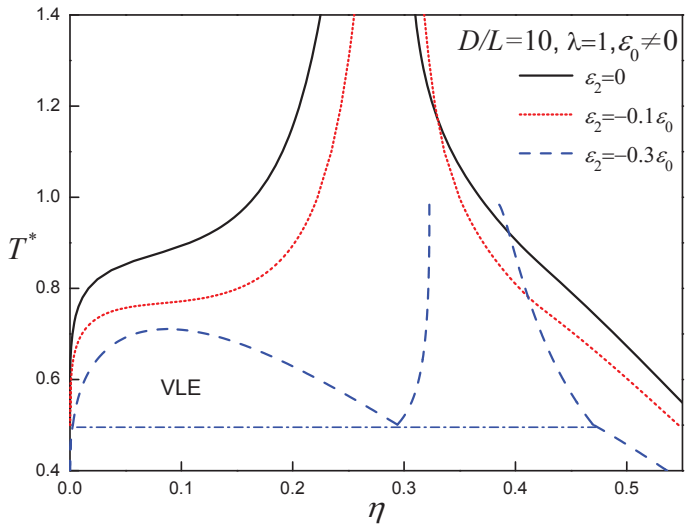

Figure 3.13: Temperature-density representation of the fluid phase equilibria of attractive cylindrical discs (ACDs) with an aspect ratio of $D/L = 10$, and an negative anisotropic attractive interaction of range $\lambda = 1$ and varying strength $\epsilon_2 < 0$. The dot-dashed line corresponds to V-L-N three-phase coexistence line. See the caption of Figure 3.2 for further details.

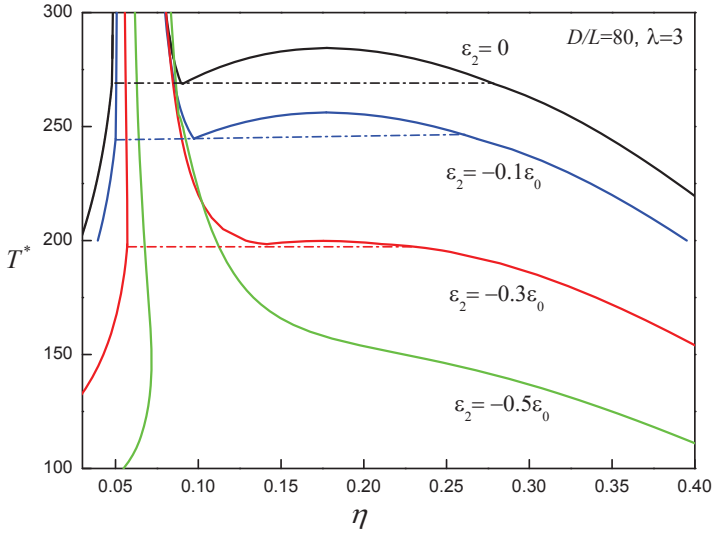

Figure 3.14: Temperature-density representation of the fluid phase equilibria of attractive cylindrical discs (ACDs) with an aspect ratio of $D/L = 80$, and an negative anisotropic attractive interaction of range $\lambda = 3$ and varying strength $\epsilon_2 < 0$. The dot-dashed lines correspond to I-N_1-N_2 three-phase coexistence lines in each case. See the caption of Figure 3.2 for further details.

in the expansion are neglected and ordered states ($\alpha \sim 10$) are considered. Using this approach we provide a qualitative description of the fluid phase diagrams of ACD particles. The separate effects of the shape anisotropy of the hard discs and the orientationally-dependent attractive interactions are examined in detail. The hard core of the particle is primarily responsible for determining the type of phase behaviour. The contribution of attractive interactions, though secondary, cannot be neglected in thermotropic LC systems. For the ACD model, the attractive range λ of the enveloping square well determines the formation of the isotropic liquid state. The anisotropic term in the ASW potential, which is controlled by the coefficient ϵ_2 (or its ratio ϵ_2/ϵ_0 relative to the isotropic term), is key to the stabilization/destablization of orientationally ordered phases.

It is important to point out that in liquid state theory [50], any perturbation approach requires an accurate description of the reference system. The reference adopted here for the ACDs is the hard cylindrical disc system described with a Parsons-Lee approach. Because of anomalous negative contributions from higher-order virial coefficients [88], the Parsons-Lee approach does not provide an accurate description of hard disc fluids, when compared with the exact simulation data, in the limit of infinitely thin discs. An improved equation of state for oblate disc-like particles has been developed [141] which incorporates these contributions and provides a better description for the isotropic and nematic phases of hard disc systems.

The methodology developed here allows other interactions to be incorporated within the attractive hard-disc model and provides a realistic free energy functional. The molecular-based statistical associating fluid theory (SAFT) [178,179] and its recent extensions [180–184], has been shown to be a powerful methodology providing accurate descriptions of phase behaviour of complex fluids and fluid mixtures. By building on the SAFT formalism, it is possible to explicitly include additional perturbation terms, such as those related to chain (or ring) geometries hence paving the path towards a more sophisticated model for disc-like LC molecules. The use of the attractive disc model to describe LC phase behaviour of real disc-like molecular fluids and the extension of the current methodology to other anisotropic phases (e.g., columnar ordering) will be the subject of future studies.

Chapter 4

Understanding and describing the liquid crystalline states of polypeptide solutions: a coarse-grained model of PBLG in DMF

The method used in the previous chapter is applied to thermotropic LC molecules of rod-like shape. We review some results of phase behaviour of attractive rod system and focus our attention on those attractive rods with large aspect ratio $L/D > 50$ which exhibit the nematic-nematic phase separation in the high-density region. The effect of positive and negative anisotropic attractions on the nematic-nematic coexistence is examined. The attractive rod model is applied to describing the liquid crystalline phase behaviour of polypeptide solutions in the late section of the chapter.

4.1 Introduction

Liquid crystals (LCs) [1–3] are substances that exhibit phases intermediate between the crystal and liquid state. Since the first discovery of this fascinated state of matter by Reinitzer as early as 1883 [4], LCs have attracted interest because of the uniqueness of their thermodynamic, structural, optical and electronic properties. Today, we recognize LC behaviour in an ever increasing number of scenarios. Apart from the common exam-

ples of solutions of soaps, detergents and surfactants [2], the existence of lyotropic liquid crystalline order in biomacromolecular systems is ubiquitous in nature including the phase behaviour exhibited by DNA [15,16], by stiff polymers such as polysaccharides [185], cellulose [186,187] and protein fibers [5,6], and by rod-like viruses such as the tobacco mosaic virus [7,8], and the *fd*-virus [9–14]. The supramolecular α-helices [17–24,188–197] formed by the self-assembly of polypeptides are also found to exhibit a rich variety of mesogenic behaviour [17–24]. In the chapter we seek to understand and describe the LC ordering exhibited by solutions of the polypeptide poly-(γ -benzyl-L-glutamate) (PBLG) in dimethylformamide (DMF) which is characterized by large regions of stable nematic order and an intriguing phase coexistence between two liquid crystalline states with markedly different concentrations of polypeptides [19–21,23,195].

An essential requirement for the stabilization of a LC phase is that the molecules be highly anisotropic in shape, such as long rigid rods or thin flat discs. For this reason, rod-like [43–45,60,62,63,134] particles are often employed as prototype models for prolate LC molecules (see reference 51 for a recent review). Hard non-spherical particles have been taken as 'zeroth order' models for lyotropic or colloidal LCs in which the appearance of anisotropic phases is controlled by the solute concentration [42, 52]. Impressively, the theoretical treatment of hard non-spherical fluids dates back to the 1940s. In his pioneering work on nematic LCs, Onsager [25,75] proposed the now well-accepted free energy functional for the nematic state and demonstrated that when only athermal (excluded volume) contributions are taken into account, the isotropic-nematic phase transition can be driven by entropy alone. Onsager's original second-order virial theory was extended by Parsons [89] and by Lee [90, 91] (PL) to incorporate the contributions from the higher-order terms based on a reference hard-sphere system [95]. Other formal approaches, such as fundamental measure theory [85, 86] and integral equation theory [83, 84], both of which have a sound basis in statistical mechanics, also offer promising routes to the development of an accurate description of the phase behaviour and structure of hard anisotropic particles. However, these theories involve a complicated mathematical treatment which make them difficult to apply to realistic LC models.

To complicate matters further, temperature often plays a key role in determining the relative stability of the LC phases. Although the Onsager viewpoint is broadly accepted, i.e. repulsive excluded-volume interactions are largely responsible for the formation of orientationally ordered phases, attractive inter-molecular interactions have to be considered on an equal footing for a proper description of the temperature dependence of the

thermodynamic properties. This reasoning is in line with the van der Waalsian view of fluids where the hard molecular core is treated as a reference which determines the fluid structure, while the dispersions (attractions) are treated as a perturbation [50, 143, 198]. A simple hard-core model which incorporates attractive interactions presumably would be appropriate to investigate the phase diagrams of thermotropic LCs. A number of studies have been carried out after the early attempts by Kimura [144] to combine Onsager's hard-rod model with anisotropic dispersion forces [145–156]. Some progress has also been made in introducing dipolar [119, 121, 159–162] or chiral [163–165, 199] interactions between LC molecules.

Of particular relevance to our current work is the closed-form algebraic equation of state developed within a van der Waals-Onsager treatment for systems of attractive hard-core particles [118], in which the attractive potential is expanded in spherical harmonics [166] representing different multipolar contributions to the anisotropic attractions.

A rigorous theoretical treatment of liquid crystalline polymers is of course complicated by the fact that an individual macromolecule of this type will have additional degrees of freedom and self-interactions. Nevertheless, several approaches for chain-like LC polymers based on Onsager's original theory have been developed to improve on the rigid-rod model. Khokhlov and Semenov (KS) [174] introduced the effect of chain flexibility as a correction to the orientational free energy of hard rods. In the KS flexible chain model, the stiffness of a chain is described with an adjustable parameter, the persistence length, conceptually defined as the characteristic length over which correlations in the direction of the chain segments are lost: for a completely flexible chain the persistence length is much smaller than the contour length which is the length at maximum physical extension of the polymer molecule. On the other hand, if the persistence length is larger than the contour length, the polymer chain can be approximated as a rigid rod-like molecule (in this case the persistence length would approach infinity). Though the KS flexible chains can provide a good representation of real LC polymer chains, it is rather difficult to obtain a general analytical expression for thermodynamic properties and orientational order due to the integro-differential equation that has to be solved to minimize the free energy of the system [200–203]. In addition to the KS flexible chain treatment, some other related models [103, 201, 202, 204–212] have been proposed all of them sharing one common feature : the hard-core backbone of the polymer chains. The major drawback in implementing these methods to represent real LC polymers is the strong coupling among the physical quantities in the model and the dependence of the model parameters on external fields.

For example, the persistence length typically depends both on the model parameters (the length of a chain segment and bending energy) and on the external environment (temperature, density, and the degree of orientational order).

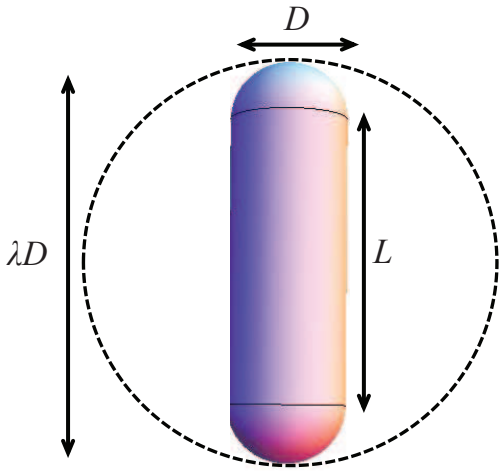

Figure 4.1: Square-well attractive hard spherocylinder (AHSC). The model is characterized by the length L of the central cylindrical core and diameter D of the hard hemispherical caps. The dashed curve represents the attractive range bounded by λD.

The fact the liquid crystalline phases of the system are found to be very sensitive to both concentration (lyotropic) and temperature (thermotropic) suggests that both repulsive and attractive interactions between the particles in the fluid should be taken into account. Here, we use an algebraic description to investigate the thermodynamics, orientational order, and fluid phase behaviour of hard spherocylinders decorated with an anisotropic square-well (ASW) potential representing the effective inter-particle attractive interactions. The equation of state is expressed in a closed algebraic form which allows one to add the contributions from other intermolecular interactions (e.g., chiral, dipolar, and associating interactions) in a straight-forward manner, or to extend the treatment to other type of inter-molecular potentials (e.g., Lennard-Jones or Yukawa). The effects of the anisotropy of the particle and the strength of the attraction on the phase behaviour of attractive rod-like particles are examined in detail. The attractive hard spherocylinder (AHSC) model is depicted in Figure (4.1). The model is characterized by the aspect ratio L/D, where L is the length of the cylindrical core and D is the diameter, and a new dimensional parameter λ is introduced to describe the range of the attractive interaction. We first describe the important details of the theoretical description (Section 2) and analyze the effect of the molecular parameters on the phase behaviour of model systems

(Section 3). An attempt to use our model to provide a quantitative representation of the orientational order and phase behaviour of solutions of PBLG in DMF over broad ranges of composition and temperature is then made in Section 4.

4.2 Theory

4.2.1 Generalised van der Waals-Onsager free energy functional

We briefly describe here a first-order thermodynamic perturbation approach [50, 167] to derive the free energy for the nematic and isotropic phases of non-spherical attractive particles. A system of N particles in a volume V at a temperature T is considered. The total Helmholtz free energy A is represented by two contributions, a reference term (hard-core repulsive) A^{ref} and a perturbation (attractive) term A^{att}:

$$\frac{A}{NkT} = \frac{A^{\mathrm{ref}}}{NkT} + \frac{A^{\mathrm{att}}}{NkT}, \tag{4.1}$$

where k is the Boltzmann constant. The reference term A^{ref} is the free energy of a fluid of hard-body particles and therefore represents a purely repulsive contribution. Following the Parsons-Lee (PL) approach [89–91], the spatial dependence of the excluded volume is decoupled from its orientational dependence, and the reference repulsive term can then be expressed as [118]

$$\begin{aligned} \frac{A^{\mathrm{ref}}}{NkT} &= \frac{A^{\mathrm{id}}_{\mathrm{iso}}}{NkT} + \int f(\vec{\omega}) \ln\{4\pi f(\vec{\omega})\} \mathrm{d}\vec{\omega} \\ &+ G(\eta) \iint V_{\mathrm{exc}}(\vec{\omega}_1, \vec{\omega}_2) f(\vec{\omega}_1) f(\vec{\omega}_2) \mathrm{d}\vec{\omega}_1 \mathrm{d}\vec{\omega}_2. \end{aligned} \tag{4.2}$$

Here, $A^{\mathrm{id}}_{\mathrm{iso}}$ is the ideal contribution to the free energy of the isotropic phase (which incorporates all of the kinetic effects), $\vec{\omega}$ is the orientation vector of the particle, and $f(\vec{\omega})$ is the single-particle orientational distribution function. In the PL approach, the density-dependent function $G(\eta) = \left(4\eta - 3\eta^2\right)/[8(1-\eta)^2]$ represents the residual free energy of an equivalent hard-sphere system (with the same molecular volume V_{m}), while $G(\eta) = \eta/2$ for the original Onsager second-virial theory [51]; in these expressions, $\eta = \rho V_{\mathrm{m}}$ is the packing fraction of the system, with $\rho = N/V$ the usual number density. The excluded volume $V_{\mathrm{exc}}(\vec{\omega}_1, \vec{\omega}_2)$ represents the region in phase space inaccessible to a particle with a fixed orientation $\vec{\omega}_1$ due to another particle with orientation $\vec{\omega}_2$, and is defined as

$$V_{\mathrm{exc}}(\vec{\omega}_1, \vec{\omega}_2) = \frac{1}{3} \int \sigma(\hat{r}_{12}, \vec{\omega}_1, \vec{\omega}_2) \mathrm{d}\hat{r}_{12}, \tag{4.3}$$

where $\sigma(\hat{r}_{12}, \vec{\omega}_1, \vec{\omega}_2)$ is the contact distance which depends on the relative orientations between $\vec{\omega}_1$ and $\vec{\omega}_2$ and the centre-of-mass interseparation of the pair of anisotropic particles, $\hat{r}_{12} = \vec{r}_{12}/r_{12}$.

At the first-order level of the perturbation theory [118], the contribution due to the attractive interactions corresponds to the statistical average of attractive energy evaluated in the reference-system ensemble. Assuming that the fluid structure of the full system with attractive interactions is unaltered by the perturbation and that pairwise additive interactions exist between particles, the perturbation contribution can be expressed as [118]

$$\begin{aligned} A^{\mathrm{att}} &= \frac{1}{2} \iiiint u_{12}^{\mathrm{att}}\left(\vec{r}_{12}, \vec{\omega}_1, \vec{\omega}_2\right) g^{\mathrm{ref}}\left(\vec{r}_{12}, \vec{\omega}_1, \vec{\omega}_2; \rho\right) \\ &\times \rho^{\mathrm{ref}}(\vec{r}_1, \vec{\omega}_1)\rho^{\mathrm{ref}}(\vec{r}_2, \vec{\omega}_2)\mathrm{d}\vec{r}_1\mathrm{d}\vec{\omega}_1\mathrm{d}\vec{r}_2\mathrm{d}\vec{\omega}_2 \\ &= \frac{\rho^2 V}{2} \iiint u_{12}^{\mathrm{att}}\left(\vec{r}_{12}, \vec{\omega}_1, \vec{\omega}_2\right) \\ &\times f(\vec{\omega}_1) f(\vec{\omega}_2) g^{\mathrm{ref}}\left(\vec{r}_{12}, \vec{\omega}_1, \vec{\omega}_2; \rho\right) \mathrm{d}\vec{r}_{12}\mathrm{d}\vec{\omega}_1\mathrm{d}\vec{\omega}_2, \end{aligned} \tag{4.4}$$

where $u_{12}^{\mathrm{att}}\left(\vec{r}_{12}, \vec{\omega}_1, \vec{\omega}_2\right)$ is the attractive pair interaction potential. The pair correlation function $g^{\mathrm{ref}}\left(\vec{r}_{12}, \vec{\omega}_1, \vec{\omega}_2; \rho\right)$ of the reference system is a complicated function [83, 84] that depends on the overall density and the relative separation and orientations of the two anisotropic particles. In order to make the approach tractable, we approximate the pair distribution function of the reference system by its low-density limit:

$$\lim_{\rho \to 0} g^{\mathrm{ref}}(\vec{r}_{12}, \vec{\omega}_1, \vec{\omega}_2; \rho) = \exp\left(-\frac{u^{\mathrm{ref}}\left(\vec{r}_{12}, \vec{\omega}_1, \vec{\omega}_2\right)}{kT}\right). \tag{4.5}$$

When considering a homogeneous nematic (anisotropic) phase, the single particle density of the system can be factorised as $\rho^{\mathrm{ref}}(\vec{r}_i, \vec{\omega}_i) = \rho f(\vec{\omega}_i)$, where the single particle orientation distribution function $f(\vec{\omega})$ has been introduced.

Since the particles of interest are non-spherical, the intermolecular pair potential is a function of the relative positions as well as orientations of particles [166, 169]. It is thus useful to expand the interaction as a series in spherical harmonics. Here we consider an anisotropic square-well (ASW) potential of the form [118, 166]:

$$\begin{aligned} u^{\mathrm{att}}(\vec{r}_{12}, \vec{\omega}_1, \vec{\omega}_2) &= -s(r_{12})[\epsilon_0 + \epsilon_2 P_2(\cos\gamma)] \\ s(r_{12}) &= \begin{cases} 1 & \lambda D > r_{12} \geq \sigma(\hat{r}_{12}, \vec{\omega}_1, \vec{\omega}_2) \\ 0 & r_{12} \geq \lambda D. \end{cases} \end{aligned} \tag{4.6}$$

where ϵ_0 and ϵ_2 characterize the isotropic and anisotropic attractive interactions respectively, λ is the range parameter, D is the reference diameter of the underlying hard-core particle, and $P_2(\cos\gamma) = \frac{3}{2}\cos^2\gamma - \frac{1}{2}$ is the second Legendre polynomial for the relative

orientation $\gamma = \arccos(\vec{\omega}_1 \cdot \vec{\omega}_2)$ between the two particles. After substituting the ASW attractive potential into Equation (4.4) and integrating over the centre-to-centre distance between particle 1 and 2, the perturbation free energy can be expressed as [118]

$$\begin{aligned}\frac{A^{\mathrm{att}}}{NkT} &= -\frac{\rho\epsilon_0}{2kT}\left[\frac{4\pi}{3}\lambda^3 D^3 - \langle V_{\mathrm{exc}}(\gamma)\rangle_{\vec{\omega}_1,\vec{\omega}_2}\right] \\ &- \frac{\rho\epsilon_2}{2kT}\left[\frac{4\pi}{3}\lambda^3 D^3 \langle P_2(\cos\gamma)\rangle_{\vec{\omega}_1,\vec{\omega}_2} - \langle V_{\mathrm{exc}}(\gamma) P_2(\cos\gamma)\rangle_{\vec{\omega}_1,\vec{\omega}_2}\right]. \end{aligned} \tag{4.7}$$

where the the double orientational average of a quantity $J(\vec{\omega}_1, \vec{\omega}_2)$ is introduced

$$\langle J(\vec{\omega}_1,\vec{\omega}_2)\rangle_{\vec{\omega}_1,\vec{\omega}_2} = \iint J(\vec{\omega}_1,\vec{\omega}_2) f(\vec{\omega}_1) f(\vec{\omega}_2) \mathrm{d}\vec{\omega}_1 \mathrm{d}\vec{\omega}_2. \tag{4.8}$$

Combining all of the contributions to the free energy one obtains an expression in terms of orientational averages of the configurational terms:

$$\begin{aligned}\frac{A[f(\vec{\omega})]}{NkT} &= \frac{A^{\mathrm{id}}_{\mathrm{iso}}}{NkT} + \int f(\vec{\omega}) \ln\left[4\pi f(\vec{\omega})\right] \mathrm{d}\vec{\omega} + G(\eta) \langle V_{\mathrm{exc}}(\gamma)\rangle_{\vec{\omega}_1,\vec{\omega}_2} \\ &- \frac{\rho\epsilon_0}{2kT}\left[\frac{4\pi}{3}\lambda^3 D^3 - \langle V_{\mathrm{exc}}(\gamma)\rangle_{\vec{\omega}_1,\vec{\omega}_2}\right] \\ &- \frac{\rho\epsilon_2}{2kT}\left[\frac{4\pi}{3}\lambda^3 D^3 \langle P_2(\cos\gamma)\rangle_{\vec{\omega}_1,\vec{\omega}_2} - \langle V_{\mathrm{exc}}(\gamma) P_2(\cos\gamma)\rangle_{\vec{\omega}_1,\vec{\omega}_2}\right]. \end{aligned} \tag{4.9}$$

A clear coupling between the repulsive (excluded volume) and attractive contributions to the pair potential can be seen in this expression: the excluded volume enters the terms corresponding to the isotropic and anisotropic attractive contributions, while the last term in $\langle V_{\mathrm{exc}}(\gamma) P_2(\cos\gamma)\rangle_{\vec{\omega}_1,\vec{\omega}_2}$ constitutes a direct coupling of the repulsions and attractions. The single-particle orientational distribution function in the isotropic state is constant which simplifies the orientational integrals in Equation (4.9); for molecular geometries with cylindrical symmetry it corresponds to $f_{\mathrm{iso}}(\vec{\omega}) = 1/4\pi$. In the anisotropic state, the equilibrium orientational distribution of molecules must be found by minimizing the total free energy functional, $A\left[f(\vec{\omega})\right]$. In order to obtain the orientational distribution function in algebraic form, we use the Onsager trial function (OTF) [25]:

$$f_{\mathrm{OTF}}(\vec{\omega}) = \frac{\alpha \cosh(\alpha\cos\theta)}{4\pi \sinh(\alpha)}, \tag{4.10}$$

where the parameter α is introduced to characterize the degree of orientational order, the polar angle $\theta = \arccos(\vec{\omega}\cdot\vec{\omega}_0)$, and $\vec{\omega}_0$ is the director of the nematic phase. On introducing the algebraic OTF into the total free energy expression (4.9), the functional variation of $A[f(\vec{\omega})]$ with respect to $f(\vec{\omega})$ can be simplified to a derivative of the free energy with respect to the parameter α. The simplification provided by the OTF makes the solution of the equilibrium orientational distribution straightforward. Details of the evaluations of orientational averages using the OTF have been discussed in earlier work [51].

4.2.2 Equation of state for hard spherocylinders with an anisotropic square-well potential

For hard spherocylinders, the excluded volume of a pair of particles can be expressed as [25]

$$V_{\text{exc}}(\gamma) = C_0 + C_1 \sin\gamma. \tag{4.11}$$

where the coefficients $C_0 = \frac{4}{3}\pi D^3 + 2\pi L D^2$ and $C_1 = 2L^2 D$ are determined by the shape of the particle. Similarly, the coupled term involving $V_{\text{exc}}(\gamma)$ and $P_2(\sin\gamma) = 1 - \frac{3}{2}\sin^2\gamma$ can also be written as a function of $\sin\gamma$:

$$V_{\text{exc}}(\gamma)P_2(\sin\gamma) = C_0 + C_1\sin\gamma - \frac{3}{2}\left(C_0\sin^2\gamma + C_1\sin^3\gamma\right). \tag{4.12}$$

The orientational averages found in the total free energy can therefore be expressed as the double orientational averages of $\left\langle \sin^i\gamma \right\rangle_{\vec{\omega}_1,\vec{\omega}_2}$ where $i = 0, 1, 2, \cdots$. The introduction of the OTF to describe the degree of orientational order of the nematic phase renders the orientational averages to an algebraic form, which provides a more tractable set of expressions [51, 118]:

$$\left\langle \sin\gamma \right\rangle_{\vec{\omega}_1,\vec{\omega}_2} \approx \sqrt{\pi}\left(\frac{1}{\alpha^{1/2}} - \frac{15}{16\alpha^{3/2}}\right) + \mathcal{O}(1/\alpha^{5/2}) \tag{4.13}$$

$$\left\langle \sin^2\gamma \right\rangle_{\vec{\omega}_1,\vec{\omega}_2} \approx \frac{4}{\alpha} + \mathcal{O}(1/\alpha^2) \tag{4.14}$$

$$\left\langle \sin^3\gamma \right\rangle_{\vec{\omega}_1,\vec{\omega}_2} \approx \sqrt{\pi}\frac{6}{\alpha^{3/2}} + \mathcal{O}(1/\alpha^{5/2}) \tag{4.15}$$

$$\left\langle \sin^4\gamma \right\rangle_{\vec{\omega}_1,\vec{\omega}_2} \approx 0 + \mathcal{O}(1/\alpha^2). \tag{4.16}$$

Using Equations (4.13)-(4.16) and the expressions for excluded volume and second Legendre polynomial, one obtains an algebraic equation of state for hard spherocylinders interacting with an anisotropic square-well potential [118]. The free energy of the nematic phase of our attractive hard spherocylinder (AHSC) particles can be expressed in algebraic

form in the terms of the OTF parameter α:

$$\begin{aligned}\frac{A^{\mathrm{nem}}(\alpha)}{NkT} &= \frac{A^{\mathrm{id}}_{\mathrm{iso}}}{NkT} + \ln\alpha - 1 \\ &+ \frac{G(\eta)}{V_{\mathrm{m}}}\left[C_0 + C_1\sqrt{\pi}\Big(\frac{1}{\alpha^{1/2}} - \frac{15}{16\alpha^{3/2}}\Big)\right] \\ &- \frac{\rho\epsilon_0}{2kT}\left[\frac{4\pi}{3}\lambda^3 D^3 - C_0 - C_1\sqrt{\pi}\left(\frac{1}{\alpha^{1/2}} - \frac{15}{16\alpha^{3/2}}\right)\right] \\ &- \frac{\rho\epsilon_2}{2kT}\left[\left(\frac{4\pi}{3}\lambda^3 D^3 - C_0\right)\left(1 - 6\alpha^{-1}\right)\right. \\ &- \left. C_1\sqrt{\pi}\left(\alpha^{-1/2} - \frac{159}{16}\alpha^{-3/2}\right)\right], \end{aligned} \tag{4.17}$$

where for hard spherocylinders the molecular volume is $V_{\mathrm{m}} = \pi D^3/6 + \pi L D^2/4$. The equilibrium value of α can be determined by minimising the total Helmholtz free energy of the system. On differentiating the free energy with respect to α, one can factor out a simple cubic equation of $x = \sqrt{\alpha}$:

$$\frac{\partial}{\partial\alpha}\frac{A(\alpha)}{NkT} = \frac{1}{x^5}\left(x^3 + a_2x^2 + a_1x + a_0\right) = 0, \tag{4.18}$$

where the coefficients depend on the repulsive and attractive intermolecular parameters and the system density through

$$a_0 = \frac{45}{32}C_1\sqrt{\pi}\left[\frac{G(\eta)}{V_{\mathrm{m}}} + \frac{\rho\epsilon_0}{2kT}\left(1 + \frac{53}{5}\frac{\epsilon_2}{\epsilon_0}\right)\right] \tag{4.19}$$

$$a_1 = 6\frac{\rho\epsilon_2}{2kT}\left(C_0 - \frac{4\pi}{3}\lambda^3 D^3\right) \tag{4.20}$$

$$a_2 = -\frac{C_1\sqrt{\pi}}{2}\left[\frac{G(\eta)}{V_{\mathrm{m}}} + \frac{\rho\epsilon_0}{2kT}\left(1 + \frac{\epsilon_2}{\epsilon_0}\right)\right]. \tag{4.21}$$

The solution for α in Equation (4.18) can be expressed as [51, 118]

$$\begin{aligned}\alpha_{\mathrm{eq}} &= \frac{1}{9}\Bigg\{a_2 - 2\sqrt{a_2^2 - 3a_1}\cos\Big(\frac{2j\pi}{3} \\ &+ \frac{1}{3}\arccos\frac{-27\left[a_0 - \frac{1}{3}a_1a_2 + \frac{2}{27}a_2^3\right]}{2\left[a_2^2 - 3a_1\right]^{3/2}}\Big)\Bigg\}^2, \quad j = \{0,1,2\}. \end{aligned} \tag{4.22}$$

The equilibrium value of α_{eq} describing the orientationally ordered nematic phase corresponds to the largest root ($j = 0$). An important quantity that characterizes the degree of orientational order is the nematic order parameter S_2, which is usually defined as the orientational average of second Legendre polynomial $P_2(\cos(\theta))$:

$$S_2 = \int P_2(\cos(\theta))f(\theta)\mathrm{d}\vec{\omega}. \tag{4.23}$$

As the OTF is used to represent the orientational distribution in nematic phase, $f(\theta) = f_{\mathrm{OTF}}(\vec{\omega})$, one can express the nematic order parameter as a function of equilibrium orientational parameter α_{eq} [51]:

$$S_2 = 1 - \frac{3\coth\alpha_{\mathrm{eq}}}{\alpha_{\mathrm{eq}}} + \frac{3}{\alpha_{\mathrm{eq}}^2}. \tag{4.24}$$

In the case of an isotropic state, the solution becomes much simpler since the orientational distribution is the constant, $f(\vec{\omega}) = 1/4\pi$. The free energy of the isotropic liquid can then be written as

$$\begin{aligned} \frac{A^{\mathrm{iso}}}{NkT} &= \frac{A_{\mathrm{iso}}^{\mathrm{id}}}{NkT} + \frac{G(\eta)}{V_{\mathrm{m}}}\left(C_0 + \frac{\pi}{4}C_1\right) \\ &- \frac{\rho\epsilon_0}{2kT}\left[\frac{4\pi}{3}\lambda^3 D^3 - C_0 + \frac{\pi}{4}C_1\left(\frac{\epsilon_2}{8\epsilon_0} - 1\right)\right]. \end{aligned} \tag{4.25}$$

The standard thermodynamic relations $A = N\mu - PV$ and $P = -\left(\partial A/\partial V\right)_T$ allow algebraic expressions for chemical potential μ and compressibility factor (pressure) $Z = PV/NkT$ in both the isotropic and nematic phases to be obtained. The solution of phase equilibria is determined by equating the chemical potential and pressure of both phases. In the case of our attractive hard spherocylinders, four possible pairs of coexisting fluid phases can be expected: vapour-liquid, vapour-nematic, liquid-nematic and nematic-nematic. There will also be a corresponding three-phase equilibrium coexistence point (e.g., vapour-liquid-nematic or vapour-nematic-nematic). The possible types of phase behaviour exhibited by this simple system are examined in the following sections.

4.3 Phase behaviour of attractive hard spherocylinders

In the present study, hard spherocylinders with an aspect ratio of L/D are enveloped by a square-well of fixed range $\lambda = L/D+1$. The calculated phase diagrams are first represented in reduced units: reduced temperature $T^* = kT/\epsilon_0$; reduced pressure $P^* = PV_{\mathrm{m}}/\epsilon_0$; and packing fraction $\eta = \rho V_{\mathrm{m}}$.

The phase behaviour of hard spherocylinders with an isotropic (spherically symmetrical) SW potential, i.e., with $\epsilon_0/k = 1$ and $\epsilon_2 = 0$, is presented in Figure 4.2. The richness of the phase behaviour exhibited by an attractive rod of varying length is consistent with the idea that hard-core interactions are to a great extent responsible for the stabilization of the nematic phase. A detailed discussion of systems of short attractive rods ($L/D < 50$) can be found elsewhere [118]. Relatively large aspect ratios can be found experimentally in the systems of rod-like colloidal suspensions [6]. The focus of our current work is on rod-like

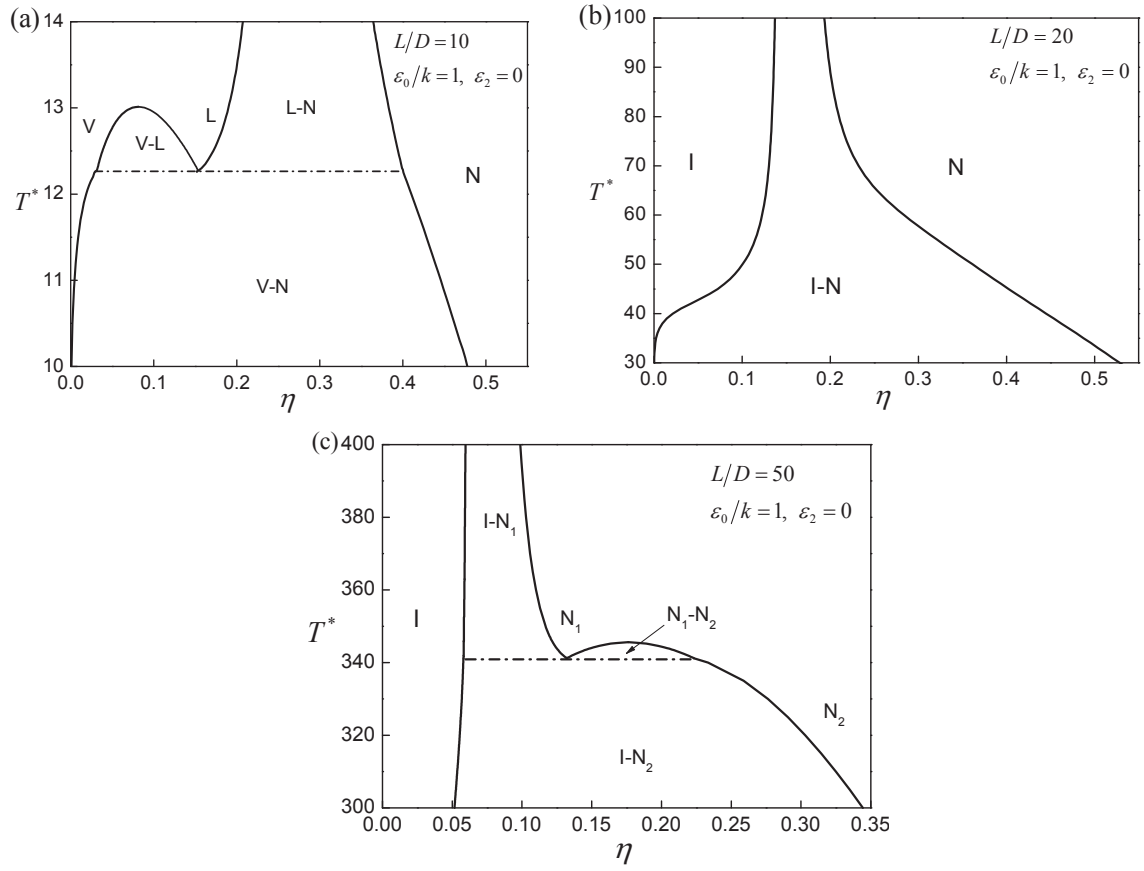

Figure 4.2: Temperature-density representation of the fluid phase behaviour of attractive hard spherocylinders (AHSC) with aspect ratios (a) $L/D = 10$, (b) $L/D = 20$ and (c) $L/D = 50$. The rod-like molecules are modelled as hard cylinders of length L and diameter D, capped by hard hemispheres of diameter D, and enveloped by an attractive square well of depth $-(\epsilon_0 + \epsilon_2 P_2(\cos\gamma))$ and range $\lambda = L/D + 1$. The stable regions are indicated as vapour (V), liquid (L), isotropic fluid (I), and nematic (N). In the case of $L/D = 50$, N_1 and N_2 correspond to the low-density and high-density nematic phases, respectively. The dot-dashed lines are the corresponding three phase lines.

particles with aspect ratios of $L/D = 50, 100$ and 150. One of most striking features of the phase behaviour is the appearance of a region of nematic-nematic phase separation for high molecular elongations [118,173–175,213]. This behaviour is a consequence of the isotropic-nematic transition moving to progressively lower densities as the molecular aspect ratio is increased. The nematic-nematic region involves the coexistence of low-density (gas-like) and high-density (liquid-like) anisotropic states, bounded at higher temperatures by a critical point. For particles of intermediate length the vapour-liquid transition becomes

metastable relative to the isotropic fluid-nematic transition; in such a case we refer to the low-density fluid state as an isotropic liquid to allow one to distinguish the two types of phase behaviour.

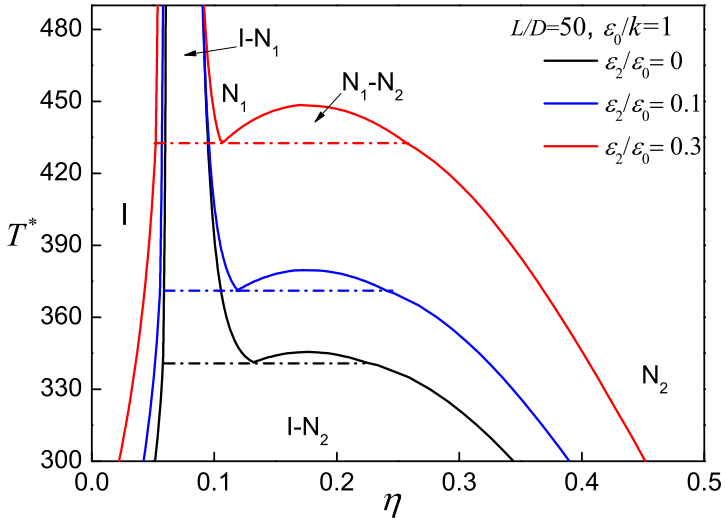

Figure 4.3: Temperature-density representation of the fluid phase behaviour of attractive hard spherocylinders (AHSC) with an aspect ratio of $L/D = 50$ and positive anisotropic interactions $\epsilon_2 > 0$. See the caption of Figure 4.2 for further details.

The effect of including a positive anisotropic attractive contribution ($\epsilon_2 > 0$) on the phase behaviour of our AHSC with $L/D = 50$ is presented in Figure 4.3. Although the weak contribution from the anisotropic attraction does not qualitatively change the type of phase behaviour of the system, the nematic-nematic transition is stabilized on increasing this anisotropic interaction as the latter leads to more favourable parallel relative orientations of the particles. On the other hand, a negative anisotropic attractive contribution to the potential ($\epsilon_2 < 0$) destabilizes the nematic-nematic coexistence, as in this case anti-parallel relative configurations of the particles are favoured, tending to reduce the effective attractive interactions in the anisotropic state. Since the region of nematic-nematic equilibrium is small, a weak negative anisotropic attraction ($\epsilon_2 = -0.1$) is sufficient to cause the nematic-nematic coexistence to become metastable with respect to the isotropic-nematic transition, as shown in Figure 4.4.

The corresponding fluid phase diagrams of AHSC particles with aspect ratios of $L/D = 100$ and $L/D = 150$ are presented in Figure 4.5, where the effect of adding both positive and

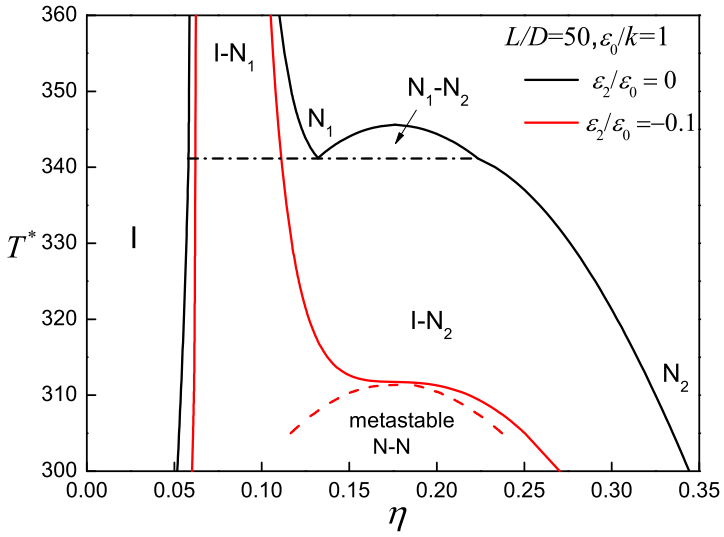

Figure 4.4: Temperature-density representation of the fluid phase behaviour of attractive hard spherocylinders (AHSC) with an aspect ratio $L/D = 50$ and a negative anisotropic interaction $\epsilon_2 < 0$. The dashed curve represents the metastable nematic-nematic coexistence. See the caption of Figure 4.2 for further details.

negative anisotropic interactions is examined. The enhanced anisotropic attractive interaction not only promotes the coexistence between two nematic phases but also leads to an increase in the isotropic-nematic-nematic (I-N_1-N_2) triple point temperature. The coexistence between the isotropic and the low-density nematic phases (N_1) is not affected by incorporation of anisotropy in the attractive interactions. As has already been mentioned the position of the isotropic-nematic transition is determined principally by the anisotropy of the rod-like molecular cores, with the coexistence shifting to lower densities as the aspect ratio is increased.

4.4 Phase behaviour of solutions of PBLG in DMF

In order to assess the capabilities of our van der Waals-Onsager approach in describing thermotropic liquid crystal behaviour, the attractive hard-spherocylinder model is used to represent the PBLG/DMF system. It has been shown experimentally [24, 193] that under certain conditions the polypeptide PBLG adopts an α-helix secondary structure in solutions of DMF; in this conformation the PBLG molecules are observed to behave as

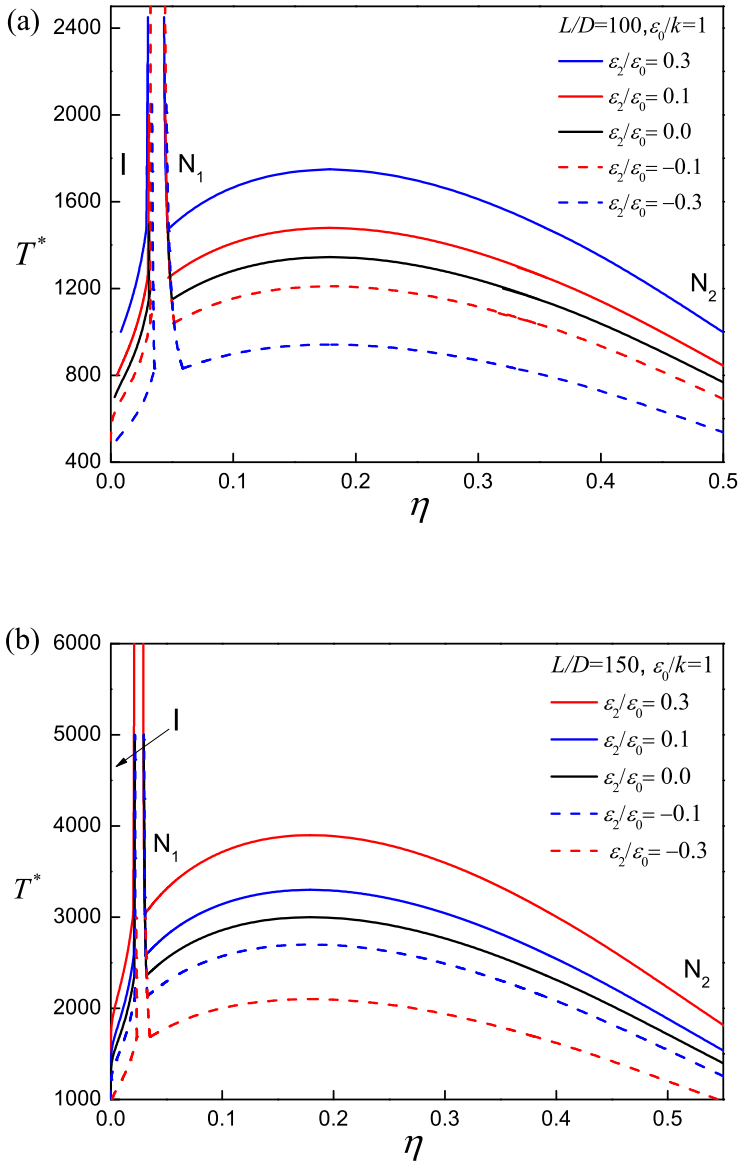

Figure 4.5: Temperature-density representation of the fluid phase behaviour of attractive hard spherocylinders (AHSC) with aspect ratios of (a) $L/D = 100$ and (b) $L/D = 150$ and a varying anisotropic interaction ϵ_2. See the caption of Figure 4.2 for further details.

rod-like particles [19, 190].

The lattice theory of Flory [172, 213] has been employed to explain the phase behaviour of the PBLG/DMF system and several qualitative similarities between the theoretical description and experiment were highlighted [19]. Because of the discrete treatment of the

medium in this type of lattice treatment and the artificial sectioning of the rod-like particles, it becomes difficult to make a direct comparison between the lattice model and the real macromolecule. By contrast, the attractive hard spherocylinder model introduced in our current work is an off-lattice (continuous) model that allows one to relate, in a coarse-grained fashion, the dimensions of the model with that of the rod-like PBLG molecules (*cf.* Figure 4.6).

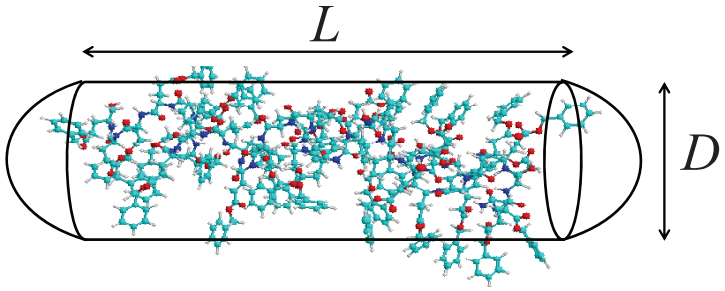

Figure 4.6: An attractive hard spherocylinder is used to represent the hard-core backbone of the PBLG molecule in its extended α-helical conformation. The length of rod L is considered to be temperature dependent to account for the flexibility and conformational changes of the polypeptide in DMF.

There are two crucial features that need to be considered carefully when modelling the PBLG/DMF system: how the conformations of PBLG molecules change over the temperature and density range of interest; and how the solvent (DMF) modulates the effective interactions between the PBLG molecules. Since our model is based on a hard rod there is no explicit account of flexibility that would enable us to incorporate the chain conformation of the macromolecule directly. The characteristic diameter D_{PBLG} of the PBLG rod is fixed as 14.2 Å in an attempt to map the extended low-temperature conformation [24], which is found to lie between the diameter corresponding to the minimum intermolecular distance (13.0 Å) and the diameter of the backbone with extended side chains (15.2 Å). We allow the rod length to vary with temperature, reflecting the state dependence of the conformations of PBLG. While the volume of the PBLG rod could be fixed hence both the length and the diameter allowed to vary with temperature; this choice is not found to provide as good a representation of the overall fluid phase equilibria. The PBLG/DMF mixture is treated as an equivalent single component system, whereby any solvent effects are subsumed into an effective PBLG intermolecular attractive interaction (which now takes on the meaning of a potential of mean force).

A simple conversion is used to interpret the packing fraction η_{PBLG} of the rod-like polymer

in terms of its volume fraction ν_{PBLG} (which is the experimentally relevant variable). The expression for volume fraction of PBLG can be obtained from

$$\nu_{\mathrm{PBLG}} = \frac{\eta_{\mathrm{PBLG}} M_{\mathrm{w}}}{N_{\mathrm{A}} \rho_{\mathrm{PBLG}} V_{\mathrm{m,PBLG}}} \tag{4.26}$$

where N_{A} is the Avogadro number and we assume an ideal (additive) volume of mixing for the PBLG/DMF system. In our simple model the molecular volume of PBLG depends on its aspect ratio through: $V_{\mathrm{m,PBLG}} = \pi D_{\mathrm{PBLG}}^3/6 + \pi L_{\mathrm{PBLG}} D_{\mathrm{PBLG}}^2/4$. Because the molecular weight M_{w} and density ρ_{PBLG} of PBLG depend on the polymerization conditions [214,215], an average prototypical molecular weight of $M_{\mathrm{w}} = 310,000$ g mol^{-1} is assumed, and a value of $\rho_{\mathrm{PBLG}} = 1.283$ g cm^{-3} is taken for its density [24].

There is experimental evidence [188, 195–197] that solutions of PBLG in some solvents (e.g., DMF or dichloromethane) exhibit a cholesteric (chiral nematic) phase rather than a nematic phase. As the difference in free energy between the two states is very small (owing to the large chiral pitches characteristic of the system), the thermodynamic properties of the cholesteric phase can be approximated by those of the nematic phase. The repulsive interactions between the various conformations of the polypeptide rods are taken into account with a simple hard-spherocylindrical core of variable aspect ratio. The effective attractive interactions between helical rods can be described with an enveloping isotropic SW potential [164, 165], where the depth of the well ϵ_0 is tuned to take into account the effect of the solvent medium (and its dielectric properties). In this sense our model is similar to the DLVO potential commonly employed to describe the interactions between colloidal particles in solution [50].

We have already shown that for long rods ($L/D = 100$ and 150) the densities of the isotropic-nematic transition are not affected to a significant degree by the anisotropic contribution (characterized by ϵ_2) to the attractive intermolecular potential (cf. Figure 4.5). In order to reduce the number of adjustable parameters we have therefore opted to include only isotropic SW attractions of strength ϵ_0 to describe the effective interaction between the PBLG molecules in solution. In summary, there are two adjustable parameters: the aspect ratio $L^*_{\mathrm{PBLG}} = L_{\mathrm{PBLG}}/D_{\mathrm{PBLG}}$ of the repulsive core and the attractive depth ϵ_0 of the enveloping SW potential. At each temperature, starting from the lowest available (260 K) at which one would expect the most extended PBLG conformation, the values of these two parameters are estimated from the experimental data for the phase boundaries of the two regions of isotropic-nematic coexistence (denoted as I-N_1 and I-N_2 in Figure 4.7). Once the values of $L^*_{\mathrm{PBLG}}(T)$ and $\epsilon_0(T)$ are determined one can predict

the nematic-nematic phase equilibrium of the PBLG solution as can be seen from Figure 4.7.

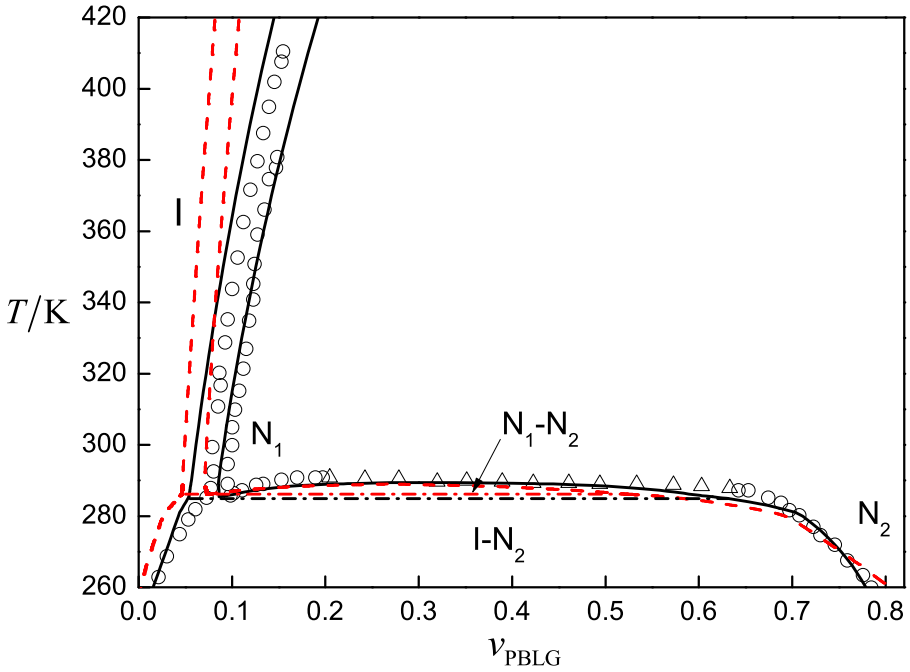

Figure 4.7: The temperature-volume fraction representation of the phase diagram of solutions of the polypeptide PBLG (molecular weight $M_w = 310,000$ g mol^{-1}) in DMF. The circles represent the experimental data (the triangles are tentative data in the inaccessible region) [19–21] and the continuous curves the description obtained using the van der Waals-Onsager theory with an attractive hard-spherocylinder model. The two regions of isotropic-nematic coexistence are denoted by I-N_1 and I-N_2, the region of nematic-nematic coexistence by N_1-N_2, and the dot-dashed line is for the I-N_1-N_2 three phase coexistence line. The description obtained assuming the volume of the PBLG rod is constant is represented as the dashed curves.

The description of the experimental data [19–21] with our algebraic van der Waals-Onsager equation of state is seen to be relatively good. At the temperature of $T = 280$ K, a low-density isotropic phase ($\nu_{\mathrm{PBLG,I}} = 0.0424$) coexists with a concentrated nematic phase ($\nu_{\mathrm{PBLG,N_2}} = 0.711$). The AHSC model successfully reproduces the fluid phase behaviour over the entire temperature range. Isotropic-nematic-nematic three-phase coexistence is predicted at a temperature of $T = 285.40$ K where an isotropic liquid phase, a low-

concentration nematic phase and a high-concentration nematic phase simultaneously coexist. The most salient feature in the phase diagram of the PBLG/DMF system is the equilibrium between low-concentration (N_1) and high-concentration (N_2) nematic phases. At a temperature of $T = 290$ K the isotropic liquid state ($\nu_{\mathrm{PBLG,I}} = 0.0564$) coexists with a low-concentration nematic state ($\nu_{\mathrm{PBLG,N_1}} = 0.0856$). Above the triple temperature, only a weak temperature dependence of the coexistence concentrations of the isotropic-nematic boundary is found. It is also clear from Figure 4.7 that the corresponding description of the fluid phase behaviour obtained by assuming that the volume of the PBLG rod remains constant (corresponding to that of the extended conformation) is not as satisfactory; we therefore do not pursue this assumption any further. It has recently been shown [216] that the effective volume of model helical hard-core particles increases as they become more elongated (less twisted); this is consistent with our assumption that the effective volume of the PBLG macromolecule is larger (corresponding to a larger aspect ratio) in the more extended low-temperature states.

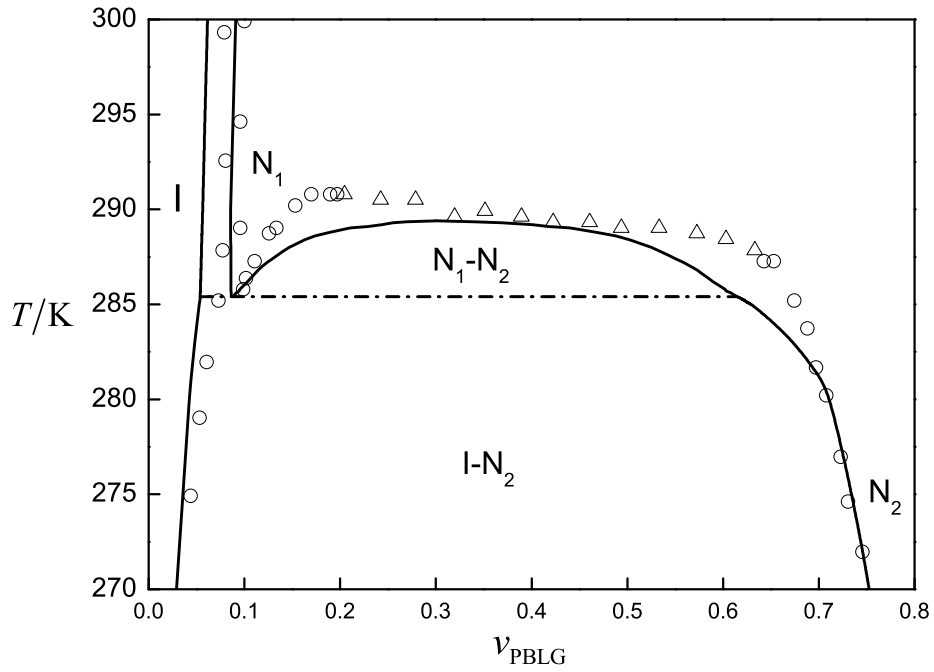

Figure 4.8: The phase diagram of Figure 4.7 highlighting the regions of nematic-nematic and isotropic-nematic-nematic three-phase coexistence.

The coexistence between two nematic phases in solutions of PBLG in DMF is well docu-

mented experimentally [17, 20, 21, 23, 195, 197]: the region of nematic-nematic coexistence is bounded between the isotropic-nematic-nematic triple point and the nematic-nematic critical temperature as can be seen clearly in the expanded scale of Figure 4.8.

The temperature-dependence of the nematic order parameter S_2 is represented in Figure 4.9: while the degree of orientational order of the high-concentration nematic state N_2, is very high and rather invariant with temperature, that of the low-concentration nematic phase N_1 is a monotonically increasing function of temperature. The volume fraction of the N_2 state at the I-N_2 coexistence boundary correspond to an effective packing fraction of $\eta_{N_2} \sim 0.35$ (volume fraction $\nu_{\mathrm{PBLG},N_2} \sim 0.61$). Considering that the aspect ratio of the PBLG rod is ~ 100 this corresponds to a relatively dense state, hence to a high degree of orientation order. The orientational order in the low-concentration nematic phase is seen to be slightly lower.

Though Miller and co-workers [19–21] reported the existence of two coexisting liquid crystalline states in solutions of PBLG in DMF, they did not observe the high-concentration anisotropic phase directly because of the high viscosity of the solutions which makes the states experimentally inaccessible. The existence of two anisotropic states in equilibrium was confirmed when two different LC textures were observed under a polarizing microscope as the characteristic fingerprint pattern of the chiral nematic (cholesteric) phase [23, 189, 195]: a high-concentration phase of relatively low pitch was found to coexist with a low-concentration phase of higher pitch. Several factors such as the molecular weight, the nature of the solvent, and the heating and cooling rates affect the phase behaviour observed in the system. With our current coarse-grained model we do not consider the cholesteric ordering of the PBLG macromolecules, assuming instead that the free energy of the system is essentially that of a nematic phase. In Figure 4.9, the less ordered nematic phase corresponds to the high-pitch cholesteric phase while the highly ordered nematic state represents the low-pitch PBLG-rich state.

The evolution of the orientational order parameter of the nematic phase in coexistence with the isotropic phase is shown in Figure 4.10. The order parameter decreases with increasing temperature along both the I-N_1 and I-N_2 boundaries as the anisotropic phases become less ordered, particularly in the low-concentration N_1 phase; a sudden drop can be seen near the isotropic-nematic-nematic I-N_1-N_2 triple point temperature.

The temperature dependence obtained for the anisotropic square-well depth ϵ_0 of our AHSC model of PBLG is depicted in Figure 4.11. The change in the attractive parameter is seen to be quite small over the entire temperature range ($\Delta\epsilon_0/k_{\mathrm{B}} \sim 0.04\,\mathrm{K}$), and is

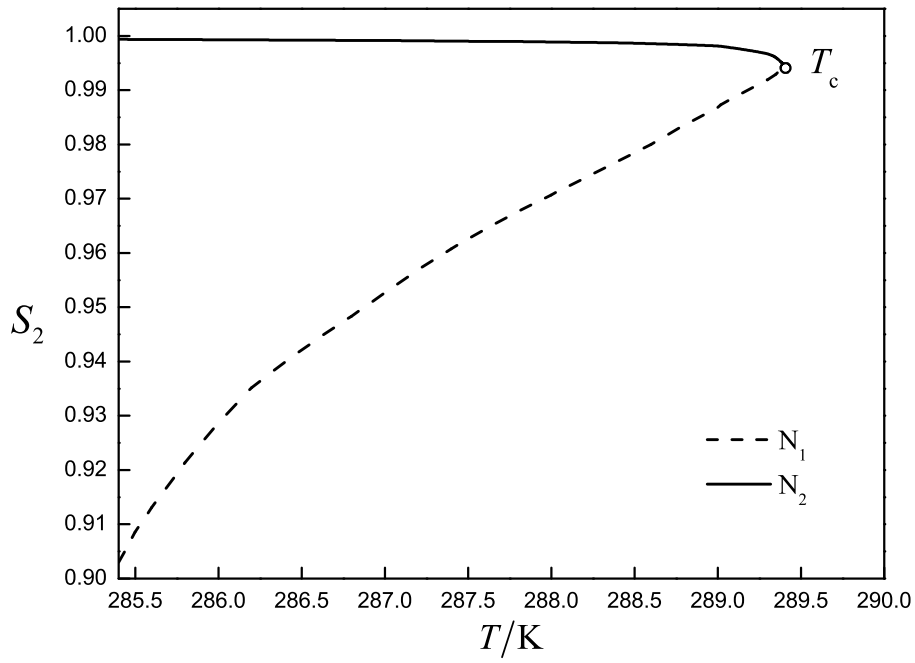

Figure 4.9: The temperature dependence of nematic order parameters S_2 in the coexisting nematic phases of solutions of PBLG (molecular weight $M_w = 310,000$ g mol^{-1}) in DMF predicted using the van der Waals - Onsager approach (continuous and dashed curves) with a simple attractive hard spherocylinder model. The nematic-nematic critical point T_c is also indicated.

found not to affect the phase behaviour of the low-concentration states. In the region below a temperature of 280 K, the energy parameter is $\epsilon_0(T < 280 \text{ K})/k_B \sim 0.26$ K, while the parameter takes a value of $\epsilon_0(T > 290 \text{ K})/k_B \sim 0.22$ K for temperatures above 290 K. In other words, the isotropic-nematic behaviour exhibited by the PBLG/DMF system can essentially be treated as two separate lyotropic liquid crystalline transitions either side of the triple point; this is not the case for the nematic-nematic coexistence region between the two anisotropic phases. The fact that the effective attractive interactions between the PBLG rods are stronger (cf. the larger values of ϵ_0) in the high-concentration low-temperature states than in the low-concentration high-temperature states would suggest a fine interplay with the properties of the solvent (e.g., the state dependence of the dielectric constant).

An assessment of the effective aspect ratio obtained for the PBLG rod with our model is

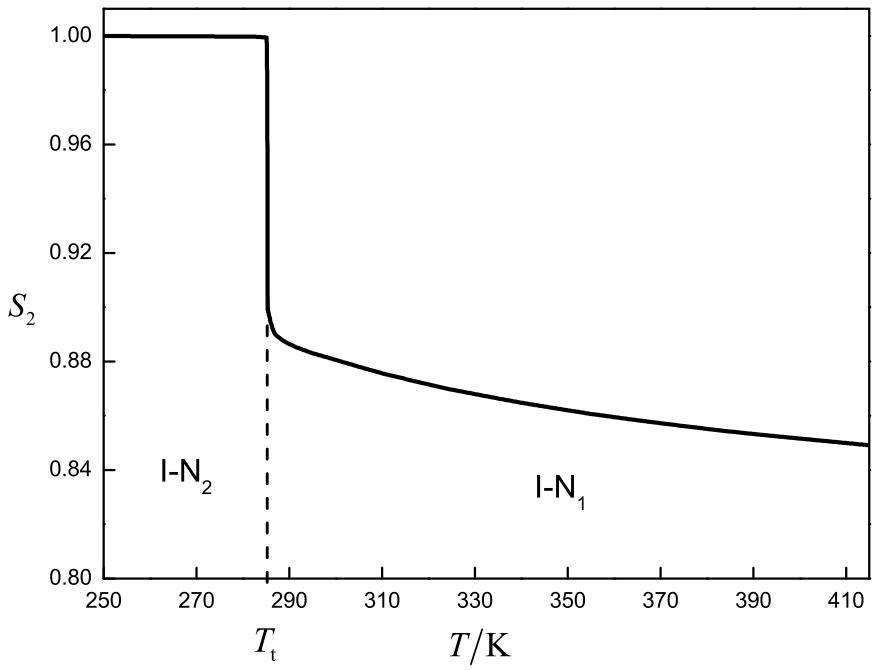

Figure 4.10: The temperature dependence of nematic order parameters S_2 of the anisotropic phase along the isotropic-nematic coexistence boundary predicted using the van der Waals - Onsager approach (continuous curve) with a simple attractive hard spherocylinder model of solutions of PBLG (molecular weight $M_w = 310,000$ g mol^{-1}) in DMF. The triple temperature T_t is indicated.

now made to ensure the overall shape of the rod is consistent with that of the real PBLG macromolecule. We find that the estimated values of the molecular anisotropy can be described with a simple linear function in the inverse temperature:

$$L^*_{\mathrm{PBLG}} = \frac{L_{\mathrm{PBLG}}}{D_{\mathrm{PBLG}}} = \frac{35003.82}{(T/\mathrm{K})} - 21.3179. \tag{4.27}$$

The effective aspect ratio is found to range from $L^*_{\mathrm{PBLG}} = 62$ to 118 over the temperature range of 420 K to 260 K. We recall here that the effective diameter of our AHSC model of the PBLG rod is fixed to the value in the extended low-temperature configuration, $D_{\mathrm{PBLG}} = 14.2$ Å. The apparent length of the PBLG rod thus varies from $L_{\mathrm{PBLG}} \sim 88$ nm to 168 nm (see Figure 4.12), which is in broad agreement with the range of persistence lengths obtained experimentally [24] from light scattering studies, $L^{\mathrm{exp}}_{\mathrm{PBLG}} \sim 70$ nm and 160 nm; the diameter of $D^{\mathrm{exp}}_{\mathrm{PBLG}}$ 15.2 Å estimated experimentally [24] by considering that

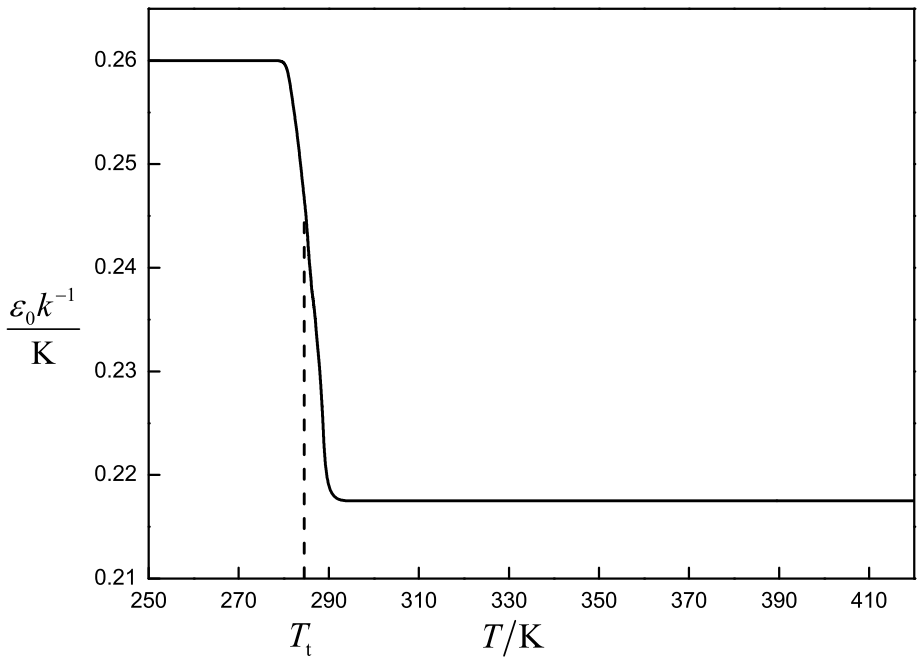

Figure 4.11: The temperature dependence of isotropic attractive parameter of solutions of PBLG (molecular weight $M_\mathrm{w} = 310,000$ g mol^{-1}) in DMF estimated using our van der Waals - Onsager approach (continuous curve) with a simple attractive hard spherocylinder model. The triple temperature T_t is indicated.

the side chains of PBLG rod are independent rotators is also in line with the predictions from our AHSC model. When the volume of the rod $V_{\mathrm{m,PBLG}}$ is assumed to be constant, a range of diameters from $D_{\mathrm{PBLG}} = 14.2$ Å at 260 K to 18.0 Å at 420 K is found to best represent the experimental phase behaviour, corresponding to an average of 16.1 Å.
It is important to emphasize that the vapour-liquid and nematic-nematic behaviour exhibited by our rod-like particles is a consequence of the interplay between the interparticle attractions and the excluded volume interactions. This is very different to the "vapour-liquid" behaviour exhibited by colloidal rod-like particles on addition of non-interacting polymer [217,218]. In polymer-colloid systems the polymer induces an effective attractive interaction (depletion force) between the colloids (that would otherwise only interact in a purely repulsive fashion) giving rise to a van der Waals-like "vapour-liquid" transition; this equivalent single component system of attractive colloids can be used to represent the phase behaviour of the mixture [33, 219] The phase diagram exhibited by PBLG in

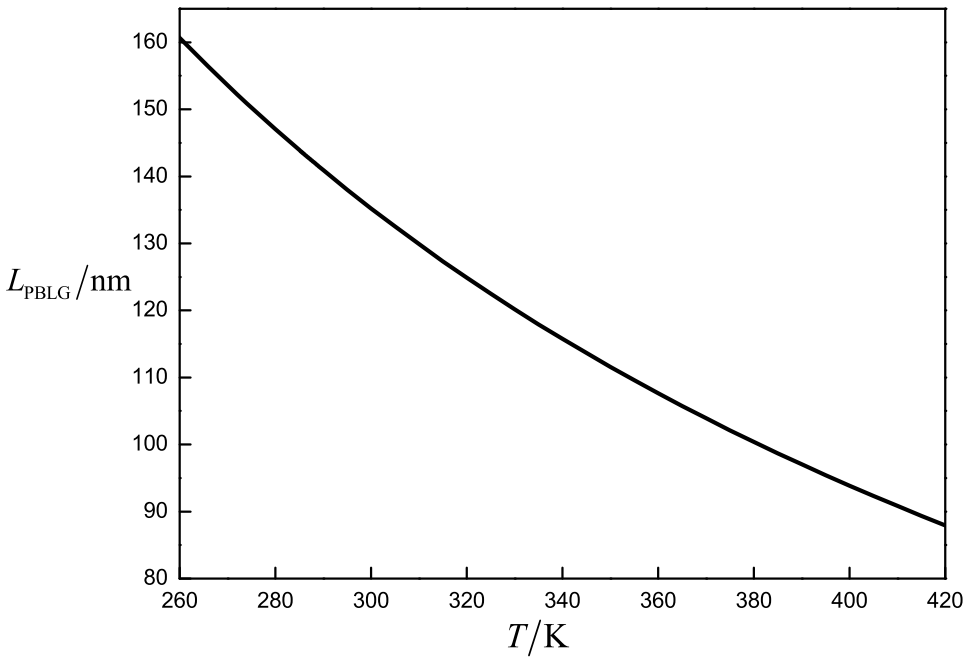

Figure 4.12: The temperature dependence of the apparent length of the PBLG rod (molecular weight $M_{\mathrm{w}} = 310,000$ g mol^{-1}) in DMF estimated using our van der Waals - Onsager approach (continuous curve) with a simple attractive hard spherocylinder model.

DMF is not a consequence of depletion interactions as the solvent is very small compared with the polypeptide and the behaviour is found to be very sensitive to the temperature of the system. This would suggest that both repulsive (excluded volume) and attractive interactions between the PBLG molecules are at play.

4.5 Conclusions

In this work, we present a theoretical framework for the description of attractive hard-spherocylinder fluids which serve as a basic model for thermotropic rod-like LC systems. The phase behaviour of prolate (spherocylinder) particles are described with a van der Waals - Onsager equation of state for the isotropic and nematic states. With the aid of the Onsager trial function to represent the orientation distribution in the nematic phase, the free energy is expressed in algebraic form and the functional variation of free energy then involves the derivative with respect to the Onsager orientational parameter α. Using this

approach, we calculate the phase diagrams of the systems of AHSC particles. The effect of the model parameters (molecular aspect ratio and strength of the isotropic/anisotropic attractive interactions) on the isotropic-nematic phase behaviour of these model attractive rods is examined in detail, and a particular emphasis is placed on the region of nematic-nematic coexistence.

The theory is applied to model the fluid phase behaviour and orientational order exhibited by solutions of the polypeptide PBLG which form rod-like structure in DMF. The PBLG macromolecules are represented as attractive rod-like particles (hard spherocylinders with an enveloping square well) with two temperature-dependent adjustable parameters: the aspect ratio of the hard-core and the well-depth of the square well. With our model one is able to faithfully reproduce the regions of isotropic-nematic coexistence as well as the more challenging nematic-nematic phase behaviour exhibited by the PBLG/DMF system. Though the effective shape of the PBLG rods obtained from our analysis is consistent with the experimental measurement, it should be recognized that our model is rather crude: the molecular flexibility is accounted for in an effective manner, and the attractive sphere enveloping the macromolecules is a highly coarse-grained representation of the specific long-range attractive interactions (e.g., surface charge, dipolar interactions, dispersion forces,etc.) present in the system.

An advantage of the perturbative methodology developed here is that it enables one to incorporate other relevant interactions into the model and construct a more realistic representation of the interactions. The Statistical Associating Fluid Theory (SAFT) and its variants [178, 180, 181, 220], which are based on more detailed information at the united atom molecular level, have been shown to provide an accurate description of fluid phase behaviour of complex fluids and fluid mixtures [179, 221]. The SAFT equation of state has recently been employed to develop coarse-grained force fields for direct use in molecular simulation [182–184]. In future work we plan to take advantage of these developments and improve our model and theoretical approach to provide a predictive platform for the the phase behaviour of thermotropic liquid crystals as well as the structures of corresponding anisotropic phases.

Chapter 5

Orientational ordering and phase behaviour of binary mixtures of hard spheres and hard spherocylinders

In this chapter, we present a Monte Carlo simulation study of the phase behaviour of binary mixtures of hard spherocylinders (HSCs) and hard spheres (HSs). Unlike the single component system of LCs studied in previous Chapters 2-4, this system is a general representation of LC systems and colloidal suspensions. We extend the Parsons-Lee and many-fluid approaches to the HSC-HS mixture and compare the theoretical descriptions with simulation results.

5.1 Introduction

Liquid crystalline phase transitions are observed experimentally in suspensions of colloidal particles such as vandium pentoxide (V_2O_5) [222], and Gibbsite ($Al(OH)_3$) [28,92], carbon nanotubes [223], and some biological systems such as protein fibers [6], tobacco mosaic virus [8], *fd*-virus [9–14], polypeptide solutions [19, 23], and DNA [16]. In order to describe the LC phase behaviour in these complex systems, some simple models of hard-core anisotropic particles have been examined [42]. Hard spherocylinders are models for rod-like LCs, exhibiting isotropic, nematic, smectic and solid phases which have been been confirmed by computer simulation [45,61,78]. The complete phase diagram of HSC has been

presented using free energy calculation technique [63, 224]. Some binary mixtures including HSC particles have also been studied, including rod-rod [12,13], rod-disc [117,225,226] and rod-sphere systems [72,227]. The rod-sphere mixtures are of particular interest due to the additional possibility of depletion forces, which can give rise to rich phase phenomena depending on the relative size ratio between rods and spheres [71, 227].

As has been mentioned earlier in the thesis a theoretical understanding of LC phase behaviour can be traced back to 1940. In his seminal work, Onsager [25] derived his simple density functional theory for the isotropic-nematic transition by truncating the virial expansion at the level of second virial coefficient. The equilibrium free energy can then be determined by functional variation of the free energy with respect to the orientational distribution function. Although Onsager's description is shown to be exact when the rods become infinitely long (because higher-order virial coefficients become negligible decaying as D/L [228]), the theory does not accurately describe the phase behaviour of rod-like system of intermediate values of L/D when higher-order virial contributions are neglected. Several attempts have been made to extend Onsager's theory by including the higher-order interactions. Recent progress in density functional theory [52, 85, 86, 229] can provide appropriate approaches to the predictions of thermodynamic properties of anisotropic fluids. A new free energy functional for inhomogeneous anisotropic fluids of arbitrary shape have been developed within the framework of fundamental-measure theory (FMT) which is based upon careful analysis of the geometry of the particles. Alternatively, the Parsons-Lee [89–91] approach provides a simple yet efficient way to incorporate the higher-order virial contributions which is neglected in Onsager's method. Parsons [89] proposed an approximation to decouple the orientational and translational degrees of freedom by mapping the properties of the rods to those of a reference hard-sphere (HS) system. Lee [90,91] approached the problem in a different way by introducing a scaling relation between virial coefficients of anisotropic particles and HS reference. Following two separate routes, Parsons and Lee reached the same expression for the free energy functional which is commonly known as the Parsons-Lee (PL) theory [45, 52, 92, 109, 141]. A straightforward extension of PL theory [73] to the mixtures is the one-fluid approximation whereby one maps the mixture on to an effective one-component HS system. A decoupling approximation is used in the PL approach in which the system is represented as the effective hard sphere of the same diameter while any information about the geometry of the LC particles is included in the term of the factorized excluded volumes. In order to improve the PL treatment for mixtures, a many-fluid (MF) approach has been proposed [112] where each component in

the mixtures are mapped on to the corresponding effective HS system separately, thus LC mixtures are represented as mixtures of HS. Following the separate routes of Parsons and of Lee, two versions of many-fluid theories can be developed: many-fluid Parsons (MFP) and many-fluid Lee (MPL) as alternatives for more accurate descriptions of LC mixtures. These many-fluid approaches have been assessed for a mixture of hard Gaussian particles and it has been shown that MFP is superior to the PL and MFL methods at moderate and high densities [112].

The focus of our current work is the isotropic-nematic phase behaviour of a HSC-HS mixture. Previous reports of the ordering in the HSC-HS binary system have been presented including direct simulation [72, 230, 231] and theoretical [69, 70, 73] studies. The work of Cuetos and coworkers is of particular relevance: the one-fluid PL approach [73] was used to study the isotropic-nematic phase diagram of the HSC-HS system characterized by rods of various lengths and diameters; comparisons where made with NPT Monte Carlo simulation [72] adopted to investigate the phase diagram and fluid structure of the mixtures. It is worth noting that in NPT ensemble the system composition remains constant overall, which will lead to an inadequate description of the phase boundary as one enters metastable states which would otherwise phase separate into phases of differing compositions.

The purpose of our current work is twofold. First, the many-fluid Parsons theory is used to describe the HS-HSC system and comparisons are made with the one-fluid Parsons-Lee approach. It should be noted that in a one-component case both approaches reduce to the standard Parsons-Lee theory. Second, we present new Monte Carlo simulation results for the mixture. The local density (packing fraction), local composition and orientational distribution are determined during the simulation to estimate the locations of the isotropic-nematic transitions of the mixture at various compositions in order to make a proper test of the accuracy of the two theories.

5.2 Theory of nematic phase in mixtures of hard particles

In this section, the main steps leading to a formulation with both one-fluid and many-fluid theories are briefly recalled; further details can be found in Ref. [112]. Consider a n-component mixture system of N hard anisotropic bodies in a volume V at a temperature T. The free energy functional of the system can expressed as a contribution from an ideal

(entropy) term (F^{id}) and a residual (configurational) part (F^{res}):

$$\frac{\beta F}{V} = \frac{\beta F^{\mathrm{id}}}{V} + \frac{\beta F^{\mathrm{res}}}{V}, \tag{5.1}$$

where $\beta = 1/(k_{\mathrm{B}}T)$ and k_{B} is the Boltzmann constant; the temperature plays a trivial role in this case since only hard repulsive interactions between particles are considered. The ideal free energy accounts for the translational and orientational entropy and can be written as

$$\frac{\beta F^{\mathrm{id}}}{V} = \sum_{i=1}^{n} \rho_i \left\{ \ln\left(\rho_i \mathcal{V}_i\right) - 1 + \sigma[f_i(\vec{\omega})] \right\}, \tag{5.2}$$

where $\rho_i = N_i/V$ ($N = \sum_{i=1}^{n} N_i$) is the number density of component i, $\rho = N/V = \sum_{i=1}^{n} \rho_i$, and $\mathcal{V}_i$ is the de Broglie volume of each species, incorporating the translational and rotational kinetic contributions of the ideal isotropic state. With the introduction of single-particle orientational distribution function $f_i(\vec{\omega})$, the orientational entropy term $\sigma[f_i]$ can be expressed as an integration over all orientations $\vec{\omega}$ of a single particle:

$$\sigma[f_i(\vec{\omega})] = \int \mathrm{d}\vec{\omega} f_i(\vec{\omega}) \ln[4\pi f_i(\vec{\omega})]. \tag{5.3}$$

For the residual part, Onsager's original expression [25] is equivalent to truncating the virial expansion at second-virial level which neglects the contributions from higher-order virial coefficients. However, the many-body correlations cannot be neglected at higher densities. Following Parsons's approach [89], we can include higher-body contributions in an approximate manner. Assuming a pairwise additive hard interaction $u_{ij}(r_{kl}, \vec{\omega}_k, \vec{\omega}_l)$ between particle k of i-th component and particle l of j-th component, the pressure of a fluid mixture of n components can be written in the virial form as

$$P = \rho k_{\mathrm{B}} T - \frac{1}{6V} \left\langle \sum_{i=1}^{n} \sum_{j=1}^{n} \sum_{k=1}^{N_i} \sum_{l=1, l\neq k}^{N_j} r_{kl} \frac{\partial u_{ij}(\vec{r}_{kl}, \vec{\omega}_k, \vec{\omega}_l)}{\partial r_{kl}} \right\rangle, \tag{5.4}$$

where $l \neq k$ is used to avoid self interactions and $\langle \cdots \rangle$ represents the ensemble average. In the canonical ensemble,

$$P = \rho k_{\mathrm{B}} T - \frac{Z^{-1}}{6V} \prod_{i=1}^{n} \int \mathrm{d}\vec{r}^{N_i} \int \mathrm{d}\vec{\omega}^{N_i} \sum_{i=1}^{n} \sum_{j=1}^{n} \sum_{k=1}^{N_i} \sum_{l=1, l\neq k}^{N_j} r_{kl} \frac{\partial u_{ij}(\vec{r}_{kl}, \vec{\omega}_k, \vec{\omega}_l)}{\partial r_{kl}} \exp(-\beta U) \tag{5.5}$$

where the configurational partition function Z is defined as

$$Z = \prod_{i=1}^{n} \int \mathrm{d}\vec{r}^{N_i} \int \mathrm{d}\vec{\omega}^{N_i} \exp(-\beta U(\vec{r}^{N_i}, \vec{\omega}^{N_i})), \tag{5.6}$$

and the total configurational energy is given by

$$U(\vec{r}^{N_i}, \vec{\omega}^{N_i}) = \frac{1}{2}\sum_{i=1}^{n}\sum_{j=1}^{n}\sum_{k=1}^{N_i}\sum_{l=1,l\neq k}^{N_j} u_{ij}(\vec{r}_{kl}, \vec{\omega_k}, \vec{\omega_l}). \tag{5.7}$$

The canonical pair distribution function is defined as

$$g_{ij}(\vec{r}_{12}, \vec{\omega_1}, \vec{\omega_2}) = \frac{N_i(N_j - \delta_{ij})}{\rho_i f_i(\vec{\omega}_1)\rho_j f_j(\vec{\omega}_2)} Z^{-1} \int \mathrm{d}\vec{r}^{N-2} \int \mathrm{d}\vec{\omega}^{N-2} \exp(-\beta U(\vec{r}^{N_i}, \vec{\omega}^{N_i})), \tag{5.8}$$

where δ_{ij} is the Kronecker delta. On integrating Equation (5.5), the expression for pressure can be written in a compact form:

$$\begin{aligned} P &= \rho k_\mathrm{B} T - \frac{1}{6}\sum_{i=1}^{n}\sum_{j=1}^{n}\rho_i\rho_j \int \mathrm{d}\vec{r}_{12} \int \mathrm{d}\vec{\omega}_1 \int \mathrm{d}\vec{\omega}_2 \\ &\times r_{12}\frac{\partial u_{ij}(\vec{r}_{12}, \vec{\omega_1}, \vec{\omega_2})}{\partial r_{12}} g_{ij}(\vec{r}_{12}, \vec{\omega_1}, \vec{\omega_2}) f_i(\vec{\omega}_1) f_j(\vec{\omega}_2). \end{aligned} \tag{5.9}$$

Following the Parsons approach, the interparticle separation $\vec{r}_{12}$ is given in terms of the contact distance $\sigma_{ij}(\vec{r}_{12}, \vec{\omega_1}, \vec{\omega_2})$ by defining a scaled distance $y_{ij} = r_{12}/\sigma_{ij}(\vec{r}_{12}, \vec{\omega_1}, \vec{\omega_2})$. The scaled distance does not explicitly depend on the orientations of the two particles and $y_{ij} = 1$ corresponds to contact value. Using the definition of y_{ij}, the pair distribution function (cf. Equation (5.8)) can be expressed as a function of scaled distance y_{ij}, $g_{ij}(y)$, which decouples the positional and orientational dependencies. In this way, a complicated pair potential u_{ij} is mapped onto the spherically symmetrical hard-sphere potential:

$$u_{ij}(\vec{r}_{12}, \vec{\omega_1}, \vec{\omega_2}) = u_{ij}(y) = \begin{cases} \infty & y < 1 \\ 0 & y \geq 1, \end{cases} \tag{5.10}$$

and the expression for the pressure becomes

$$\begin{aligned} P &= \rho k_\mathrm{B} T - \frac{1}{6}\sum_{i=1}^{n}\sum_{j=1}^{n}\rho_i\rho_j \int \mathrm{d}y_{ij} y_{ij}^3 \frac{\mathrm{d}u_{ij}}{\mathrm{d}y_{ij}} g_{ij}(y) \\ &\quad \times \int \mathrm{d}\hat{r}_{12} \int \mathrm{d}\vec{\omega}_1 \int \mathrm{d}\vec{\omega}_2 f_i(\vec{\omega}_1) f_j(\vec{\omega}_2) \sigma_{ij}^3(\hat{r}_{12}, \vec{\omega_1}, \vec{\omega_2}) \\ &= \rho k_\mathrm{B} T - \frac{1}{2}\sum_{i=1}^{n}\sum_{j=1}^{n}\rho_i\rho_j \int \mathrm{d}y_{ij} y_{ij}^3 \frac{\mathrm{d}u_{ij}}{y_{ij}} g_{ij}(y) \\ &\quad \times \int \mathrm{d}\vec{\omega}_1 \int \mathrm{d}\vec{\omega}_2 f_i(\vec{\omega}_1) f_j(\vec{\omega}_2) V_{ij}^{\mathrm{exc}}(\vec{\omega_1}, \vec{\omega_2}) \end{aligned} \tag{5.11}$$

where the excluded volume between a pair of particles is defined as $V_{ij}^{\mathrm{exc}}(\vec{\omega_1}, \vec{\omega_2}) = \frac{1}{3}\int \mathrm{d}\hat{r}_{12}\sigma_{ij}^3(\hat{r}_{12}, \vec{\omega_1}, \vec{\omega_2})$ and $\hat{r}_{12} = \vec{r}_{12}/r_{12}$. The form of hard repulsive pair interaction is a step function (cf. Equation (5.10)), thus $\beta \mathrm{d}u_{ij}/\mathrm{d}y_{ij} = -\exp(\beta u_{ij})\delta(y_{ij} - 1)$ [232].

Integrating over the scaled variable y_{ij} and noting that $u_{1^+}(y) = 0$ when $y = 1$, we then obtain

$$P = \rho k_{\mathrm{B}} T + \frac{1}{2} \sum_{i=1}^{n} \sum_{j=1}^{n} \rho_i \rho_j g_{ij}^{\mathrm{HS}}(1^+) \int \mathrm{d}\vec{\omega}_1 \int \mathrm{d}\vec{\omega}_2 f_i(\vec{\omega}_1) f_j(\vec{\omega}_2) V_{ij}^{\mathrm{exc}}(\vec{\omega_1}, \vec{\omega_2}), \tag{5.12}$$

where $g_{ij}(1^+) \approx g_{ij}^{\mathrm{HS}}(1^+)$ has been approximated as the corresponding hard-sphere contact value of pair distribution function.

The residual free energy can then be obtained from the formal thermodynamic definition $(\partial F/\partial V)_{NT} = -P$ by integrating Equation (5.12) over the volume:

$$\frac{\beta F^{\mathrm{res}}}{V} = \frac{1}{2} \sum_{i=1}^{n} \sum_{j=1}^{n} \rho_i \rho_j G_{ij} \int \mathrm{d}\vec{\omega}_1 \int \mathrm{d}\vec{\omega}_2 f_i(\vec{\omega}_1) f_j(\vec{\omega}_2) V_{ij}^{\mathrm{exc}}(\vec{\omega_1}, \vec{\omega_2}), \tag{5.13}$$

where $G_{ij} = \rho^{-1} \int_0^{\rho} \mathrm{d}\rho' g_{ij}^{\mathrm{HS}}(1^+)$. Within this notation, Onsager's second-virial theory can be recovered with $G_{ij} = 1$ (i.e., $g_{ij}^{\mathrm{HS}}(1^+) = 1$) corresponding to the low-density limit.

In this way, the theory of Parsons for a one-component fluid can be reformulated to describe a n-component mixtures of anisotropic bodies. As shown in Ref. [112], the standard [73] "one-fluid" approach corresponds to $G_{ij} = G^{\mathrm{PL}}$, where $G^{\mathrm{PL}} = \rho^{-1} \int_0^{\rho} \mathrm{d}\rho' g_{\mathrm{CS}}^{\mathrm{HS}}(1^+)$, given in terms of the Carnahan-Starling form of the radial distribution function at contact [50,95],

$$g_{\mathrm{CS}}^{\mathrm{HS}}(1^+) = \frac{1 - \eta/2}{(1-\eta)^3}, \tag{5.14}$$

with $\eta = \sum_{i=1}^{n} \rho_i V_{\mathrm{m},i}$, and $V_{\mathrm{m},i}$ is the volume of the i-th species. The Parsons-Lee residual free energy can then be expressed as

$$\frac{\beta F^{\mathrm{res,PL}}}{V} = \frac{\rho^2}{8} \frac{4 - 3\eta}{(1-\eta)^3} \sum_{i=1}^{n} \sum_{j=1}^{n} x_i x_j \int \mathrm{d}\vec{\omega}_1 \int \mathrm{d}\vec{\omega}_2 f_i(\vec{\omega}_1) f_j(\vec{\omega}_2) V_{ij}^{\mathrm{exc}}(\vec{\omega_1}, \vec{\omega_2}), \tag{5.15}$$

Alternatively, in developing the many-fluid theory proposed in Ref. [112] one treats the size (volume) of each species individually, i.e.,

$$V_{\mathrm{m},i} = V_{\mathrm{HS},i} = \frac{\pi}{6} \sigma_i, \quad i = 1, 2, \cdots, n. \tag{5.16}$$

An expression for the contact value of the distribution function for hard sphere mixture is given by Boublik [233]:

$$g_{ij,\mathrm{B}}^{\mathrm{HS,Mix}}(1^+) = \frac{1}{1-\zeta_3} + \frac{3\zeta_2}{(1-\zeta_3)^2} \frac{\sigma_{ii}\sigma_{jj}}{\sigma_{ii} + \sigma_{jj}} + \frac{2\zeta_2^2}{(1-\zeta_3)^3} \frac{(\sigma_{ii}\sigma_{jj})^2}{(\sigma_{ii} + \sigma_{jj})^2} \tag{5.17}$$

where the moments of the density are defined as $\zeta_\alpha = (\pi/6) \sum_{i=1}^{n} \rho_i \sigma_{ii}^{\alpha}, \quad \alpha = 0, 1, 2, 3.$ Combining Equations (5.13) and (5.17) and noting the separate definition of G_{ij} for each

$i-j$ pair, one obtains the many-fluid Parsons (MFP) form of the residual free energy $F^{\text{res,MFP}}$.

In the one-component limit the contact value of the radial distribution function of the HS mixture (Equation (5.17)) reduces to the Carnahan-Starling expression (cf. Equation(5.14)). Thereby, the MFP approach yields same descriptions as PL treatment for the pure-component systems. In the standard extension of the PL theory to mixtures one therefore adopts a van der Waals one-fluid (VDW1) approximation using an equivalent hard-sphere system with the effective diameter given by the VDW1 mixing rule to represent the anisotropic mixtures. In contrast to the PL approach, each component is represented as a separate effective hard-sphere component, so that the excluded volume between a pair of i-th component and j-th component is weighted by the corresponding contact value of the HS mixture, g_{ij}^{HS} . The equilibrium free energy of the system is determined from a functional variation with respect to the orientational distribution function $f_i(\vec{\omega})$ of each component which leads to an integral equation for $f_i(\vec{\omega})$. The set of integral equations are solved numerically using an iterative procedure, details of which can be found in Ref. [112].

In this work, we assess the adequacy of many-body theories such as the MFP for a binary mixture of hard spheres (HSs) and hard spherocylinders (HSCs). The modles are depicted in Figure 5.1: the aspect ratio of the HSC is $L/D = 5$ and the diameter of the HS is taken to be the same as the diameter of the HSC, i.e., $\sigma = D$. The excluded volumes

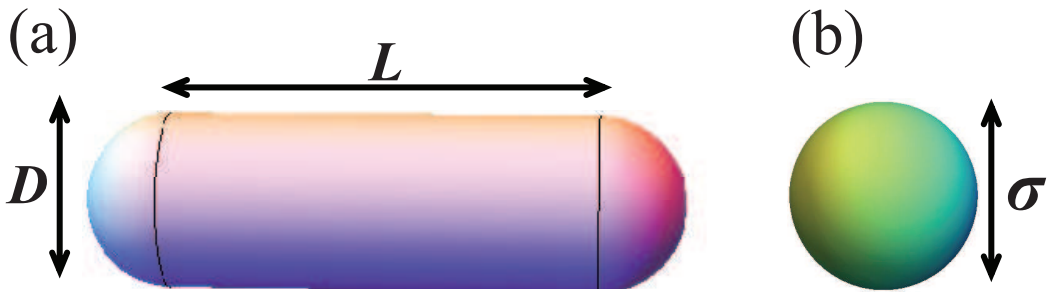

Figure 5.1: The hard-core models: (a) hard spherocylinder (HSC) of length L and diameter D; and (b) hard sphere (HS) of diameter σ. In the current study, the length of the HSC is fixed to $L = 5D$ and the diameter of the HS is the same value as that of the HSC, i.e., $\sigma = D$.

corresponding to the HSC-HSC, HSC-HS and HS-HS interactions are given as

$$\begin{aligned} V^{\rm exc}_{\rm HSC-HSC} &= \frac{4}{3}\pi D^3 + 2\pi L D^2 + 2L^2 D|\sin\gamma| \\ V^{\rm exc}_{\rm HSC-HS} &= \frac{\pi}{6}(D+\sigma)^3 + \frac{\pi}{4}L(D+\sigma)^2 \\ V^{\rm exc}_{\rm HS-HS} &= \frac{4}{3}\pi\sigma^3. \end{aligned} \tag{5.18}$$

where $\gamma = \arccos(\vec{\omega}_1 \cdot \vec{\omega}_2)$ is the relative orientation of the two HSC particles. The total excluded volume of the mixture is $V^{\rm exc} = x^2_{\rm HSC} V^{\rm exc}_{\rm HSC-HSC} + 2x_{\rm HSC}x_{\rm HS}V^{\rm exc}_{\rm HSC-HS} + x^2_{\rm HS}V^{\rm exc}_{\rm HS-HS}$ where $x_{\rm HS}$ and $x_{\rm HSC}$ are mole fractions of HS and HSC species, respectively. Since the HSC particles are the anisotropic component in the system, $f(\vec{\omega})$ is used to describe the orientation distribution of the HSC rods which is related to the nematic order parameter S_2 of the system through

$$S_2 = \int {\rm d}\vec{\omega} f(\vec{\omega}) \left(1 - \frac{3}{2}\sin^2\gamma\right). \tag{5.19}$$

In particular, $S_2 = 0$ corresponds to the isotropic state and $S_2 = 1$ for a perfectly-aligned nematic phase.

5.3 Monte Carlo simulation of phase coexistence in mixtures of hard spheres and hard spherocylinders

A common approach to studying fluid phase separation by molecular simulation is a direct procedure whereby the two coexisting phases are treated simultaneously in the presence of an interface with the usually periodic boundary conditions [234, 235]. The stabilization of a fluid interface corresponding to a system with a nonuniform density within a single simulation box is relatively straightforward with either molecular dynamics (MD) or Monte Carlo (MC) techniques. This was first demonstrated by Croxton and Ferrier [236] who performed MD simulations of the vapor-liquid interface of a Lennard-Jones system in two dimensions, and shortly afterwards by Leamy et al. [237] who stabilized the interface of a three-dimensional lattice gas (Ising moded) by MC simulation. For a system which is sufficiently large one can simultaneously examine the bulk properties, in the central region of the coexisting phases, and the properties in the surface region.

The direct molecular simulation of the isotropic-nematic (I-N) phase transition in mixtures of hard spheres and hard spherocylinders is particularly challenging because of the very low interfacial tension between the two phases; for example, the I-N interfacial tension of a hard-core system of for thin disc-like particles has be estimated to be a few tenth of $k_{\rm B}T$

in units of the particle's area [135]. As a consequence there is a very low energetic penalty to the deformation of the interface in such systems leading to large interfacial fluctuations with the interface moving within the simulation cell with little hindrance. The location of the bulk coexistence regions and the determination of the density and compositional profiles becomes a difficult task as a result. In order to break the symmetry of the system and reduce the effect of the interfacial fluctuations one can introduce an external field by placing the system within structureless hard walls; this corresponds to removing the periodicity in one dimension (say the z direction). An issue with this type of approach is that large systems have to be considered in order to study the true bulk phase behaviour and avoid capillary effects. By keeping the separation between the walls large compared to the dimensions of the particles, one can simulate the phase coexistence in the hard-core HS-HSC mixtures with minimal effect from the hard surfaces.

An appropriate ensemble for a system with planar surfaces is one where the component P_N of the pressure tensor normal to the surface is kept constant, so that the condition of mechanical equilibria is satisfied within the entire simulation cell [74, 232, 238]. There are advantages in employing the $NP_{\mathrm{N}}T$ ensemble to study the bulk properties of the HSC-HS mixture. A popular direct MC method for the simulation of the fluid phase equilibria of mixtures is Gibbs ensemble technqiues [234, 235] in which the coexisting phase are retained in separate boxes and coupled volume changes and particles exchanges between the boxes are undertaken to meet the requirements of mechanical and chemical equilibria. In the case of hard anisometric particles, the acceptance ratio for the insertion of anisotropic particles will be very low, particularly at the high densities of the dense anisotropic phases of interest, requiring an impracticably large number of trial insertions for a proper equilibration of the system [239]. A conventional simulation of the system within a single box will partially solve the problem since trial insertions of the particles are no longer required. There is however a complication with the simulation of bulk phase equilibria of mixtures with a single simulation cell: though the phase transition between the various states can be traced as for a pure component system, the overall composition remains fixed preventing the fractionation of the different species in the various phases. There is therefore an added advantage of simulating the phase separation of mixtures by simultaneously considering the coexisting phases and the interface in a single cell as this will allow for inhomogeneities in both the density and the composition of the system. By introducing an external field such as a hard surface one is able to examine both the bulk and interfacial regions of mixtures of hard core particles without constraining the density

or composition of the individual bulk phases.

We perform constant normal-pressure Monte Carlo simulation ($NP_{\mathrm{N}}T$-MC) for a system of $N_{\mathrm{HSC}} = 1482$ HSC particles of the aspect ratio $L/D = 5$ where the number of hard spheres is varied depending on mole fraction of the binary mixture $x_{\mathrm{HS,tot}} = N_{\mathrm{HS}}/(N_{\mathrm{HS}} + N_{\mathrm{HSC}})$. In this system, the intermolecular potential between any two particles is restricted to a pure repulsion. The simulation cell is shown in Figure 5.2, the system is a rectangular box of dimension $L_x = L_y = 25D$ (corresponding to a fixed surface area in the $x - y$ plane of $625D^2$) and L_z varies according to the value set for P_{N}. The parallel hard walls are positioned at $z = 0$ and $z = L_z$ and standard periodic boundary conditions are applied in x and y directions. Since a fixed normal pressure is imposed along the z axis, the system volume in our $NP_{\mathrm{N}}T$-MC simulation is allowed to fluctuate by scaling the length of the z axis which moves the walls closer together or farther apart, while the system dimensions of the x and y axes and the $x - y$ surface area are kept fixed.

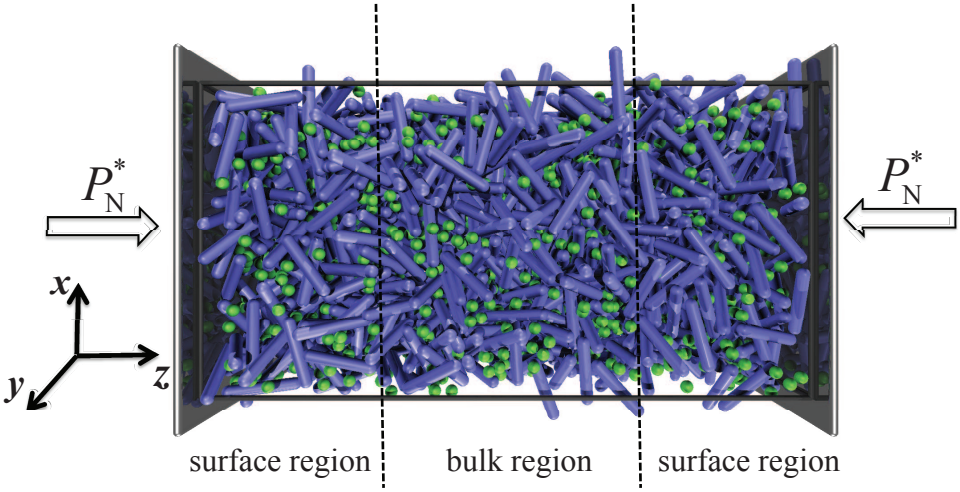

Figure 5.2: The $NP_{\mathrm{N}}T$-MC simulation cell: hard walls are placed along the z axis and the cell is divided into three large bins: two surface regions close to the hard walls and a bulk region in the central part of the cell. A fixed normal pressure is imposed and the dimension of the system is allowed to fluctuate in the z direction. In this example a mixture system of hard spherocylinders (purple rods) and hard spheres (green spheres) is depicted.

The $NP_{\mathrm{N}}T$-MC simulation of the HSC-HS mixture is performed for 5×10^6 cycles to equilibrate the system and 5 to 8×10^6 cycles to obtain the average properties. Each MC cycles consist of N (N again being the total number of particles in the system) attempts to displace and rotate randomly chosen particles and one trial volume change corresponding to a contraction or extension in the z direction. The breaking of symmetry caused

by the hard walls leads to inhomogeneous positional, orientational, and compositional distributions of the system along the z-axis, so that the thermodynamic and structural properties have to be determined locally. Smooth density and composition profiles are required to identify the uniform region in the centre of the box which correspond to the bulk phase. In order to evaluate the packing fraction ($\eta_i(z)$), composition ($x_{\rm HS}(z)$), and order parameter ($S_2(z)$) profiles, the simulation box is divided into several bins of equal width δz in the z direction; $n_{\rm bin} = 200$ are used to calculate the packing fraction profile $\eta_i(z) = \rho_i(z)V_{{\rm m},i}, i = {\rm HS, HSC}$, where the number density profile of the component i is obtained from

$$\rho_i(z) = \frac{< N_i >}{L_x L_y \delta z} \qquad i = {\rm HS, HSC} \tag{5.20}$$

and the local composition is then obtained as $x_{\rm HS}(z) = \rho_{\rm HS}(z)/(\rho_{\rm HS}(z) + \rho_{\rm HSC}(z))$. The packing fraction $\eta_{\rm b}$ and composition $x_{\rm HS,b}$ of the bulk phase is then determined to be the values corresponding to the uniform regions of the packing fraction and composition profiles in the centre of the simulation cell.

The nematic order parameter profile S_2 is obtained by determining the local nematic order parameter tensor $\mathbf{Q}(j)$ in each bin j:

$$\mathbf{Q}(j) = \left\langle \frac{1}{2N_{{\rm HSC},j}} \sum_{i=1}^{N_{{\rm HSC},j}} (3\vec{\omega}_i \bullet \vec{\omega}_i - \mathbf{1}) \right\rangle \tag{5.21}$$

where $N_{{\rm HSC},j}$ is the number of HSC particles in the j-th bin and $\mathbf{1}$ is the unit matrix. On diagonalising the tensor $\mathbf{Q}(j)$, three eigenvalues can be obtained and the largest eigenvalue defines the local nematic order parameter $S_2(z)$ of the j-th bin. Special care is required in calculating the order parameter profile because of finite-size effects. It has been shown by Eppenga and Frenkel [46] that the value of the nematic order parameter depends on the number of particles considered and the error in local order parameter is $\sim 1/(\sqrt{N_{\rm HSC}/n_{\rm bin}})$. If we use $n_{\rm bin} = 200$ which is the same number of bins used for density profile, there are on average only $7(\approx 1482/200)$ rods in each bin and the expected error in $S_2(z)$ of ~ 0.367 is large. Richter and Gruhn [240] have employed a methodology to correct for finite-size effects by introducing a function which bridges $S_{2,N_{\rm HSC}\to\infty}(z)$ and $S_{2,N_{\rm HSC}}(z)$ by correlating the simulation data. A more direct way [74] to reduce the error in the local nematic order parameter is to examine a larger system; for example, in the case of a system of 14820 rods (an order of magnitude larger than the system studied here) and 200 bins reduces the error in $S_2(z)$ to ~ 0.11. However, the simulation of a system of this size is very computationally expensive. As in our current work the focus is the

bulk phase behaviour not the interfacial region, we divide the system into 3 large bins: 2 surface regions adjacent to the hard walls and the bulk region (cf. Figure 5.2). With $n_{\rm bin} = 3$ system-size error in $S_2(z)$ decreases to ~ 0.04 where there are now an average of 500 rods in each bin. The value of $S_2(z)$ corresponding to the central region is then taken to represent the nematic order parameter of the bulk phase $S_{2,\rm b}$. The reduced normal pressure is defined as $P^*_{\rm N} = P_{\rm N} D/k_{\rm B}T$.

5.4 Results and discussion

5.4.1 Pure hard spherocylinders

We begin by studying a system of pure HSC particles with aspect ratio of $L/D = 5$. As is well known, the simple HSC model of a mesogen exhibits isotropic, nematic, smectic-A, and solid phases as the density of the system is increased [45, 61–63, 78, 228, 241, 242]. As an preliminary assessment we demonstrate that the bulk isotropic-nematic transition for the $L/D = 5$ HSC system contained between well separated parallel hard surfaces simulated using our NP_NT-MC methodology is essentially unaffected by the external field. The bulk phase behaviour for the homogeneous system obtained using conventional constant pressure NPT-MC with full three dimensional periodic boundary conditions [45] is compared with the corresponding data obtained using the constant normal-pressure $NP_{\rm N}T$-MC methodology for the system between parallel hard surfaces in Figure 5.4 and corresponding simulation data is reported in Table 5.1).

The predictions of the isotropic and nematic branches with the MFP theory [112] is also shown in Figure 5.4 which reduces to the commonly employed PL theory [89–91] for one-component system: the theory is seen to provide a reasonably quantitative description of the isotropic and nematic branches of the equation of state and the position of the isotropic-nematic transition. We can infer that the results obtained for the HSC particles contained between the parallel hard surfaces are fully consistent with those of the fully periodic homogeneous system, confirming that at least for this system size and geometry of the simulation cell the presence of hard surfaces only has a small (stabilizing) effect on the isotropic-nematic transition; in this case the separation between the surfaces, which defines the dimension the box in the z direction, ranges from $L_z = 899.85D$ at the lowest density ($P^*_{\rm N} = 0.001$) studied to $L_z = 23.57D$ for the highest density ($P^*_{\rm N} = 1.26$) nematic state. Example of the packing fraction (density) profiles $\eta(z)$ obtained for a low-density isotropic state, an intermediate-density nematic state, and a moderately high-density nematic state

Table 5.1: Constant normal-pressure MC ($NP_{\mathrm{N}}T$-MC) simulation results for bulk isotropic-nematic phase behaviour of hard spherocylinders with an aspect ratio $L/D = 5$. The reduced normal pressure P^*_{N} is set in the simulation and corresponding bulk values of packing fraction (η_{b}) and nematic order parameter ($S_{2,\mathrm{b}}$) are obtained as configurational averages. The isotropic phase is denoted by Iso, the nematic by Nem, the pretransitional states (Pre) are considered to be metastable.

P^*_{N}	η_{b}	$S_{2,\mathrm{b}}$	L_z/D	Phase
0.001	0.004	0.042	899.85	Iso
0.003	0.011	0.042	881.84	Iso
0.005	0.018	0.042	562.67	Iso
0.01	0.031	0.042	327.44	Iso
0.02	0.057	0.043	183.67	Iso
0.05	0.098	0.045	105.10	Iso
0.10	0.144	0.046	71.12	Iso
0.20	0.199	0.049	51.17	Iso
0.30	0.235	0.053	43.39	Iso
0.40	0.271	0.056	38.84	Iso
0.50	0.300	0.067	35.12	Iso
0.60	0.318	0.072	32.81	Iso
0.70	0.340	0.074	30.85	Iso
0.80	0.348	0.085	29.23	Iso
0.90	0.372	0.099	27.68	Iso
1.00	0.386	0.116	26.75	Iso
1.10	0.397	0.371	25.40	Pre
1.12	0.401	0.456	25.18	Pre
1.14	0.419	0.553	24.88	Nem
1.16	0.420	0.555	24.82	Nem
1.18	0.425	0.570	24.61	Nem
1.20	0.433	0.619	24.22	Nem
1.22	0.434	0.692	23.95	Nem
1.24	0.435	0.727	23.73	Nem
1.26	0.443	0.739	23.57	Nem

are displayed in Figure 5.3; the flat part of the profiles correspond to the homogenous bulk phases in the central region of the simulation cell which allows one to determine the equilibrium bulk density with confidence. Significant structure is also apparent close to the surfaces but a full analysis of the surface effects such as wetting, de-wetting, surface nematization, and adsorption will be left for the following chapter.

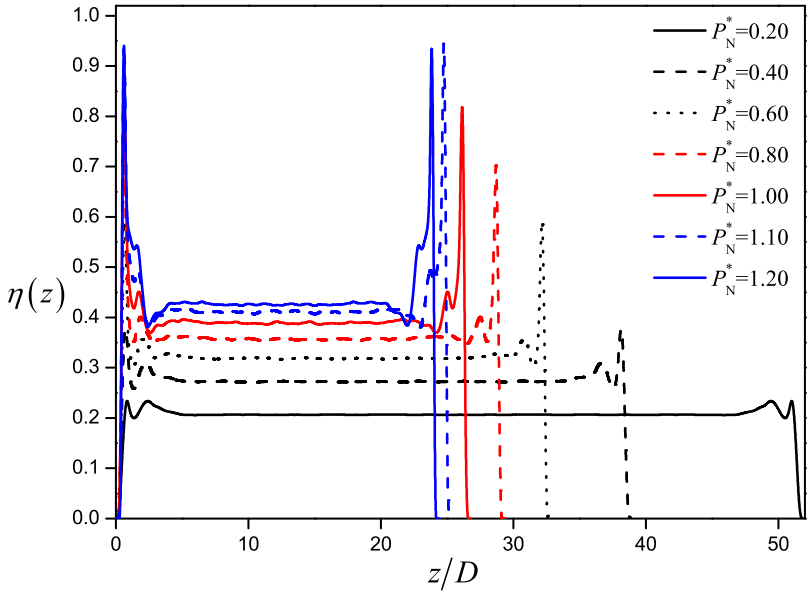

Figure 5.3: Packing fraction profile $\eta(z)$ for pure HSC with normal pressure $P_{\mathrm{N}}^{*} = 0.2 - 1.2$ obtained using $NP_{\mathrm{N}}T$-MC. Two hard walls are positioned at $z = 0$ and $z = L_z$ where L_z is the length of the z axis.

In order to estimate the location of the bulk isotropic-nematic bulk phase transition, we examine the density dependence of the nematic order parameter in Figure 5.5. The order parameter of a finite system $S_{2,N_{\mathrm{HSC}}}(z)$ converges quickly to the limiting bulk thermodynamic value $S_{2,N_{\mathrm{HSC}}\to\infty}(z)$ for states with intermediate to high orientational order. In Figure 5.6 we display the order parameter profiles for states of low to moderate orientational order in the close vicinity of the isotopic-nematic transition. Snapshots of typical configurations of these two states are shown in Figure 5.7: the low density configuration corresponds to an bulk isotropic state, the intermediate density configuration to a pre-transitional metastable state, while the higher density configuration has clearly undergone a transition to a bulk nematic phase.

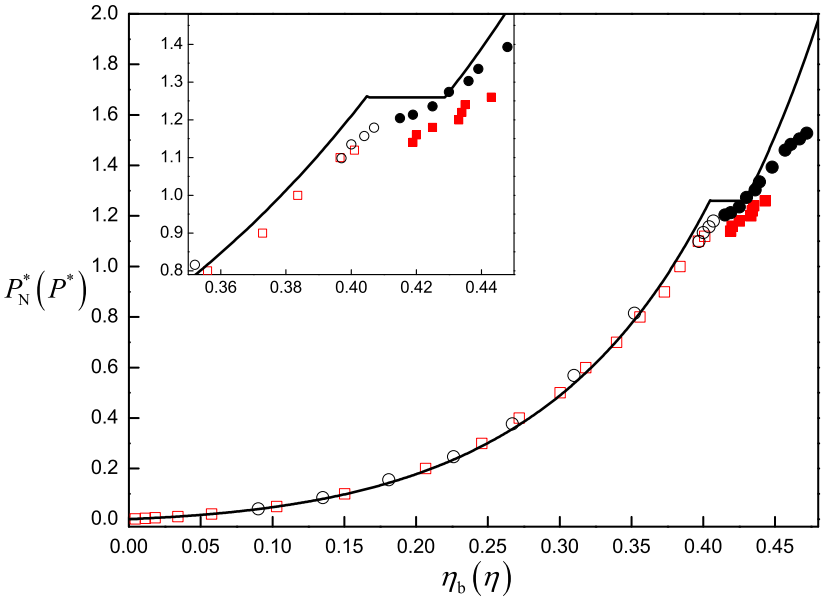

Figure 5.4: The isotropic-nematic phase behaviour of hard-spherocylinder (HSC) rods with an aspect ratio of $L/D = 5$. The simulation data obtained for the system of $N = 1482$ particles contained between parallel hard surfaces using our $NP_{\mathrm{N}}T$-MC approach (squares), where $P_{\mathrm{N}}^* = P_N D^3/(k_{\mathrm{B}}T)$ is the dimensionless normal pressure and $\eta_{\mathrm{b}} = \rho_{\mathrm{b}} V_{\mathrm{HSC}}$ is the bulk value of the packing fraction in the central region of the cell, are compared with the corresponding simulation data obtained for the fully periodic system using the conventional NPT-MC approach (circles) [45], where now $P^* = P/(k_{\mathrm{B}}T)$ and $\eta = \rho V_{HSC}$ are the values for the homogeneous system. The empty symbols correspond to the isotropic states and the filled symbols to the nematic states. The curve correspondes to the theoretical predictions obtained with the PL theory. An enlargement of the isotropic-nematic transition region is shown in the inset.

The discrepancy between the values of the nematic order parameter obtained for profiles with $n_{\mathrm{bin}} = 3$ and $n_{\mathrm{bin}} = 20$ histogram bins in the z direction is very small so that the size effects are expected to be small in this case. An isotropic bulk phase region is clearly found in the case of the state with a pressure of $P_{\mathrm{N}}^* = 1.00$; in this case the orientational order in the bulk region is found to be low corresponding to an nematic order parameter of $S_{2,b}$ 0.11. The order parameter profile for the pre-transitional state with a normal pressure of $P_{\mathrm{N}}^* = 1.12$ exhibits a "V"-shaped curve with no uniform bulk region; the average of the

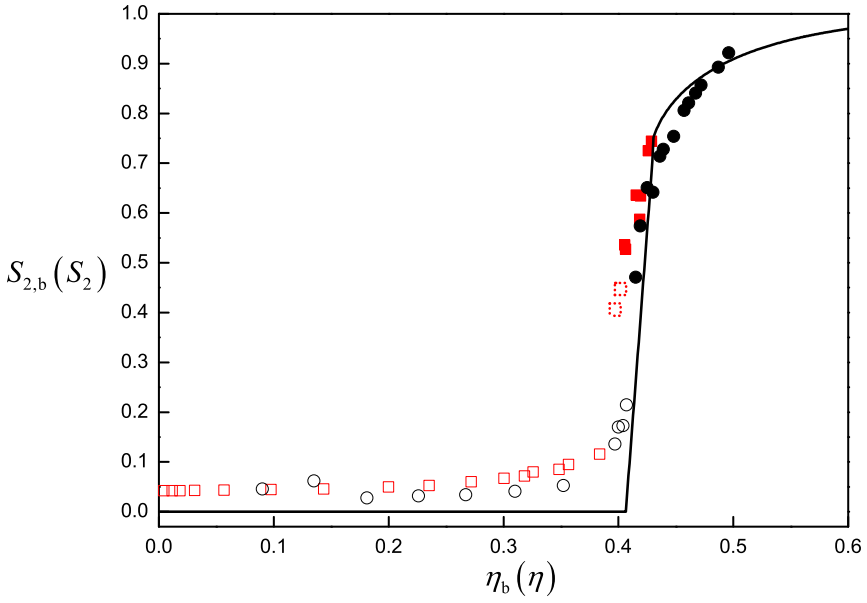

Figure 5.5: The density dependence of the bulk nematic order parameter $S_{2,\mathrm{b}}$ for hard spherocylinder (HSC) rods with aspect ratio $L/D = 5$. The simulation data obtained for the system of $N = 1482$ particles contained between parallel hard surfaces using our $NP_{\mathrm{N}}T$-MC approach (squares), where $S_{2,\mathrm{b}}$ is the bulk value of the nematic order parameter and $\eta_{\mathrm{b}} = \rho_{\mathrm{b}} V_{\mathrm{HSC}}$ is the bulk value of the packing fraction in the central region of the cell, are compared with the corresponding simulation data obtained for the fully periodic system using the conventional NPT-MC approach (circles) [45], where now S_2 and $\eta = \rho V_{HSC}$ are the values for the homogeneous system. The empty symbols correspond to the isotropic states and the filled symbols to the nematic states and the dashed squares represents the metastable states in the vicinity of isotropic-nematic transition. The curve is the theoretical predictions obtained with the PL theory.

nematic order parameter of $S_{2,\mathrm{b}} = 0.456$ obtained in the central part of the cell does not therefore represent that of a true bulk phase. In the case of the denser state corresponding to $P_{\mathrm{N}}^{*} = 1.14$, the value of the bulk nematic order parameter $S_{2,\mathrm{b}} = 0.553$ obtained as an average over $n_{\mathrm{bin}} = 3$ bins is essentially equivalent to the value of $S_{2,\mathrm{b}} = 0.556$ obtained with $n_{\mathrm{bin}} = 20$ bins in the homogeneous central region of the simulation cell. The difference in the orientational ordering for the states corresponding to normal pressures of $P_{\mathrm{N}}^{*} = 1.12$ and $P_{\mathrm{N}}^{*} = 1.14$ is also apparent from Figure 5.7 where the orientations of HSC rods have

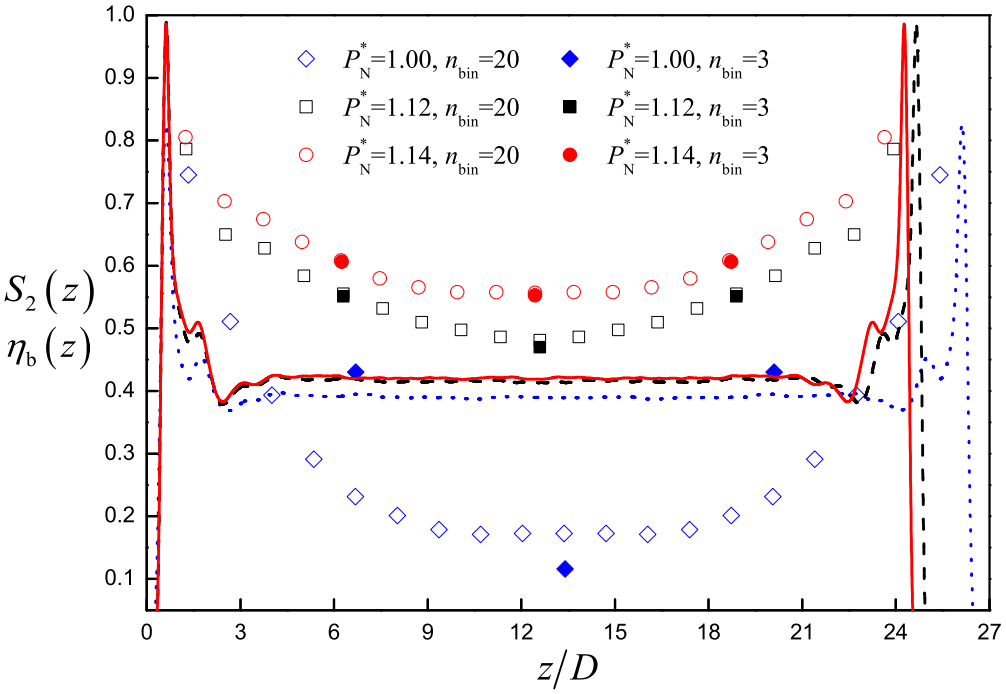

Figure 5.6: The nematic order parameter $S_2(z)$ (symbols) and packing fraction $\eta(z)$ (curves) profiles for hard-spherocylinder (HSC) rods with an aspect ratio of $L/D = 5$ obtained by simulating the system of $N = 1482$ particles between parallel hard surfaces places along the z direction. Isotropic ($P_N^* = 1.00$), metastable ($P_N^* = 1.12$), and nematic ($P_N^* = 1.14$) states in the vicinity of the isotropic-nematic transition are examined; the thermodynamic state is characterized by the value of the normal pressure tensor, $P_N^* = P_N D^3/(k_B T)$. In the case of $S_2(z)$ the profiles are constructed from histograms with $n_{bin} = 3$ and $n_{bin} = 20$ to assess possible system size effects. The dotted (blue) curve corresponds to the $\eta(z)$ profile for the isotropic ($P_N^* = 1.00$) state, the dashed (black) curve that for the metastable state($P_N^* = 1.12$), and the continuous (red) curve that for the nematic ($P_N^* = 1.14$) state.

been colourly coded to aid the visualization. Clearly, the equilibrium state at the pressure

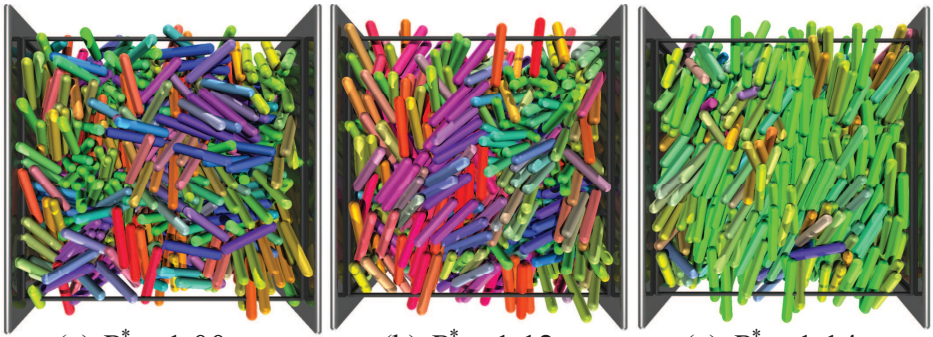

Figure 5.7: Snapshots of typical configurations of hard-spherocylinder (HSC) rods with an aspect ratio of $L/D = 5$ obtained by simulating the system between parallel hard surfaces places along the z axis. a) Isotropic ($P_N^* = 1.00$), b) metastable ($P_N^* = 1.12$), and c) nematic ($P_N^* = 1.14$) states in the vicinity of the isotropic-nematic transition are examined (see the Caption of Figure 5.6 for further details). The colours denote the orientation of the rod-like particles relative to the frame of the simulation box.

of $P_N^* = 1.14$ corresponding to a bulk density of $\eta_b = 0.419$ and nematic order parameter of $S_{2,b} = 0.553$ can be taken to correspond to the lowest-density nematic state, while the state at the slightly lower pressure of $P_N^* = 1.12$ is seen to exhibit some small nematic clusters which would correspond to a pre-transitional metastable state; large region with random orientations corresponding to a bulk isotropic liquid can be seen in the case of the system with $P_N^* = 1.00$. Our estimate of the isotropic-nematic transition for the $L/D = 5$ HSC system from an analysis of this data is $\eta_{b,iso} = 0.401$, $\eta_{b,nem} = 0.419$ for the bulk nematic phase which are in good agreement with the corresponding results estimated from conventional NPT-MC simulation with full three-dimensional periodic boundary conditions ($\eta_{iso} = 0.407, \eta_{nem} = 0.415$) [45]; the coexistence pressure is estimated to be the arithmetic average between the normal pressures corresponding to the highest-density isotropic state and the lowest-density nematic state, $P_N^* = 1.10$, which is slightly lower than that estimated for the system with full periodicity ($P_N^* = 1.19$) [45]. A determination of the free energy and chemical potential of the system would allow one to get a more precise estimate of the position of the phase transition, but this is beyond the scope of the current study. A slight stabilization of the isotropic-nematic transition (corresponding to a lowering the transition packing fraction by 1 to 2% is therefore found in our systems of HSC rods placed between two parallel hard walls. One would certainly expect surface

induced nematization to stabilize the transition to a bulk nematic phase. These surface effects are however not the focus of the current study and will be discussed in detail in subsequent chapters. When the two confining walls are well separated the effect on the bulk isotropic-nematic transition is inappreciable. However, the effects of confinement will become increasingly more important as the surfaces are brought closer together. For the systems studied in our current work the two hard walls in our simulation cells are far enough apart (even for the highest density states) to ensure that the effect of the surfaces on the bulk phase transition will be small.

5.4.2 HSC-HS mixture

We now turn our attention to a binary mixture of HS and HSC particles characterized by overall HS composition x_{HS} ranging from 0.05 to 0.20. As with the pure component system the mixture is contained between parallel hard structureless surfaces and the isotropic-nematic phase transition is simulated using the $NP_{\mathrm{N}}T$-MC method as described in Section 5.3. As well as being of different density the coexisting isotropic and nematic phases will exhibit a fractionation of the two components, with an accumulation of the the rod-like particles in the orientationally ordered nematic phase. The fluid phase separation in hard-core system of this type is an entropy driven process. This is not to be confused with the depletion driven phase behaviour exhibited by anisometric colloidal particles on addition of polymer where the polymer induces an effective attractive interaction (depletion force) between the colloids, that would otherwise only interact in a purely repulsive fashion, giving rise to a van der Waals like "vapour-liquid" transition (see for example references [67, 217, 218] and the excellent monograph by Lekkerkerker and Tuiner [33]. The simulated phase boundaries of our HSC-HS mixture will be compared with the theoretical corresponding predictions obtained with the one-fluid PL and two-fluid MFP approaches. A simulation cell in a low-density thermodynamic state is slowly compressed and equilibrated to obtain the dependence of bulk packing fraction and bulk composition on the equilibrium bulk pressure (which for our system with planar symmetry also corresponds to the normal component of the pressure tensor, P_{N}). The bulk values of the phases are again obtained as averages of the density and composition profiles in the central region of the simulation cell. Typical density, composition and nematic order parameter profiles for bulk isotropic, intermediate isotropic-nematic, and bulk nematic states of mixtures with overall HS composition $x_{\mathrm{HS}} = 0.10$ are shown in Figures 5.8, respectively.

The dependence of the bulk packing fraction η_{b} on the applied normal pressure P_{N}^{*} for

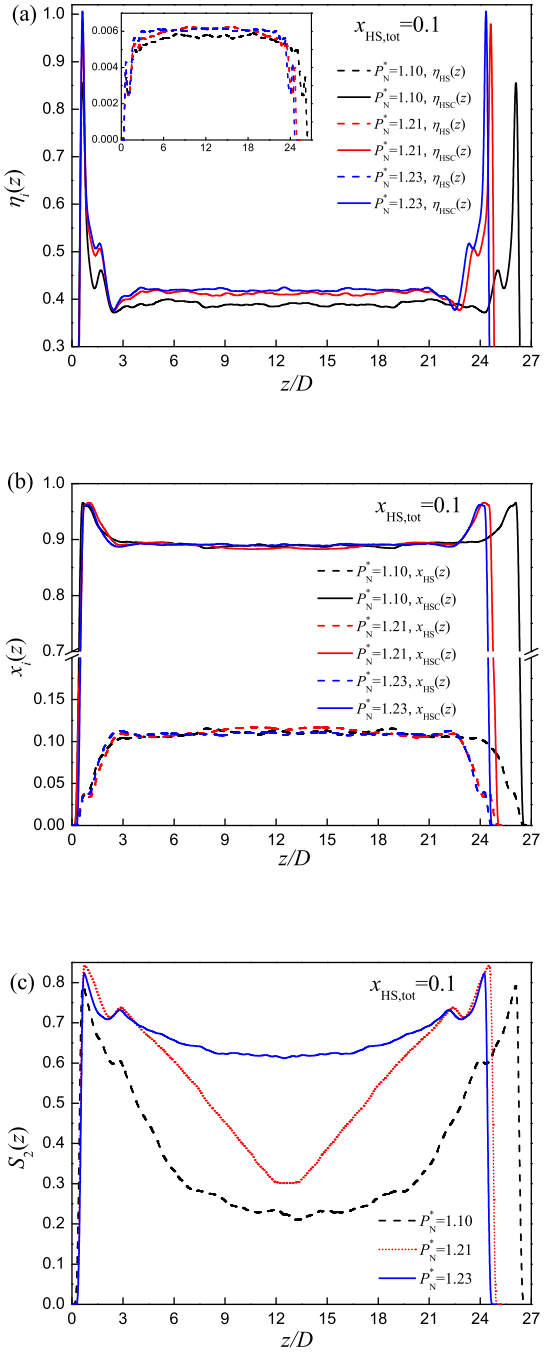

Figure 5.8: The packing fraction $\eta_i(z)$ (a), composition $x_{\rm i}(z)$ (b), and nematic order parameter $S_2(z)$ (c) profiles for mixtures of $N_{\rm HSC} = 1482$ HSC and $N_{\rm HS} = 371$ HS particles for an overall composition of $x_{\rm HS,tot} = 0.10$. Typical bulk isotropic ($P_{\rm N}^* = 1.10$), metastable ($P_{\rm N}^* = 1.21$), and nematic ($P_{\rm N}^* = 1.23$) states are examined. The packing fraction profiles of HS particles are shown in the inset of (a).

the HSC-HS system with an overall composition of $x_{\mathrm{HS,tot}} = 0.1$ is illustrated in Figure 5.9(a). The theoretical description of isotropic and nematic branches of the equation of state obtained with the PL and MFP approach at the same overall composition are also plotted in Figure 5.9(a) for comparison. There is only a negligible difference between the PL and MFP results in the isotropic state. This is to be expected, since both the density and the ordering in this region is small and as a consequence the sphericalized averages of the excluded volume contributions with a one- or two-fluid approximation should be similar for the isotropic state. One should note that while within the theories (both PL and MFP) the density and composition are input variables for a given system and the pressure is an output, while for our $NP_{\mathrm{N}}T$-MC simulation the equilibrium pressure is specified and the bulk density and composition are obtained as averages from the central region of the cell. A marked difference between the one- and two-fluid theories can be seen in the vicinity of the isotropic-nematic transition where the branches of the equation of state obtained by simulation data experience an abrupt change in slope indicating the transition to the orientationally ordered state. From the results depicted in Figure 5.9, one can infer that predictions with the two-fluid MFP apporach is superior to that with the one-fluid PL at least for the nematic phase.

The isotropic-nematic transition point can be identified from the change in nematic order parameter as is apparent from in Figure 5.9(b). The typical snapshots of configurations for the highest-density bulk isotropic state ($\eta_{\mathrm{b}} = 0.400, x_{\mathrm{HS,b}} = 0.116$) and the lowest-density bulk nematic state ($\eta_{\mathrm{b}} = 0.419, x_{\mathrm{HS,b}} = 0.108$)are also included in order to visualise differing degrees of orientational order. The corresponding results for the HSC-HS system with the highest overall HS composition $x_{\mathrm{HS,tot}} = 0.20$, are shown in Figure 5.10. The isotropic-nematic transition lies somewhere between highest-density bulk isotropic state at $P^*_{\mathrm{N}} = 1.23$ and the lowest-density bulk nematic state at $P^*_{\mathrm{N}} = 1.32$ where a clear change in the density and composition is exhibited: the values of the packing fraction and composition for these two states are $\eta_{\mathrm{b}} = 0.410$ and $x_{\mathrm{HS,b}} = 0.222$ for the bulk isotropic phase and $\eta_{\mathrm{b}} = 0.429$ and $x_{\mathrm{HS,b}} = 0.219$ for the bulk nematic phase.

The isotropic-nematic phase boundaries estimated for the HSC-HS mixtures for bulk phase compositions ranging from the pure HSC system ($x_{HS,b} = 0$) to $x_{HS,b} \sim 0.3$ is shown in Figure 5.11. Here, we compare the predictions of PL and MFP theories with our $NP_{\mathrm{N}}T$-MC simulations as well as with the previously reported NPT-MC data for systems in full three-dimensional periodic boundary conditions [72]. The one-fluid and two-fluid approaches are both seen to describe the coexisting packing fractions as monotonically

Table 5.2: Constant normal-pressure MC ($NP_{\mathrm{N}}T$-MC) simulation results for bulk isotropic-nematic phase behaviour of mixtures of $N_{\mathrm{HSC}} = 1482$ HSC and $N_{\mathrm{HS}} = 165$ HS particles for an overall HS composition of $x_{\mathrm{HS,tot}} = 0.10$. The reduced normal pressure P_{N}^{*} is set in the simulation and corresponding bulk values of packing fraction (η_{b}), composition ($x_{\mathrm{HS,b}}$), and nematic order parameter ($S_{2,\mathrm{b}}$) are obtained as configurational averages. The isotropic phase is donated by Iso, the nematic by Nem, the pretransitional states (Pre) are considered to be metastable.

P_{N}^{*}	η_{b}	$x_{\mathrm{HS,b}}$	$S_{2,\mathrm{b}}$	L_z/D	Phase
0.70	0.336	0.104	0.069	32.07	Iso
0.80	0.355	0.105	0.076	30.34	Iso
0.90	0.370	0.107	0.092	28.58	Iso
1.00	0.383	0.109	0.118	27.56	Iso
1.10	0.396	0.109	0.167	26.71	Iso
1.16	0.408	0.109	0.233	25.84	Iso
1.20	0.410	0.114	0.287	25.30	Pre
1.21	0.414	0.114	0.345	25.35	Pre
1.22	0.416	0.114	0.339	25.27	Pre
1.23	0.419	0.108	0.506	25.18	Nem
1.24	0.420	0.108	0.577	24.97	Nem
1.25	0.421	0.112	0.610	24.66	Nem
1.26	0.423	0.121	0.614	24.58	Nem
1.28	0.430	0.111	0.661	24.35	Nem
1.30	0.436	0.110	0.708	24.13	Nem
1.32	0.441	0.109	0.724	23.89	Nem

Table 5.3: Constant normal-pressure MC ($NP_{\mathrm{N}}T$-MC) simulation results for bulk isotropic-nematic phase behaviour of mixtures of $N_{\mathrm{HSC}} = 1482$ HSC and $N_{\mathrm{HS}} = 371$ HS particles for an overall HS composition of $x_{\mathrm{HS,tot}} = 0.20$. The reduced normal pressure P^*_{N} is set in the simulation and corresponding bulk values of packing fraction (η_{b}), composition ($x_{\mathrm{HS,b}}$), and nematic order parameter ($S_{2,\mathrm{b}}$) are obtained as configurational averages. The isotropic phase is donated by Iso, the nematic by Nem, the pretransitional states (Pre) are considered to be metastable.

P^*_{N}	η_{b}	$x_{\mathrm{HS,b}}$	$S_{2,\mathrm{b}}$	L_z/D	Phase
0.80	0.348	0.206	0.131	31.05	Iso
0.90	0.361	0.211	0.151	29.75	Iso
1.00	0.378	0.212	0.171	28.68	Iso
1.10	0.391	0.213	0.163	27.85	Iso
1.20	0.404	0.222	0.254	26.45	Iso
1.26	0.408	0.226	0.301	25.62	Pre
1.28	0.414	0.225	0.404	25.53	Pre
1.30	0.415	0.230	0.415	25.35	Pre
1.31	0.417	0.233	0.419	25.26	Pre
1.32	0.429	0.219	0.611	25.02	Nem
1.34	0.430	0.223	0.612	24.71	Nem
1.36	0.431	0.226	0.628	24.50	Nem
1.38	0.432	0.226	0.619	24.64	Nem
1.39	0.435	0.226	0.650	24.53	Nem

increasing functions of the bulk composition for the isotropic and nematic phases. For the phase boundary of the nematic states found at the higher packing fractions, the difference between the description obtained with the PL and MFP approaches becomes more marked with increasing composition of the spherical particles. Our simulated values for the nematic and isotropic phase boundaries are consistent with those obtained with a fully periodic system; the simulation data are in reasonably good agreement with the PL and MFP theoretical descriptions. This can be partly attributed to the overestimate of the first-order character of the isotropic-nematic transition with scaled Onsager theories of this type which are based on a underlying description at the level of the second virial coefficient [45]. The approximations inherent in mapping HSC-HS mixture on to an equivalent HS mixture in order to simplify the computation of higher-order virial contribution may also lead to an exaggeration of the first-order nature of the transition. On increasing the overall composition of the HS particles,the density gap between the isotropic and nematic coexisting states is seen to become larger as found with our simulations. By contrast,the density gap between the phase boundaries obtained from conventional NPT-MC simulations of the fully periodic system [72] appears to shrink slightly. In fully periodic NPT-MC simulations of this type the system remains essentially homogeneous so that the composition of the state remains fixed. As the pressure is increased the system will undergo a transition from an isotropic to a nematic phase but the states will be constrained to have the same composition. As a consequence of lack of fractionation of the species between the two phases with the NPT-MC simulations it is difficult to differentiate metastable states within the binodal region from those corresponding to the coexistence boundaries. The $NP_{\rm N}T$-MC simulation data for the HSC-HS mixture are also reported in Table 5.4 where the slight composition asymmetry between coexisting isotropic and nematic phases is clearly apparent. For the HSC-HS system, the addition of spherical particles is found to destabilize. The formation of a bulk nematic state predominantly composed of HSC rods will cause a reduction in the concentration of the HS particles in the same region, and as a consequence the orientational ordered state which is of higher density but lower bulk HS composition coexists with an isotropic state of lower-density and higher bulk HS composition.

Finally, a phase diagram in the pressure-composition ($P^*_{\rm N} - x_{\rm HS,b}$) plane is shown in Figure 5.12. A very narrow region of isotropic-nematic coexistence is obtained with our $NP_{\rm N}T$-MC simulation approach. The coexistence region is seen to be at lower pressures that that predicted with the PL and MFP theories or obtained by fully periodic NPT-MC

simulation [72]. It should be noted that the results obtained at higher compositions with the fully periodic simulations is in good agreement with the nematic branch predicted with MFP theory. It is apparent the estimates of the phase boundaries for the HSC-HS mixture obtained with both the PL and MFP approaches deviate considerably from the simulation data. The predictions with the two-fluid MFP theory are seen to be much better than one-fluid PL theory, particularly for systems of higher composition. It is therefore apparent that at least for this system the representation of HSC-HS mixtures as two separate effective HS fluids improves the description of the fluid phase behaviour.

Table 5.4: The isotropic-nematic transition estimated from $NP_{\mathrm{N}}T$-MC simulations of mixtures of $N_{\mathrm{HSC}} = 1482$ hard-spherocylinder (HSC) and N_{HS} hard-sphere (HS) particles for varying overall HS compositions of $x_{\mathrm{HS,tot}}$ contained between well separated parallel hard walls. The normal pressure $P^*_{\mathrm{N}} = P_{\mathrm{N}}D^3/(k_{\mathrm{B}}T)$ is set during the simulation, bulk packing fractions η_{b} and bulk compositions $x_{\mathrm{HS,b}}$ of coexisting isotropic (iso) and nematic (nem) states are obtained as averages from the central region of the cell. The bulk nematic order parameter $S_{2,\mathrm{b}}$ of the lowest-density nematic bulk phase is also shown.

$x_{\mathrm{HS,tot}}$	$P^*_{\mathrm{N,iso}}$	$\eta_{\mathrm{b,iso}}$	$x_{\mathrm{HS,b,iso}}$	$P^*_{\mathrm{N,nem}}$	$\eta_{\mathrm{b,nem}}$	$x_{\mathrm{HS,b,nem}}$	$S_{2,\mathrm{b}}$
0	1.10	0.401	0	1.10	0.419	0	0.570
0.05	1.12	0.405	0.0568	1.17	0.418	0.0567	0.574
0.10	1.18	0.400	0.116	1.23	0.419	0.108	0.551
0.15	1.22	0.413	0.172	1.27	0.428	0.167	0.577
0.20	1.23	0.410	0.222	1.32	0.429	0.219	0.611

5.5 Conclusions

The focus of the work presented in this chapter has been on the fluid phase behaviour of mixtures of purely repulsive rod-like (hard spherocylinders) and spherical (hard spheres) particles and the effect of the composition on the orientationally ordering into a nematic state. In order to facilitate the study of the fluid phase separation in repulsive systems of this type which are characterized by low interfacial tension an external potential is employed by containing the mixture between parallel hard structureless walls. The separation between the walls is made sufficiently large in order to minimize the effect of the surface on the bulk fluid phase transition. The planar symmetry of the system allows one fix the

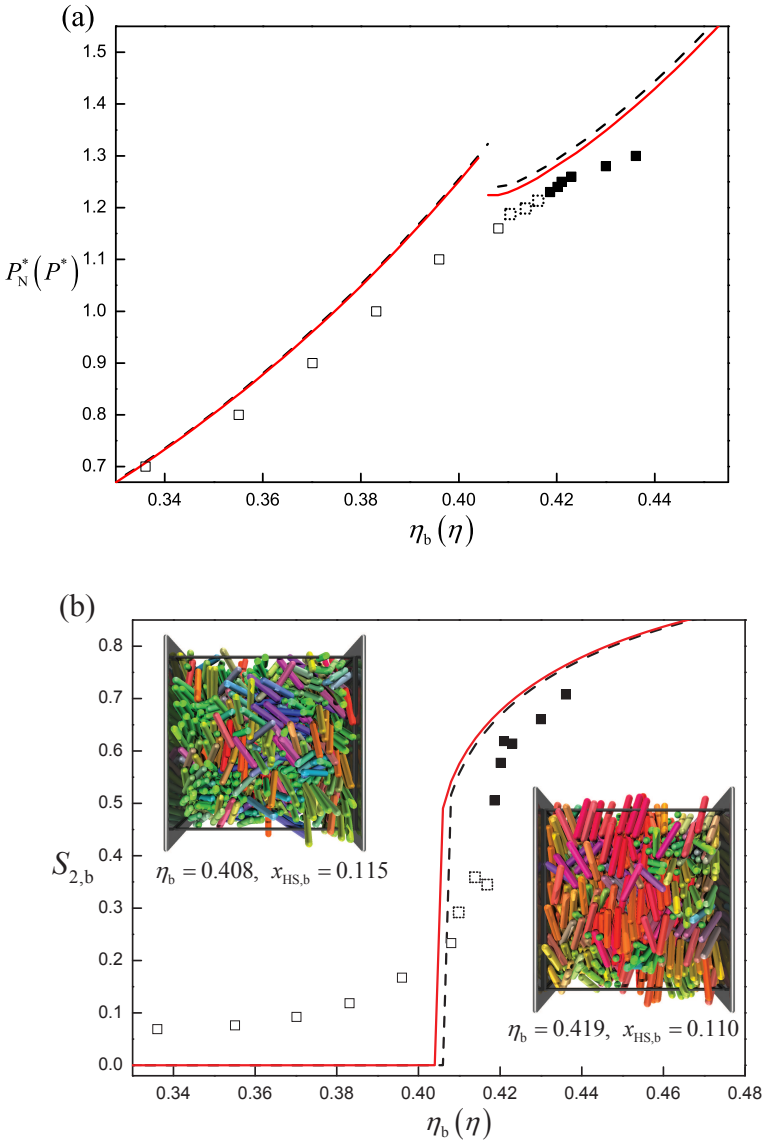

Figure 5.9: (a) The equation of state (pressure-density, $P_N^* - \eta_b$), and (b) orientational order (nematic order parameter S_2, b) of mixtures of hard spherocylinders (HSCs) and hard spheres (HSs). The results of NP_NT-MC simulations for mixtures of $N_{HSC} = 1482$ HSC and $N_{HS} = 165$ HS particles for an overall HS composition of $x_{HS,tot} = 0.10$ contained between well separated parallel hard walls are represented as open (isotropic branch) and filled (nematic branch) squares, while the metastable states are shown as dashed. The dashed and continuous curves predicted using the one-fluid PL and two-fluid MFP theories, respectively; the lower-density branch corresponds to isotropic states and the higher density branch to nematic states. The snapshots in (b) correspond to the highest-density bulk isotropic state ($\eta_b = 0.408, x_{HS,b} = 0.115$) and the lowest-density bulk nematic state ($\eta_b = 0.419, x_{HS,b} = 0.110$).

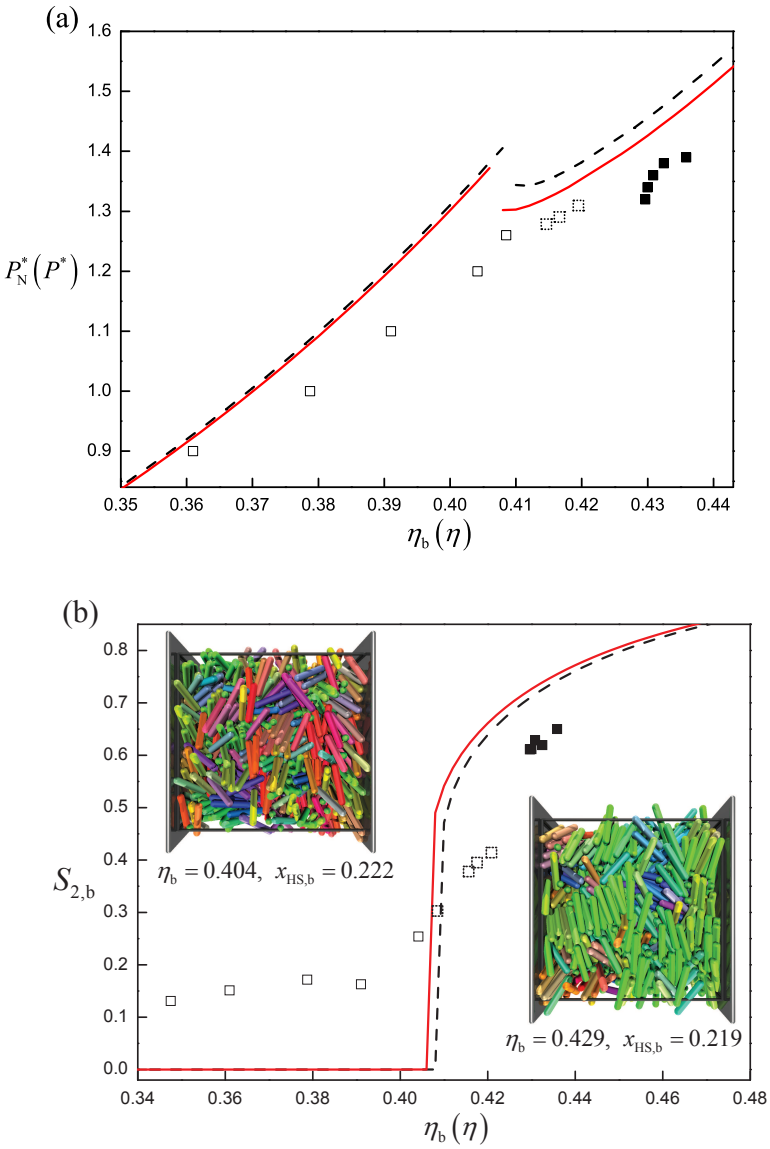

Figure 5.10: (a) The equation of state (pressure-density, $P_N^* - \eta_b$), and (b) orientational order (nematic order parameter S_2, b) of mixtures of hard spherocylinders (HSCs) and hard spheres (HSs). The results of NP_NT-MC simulations for mixtures of $N_{HSC} = 1482$ HSC and $N_{HS} = 371$ HS particles for an overall HS composition of $x_{HS,tot} = 0.20$ contained between well separated parallel hard walls are represented as open (isotropic branch) and filled (nematic branch) squares, while the metastable states are shown as dashed. The dashed and continuous curves predicted using the one-fluid PL and two-fluid MFP theories, respectively; the lower-density branch corresponds to isotropic states and the higher density branch to nematic states. The snapshots in (b) correspond to the highest-density isotropic state ($\eta_b = 0.404, x_{HS,b} = 0.222$) and the lowest-density nematic state ($\eta_b = 0.429, x_{HS,b} = 0.219$).

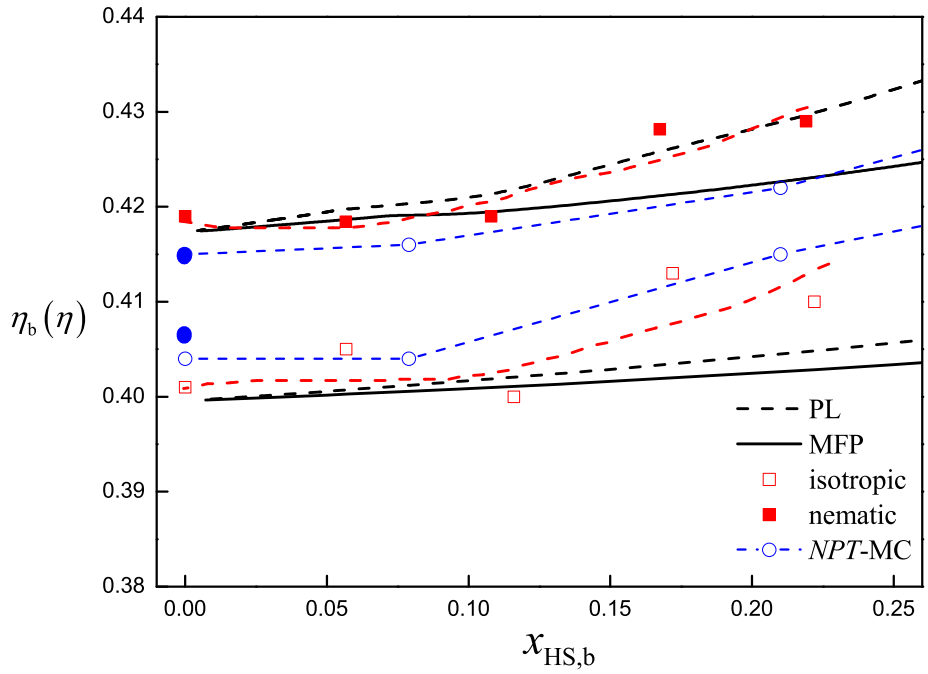

Figure 5.11: The isotropic-nematic phase diagram of mixtures of hard spherocylinders (HSCs) and hard spheres (HSs) in $\eta_b(\eta) - x_{HS,b}$ plane. The results of NP_NT-MC simulations for mixtures of $N_{HSC} = 1482$ HSC and N_{HS} HS particles for an overall HS composition of $x_{HS,tot} = 0.1$ are represented as open (isotropic branch) and filled (nematic branch) squares. The NP_NT-MC data are compared with predictions obtained with the one-fluid PL (dashed curves) and two-fluid MFP (continuous curves)theories, and with previously reported NPT-MC simulation data for fully periodic systems: open circles [72] and filled circles [45].

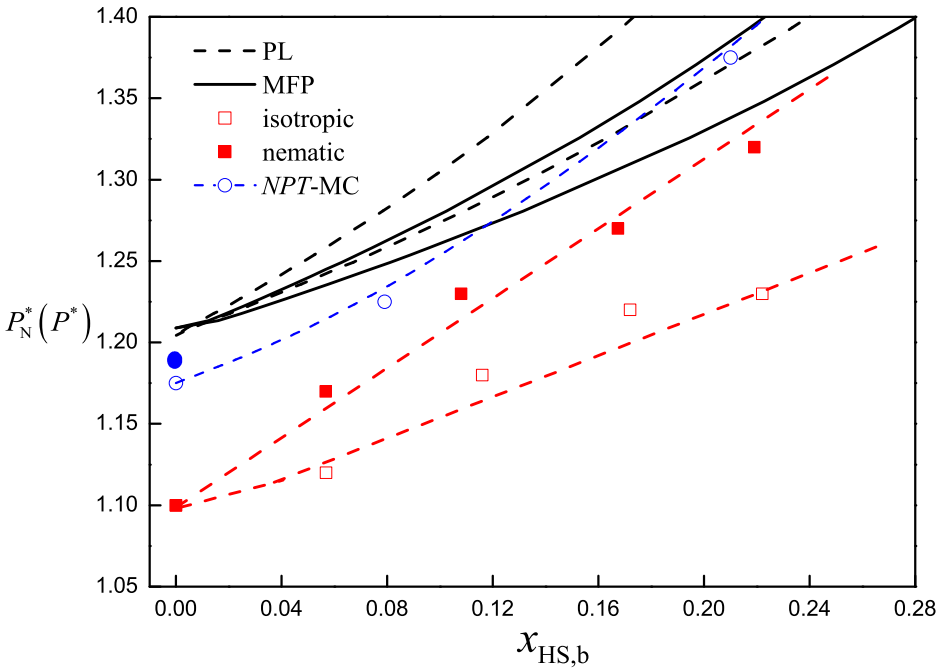

Figure 5.12: The isotropic-nematic phase diagram of mixtures of hard spherocylinders (HSCs) and hard spheres (HSs) in $P_{\mathrm{N}}^{*}(P^{*}) - x_{\mathrm{HS,b}}$ plane. The results of NP_NT-MC simulations for mixtures of $N_{\mathrm{HSC}} = 1482$ HSC and N_{HS} HS particles for an overall HS composition of $x_{\mathrm{HS,tot}} = 0.1$ are represented as open (isotropic branch) and filled (nematic branch) squares. The $NP_{\mathrm{N}}T$-MC data are compared with predictions obtained with the one-fluid PL (dashed curves) and two-fluid MFP (continuous curves)theories, and with previously reported NPT-MC simulation data for fully periodic systems: open circles [72] and filled circles [45].

component P_{N} of the pressure tension normal to the surface (which owing to mechanical equilibrium also corresponds to the bulk pressure) and simulate the system with an NP_T-MC algorithm by allowing the separation between the walls to fluctuate. The advantage of this technique is that the fluid phase separation in such a system can be studied within a single simulation cell which circumvents the problem of inserting anisotropic particles inherent in other techniques such as Gibbs ensemble MC (GEMC). Additionally, particle exchanges are allowed between the surface and bulk regions so that one is able to treat the two bulk states coexisting at different bulk densities (packing fractions) as well as different bulk compositions. In the case of conventional fully periodic NPT-MC method simulation of a system characterized by a low interfacial tension between the coexisting bulk phases it is very challenging to stabilize the bulk phase separation.

In order to analyse the bulk phases the simulation box is divided into two surface regions which are close to the hard walls and one large region in the centre of the box representing the bulk phase.The adequacy of the approach is first assessed for the isotropic-nematic phase transitions exhibited by pure hard spherocylinders with an aspect ratio of $L/D = 5$: only a small surface stabilization of the transition is observed on comparison with the data for the fully periodic system providing the separation between the surfaces is sufficiently large. The isotropic-nematic phase behaviour of the mixtures of $L/D = 5$ hard spherocylinders and hard spheres of diameter $\sigma = D$ is then examined in detail. The approximate phase boundary obtained with our $NP_{\mathrm{N}}T$-MC approach is compared with the results of NPT-MC in which suppressed the fractionation of the particles between the various phases. Our work provides a more comprehensive understanding of phase behaviour of HSC-HS mixtures allowing for the asymmetry in the overall composition of the two coexisting bulk phases. In contrast to the findings of previous studies, the degree of fractionation of the species between the two phases is found to increase with increasing concentration of spherical particles. A more precise location of phase boundaries of the HSC-HS mixture will be determined in future work by using thermodynamic integration. A comparison of the simulation data for the HSC-HS mixture also enables one to undertake a stringent test of the adequacy of theoretical predictions with multi-fluid approaches of the nematic state.

The comparison reveals both the one- and two-fluid approaches provide a reasonably quantitative description of the simulation data for the isotropic-nematic phase boundary and degree of orientational order of the HSC-HS mixtures. The two-fluid MFP predictions of coexistence pressure are better than those obtained with the one-fluid PL method. Here

we have restricted our attention to systems of HSC rods with an aspect ratio of $L/D = 5$ and HS particles of diameter $\sigma = D$. For larger aspect ratios, one would expect a more significant improvement of the two-fluid treatment compared to the one-fluid approach.. The focus of this work has been the bulk properties of HSC-HS mixtures and not on the surface effects. It is well known that the surfaces play an important role in inducing rich surface behaviour in liquid crystalline systems [243, 244]. In the next two chapters we will employ the NP_NT-MC technique to provide a detailed investigation of the surface phenomena (adsorption, wetting, de-wetting, nematization, smectization etc.) of mixtures of hard spherocylinders and hard spheres in contact with hard structureless walls.

Chapter 6

Demixing of a binary mixture of hard rods and hard spheres in contact with hard surfaces: surface nematization and competing adsorption

The bulk phase behaviour of hard spherocylinders (HSCs) and hard spheres (HSs) mixture has been studied in the previous chapter. Since the two parallel hard walls placed along the z axis of the simulation cell lead to the inhomogeneity of density and orientational distributions of rods, these simulations can also be used directly to provide very detailed information on the surface behaviour of HSC-HS mixture. We assess effects of the surfaces and the addition of spherical particles on the structure and the local orientational order of the HSC-HS mixture near the wall, the surface nematization and adsorption.

6.1 Introduction

In addition to the vast literature on bulk phase behaviour of liquid crystalline (LC) systems, numerous papers have been devoted to modelling and understanding the LC ordering induced by a surface [245–247]. The inhomogeneity in the fluid structure brought out by the surface couples with the inherent anisotropy of LC states to bring about a rich and complex phenomenology. Much of the early work on surface effects and anchoring in LC

systems was reviewed by Jerome [246]; we highlighted some of the representative studies here and mention a few examples of more recent work. Before direct molecular simulation of liquid crystalline systems had been attempted, Sheng [248] provided a theoretical framework within the Landau-de Gennes phenomenological approach to assess the effect of surface alignment of LC on the bulk isotropic-nematic phase separation, showing that that there is a critical thickness of the surface nematic film below which the transition to the isotropic phase becomes continuous. A mean-field density functional theory (DFT) of the induced orientational order and wetting transitions of a nematic phase at a solid interface was presented by Telo da Gama [249, 250]; the use of Maier-Saupe model to represent the mesogens does not however allow one to relate effects of molecular anisotropy of the fluid particles to the extent of surface ordering. The surface effect on the LC transition of the Lebwohl-Lasher model was examined by Telo da Gama *et al.* [251]. Poniewierski and co-workers [252–255] have used the Maier-Saupe and generalised Onsager free-energy functionals to examine surface ordering of LCs including systems of hard-rod fluids in contact with a hard wall, treating the rods as hard needle-like particles of vanishing diameter. Surface drying was observed for the latter system in the vicinity of the surface followed by a cusp in the density profiles at a distance of half the length of the rod. This type of dewetting behaviour has also been examined in systems of hard rods confined between two parallel walls [243]. In a thorough study, van Roij *et al.* [256] used a second virial Onsager theory to treat confined rectangular rods in which the orientations are restricted to three possible directions (Zwanzig) rather than the continuous degrees of orientational freedom and a continuous uniaxial-biaxial nematic surface phase transition is found for an isotropic fluid in contact with a single planar hard wall, followed by wetting of the wall by a nematic film oriented parallel before a bulk nematic phase is observed; a first-order capillary nematization transition is seen in the case of the system confined between two well separated parallel hard walls at large wall separation, and a capillary critical point when the wall separation is about twice the length of the rods. Similar effects have been observed by Harnau and Dietrich [257] and by Reich and Schmidt [137] with density functional theories of disc-like particles at planar walls; in this case however homeotropic wall anchoring is induced. An example of more recent theoretical work is the analysis of confinement effects on the positional order of hard cylinders using the Onsager free-energy functional [258]. It is fair to say that despite these efforts, an accurate theoretical description of LCs in the close proximity of surfaces is still very challenging and in its infancy.

Computer simulation methods [234, 235] provide a more reliable approach to investigate

the LC phase behaviour of anisotropic particles both in bulk phase and and in the vicinity of surfaces. Examples of recent research focus on LC ordering at surfaces for prototypical models of mesogenic molecules include studies of hard spherocylinders [243, 244, 259–261], hard needles [255], hard ellipsoids [262, 263], hard cut spheres [142, 261], hard Gaussian overlap particles [264], Gay-Berne particles [265–268], and the Zwanzig model [256], as well as spherical particles decorated with an anisotropic Lennard-Jones potential [269], and rod-like particles with chiral interactions [163, 199]. Several types of surface-particle potentials and heterogeneities including roughness [270], softness [142], surface anchoring [247], competing walls [271] and spherical confinement [272] have been examined in simulation studies of the surface behaviour of LCs.

From the experimental perspective, the LC phases exhibited by suspensions of colloidal particles such as vandium pentoxide (V_2O_5) [222], Gibbsite ($Al(OH)_3$) platelets [28, 92], by carbon nanotubes [223] and some biological systems such as protein fibers [6], tobacco mosaic virus [8], *fd*-virus [9], polypeptide solutions [19, 23], and DNA chains [16] offer convenient test beds for an assessment of the simple hard core models of mesogenic systems. The interfacial properties of colloidal dispersions of gibbsite platelets have been studied by van der Beek *et al.* [135]: the nematic phase is found to wet the glass surface with homeotropic surface anchoring of the disc-like particles, as seen at the isotropic-nematic interface. The work by Galanis *et al.* [273] provides a very useful insight into the surface behaviour of granular rod-like particles ($L/D \approx 20$) for very thin layers of rods in a quasi-2D circular container. The number-density profiles measured are in excellent agreement with previous results obtained by simulation. The influence of a flat wall on the surface anchoring of colloidal rods has been examined in a recent study of aqueous suspensions of silica particles [274]. As with other colloidal systems of this type, the silica rods basically behave as an athermal (purely repulsive) system and are of sufficiently low polydispersity that they exhibit isotropic, nematic, and smectic phase behaviour on increasing concentration as is observed in molecular simulation studies of hard spherocylinders [42, 45, 61, 61–63, 224, 228]. This interesting work provides experimental confirmation that the rods adopt a planar anchoring configuration in the vicinity of the surface. In this experimental analog of the hard-core system, the effect of the surface is active over tens of microns.

It is appropriate to pay additional attention to to some previous work of particular relevance to our current study. Mao *et al.* [243] have presented a Monte Carlo (MC) simulation study of hard-spherocylinder (HSC) particles (with aspect ratios of $L/D = 10, 20$) con-

fined between two parallel hard structureless walls for relatively low density states. The emphasis of their work is on understanding the depletion force induced by the walls, the surface adsoprtion, and the determination of the fluid-wall surface tension. An impressively detailed simulation study has been undertaken by Dijkstra *et al.* [244] to investigate the surface adsorption, the wetting behaviour, and capillary nematization of HSC particles with an aspect ratio of $L/D = 15$. By simulating the HSC fluids in contact with a single wall allowing the thickness of the nematic film remain well defined in the simulation.

A more recent simulation study [74, 232] of the HSC system with $L/D = 10$ confined between two impenetrable parallel walls has also been carried out to determine the profiles of the density profile, nematic order parameter, and the degree of biaxiality, normal and tangential components of the pressure tensor which allow one to determine the fluid-wall interfacial tension of the system. As may have become become apparent the focus of the aforementioned work has been on the surface behaviour of one-component LC systems. On the other hand, there is a large body of work devoted to modelling and understanding the bulk phase transitions exhibited by athermal mixtures of mesogenic components including rod-rod [12,13,53,275,276], rod-sphere [67–73,277,278], rod-disc [77,115–117,124,225,226, 279] and disc-disc [93, 280] and discs-sphere [281] hard-core systems (the reader is direct to reference [112] for a recent review).

The main objective of our current work is to study the influence of hard walls on the bulk phase behaviour of athermal rod-sphere mixtures as well as on the surface. Particular attention is paid to understanding of the effect of the spherical particles on the adsorption and surface nematization of rods. A detailed MC simulation study of binary mixtures of hard spherocylinders and hard spheres in the constant-stress (normal pressure) ensemble to facilitate the investigation of the surface behaviour of the system. The focus in this chapter is on the phase behaviour from low pressures (density) states to the higher pressure (density) states where system exhibits a the bulk isotropic-nematic transition. Both pure rods and binary mixtures are studied to uncover the role that the addition of spheres has on the surface behaviour of the rod-sphere mixture. The density and nematic order parameter profiles are determined in order to quantify the adsorption and orientational effects of the surface on the system.

6.2 Simulation details

Constant normal-pressure Monte Carlo simulations ($NP_{\mathrm{N}}T$-MC, where P_{N} is normal pressure) are performed for a binary mixture of $N_{\mathrm{HSC}} = 1482$ hard spherocylinder (HSC) particles of aspect ratio $L/D = 5$ and a number N_{HS} of HS particles of diameter $\sigma = D$ defined from the values of the overall mole fraction set for the system, $x_{\mathrm{HS}} = N_{\mathrm{HS}}/(N_{\mathrm{HS}} + N_{\mathrm{HSC}})$. Further details of the $NP_{\mathrm{N}}T$-MC algorithm and specifics of its application to the determination of the interfacial properties can be found in a previous work [74]. As the intermolecular potential between particles is purely repulsive and the system is athermal and the temperature only plays a trivial (kinetic) role. As can be seen from a typical snapshot presented in Figure 6.1, the system comprises a rectangular box of dimensions $L_x = L_y = 25D$ and L_z in the usual Cartesian coordinates. Two parallel hard structureless walls are positioned at $z = 0$ and $z = L_z$ and standard periodic boundary conditions are applied in the x and y dimensions. In the $NP_{\mathrm{N}}T$ ensemble, the component of the pressure tensor $\mathbf{P}$ normal to the hard walls P_{N} is imposed (i.e., along the z axis) and the system volume fluctuates by varying the dimension of the z axis (L_z) moving the walls closer together or farther apart about the equilibrium value, while the dimensions of the system along the x and y axes (L_x and L_y) remain fixed. For a systems with this type of planar symmetry the condition of mechanical equilibrium ($\nabla \cdot \mathbf{P} = 0$) requires that the normal component of the pressure tensor is constant throughout the sample: as a consequence the normal component is also equivalent to the equilibrium pressure of the system, i.e., $P_{\mathrm{N}} = P$. The relevant thermodynamic variables that define the system in this ensemble are therefore the total number of particles, composition, pressure, and surface area in the $x - y$ plane (L_xL_y); one should therefore strictly include the area and composition in the designation of the ensemble but we chose to retain the $NP_{\mathrm{N}}T$ for conciseness, implicitly recognizing the the latter variables are constant.

The $NP_{\mathrm{N}}T$-MC simulations are performed for 5×10^6 cycles to equilibrate the system and $5-8\times10^6$ cycles to accumulate the averages. Each MC cycle consists of N (where N is the total number of molecules) attempts to displace and rotate a randomly chosen molecule and one trial volume change; the later involves an affine scaling z dimension where the relative positions of the particles along the z axis L_z remain constant. The breaking of symmetry caused by the hard surfaces leads to inhomogeneous positional and orientational distributions of the particles along the z axis, apart from the central region of the box when the separation between the walls is sufficiently large. The thermodynamic and structural properties of the system are therefore determined locally. In order to evaluate the number

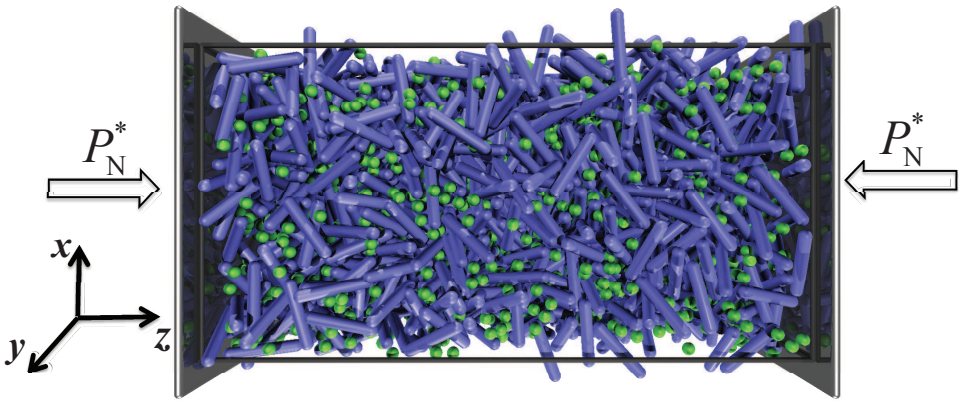

Figure 6.1: A typical snapshot of the mixture of hard spherocylinders and hard spheres in the NP_NT-MC simulation cell employed in our current work. The structureless hard walls are placed along the z axis and the normal pressure P_N is imposed along the z direction perpendicular to the surfaces.

density profile $\rho_i(z), i = \mathrm{HS}, \mathrm{HSC}$, and order parameter profile ($S_2(z)$), the simulation box is divided into n_{bin} bins of equal width δz in the z direction. The density profile $\rho_i(z), i = \mathrm{HS}, \mathrm{HSC}$ is obtained from

$$\rho_i(z) = \frac{< N_i(z) > D^3}{L_x L_y \delta z} \qquad i = \mathrm{HS}, \mathrm{HSC}, \tag{6.1}$$

where $< N_i(z) >$ represents the ensemble average of the local number density of component i; typically $n_{\mathrm{bin}} = 200$ bins are used to accumulate the averages. The composition profile of the two component can be determined from

$$x_i(z) = \frac{\rho_i(z)}{\rho_{\mathrm{HS}}(z) + \rho_{\mathrm{HSC}}(z)} \qquad i = \mathrm{HS}, \mathrm{HSC}. \tag{6.2}$$

When the system is large enough one would expect an equilibrium region of bulk-like behaviour in the central part of the cell, well removed from the walls. In this region, the density profiles $\rho_i(z), i = \mathrm{HS}, \mathrm{HSC}$ in the z direction should level out, indicating a bulk density of HSC ($\rho_{\mathrm{HSC,b}}$) and HS ($\rho_{\mathrm{HS,b}}$) particles, respectively. With the bulk densities of each components, we can calculate the adsorption Γ_i of component i from the following integral:

$$\Gamma_i = \frac{1}{D} \int_0^{L_z} [\rho_i(z) - \rho_{i,\mathrm{b}}] \mathrm{d}z, \quad i = \mathrm{HS}, \mathrm{HSC} \tag{6.3}$$

Because hard spheres are isometric, one only need to calculate the orientational order of the anisometric hard spherocylinders in the cell. The degree of orientational order in anisotropic systems is commonly quantified by computing the nematic order parameter

S_2 [3]. The nematic order parameter profile $S_2(z)$ is obtained by measuring the standard nematic order parameter tensor $\mathbf{Q}(j)$ in each bin j:

$$\mathbf{Q}(j) = \left\langle \frac{1}{2N_{\mathrm{HSC},j}} \sum_{i=1}^{N_{\mathrm{HSC},j}} (3\vec{\omega}_i \bullet \vec{\omega}_i - \mathbf{1}) \right\rangle \tag{6.4}$$

where $\vec{\omega}_i$ is the orientation of the i-th rod, $N_{\mathrm{HSC},j}$ is the number of HSC particles in the j-th bin, and $\mathbf{1}$ is the unit matrix. On diagonalization of the $\mathbf{Q}(j)$ tensor [105], three eigenvalues are obtained and the largest of which is defined as the local nematic order parameter $S_2(z)$ associated with the j-th bin. Particular care should be taken with the calculation of the order parameter profile because of finite-size effect. It has been shown by Eppenga and Frenkel [46] that the order parameter depends on the number of anisometric molecules considered the error in local order parameter is $\sim 1/(\sqrt{N_{\mathrm{HSC}}/n_{\mathrm{bin}}})$. If we use $n_{\mathrm{bin}} = 200$ histogram bins which is the same as that used for density profile, there will be on average only $7(\sim 1482/200)$ rods in each bin and the expected error ~ 0.367 corresponds to a large deviation from the correct value of order parameter $S_{2,N_{\mathrm{HSC}}\to\infty}(z)$ in the thermodynamic limit. One can employ a function [240] to bridge between $S_{2,\infty}(z)$ and $S_{2,N_{\mathrm{HSC}}}(z)$ by postprocessing the simulation data. An obvious (and trivial) way to minimize the error is to use a larger size system, however this comes at an increasing prohibitive computational cost. For example, a large system of 14820 rods (an order of magnitude larger than the current system) with $n_{\mathrm{b}} = 200$ accumulation bins barely reduces the error in $S_2(z)$ to ~ 0.11. Instead we opt to reduce the number of bins by using $n_{\mathrm{bins}} = 20$ to calculate the order parameter profile. The expected error ~ 0.11 ($n_{\mathrm{bin}} = 20$) is deemed to be small enough to render the results and trends meaningful.

In the remainder of this chapter the following dimensional quantities will be employed: the pressure is $P^*_{\mathrm{N}} = P_{\mathrm{N}} D^3/(k_{\mathrm{B}}T)$, the number density $\rho^* = ND^3/V = \rho D^3$, the packing fraction $\eta = (N_{\mathrm{HSC}}V_{\mathrm{HSC}} + N_{\mathrm{HS}}V_{\mathrm{HS}})/V$ (with V_{HSC} and V_{HS} the volumes of the HSC and HS particles, respectively), and the z dimension $L^*_z = L_z/D$.

6.3 Results and discussion

6.3.1 Pure hard spherocylinders in contact with hard walls

We begin our discussion of results with the surface behaviour of pure HSC rods over a wide range of equilibrium (normal) pressures up to the point where the bulk isotropic-nematic transition is observed. The local density near to a hard wall in the low-pressure region of $P^*_{\mathrm{N}} = 0.001$-0.005 is shown in Figure 6.2(a). Appreciable differences between the local

density in the region close to the wall and the density of the bulk fluid which is observed at a sufficient distance from the wall, i.e., $z > 9D$. For a pressure of $P_{\mathrm{N}}^{*} = 0.1$, a kink is found at $z \sim 3D$ away from the wall which progressively becomes a small peak with increasing pressure. The appearance of this peak is explained by the fact that for these very low density states, HSC particles with an aspect ratio of $L/D = 5$ maintain their orientational freedom at $z = 3D$ (which is half the length $L + D$ of the rod) [243, 259]. In these cases, the wall is actually dried (dewetted) of rods. The dependence of density profiles at higher pressures ($P_{\mathrm{N}}^{*} = 0.2 - 1.2$) is shown in Figure 6.2(b). The peak at $z = 3D$ weakens while a new peak near $z \sim 0.5D$ quickly become the dominant feature with increasing P_{N}^{*}. The peak near $z \sim 0.5D$ indicates an increasing probability of rods wetting the wall by adopting planar anchoring in the first wetting layer. As the pressure is increased, a second wetting layer can also be identified between $z \sim 2D$ to $\sim 2.5D$.

In order to investigate the effect of the presence of the hard surface on the orientations of the HSCs, we display the local order parameter $S_2(z)$ in Figure 6.3 as a function of the position z from the wall. Taking into account the finite size of the system ($N = 1482$) and of the histogram bins ($n_{\mathrm{bins}} = 20$) used for the local order parameter profile, we take $S_2(z) < 0.4$ to represent a disordered state and $S_2(z) > 0.4$ to represent a local orientationally ordered nematic structure. For a pressure of $P_{\mathrm{N}}^{*} > 0.8$, the peak in $S_2(z)$ close to the wall at $z < 4D$ is associated with the formation of an ordered nematic film on the surface. The peak in the local nematic order parameter near the wall ($z < 4D$) grows with increasing P_{N}^{*} indicating the enhancement in the orientational order of the HSC particles at the wall for states of progressively higher density. The density profiles shown in Figure 6.2b resemble those seen in previous studies of wetting transitions. In particular, these density profiles provide some evidence of a prewetting transition, where the thin nematic layer at the surface builds up a second and further layers in a discontinuous fashion before the onset of the bulk isotropic-nematic transition (see discussion below). This has been seen in hard-rod [244, 256] and Gay-Berne [266, 267] models in contact with surfaces.

Three regimes corresponding to different patterns in the surface phase behaviour can be distinguished. In the first low-density regime ($P_{\mathrm{N}}^{*} = 0.001$-$0.01$), the density profiles are characterized by monotonic functions, where the HSC particles are simply being pushed away from the wall. For the second moderate bulk density regime ($P_{\mathrm{N}}^{*} = 0.02$-$0.4$), the interplay between the orientational entropy and packing entropy gives rise to a non-monotonic behaviour of the density profile with a pronounced maximum at $\sim (L + D)/2$

beyond which the rods are free to rotate. The third regime seen at higher bulk densities (P_{N}^{*} = 0.5-1.2) is characterized by surface nematization of the rods at the wall with the rods adjacent to the wall preferentially orientated parallel to the wall. This surface wetting manifests itself with a shift of the first maximum in the density profile to $z \sim 0.5D$. The second maximum located at $z \sim 2D$ which indicates an effect of the orientation entropy of the rods (S_2 is large in this region) in contrast with what is found for the hard-sphere fluid in which case the second maximum lies at $z = 1.5D$ [282–284].

In addition, a bulk phase transition between isotropic and nematic states is found in the higher density regime. There is a change in behaviour between the density profile corresponding to $P_{\mathrm{N}}^{*} = 1.10$ where the shape of the curve suggests the onset of bulk isotropic-nematic transition and that corresponding to $P_{\mathrm{N}}^{*} = 1.14$ where a fully developed nematic phase can be seen within the cell. The intermediate state observed for $P_{\mathrm{N}}^{*} = 1.12$ corresponds to a state dominated by the local nematic clusters, which are presumably stabilized by the alignment at the wall. Hence, the bulk transition from an isotropic phase to a nematic phase is delimited by the pressure range $P_{\mathrm{N}}^{*} = 1.00 - 1.14$ and the corresponding bulk densities are $\rho_{\mathrm{iso}}^{*} = 0.0867$ and $\rho_{\mathrm{nem}}^{*} = 0.0941$ (corresponding to packing fraction of $\eta_{\mathrm{iso}} = 0.386$ and $eta_{\mathrm{nem}} = 0.419$). When compared to previously reported results for the coexistence pressure and densities [45] ($P^{*} = 1.19$, $\rho_{\mathrm{iso}}^{*} = 0.0914$ and $\rho_{\mathrm{nem}}^{*} = 0.0932$, corresponding to $\eta_{\mathrm{iso}} = 0.407$ and $\eta_{\mathrm{nem}} = 0.415$) obtained from isobaric-isothermal MC simulation of the fully periodic system, the $NP_{\mathrm{N}}T$-MC simulations of the system with parallel walls appears to predict a slightly lower pressure and lower bulk coexistence densities. It stems from the weak stabilizing effect of the hard walls on the nematic state for these surface separations which though not negligible, does not have a significant impact on the bulk isotropic-nematic phase behaviour.

We further analyze the dependence of adsorption on the equilibrium pressure which is shown in Figure 6.4. It is should be mentioned that due to the hard core of the HSC and HS particles, the regions of $z < 0.5D$ and $z > L_z - 0.5D$ are inaccessible to the centres of mass of both species. A different definition for surface adsorption with the Gibbs dividing surface defined at $z = 0.5D$ and $z = Lz - 0.5D$ leads to numerically different but qualitatively consistent results for the surface adsorption [74]. From the surface adsorption curve, several previously reported adsorption phenomena exhibited in pure HSC systems are confirmed. At very low pressures ($P_{\mathrm{N}}^{*} = 0.001 - 0.08$) the system exhibits a negative net adsorption of rods on the surface, and the behaviour is characterized by a dominance of the orientation entropy which is restricted by the presence of the wall.

In these de-wetted low density states, the reduction in entropy associated with surface wetting is prohibitively large. The wall remains dry as the HSC particles only occupy the space where full orientational degrees of freedom are retained. Beyond the minimum of Γ seen at $P_{\mathrm{N}}^{*} = 0.08$, the surface adsorption increases monotonically in the range of normal pressures $P_{\mathrm{N}}^{*} = 0.1 - 1.1$; a net positive adsorption of the HSC particles at the wall is apparent at $P_{\mathrm{N}}^{*} = 0.6$. In this region, the structure of the fluid is dominated by the packing effects due to repulsive forces between the particles which causes an increase in adsorption with P_{N}^{*}. This broad region can be further divided into two sub-regions. First, at low to intermediate pressures, $P_{\mathrm{N}}^{*} = 0.1 - 0.6$, the system is characterized by an isotropic structure of the fluid (even locally close to the wall) with a development of a maximum in the density profile $\rho(z)$ at about $z = (L + D)/2$. Thus, the presence of the wall is still restrictive to the HSC rods and $\Gamma < 0$. The second sub-region features by a partial wetting of the wall by a nematic film of the HSC rods and thus $\Gamma > 0$ in the higher pressure region $P_{\mathrm{N}}^{*} = 0.7 - 1.1$. The boundary pressure between these two states ($P_{\mathrm{N}}^{*} = 0.5 - 0.6$) at which $\Gamma \sim 0$ is analogous to the point at which the contact angle of a sessile liquid drop deposited on a planar (attractive) wall is $\theta = \pi$. The formation of the bulk nematic phase results in an abrupt drop of adsorption as one approaches the bulk isotropic-nematic transition due to the increase in the bulk density. The bulk transition point is located between $P_{\mathrm{N}}^{*} = 1.00$ and 1.14, thus the development of a nematic layer on the hard surfaces may be regarded as a capillary condensation of the nematic phase (capillary nematization) prior to the bulk isotropic-nematic transition. Some illustrative snapshots of equilibrium configurations for selected states are shown in Figure 6.5. It can clearly be seen that the rods do not favour wetting of the wall at $P_{\mathrm{N}}^{*} = 0.02$, while a planar anchoring is adopted at $P_{\mathrm{N}}^{*} = 0.20$. At the higher pressures of $P_{\mathrm{N}}^{*} = 0.90$, a nematic surface is formed while a bulk nematic phase is stabilized at $P_{\mathrm{N}}^{*} = 1.14$.

6.3.2 Binary mixtures of hard spherocylinders and hard spheres in contact with hard walls

We are now in a position to assess how the addition of hard spheres affects the surface and bulk phase behaviour of the hard spherocylinders for mixtures with an equimolar overall concentration. The individual density profiles of the equimolar HSC-HS mixture for pressures in the range of $P_{\mathrm{N}}^{*} = 0.02 - 0.1$ is shown in Figure 6.6. As for the system of pure rods, the HSC particles dewet the wall at low densities driven by the entropic gain in free energy of retaining their rotational degrees of freedom near a wall. This

essentially leaves a free space close to the wall that is free to be occupied by the hard-sphere components of the mixture. In this low-pressure region, the HSC particles do not exhibit an orientationally-order structure shown by HSCs and thus rods behave like hard spheres with a larger effective diameter of $(L+D)/2$. The hard spheres are preferentially adsorbed by the wall and form a small peak at $z \sim 1D$. The spheres form a layer on the surface (dashed curves) while an accomodation of rods around $z \sim 3D$ (continuous curves) give rise to a second layer next to the thin film of HS particles. In Figure 6.7 we show how the HSC rods progressively wet the wall as the pressure is increased in the range $P_{\mathrm{N}}^{*} = 0.1 - 0.4$. At a pressure of $P_{\mathrm{N}}^{*} = 0.3$, the number density of HSC corresponding to the first peak around $z \sim 0.5D$ is higher than that of HS; the crossover of competing wetting between the HSC and HS particles occurs in the range of $P_{\mathrm{N}}^{*} = 0.2 - 0.3$. As the pressure is further increased, the second peak in the density profile for the HSC particles moves towards the hard wall from $z \sim 3D$ to $z \sim 2D$ because the HSC is parallel to the wall, so it oscillates with a periodicity corresponding to the diameter D of the rod (not a half of the rod's length as in the case of the isotropic state). Since the HSCs progressively occupy more of the space close to the wall, there is a corresponding marked decrease in the density of HS particles near the wall.

The corresponding behaviour of the HSC-HS mixture in higher pressure range of $P_{\mathrm{N}}^{*} = 0.4 - 1.4$ is shown in Figure 6.8. It is clear from the density profiles that higher pressures enhance the wetting of the wall by the rod-like particles; the degree of nematic order of the HSC particles in the wetting layer increases with pressure and at sufficient high pressure ($P_{\mathrm{N}}^{*} = 1.0$), nematic wetting is induced on the surface in coexistence with a bulk isotropic state. In this interval of the pressure the packing effects are strong enough to form a thin nematic layer at the wall, since the additional nematic ordering at the wall prevails over the loss of the orientational entropy in this region. Because the excluded volume of the rods is larger than that of spherical particles, the wall preferentially adsorbs the HSC rods while the HS particles are pushed away from the wall. As a result, the density of HSs near the wall ($z < 2D$) decreases gradually with increasing pressure accompanied by an increase in the partial demixing of the fluid. When compared with the behaviour of the pure HSC rods, where the onset of nematic wetting is seen at $P_{\mathrm{N}}^{*} = 0.7$, the HSs destabilize the nematic order of the HSCs on the surface and the first instance of nematic layering at the high pressure of $P_{\mathrm{N}}^{*} = 1.0$. It should also be noted that the presence of the HS particles causes the system to be more isotropic, which is consistent with the higher value of the pressure at which the first nematic layer forms (cf. Figure 6.2).

We further show in Figure 6.9 the surface adsorption $\Gamma_i, i = \mathrm{HSC}, \mathrm{HS}$ of both species in the equimolar HSC-HS mixture, as obatined from Eq. (6.3). It is clear from this figure that both HSC and HS particles dry the walls at very low pressures, with a slightly higher (less negative) value of the adsorption for the HS particles than for the HSC particles. A crossover in the adsorption behaviour can be seen at a pressure of $P_{\mathrm{N}}^* \sim 0.16$ at which point the spheres are excluded from the region close to the surface and rods begin to wet the wall, forming a nematic wetting layer from $P_{\mathrm{N}}^* \sim 1.0$. The presence of the hard spheres shifts the value of the pressure corresponding to $\Gamma \geq 0$ to a lower pressure of $P_{\mathrm{N}}^* = 0.3$, compared with the value for the pure HSC of $P_{\mathrm{N}}^* \sim 0.5$. A further increase in the pressure leads to an enhancement in the preferential adsorption of the HSC particles by the hard wall while the (negative) adsorption of the HS particles is seen to further decrease. The dependence of the bulk compositions of HSC and HS species with pressure is presented in Figure 6.10. The trends for the bulk compositions are expected to be opposite to those for the surface adsorption. A slight demixing in the bulk region is seen at low pressures ($P_{\mathrm{N}}^* < 0.16$) because the rods preferentially occupy the bulk region and the spheres enter the space close to the surface. For pressures $P_{\mathrm{N}}^* > 0.16$, more spheres are displaced into the central of the cell due to the preferential adsorption of the rods at the hard wall, and a HS-rich bulk phase state is observed in coexistence with a rod-rich surface phase. Representative snapshots of configurations for pressures ranging from the low density (isotropic) to the high density (nematic) states are shown Figure 6.11. It can be seen there are a few spheres close to the wall at the very low density state ($P_{\mathrm{N}}^* = 0.04$) and the HS surface density decreases as the pressure is increased to $P_{\mathrm{N}}^* = 1.4$ where a nematic film is formed on the surface.

It is known [72] that the addition of spherical particles to a bulk phase of rod-like particles destabilize the formation of the bulk nematic phase. An analysis of the effect of increasing the overall HS composition on the nematic film of the HSC particles is shown in Figure 6.12. At a pressure of $P_{\mathrm{N}}^* = 1.0$, the four systems ($x_{\mathrm{HS}} = 0, 0.1, 0.2, 0.5$) are found to exhibit nematic surfaces on the hard walls, and degree of orientational order of the nematic layer decreases with increasing HS composition. This confirms that the nematic ordering at the surface is destabilized by increasing the concentration of hard spheres in the mixture. The dependence of surface adsorption on the HS compositions are shown in Figure 6.13 where we introduce the quantity $\Delta_{\mathrm{W}} = \Gamma_{\mathrm{HSC}} - \Gamma_{\mathrm{HS}}$ to describe the preferential adsorption of the HSC and HS particles on the hard walls. It is apparent that on increasing the overall hard-sphere concentration x_{HS}, the adsorption of HSs decreases more dramatically

than that of HSC; the preferential adsorption of the HSC particles even when there are more hard-sphere particles in the system is a consequence of the formation of the nematic ordering of HSCs at the wall.

6.4 Conclusions

A detailed MC simulation study of pure rods and of binary equimolar HSC-HS mixtures has been presented both in the bulk and at a hard surface. The surface phase behaviour of HSC at $L/D = 5$ is studied and adsorption the Γ is calculated. Surface drying is observed for the low-density isotropic system as the rods are displaced by the hard walls causing a reduced probability of finding a rod in the vicinity of the walls. Partial wetting and surface nematization is also found in the pure HSC system at intermediate-high pressures. The predicted bulk transition obtained in our simulation is in good agreement with previous results obtained using conventional NPT-MC simulation of the fully periodic system.
In the case of HSC-HS mixtures one can conclude that the preferential adsorption of the rods at the wall due to the formation of a nematic layering leads to an enhanced demixing between the HS and HSC species. At low densities (pressures), the rod-like particles dry (de-wet) the surface to retain orientational freedom while the spherical particles form a very thin absorbent film on the wall. A crossover in the preferential surface adsorption between HSC and HS particles occurs at intermediate pressures where the HSCs form a nematic wetting layer on the wall and the spheres progressively move to the bulk region. A positive adsorption of HSC occurs at lower pressures than for the pure component HSC system. By contrast, the destabilization of the nematic ordering on the wall due to the addition of HSs causes the formation of a nematic wetting layer at higher pressures.
In this chapter the focus has been restricted to isotropic and nematic states. Other surface induced structures are expected at higher pressures. The smectic order of HSC particles in confinement [258] and the layered structure observed in rod-sphere mixtures [227] are of particular interest to us. Another important feature which has been omitted from our current work is an analysis of the expected biaxiality of the rod-like particles close to wall [74,244]. The method adopted here to characterise the spatial distribution of the order parameter tensor is not sufficiently accurate to compute the biaxiality of HSC particles induced by the surface. We also plan to use advanced DFT methodologies [69, 86, 229] to predict the surface behaviour of HSC-HS systems and make comparisons with the results obtained in our current work.

The surface phase behaviour of HSC-HS mixtures in the higher-density region is investigated in next chapter where we will see the hard rods form a smectic monolayer on the hard wall.

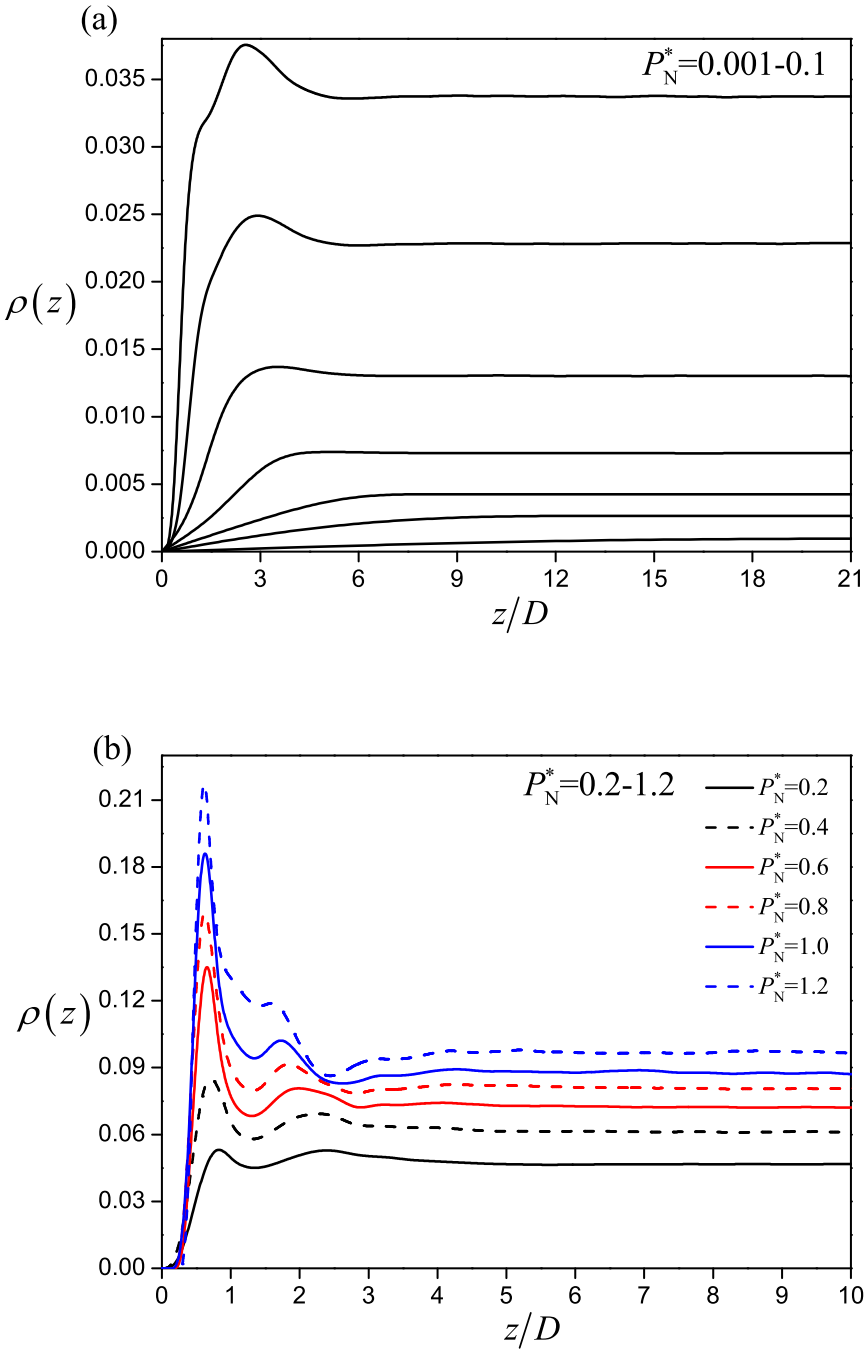

Figure 6.2: Density profiles $\rho(z)$ of a HSC fluid with $L/D = 5$ close to a hard wall. The curves correspond to varying normal pressures P_N^* (from bottom to top): (a) $P_N^* = 0.001, 0.003, 0.005, 0.01, 0.02, 0.05, 0.1$; (b): $P_N^* = 0.2 - 1.2$ with the increments of $\Delta P_N^* = 0.2$.

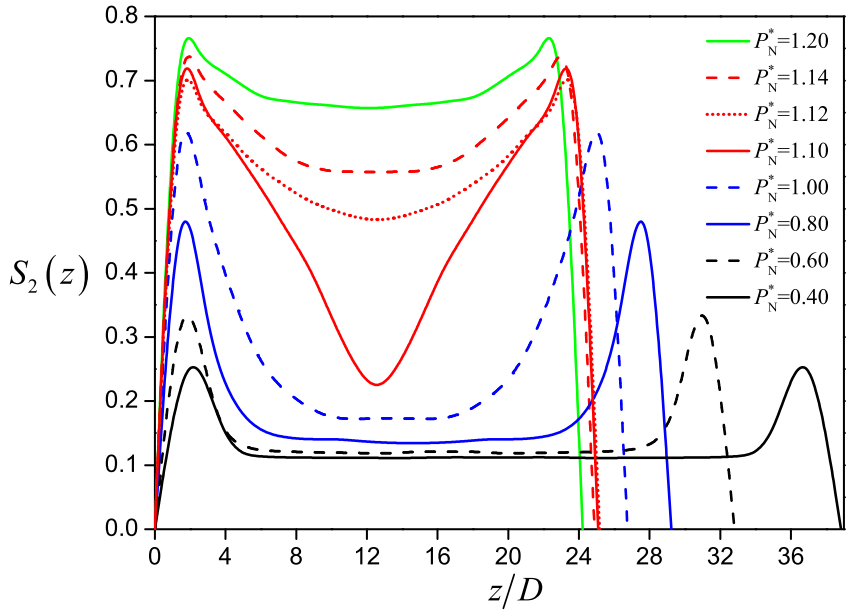

Figure 6.3: Nematic order parameter profiles of a HSC fluid with $L/D = 5$. The curves correspond to different normal pressures in the range $P_N^* = 0.4 - 1.2$.

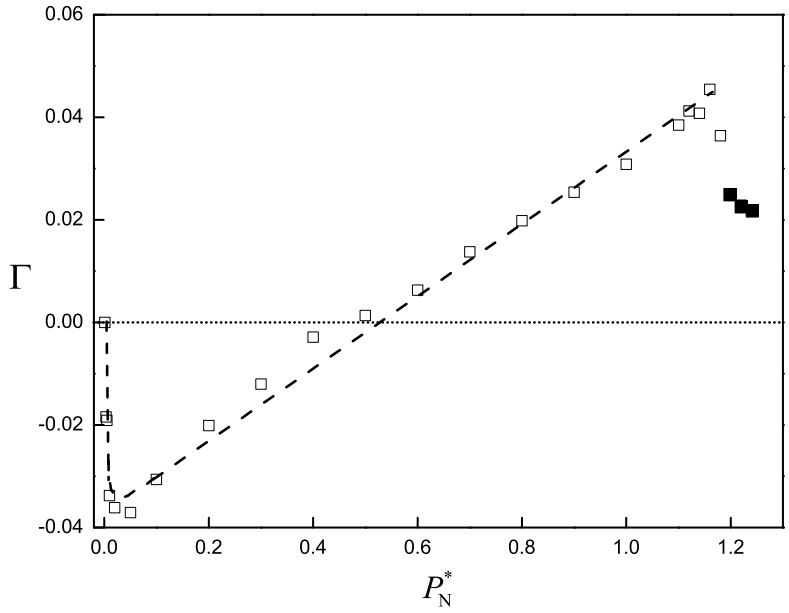

Figure 6.4: Surface adsorption as a function of the pressure P_N^* for a system of pure HSC. The open squares correspond to bulk isotropic states and the filled squares represent bulk nematic states and the dashed black curve is drawn to guide the eye.

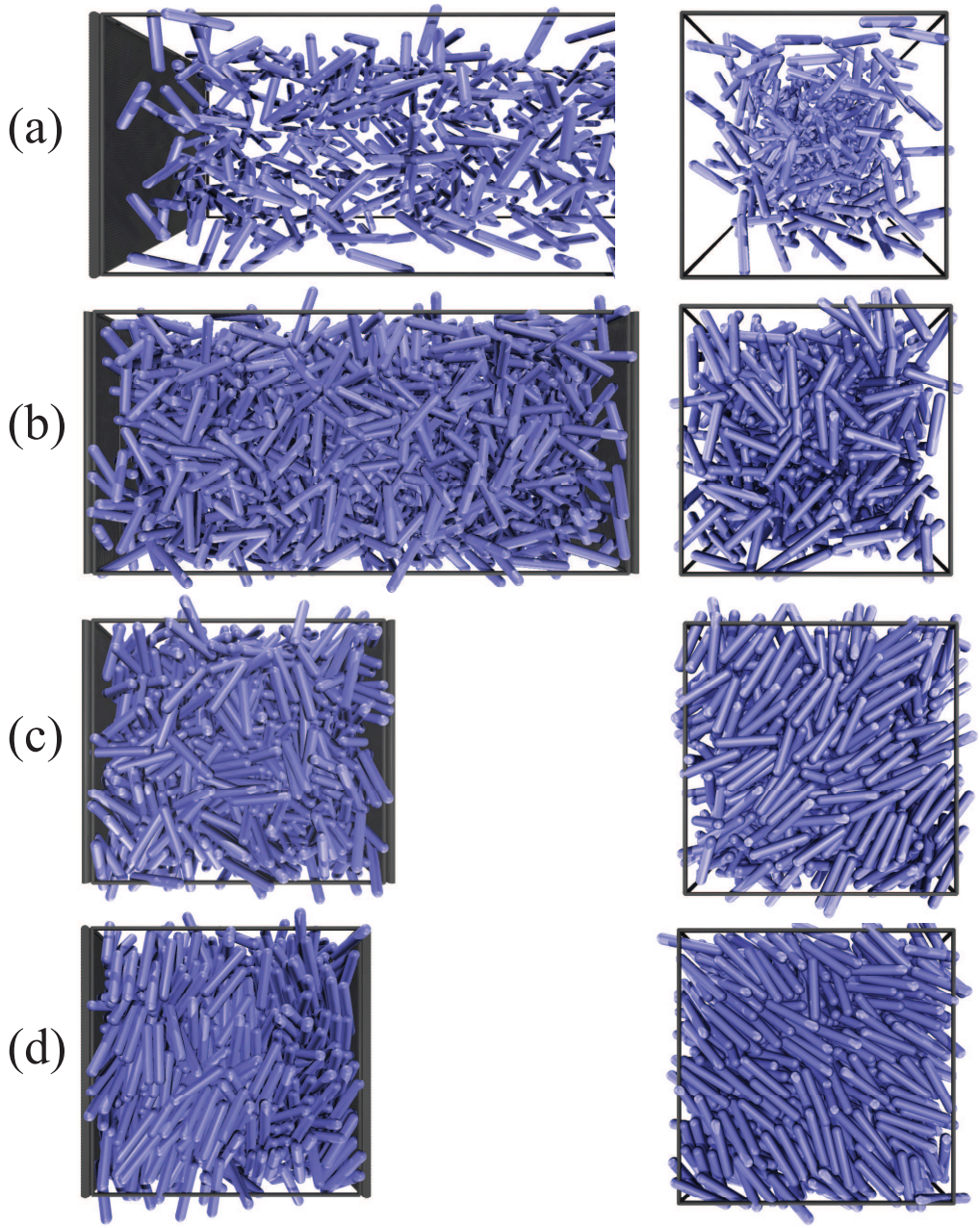

Figure 6.5: Snapshots of typical configurations for systems of pure HSC at various normal pressures: (a) $P_N^* = 0.02$, (b) $P_N^* = 0.20$, (c) $P_N^* = 0.90$, (d) $P_N^* = 1.14$. The configurations are viewed in a direction parallel to the surface (xy plane) on the left, and a direction perpendicular to the hard surface (perpendicular to the xy plane) on the right.

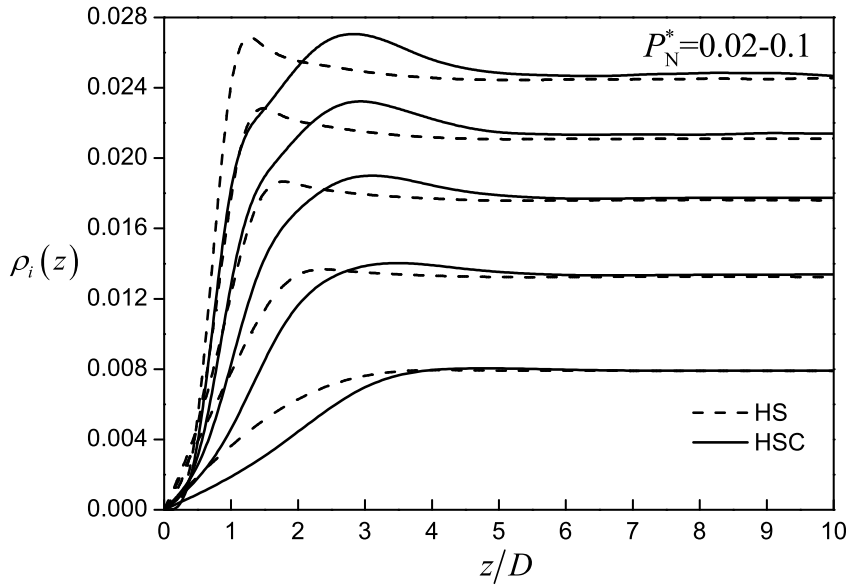

Figure 6.6: Density profiles $\rho_i(z)$ of HSC (continuous curves) and HS (dashed curves) particles close to a hard wall for an equimolar HSC-HS mixture ($x_{\mathrm{HS}} = 0.5$). The various curves correspond to states for different normal pressures P_{N}^*: bottom to top, $P_{\mathrm{N}}^* = 0.02 - 0.1$ with increments of $\Delta P_{\mathrm{N}}^* = 0.02$.

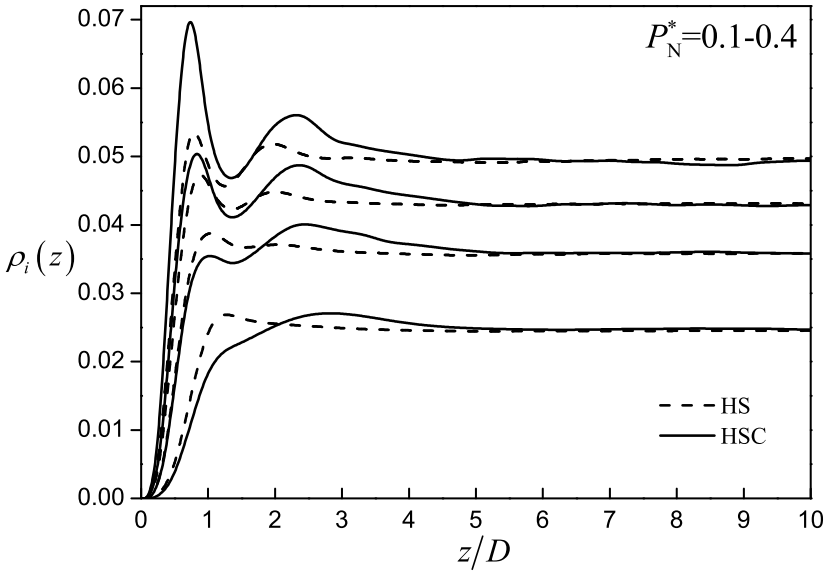

Figure 6.7: Density profiles $\rho_i(z)$ of HSC (continuous curves) and HS (dashed curves) particles close to a hard wall for an equimolar HSC-HS mixture ($x_{\mathrm{HS}} = 0.5$). The various curves correspond to states for different normal pressures P_{N}^*: bottom to top, $P_{\mathrm{N}}^* = 0.1, 0.2, 0.3, 0.4$.

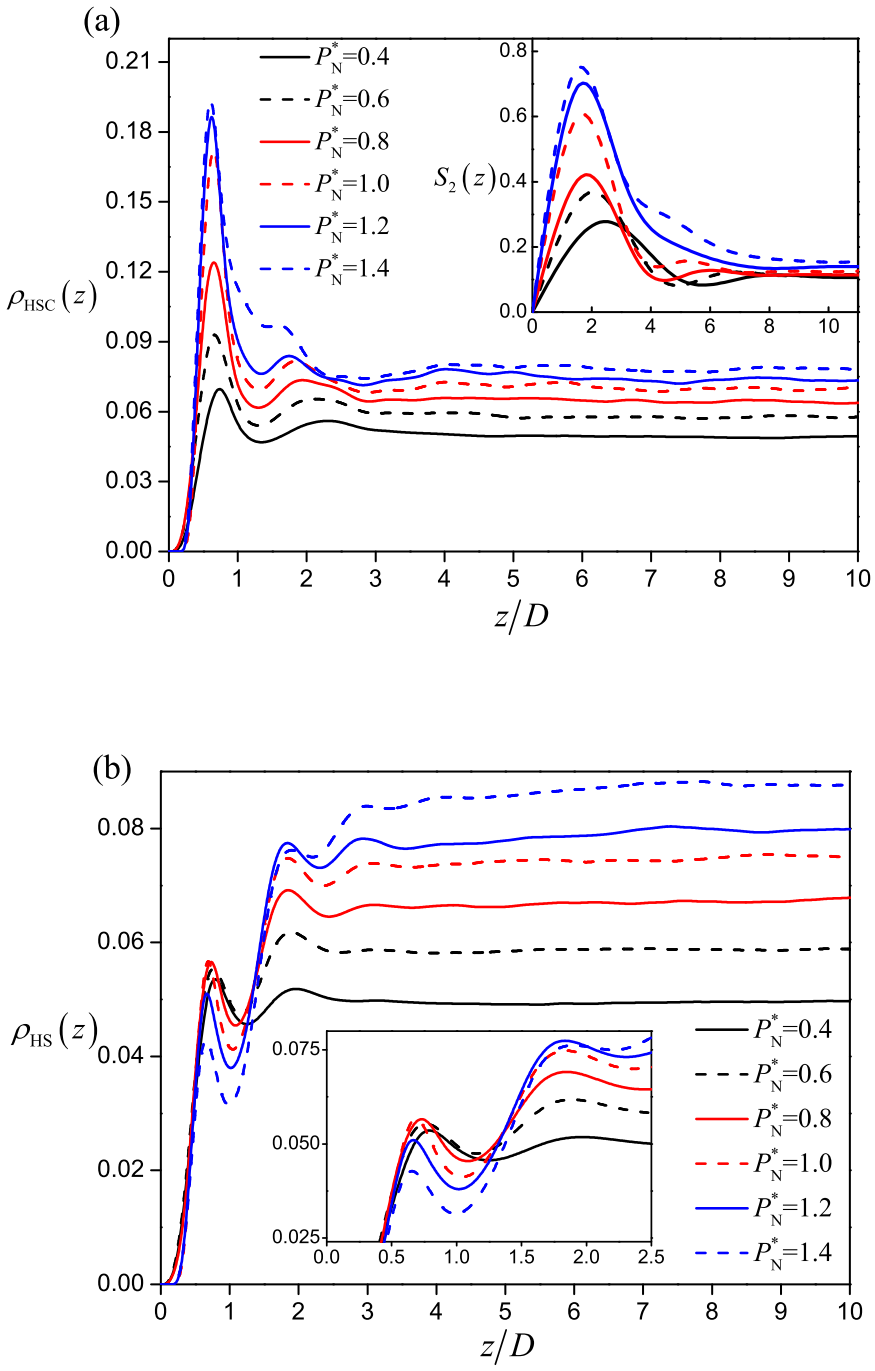

Figure 6.8: Individual density profiles of (a) HSC $\rho_{\mathrm{HSC}}(z)$ and (b) HS $\rho_{\mathrm{HS}}(z)$ particles in an equimolar HSC-HS mixture ($x_{\mathrm{HS}} = 0.5$). The various curves correspond to states for different normal pressures P_{N}^*: from bottom to top, $P_{\mathrm{N}}^* = 0.4 - 1.4$. The nematic order parameter profiles $S_2(z)$ of the HSC particles is shown in the inset of (a). The behaviour of the density profiles for HSs near a hard wall is highlighted in the inset of (b)

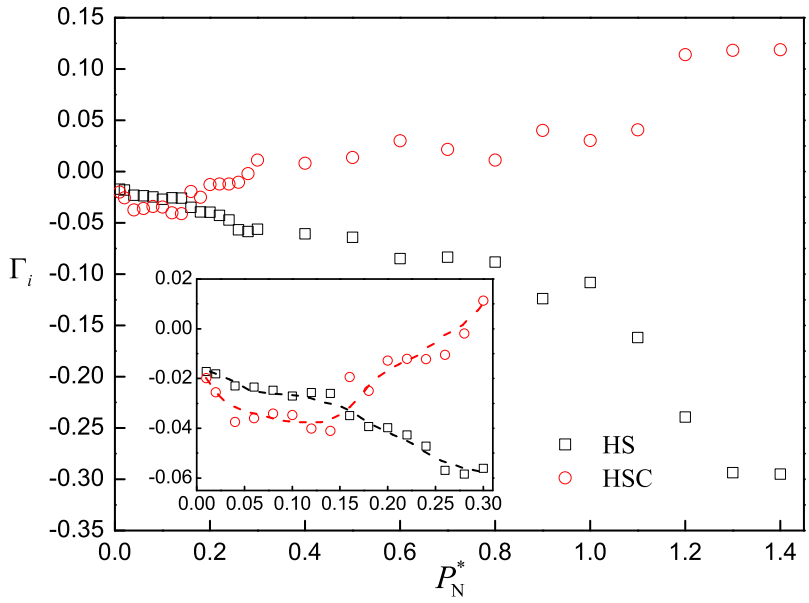

Figure 6.9: Surface adsorption Γ_i $(i = \mathrm{HSC}, \mathrm{HS})$ of the HSC-HS mixture plotted as a function of normal pressure P_{N}^*. The competing adsorption between the HSC and HS particles is highlighted in the inset. Dashed curves are drawn to guide the eye.

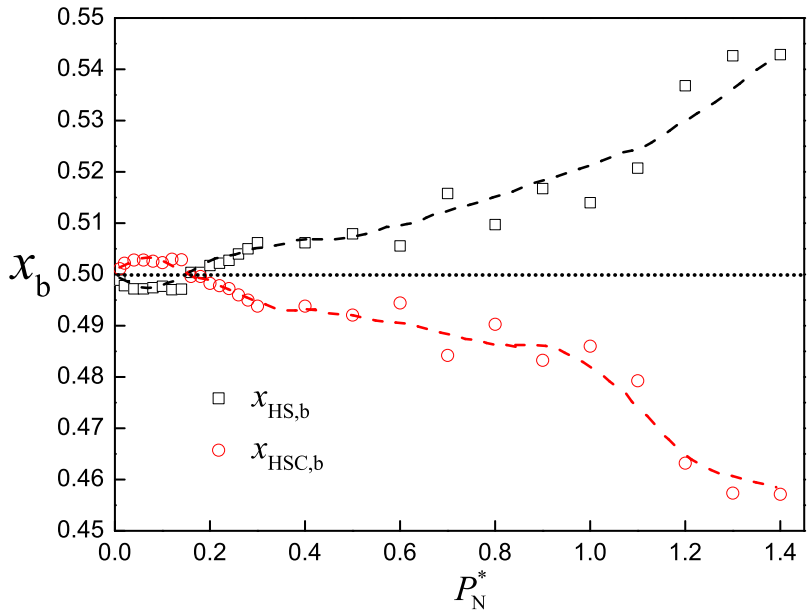

Figure 6.10: The bulk composition of the HSC-HS mixture as a function of the normal pressure P_N^*. The dotted line corresponds to the global overall composition of the mixture and the dashed curves are drawn to guide the eye.

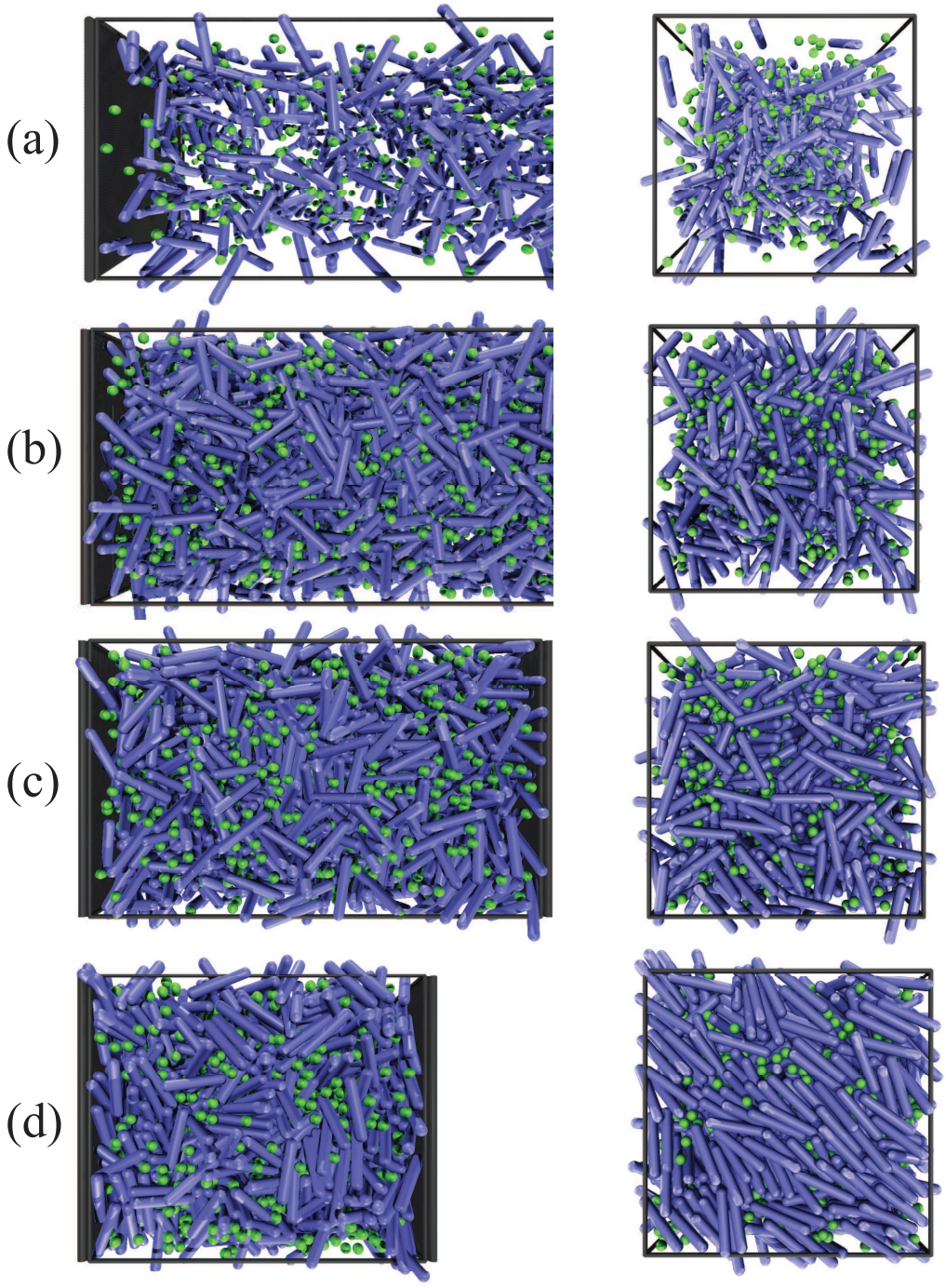

Figure 6.11: Snapshots of the HSC-HS mixture of $x_{\mathrm{HS}} = 0.5$ at various normal pressures: (a) $P^*_{\mathrm{N}} = 0.04$, (b) $P^*_{\mathrm{N}} = 0.26$, (c) $P^*_{\mathrm{N}} = 0.60$, (d) $P^*_{\mathrm{N}} = 1.40$. The configurations are viewed in a direction parallel to the surface (xy plane) on the left, and a direction perpendicular to the hard surface (perpendicular to the xy plane) on the right.

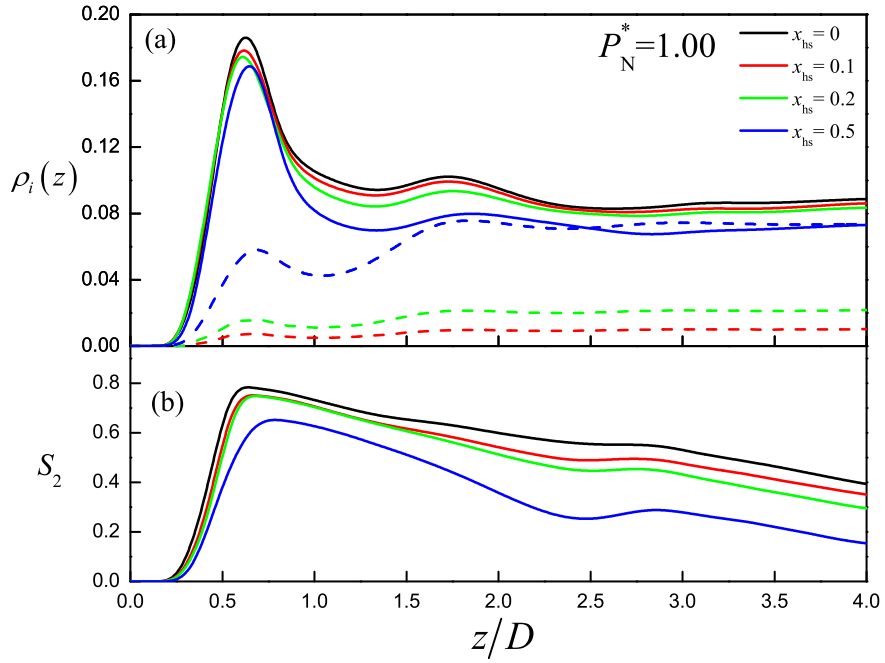

Figure 6.12: (a) density profiles $\rho_i(z)$ of HSC-HS mixture; and (b) nematic order parameter profiles $S_2(z)$ of the HSC against a hard wall at varying compositions. The continuous curves in (a) represent the density profiles of the HSC particles and the dashed curves are those for the HS particles.

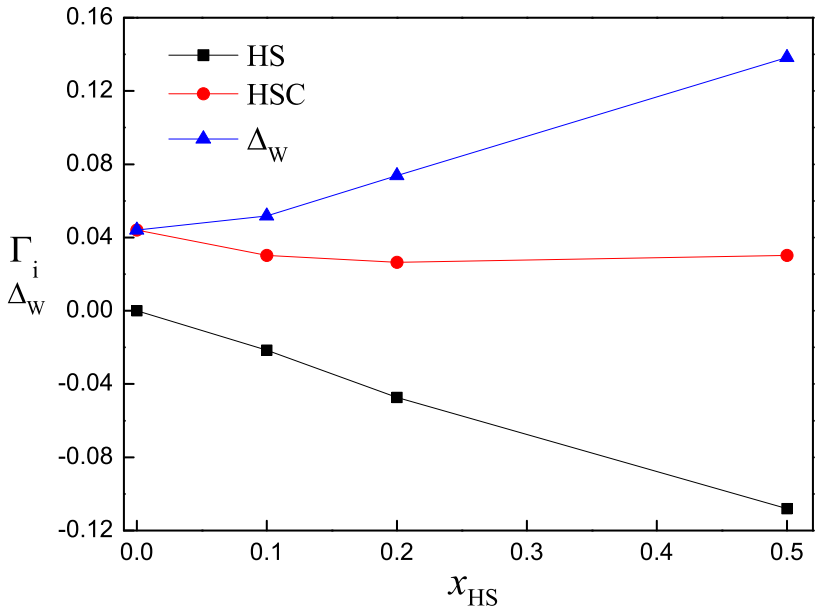

Figure 6.13: Dependence of surface adsorption on the overall HS composition of the HSC-HS mixtures in the presence of hard walls for a fixed pressure of $P_N^* = 1.0$. The trend for the differential adsorption $\Delta_W = \Gamma_{HSC} - \Gamma_{HSC}$ is also included.

Chapter 7

Entropy-driven surface smectization in a binary mixture of hard rods and hard spheres

This chapter is the continuation of our MC simulation study of HSC-HS mixture, but now devoted to the surface behaviour at high pressures. For sufficiently high-density states the formation of a smectic layer of hard rods is observed on the surface. The transition between nematic and smectic layers is related to a change of orientations adopted by rods at the surface on varying the pressure.

7.1 Introduction

Industrial applications of liquid crystals (LCs) in the display technology has led to a enormous market of optoelectronic devices [1]. In LC display, the LC materials are placed between two substrates. The interaction between LCs and solid surfaces is thus a problem of fundamental importance [246]. The phase behaviour of liquid crystals on a surface has attracted considerable interests both academically and industrially. The presence of substrates in LC systems introduces surface interactions which affect the LC ordering and causes inhomogeneities in the degree of positional and orientational order. A very rich surface phenomenology including surface drying/wetting and surface anchoring is therefore exhibited in LC systems in contact with surfaces

The discussion of the previous chapter was restricted to the behaviour of isotropic and nematic phases at surfaces or under confinement. Smectic ordering on the surface is com-

mon in thermotropic liquid crystals and has been observed in several experimental studies for example using X-ray scattering techniques [285–287], differential scanning calorimetry [288–290] and atomic force spectroscopy [291–293]. Only a few theoretical studies have shed light on capillary effects of smectic phases of rod-like LC which occurs in the high-density region. In earlier work, some theoretical attempts [294, 295] were made to predict and explain the mechanism of stabilization of smectic films and related wetting and layering transition [296, 297]. In more recent studies, de las Heras *et al.* [298–300] have used a generalised Onsager density functional theory to analyze the phase diagram of HSCs confined between two parallel planar substrates. The capillary smectization transition, which is found to be closely related with the layering transition, occurs at the thermodynamic state which is shifted from the corresponding bulk nematic-smectic transition. The interplay between the wall separation and smectic layer spacing which is referred to as the commensuration effect [296], enhances the degree of smectic ordering in the confined system of rod-like particles . It is important to note that in their analysis, the interaction between the rod particles and the walls is treated as an external field promoting homeotropic alignment at the walls (with the long molecular axes parallel to the surface). Steuer *et al.* [271] have examined isotropic, nematic, and smectic ordering in a confined LC system using MC simulation in NPT ensemble. In their system, the wall-fluid interaction is described with a Lennad-Jones type potential with an additional functional form that can be adjusted o give the desired surface anchoring (planar/homotropic). Malijevský and Varga [258] have studied the phase behaviour of perfectly aligned hard rods under confinement using an Onsager density functional theory (DFT). The hard rod is hereby represented by hard cylinder model which is slightly different from HSC model but they assume that the homogeneous alignment of rods (with the long molecular axes perpendicular to the surface) on the wall is preferred. Although there has been much attention on the bulk phase behaviour and fluid structure of LC mixtures [72, 112, 226], we note few studies involve the surface phase behaviour of such systems. In recent work [301] a version of fundamental-measure theory (FMT) was extended to binary mixtures of hard rods in contact with a single hard wall and perfect homeotropic alignment of the nematic director with the wall is assumed.

In this chapter, we apply the constant normal-pressure simulation method ($NP_{\mathrm{N}}T$-MC) described in Chapters 5 and 6 to the phase behaviour of a binary mixture of hard spherocylinders (HSCs) and hard spheres (HSs) between two parallel hard walls. Unlike previous investigations in which a surface potential is used to control the orientations of the rods

on the wall, the hard wall in our simulation is fully repulsive impenetrable surface. Because all of the interactions of HSC-HSC, HSC-HS, HS-HS and HSC/HS-wall involve hard-core repulsions, according to thermodynamics, the phase behaviour of the system is driven by maximising the entropy. The system is progressively compressed and equilibrated by increasing the component of the pressure tensor in the direction. The structural and orientational properties are determined and a particular emphasis is placed on the characterization of the surface smectization formed by the HSC particles at the surface. Additionally, we examine the effect of the addition of hard spheres on the surface smectization behaviour of the HSC particles and bulk phase behaviour of the HSC-HS mixtures.

7.2 Simulation details

As in the previous chapters constant normal-pressure Monte Carlo simulation ($NP_{\mathrm{N}}T$-MC, P_{N} is normal pressure) are performed for binary mixtures of $N_{\mathrm{HSC}} = 1482$ hard spherocylinder (HSCs) with an aspect ratio of $L/D = 5$ and N_{HS} hard spheres of diameter $\sigma = D$ where the number is determined by the overall mole fraction HS (x_{HS}) set for the system. As depicted in Figure 7.1, the simulation is undertaken in a rectangular box of dimensionless length $L_x = L_y = 25D$ and L_z in the usual Cartesian coordinates. Parallel hard walls are positioned at $z = 0$ and $z = L_z D$ and standard periodic boundary conditions are applied in x and y dimensions. In these simulations a fixed pressure normal to the hard walls is imposed along the z axis, so that the volume of the system fluctuates as the L_z box length changes moving the walls closer together or farther apart, while the box length in x and y axes directions remain fixed.

The $NP_{\mathrm{N}}T$-MC simulations are performed for 5×10^6 cycles to equilibrate the system and $5 - 8 \times 10^6$ cycles to accumulate the averages of the various properties. Each MC cycles consist of N ($N = N_{\mathrm{HSC}} + N_{\mathrm{HS}}$ is the total number of particles in the system) attempts to displace and rotate the randomly chosen particles and one trial volume change of the box along the z direction. As before the breaking of symmetry caused by the hard walls leads to inhomogeneous positional and orientational distributions of the HSCs and HSs throughout the system along the z axis, and the thermodynamic and structural properties are determined locally as appropriate profiles in terms of the distance from the walls. We recall here that in order to evaluate the density profile $\rho_i(z), i = \mathrm{HS}, \mathrm{HSC}$ and order parameter profile $S_2(z)$, the simulation box is divided in the z direction into several bins of equal width δz ($n_{\mathrm{bin}} = 200$ bins are used in order to be able to identify the constant

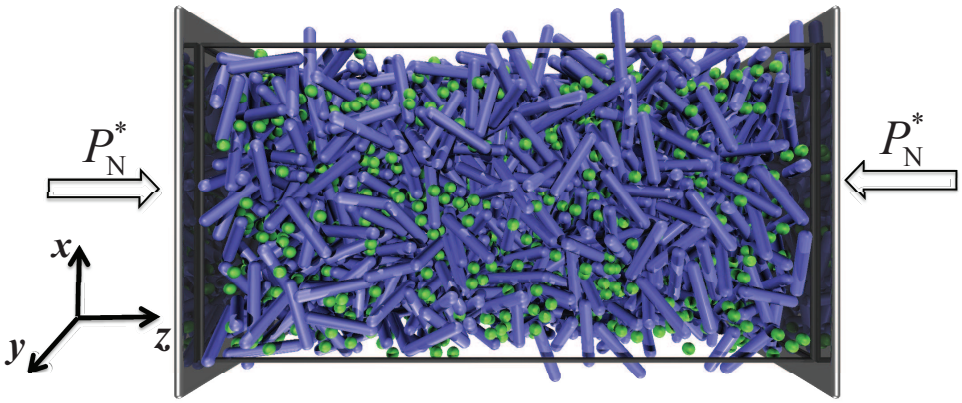

Figure 7.1: A typical snapshot of the mixture of hard spherocylinders and hard spheres in the NP_NT-MC simulation cell employed in our current work. The structureless hard walls are placed along the z axis and the normal pressure P_N is imposed along the z direction perpendicular to the surfaces.

homogeneous regions in the central part of the simulation cell):

$$\rho_i(z) = \frac{< N_i(z) >}{L_x L_y \delta z} \qquad i = \mathrm{HS}, \mathrm{HSC} \tag{7.1}$$

where $< \cdots >$ represents the ensemble average of the quantity in the brackets. The local composition profiles can also be determined from the corresponding density profiles:

$$x_i(z) = \frac{\rho_i(z)}{\rho_{\mathrm{HS}}(z) + \rho_{\mathrm{HSC}}(z)} \qquad i = \mathrm{HS}, \mathrm{HSC}. \tag{7.2}$$

and the adsorption Γ_i of component $i, i = \mathrm{HS}, \mathrm{HSC}$, is obtained from

$$\Gamma_i = \int_0^{L_z} [\rho_i(z) - \rho_{i,\mathrm{b}}] \mathrm{d}z \tag{7.3}$$

where $\rho_{i,\mathrm{b}}$ is bulk density of i-th species.

The nematic order parameter profile S_2 is obtained by measuring the standard nematic order parameter tensor $\mathbf{Q}(j)$ in each bin j:

$$\mathbf{Q}(j) = \left\langle \frac{1}{2N_{\mathrm{HSC},j}} \sum_{i=1}^{N_{\mathrm{HSC},j}} (3\vec{\omega}_i \bullet \vec{\omega}_j - \mathbf{1}) \right\rangle \tag{7.4}$$

where $\vec{\omega}_i$ is the orientation of the i-th rod, $N_{\mathrm{HSC},j}$ is the number of HSC particles in the j-th bin, and $\mathbf{1}$ is the unit matrix. On diagonalization of the $\mathbf{Q}(j)$ tensor [105], three eigenvalues are obtained and the largest of which is defined as the local nematic order parameter $S_2(z)$ associated with the j-th bin. Particular care should be taken with the calculation of the order parameter profile because of finite-size effect. It has been

shown by Eppenga and Frenkel [46] that the order parameter depends on the number of anisometric molecules considered the error in local order parameter is $\sim 1/(\sqrt{N_{\rm HSC}/n_{\rm bin}})$. In simulation we use $n_{\rm bins} = 20$ to calculate the order parameter profile and the expected error reduces to ~ 0.11 ($n_{\rm bin} = 20$).

The orientational order parameter profile $S_2(z)$, provides information about the degree of local nematic order as a function of the distance from the wall; in this case the order is quantified relative to the local nematic director $\hat{n}(z)$. In order to further study the nature of the orientational ordering close to the surface it is also useful to assess the relative orientation of the particles with respect to the planar surface. For this purpose we define the quantity $\bar{\theta}_{\rm w}(z)$ which represents a measure of the average angle between rods and the unit vector ($\hat{u}_{\rm w}$) normal to the surface of the hard wall (Fig. 7.2). The value of $\bar{\theta}_{\rm w}(z)$ in the j-th bin can be computed by:

$$\bar{\theta}_{\rm w}(j) = \frac{1}{N_{{\rm HSC},j}} \left\langle \sum_{i=1}^{N_{{\rm HSC},j}} \arccos(\vec{\omega}_i \cdot \hat{u}_{\rm w}) \right\rangle . \tag{7.5}$$

The average relative orientations distribution of the rods with respect to the wall normal are accessible from $\theta_w(z)$: the rods are parallel to the wall when $\theta_{\rm w} = 90^\circ$ and perpendicular to the wall if $\theta_{\rm w} = 0^\circ$.

In the remainder of this chapter the following dimensional quantities will be employed: the pressure is $P^*_{\rm N} = P_{\rm N} D^3/(k_{\rm B}T)$, the number density $\rho^* = ND^3/V = \rho D^3$, the packing fraction $\eta = (N_{\rm HSC}V_{\rm HSC} + N_{\rm HS}V_{\rm HS})/V$ (with $V_{\rm HSC}$ and $V_{\rm HS}$ the volumes of the HSC and HS particles, respectively), and the z dimension $L^*_z = L_z/D$.

7.3 Results and discussion

7.3.1 Pure hard spherocylinders at hard surfaces

The number density profiles of hard-spherocylinder particles contained between hard structureless parallel walls at various states of $P^*_{\rm N} = 1.10 - 1.30$ are shown in Fig. 7.3. At an intermediate pressure $P^*_{\rm N} = 1.10$ the system corresponds is at moderate density and is found to exhibit a nematic surface on the hard surfaces which is in coexistence with a bulk and isotropic state in centre of the simulation cell. The pressure is increased in a step wise manner from this state to $P^*_{\rm N} = 1.26$. On increasing the pressure the bulk density fluctuates at $\rho^* = 0.1$ while the density at $z \sim 0.5D$ decreases and the peak in the density profile between $z \sim 1D$ and $2D$ grows. This behaviour is associated with a change in the average position and orientation of the rod-like particles in the vicinity of

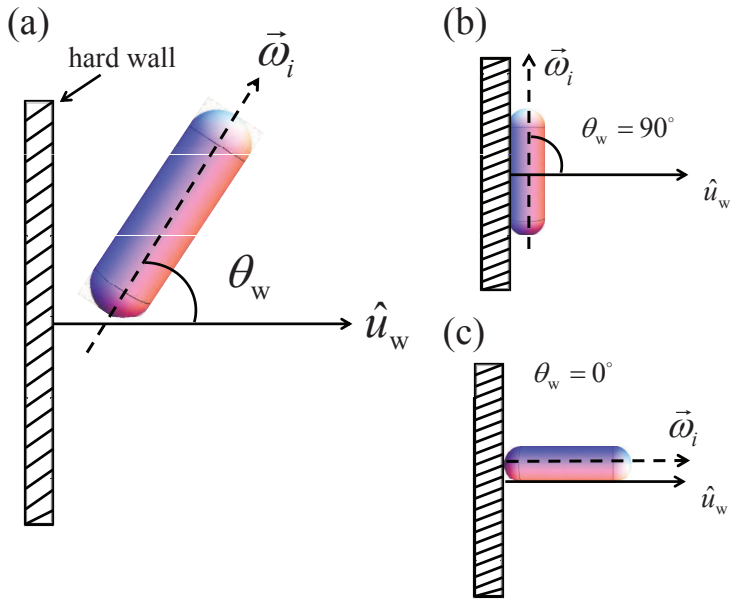

Figure 7.2: (a) The relative angle θ_w between the orientation of a hard-spherocylinder (HSC) particle ($\vec{\omega}_i$) and the unit vector $\hat{u}_w$ which is normal to the hard wall (represented as the shaded rectangular box). Two surface anchoring scenarios: (b) homogeneous (planar with surface) anchoring $\theta_w = 90°$ and (c) homeotropic (perpendicular with surface) anchoring $\theta_w = 0°$.

the surface. From the inset of Fig. 7.3, it is clear that the HSC particles form a very high-density layer on the surface when the pressure is increased to $P^*_N = 1.28$. The high peak in the density profile is seen to be located at $z \sim 3D$ which is half the length of the HSC particle. Recalling that the density profiles are obtained by computing the statistical average of the coordinates of centres of mass of rods in the box, the vanishing density of HSC particles found at distances $0 < Z < 2D$ and $4D < z < 5D$, corresponding to the states with $P^*_N = 1.28$ and 1.30, means that there are essentially no particles in these two regions. This supports the suggestion that the high-density layer formed by rods is of smectic-like nature where the rods adopt homeotropic alignment on the hard wall.
Compared with the the previous results obtained for the fully periodic $L/D = 5$ pure HSC system where a bulk nematic-smectic transition is observed at an isotropic pressure $P^* = 1.438$ [45], the surface transition exhibited in the presence of the hard walls at $P^* = 1.28$ corresponding to smectic layer can be considered as the onset of capillary smectization. The density profile is found to exhibit oscillations in the bulk region of the simulation box with peak spacings of $\sim 1D$ which indicates long-range positional order of

the HSC rods along the z axis. Surprisingly, however, the particles in the bulk smectic region are on average orientated parallel to the surfaces in contrast to the homeotropic perpendicular arrangement of the smectic surface layer.

The corresponding nematic order parameter profiles $S_2(z)$ for the different pressures are shown in Fig. 7.4. The orientational order is found to progressively increase in the pressure range from $P_{\mathrm{N}}^{*} = 1.10$ to 1.26 both in the bulk and in the vicinity of the hard surface. The large jump in bulk order parameter between $P_{\mathrm{N}}^{*} = 1.10$ and $P_{\mathrm{N}}^{*} = 1.20$ is associated with the a bulk phase transition from the isotropic state to the nematic state in the centre of the box. The value of local orientational nematic order parameter for the states characterized by $P_{\mathrm{N}}^{*} = 1.28$ and 1.30 is close to 1 in the region of $2D < z < 3D$ which corresponds to the location of the smectic monolayer on the hard wall. The spatial distribution of relative orientation of the HSC rods with respect to the wall normal is depicted in Fig. 7.5. For the nematic wetting layer which corresponds to the states of $P_{\mathrm{N}}^{*} = 1.10 - 1.26$, the value of $\bar{\theta}_{\mathrm{w}}(z)$ near the wall ($0 < z < 1D$) is 70 to 80° corresponding to a near planar anchoring. A small decrease in the effect of the planar anchoring is seen as the particles move away from the surface. When the smectic surface layer is formed at the higher pressures, the average of the angle between the orientations of the HSC rods and the unit vector $\hat{u}_{\mathrm{w}}$ corresponding to the surface normal lies 20 to 30° indicating that the rods in smectic wetting layer are slightly tilt on the hard wall rather than in a perfect perpendicular orientation. We do not however find any evidence for the formation of a second smectic layer before the formation of a bulk smectic region in the centre of the box which is orientated in a perpendicular geometry relative to the smectic surface layer.

Typical snapshots of configurations obtained from the simulation for states corresponding to pressures of $P_{\mathrm{N}}^{*} = 1.26$ (nematic surface layer in coexistence with a bulk nematic phase) and $P_{\mathrm{N}}^{*} = 1.28$ (smectic surface layer in coexistence with a bulk smectic phase) are illustrated in Fig. 7.6. It is apparent for the colour scheme to denote the orientations of the particles that the rods in the smectic layer corresponding to a homeotropic alignment (perpendicular to the surface) while a homogeneous/planar alignment (parallel to the surface) is adopted in the nematic layer. Since the particle-particle and particle-wall interactions are purely repulsive in nature, the surface transition between the nematic and smectic layerd is driven by entropy: the entropy loss due to the formation of smectic monolayer at the surface is compensated by an increase in the translational entropy of the rods. The surface adsorption in the HSC system for pressures ranging from $P_{\mathrm{N}}^{*} = 1.10$ to 1.30 is presented in Fig. 7.7. Three different regions can be identified: for $P_{\mathrm{N}}^{*} = 1.10$

to 1.12, a nematic layer is formed on the hard surface; in the higher pressure region of $P_{\mathrm{N}}^{*} = 1.14$ to 1.26, the slight decrease seen for the surface adsorption is due to the rise in bulk density associated with the phase transition from the bulk isotropic state to the bulk nematic state in the centre of the box; for the states corresponding to the appearance of the smectic monolayer, the surface adsorption curve experiences a discontinuous jump with values of Gamma as high as 0.20 to 0.25.

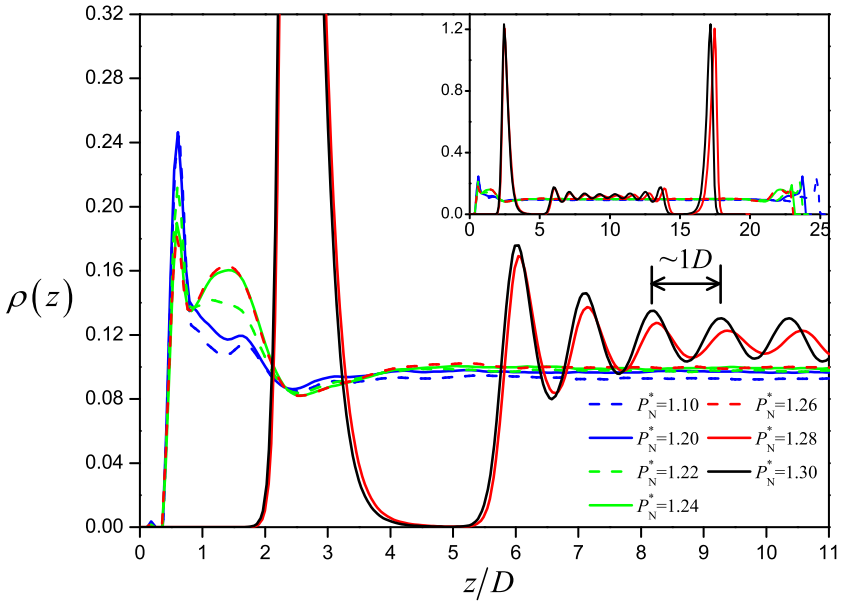

Figure 7.3: Density profiles $\rho(z)$ of a HSC fluid with $L/D = 5$ close to a hard wall. The curves correspond to varying normal pressures in the range $P_{\mathrm{N}}^{*} = 1.10 - 1.30$. The inset shows the density profiles throughout the simulation box.

7.3.2 Mixtures of hard spherocylinders and hard spheres at hard surfaces.

The surface phase behaviour of binary HSC-HS mixtures has also been investigated for an equimolar overall composition $x_{\mathrm{HS,tot}} = 0.5$. In Fig. 7.8, we present the density profiles of the HSC and HS particles determined for a range of high density states corresponding to pressures from $P_{\mathrm{N}}^{*} = 1.5$ to 1.62. The rods form a nematic wetting layers at $z \sim 0.5D$ when $P_{\mathrm{N}}^{*} = 1.50$ to 1.58. The broad peak in the density profile seen $z \sim 1.5D$ is found to grow while the surface peak at $z \sim 0.5D$ shrinks with increased pressure. As mentioned in the

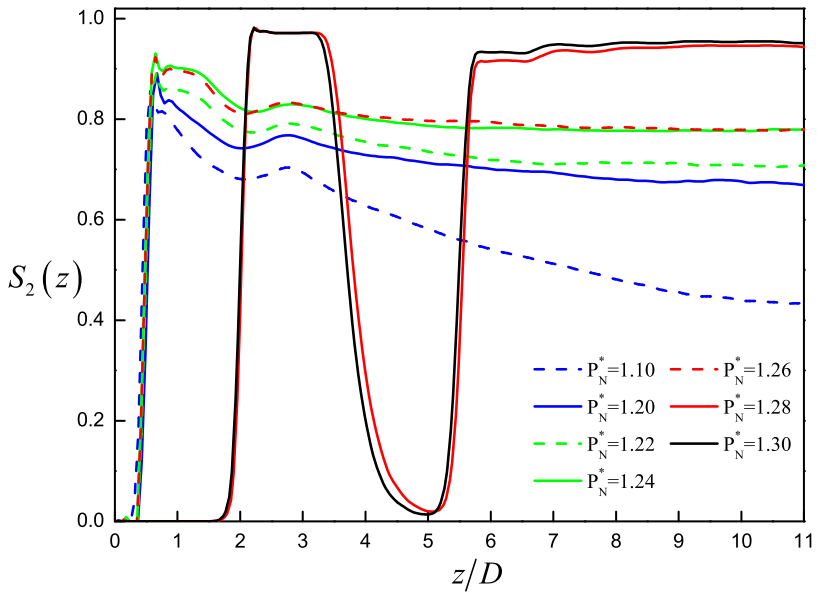

Figure 7.4: Nematic order parameter profiles of a HSC fluid with $L/D = 5$. The curves correspond to different normal pressures in the range $P_{\mathrm{N}}^{*} = 1.10 - 1.30$.

previous discussion, we relate the emergence of the peak at $z \sim 1.5D$ and the disappearance of the peak at $z \sim 0.5D$ with re-orientations of the HSC particles relative to the hard wall which precedes the formation of the smectic monolayer at higher pressures. The high-density smectic layer can clearly be observed in the density profiles of Fig. 7.8 for the highest pressure $P_{\mathrm{N}}^{*} = 1.60$ and 1.62. Compared with the surface behaviour of the system comprising pure HSC rods ($x_{\mathrm{HS}} = 0$), the equimolar HSC-HS mixture ($x_{\mathrm{HS}} = 0.5$) exhibits smectic layering at higher pressure and no oscillations of HSC density are exhibited in the bulk region. This means that in contrast to the behaviour found for the pure component system, the smectic monolayer formed by the HSC-HS mixture does not coexist with a bulk smectic phase in the central part of the box. The differences are certainly caused by the destabilization of orientationally ordered phases on addition of spherical particles to the system. The density profile of the HS particles shown in Fig. 7.8(b) indicate that the wall is almost completely depleted (dried) of the spheres for the whole range of pressures studied. Once the smectic monolayer appears at the wall, the hard spheres are found to form a second layer on the smectic surface at $z \sim 6D$, with a marked increase in the bulk HS density caused by their exclusion from the high-density smectic layer of HSCs.

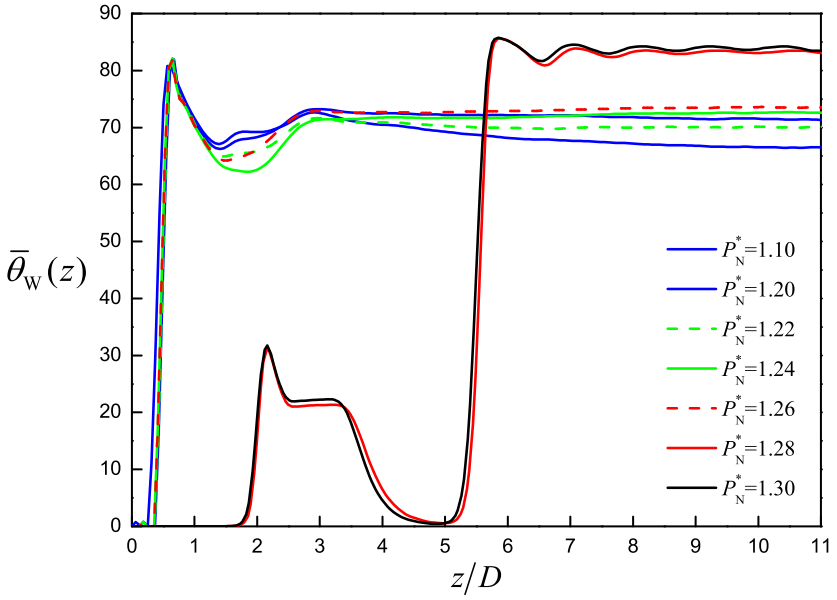

Figure 7.5: The profiles of of the average of the relative angle $\bar{\theta}_{\mathrm{w}}(z)$ between principal axes of the hard spherocylinders and the unit vector $\hat{u}_{\mathrm{w}}$ normal to the hard walls for states corresponding to pressures of $P_{\mathrm{N}}^{*} = 1.10$ to 1.30.

Profiles of the local orientational nematic order along the z direction obtained for the equimolar HSC mixture are shown in Fig. 7.9. For the states with pressures of $P_{\mathrm{N}}^{*} = 1.50$ to 1.58, peaks can be seen in the $S_2(z)$ profiles at $z \sim 0.5D$, The smectic monolayer that appears at $z \sim 3D$ for the state with $P_{\mathrm{N}}^{*} = 1.60$ is found to possess a high degree of orientational order ($S_2 > 0.9$). It is interesting to see that a weakly ordered nematic layer is formed by HSCs on the surface of the smectic monolayer which is now play the part of a hard surface of a certain roughness due to the hemispherical caps of the HSC particles. In bulk region of the state corresponding to the relatively high pressure of $P_N^{*} = 1.60$, the equimolar HSC-HS mixture is still seen to exhibit an isotropic state presumably because of the relatively high HS concentration in the bulk (which increases with pressure) that leads to a destabilization of the nematic order. In Fig. 7.10, we show the relative orientation $\bar{\theta}_{\mathrm{w}}(z)$ of the HSCs with respect to the surface normal. For the states corresponding to pressures of $P_{\mathrm{N}}^{*} = 1.50$ to 1.58 , the value of $\bar{\theta}_{\mathrm{w}}$ in the region of $z \sim 2$ to $3D$ gradually decreases from 70° to 63° which signals the formation of the smectic monolayer; once the smectic layer has been stabilized in the higher-density states, the relative orientation of

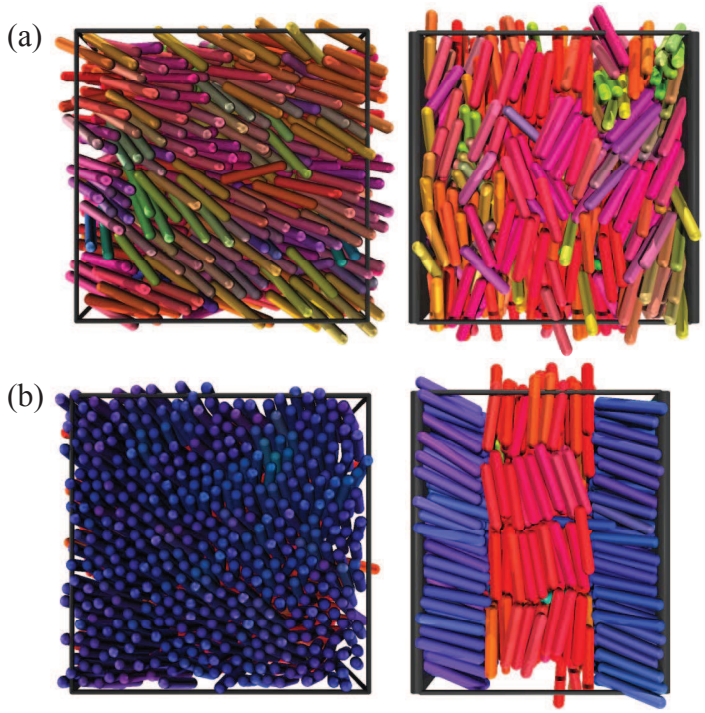

Figure 7.6: Snapshots of typical configurations for systems of pure HSC at pressures: (a) nematic layer at the surface ($P_{\mathrm{N}}^{*} = 1.26$), (b) smectic layer at the surface ($P_{\mathrm{N}}^{*} = 1.28$). The configurations are viewed in a direction perpendicular to the hard surface (perpendicular to the xy plane)on the left, and a direction parallel to the surface (xy plane)on the right. The colours denote the orientation of the HSC particles relative to the frame of the simulation box.

the rods at $z \sim 2D$ to $3D$ ranges from $\bar{\theta}_{\mathrm{w}} = 28°$ to $45°$ indicating that the smectic layer is tilted with respect to the hard wall. The rods near the smectic monolayer are oriented parallel with the wall form a weakly ordered film at $z \sim 6D$ which corresponds to the surface of the smectic layer.

The surface adsorption $\Gamma_i$for $i = \mathrm{HSC}, \mathrm{HS}$, determined for the equimolar HSC-HS mixtures over the pressure range of $P_{\mathrm{N}}^{*} = 1.00$ to 1.70 is shown in Fig. 7.11. The discontinuous jump in Γ_{HSC} for the HSC rods at $P_{\mathrm{N}}^{*} = 1.60$ is associated with formation of the smectic monolayer of the HSC rods which results in a corresponding dramatic drop in Γ_{HS} of the spherical particles. In Fig. 7.12 we compare the configurations of two states of the HSC-HS mixtures, one exhibiting the nematic layer ($P_{\mathrm{N}}^{*} = 1.58$) and the other the smectic monolayer ($P_{\mathrm{N}}^{*} = 1.60$).

We have observed smectic monolayer ordering at hard walls in HSC-HS mixtures with

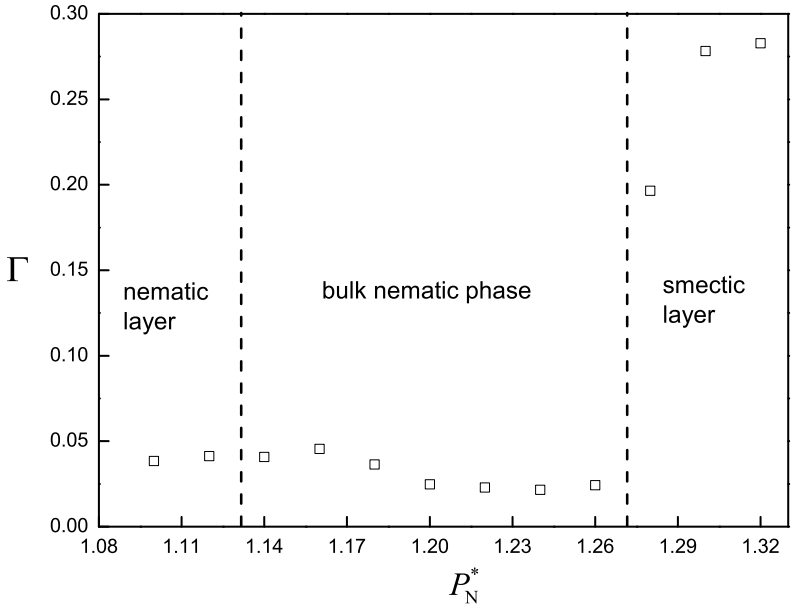

Figure 7.7: The surface adsorption Γ of hard spherocylinders (HSC) particles obtained from NP_NT-MC simulations of $N = 1482$ HSCs contained between hard parallel walls as a function of normal pressure P_N^*. Three different adsorption regions can be identified: nematic layer, bulk nematic phase, and smectic layer.

a range of overall HS composition, i.e., $x_{HS,tot} = 0 - 0.5$. Snapshots of typical configurations simulated for the mixtures are presented in Fig. 7.13. As shown in Fig. 7.14, the pressure corresponding to the smectic monolayer transition depends critically on the overall composition. The profiles for the density and nematic order parameter of the lowest-density (pressure) states exhibiting the smectic monolayer are shown in Fig. 7.14 and 7.16, respectively. All of these systems exhibit the similar pattern for the behaviour of the profiles near the wall while there is a noticeable difference in the bulk region. The degree of nematic order in the bulk phase is weaken by the increasing concentration of spherical particles, and eventually the systems with $x_{HS,tot} = 0.4$ and 0.5 are characterized by an isotropic bulk state.

In order to examine the effect of the system size on the surface transition of the HSC-HS mixtures, we simulate systems with double the size corresponding to $N_{HSC} = 2964$ rods for compositions of $x_{HS} = 0, 0.2$, and 0.5. Surface transitions between a state with a nematic layer and smectic monolayer are also observed, and the corresponding snapshots of the

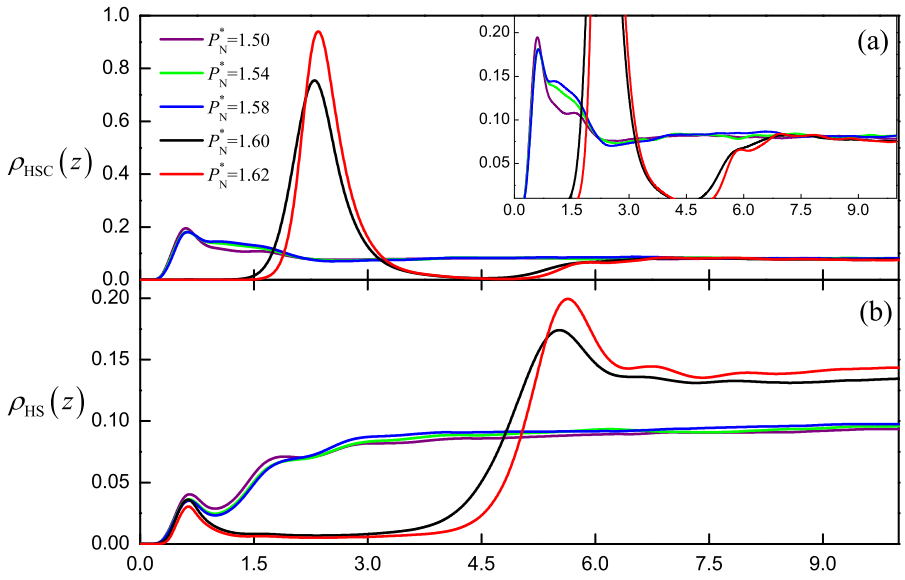

Figure 7.8: Density profiles $\rho_i(z)$ of HSC (a) and HS (b) particles close to a hard wall for an equimolar HSC-HS mixture ($x_{HS} = 0.5$). The various curves correspond to states for different pressures in the range of $P_N^* = 1.50$ to 1.62. The density profile of the HSC particles close to the hard wall is shown in the inset of (a).

molecular configurations are presented in Fig. 7.17. No qualitative difference is found with the results obtained for smaller system ($N_{HSC} = 1482$), though a small quantitative deviation in the precise position of the phase transition can be seen (c.f. Fig. 7.15): the transition pressures for systems of double the size are found to be slightly larger than those of the smaller systems, indicating a small but noticeable capillary effect due due to the two confining walls.

7.4 Conclusions

The results of a NP_NT-MC simulation study have been presented for the surface behaviour of mixtures of hard spherocylinders and hard spheres of varying composition ($x_{HS} = 0$ to 0.5) in the high-density region. We observe the so-called capillary surface smectization phenomena in which a smectic layer is formed on smooth hard walls which are at a lower pressure compared with the bulk nematic-smectic transition of the corresponding pure fully periodic HSC system. The smectic monolayer is characterized in terms of the density

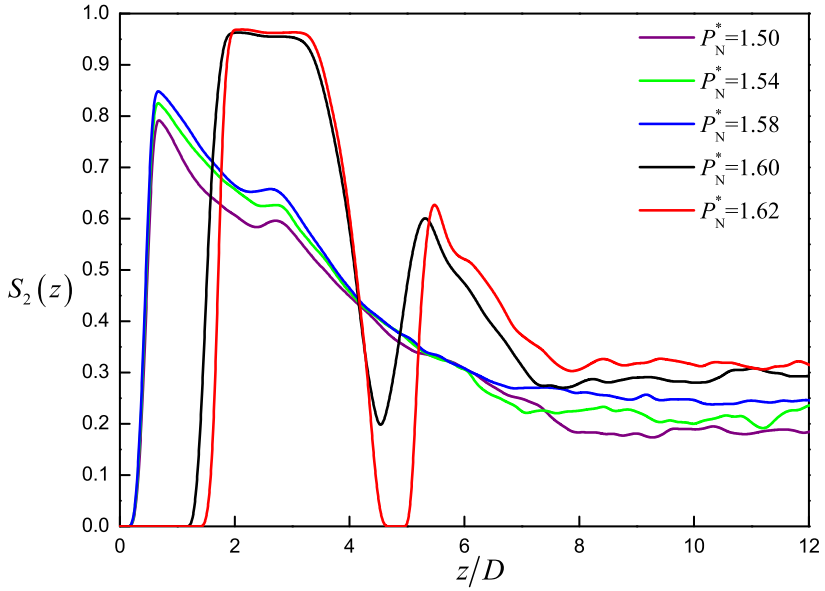

Figure 7.9: Nematic order parameter profiles for an equimolar HSC-HS mixture ($x_{\mathrm{HS}} = 0.5$). The curves correspond to different normal pressures in the range of $P_{\mathrm{N}}^* = 1.50$ to 1.62.

and nematic order parameter profiles of the HSC rods, and the average of the relative orientation between the principal axis of the rods and the surface normal.

The formation of smectic monolayer results in a transition from homogeneous planar anchoring (parallel to the hard surface) to homeotropic alignment (perpendicular to the planar surface) in the high-density region. In the case of HSC-HS mixture system, the formation of the smectic monolayer in the vicinity of the hard wall results in the increase in concentration of spherical particles in the bulk. A mixed wetting film of HSs and orientationally ordered HSC rods forms near the surface of the smectic monolayer. The surface transition between nematic film and smectic layer determined for systems of various HS compositions. The transition pressure is found to follow a roughly linear dependence on the overall mole fraction of spherical particles. By simulating systems of a larger size we have shown that though there is a small effect of confinement, the formation of the smectic monolayer does not appear to an artefact of system size effects.

There are several choices for further studies. Simulating the phase behaviour of HSC-HS mixtures on the single wall [244] allow one to ensure that the formation of smectic wetting

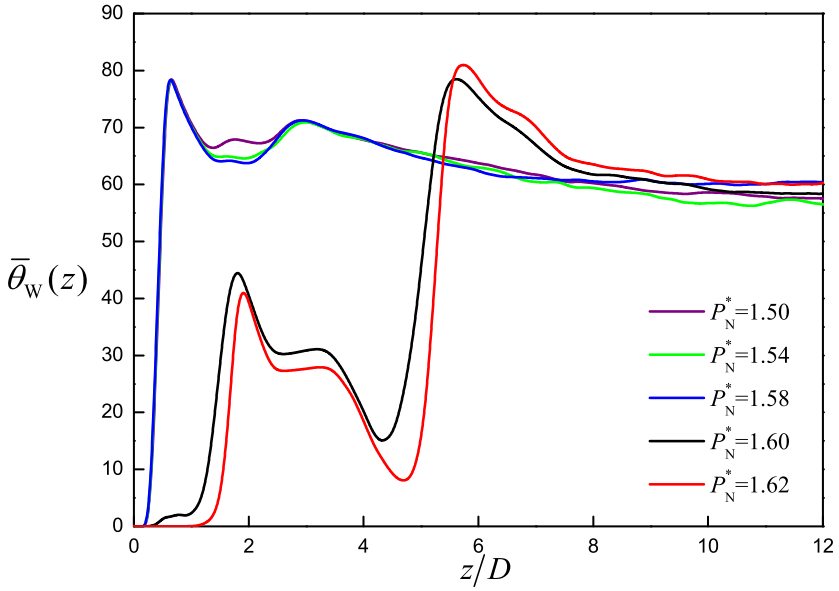

Figure 7.10: The profiles of of the average of the relative angle $\bar{\theta}_{\mathrm{w}}(z)$ between principal axes of the hard spherocylinders and the unit vector $\hat{u}_{\mathrm{w}}$ normal to the hard walls for states of an equimolar HSC-HS mixture ($x_{\mathrm{HS}} = 0.5$)corresponding to pressures of $P_{\mathrm{N}}^{*} = 1.50$ to 1.62.

layer is a well defined surface transition that does not result from confinement effects. It would also be interesting to examine geometric effects of the wall on the surface behaviour of LCs rather than confine the study to planer surfaces, e.g., spherical or cylindircal pores [268,272,302] or the roughness of the wall [270]. The use of the latest developments in density-functional theory [69,86,229] to determine the fluid structure of HSC-HS mixtures on the hard wall would also be useful to obtain a better understanding of the phenomena studied in the current work.

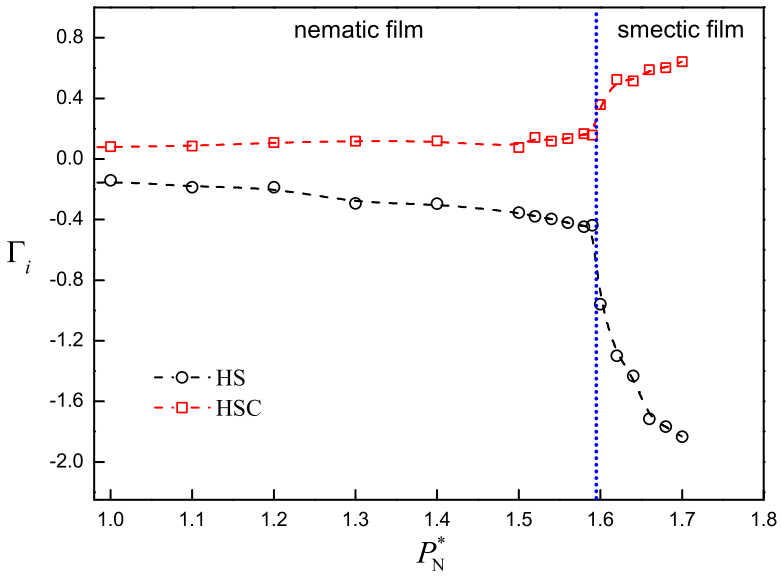

Figure 7.11: The surface adsorption Γ of hard spherocylinders (HSC) particles obtained from NP_NT-MC simulations of an equimolar HSC-HS mixture ($x_{HS} = 0.5$) contained between hard parallel walls as a function of normal pressure P_N^*. Two different adsorption regions can be identified: nematic layer and smectic monolayer. The dashed curves are drawn to guide the eye.

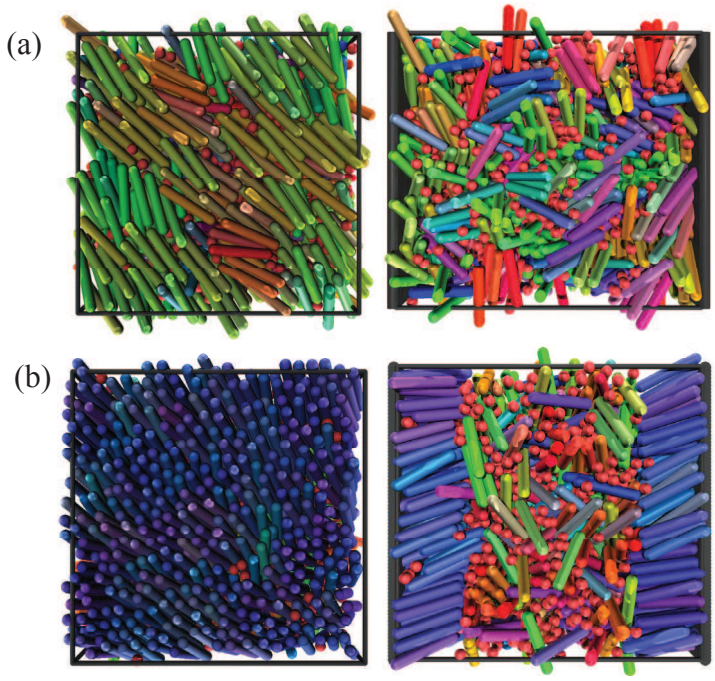

Figure 7.12: Snapshots of typical configurations for systems of pure HSC at pressures: (a) nematic layer at the surface ($P^*_{\mathrm{N}} = 1.58$), (b) smectic layer at the surface ($P^*_{\mathrm{N}} = 1.60$). The configurations are viewed in a direction perpendicular to the hard surface (perpendicular to the xy plane)on the left, and a direction parallel to the surface (xy plane)on the right. The colours denote the orientation of the HSC particles relative to the frame of the simulation box.

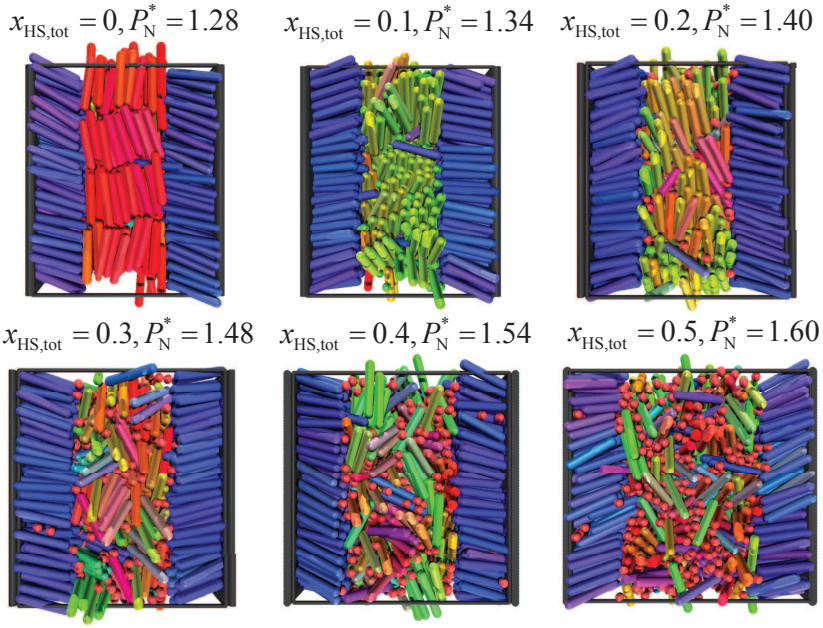

Figure 7.13: The snapshots for lowest-density (pressure P_{N}^{*}) states of HSC-HS mixture for HSC-HS mixtures with various overall composition $x_{\mathrm{HS,tot}}$ exhibiting smectic monolayer at the wall. The colours denote the orientation of the HSC particles relative to the frame of the simulation box.

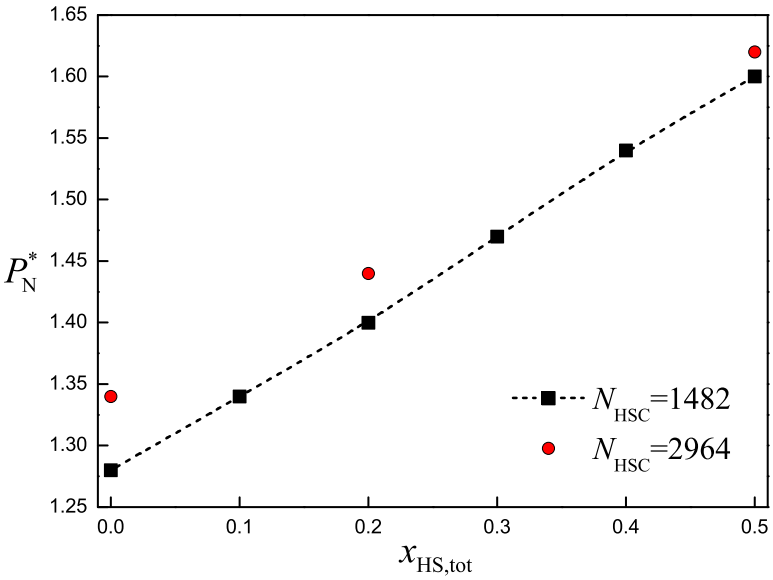

Figure 7.14: The lowest value of the pressure P_N^* necessary to induce the formation of a smectic monolayer for mixtures of hard spherocylinders (HSCs) and hard spheres (HSs) on hard surfaces is plotted as a function of overall HS mole fraction $x_{HS,tot}$. The dashed line is to guide the eye.

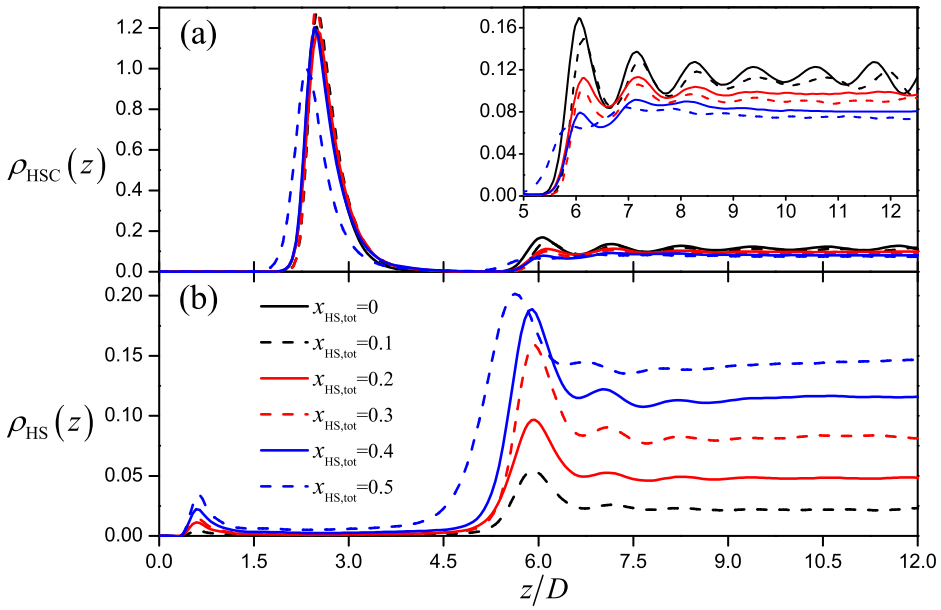

Figure 7.15: Density profiles $\rho_i(z)$ of HSC (a) and HS (b) particles close to a hard wall. The curves correspond to the lowest-density states of HSC-HS mixtures with various overall compositions exhibiting smectic monolayer. The density profiles of the HSC rods in the bulk region are shown in the inset of (a).

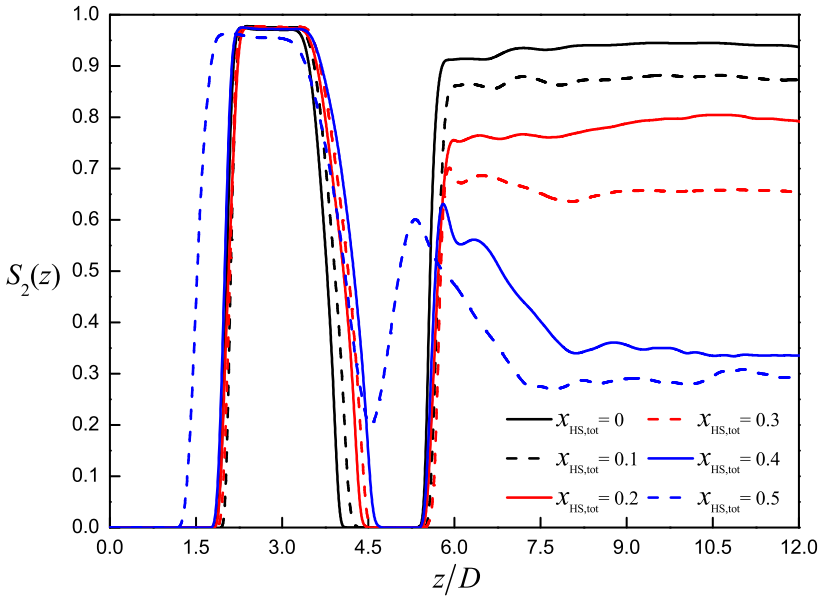

Figure 7.16: Nematic order parameter profiles for HSC-HS mixture mixtures with various overall compositions. The curves correspond to different pressures necessary to induce the formation of a smectic monolayer for the mixtures with various overall compositions.

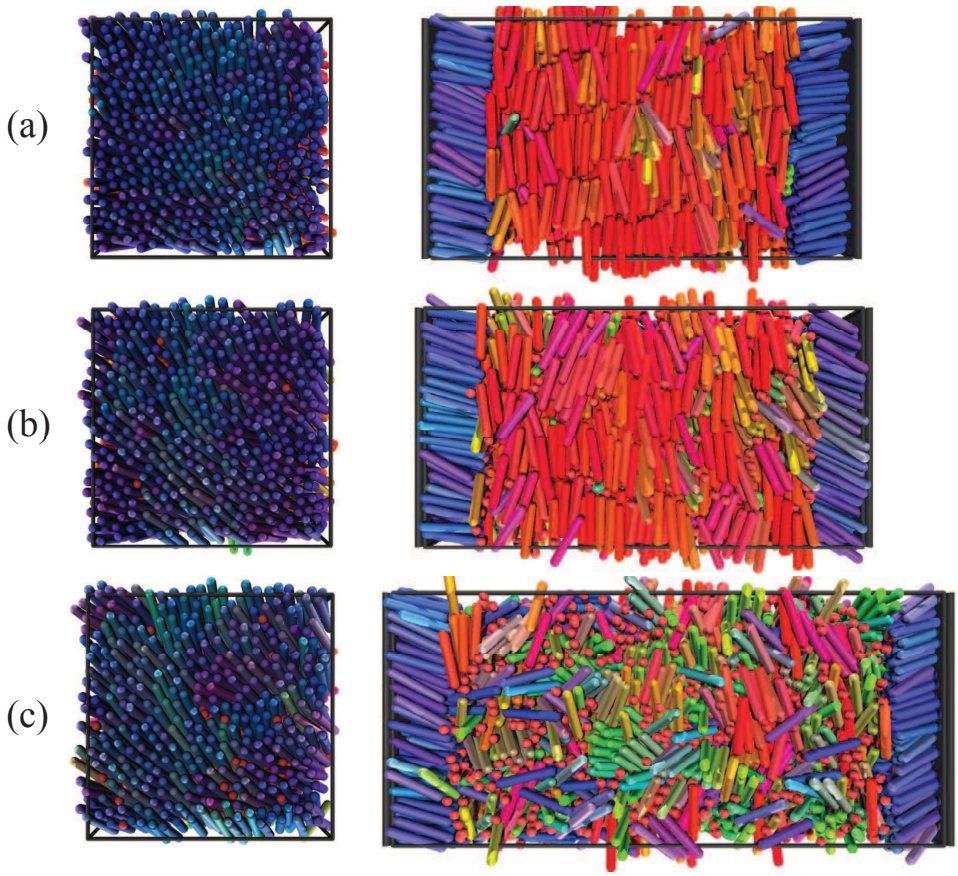

Figure 7.17: The snapshots for lowest-density states of HSC-HS mixtures ($N_{\mathrm{HSC}} = 2964$) with overall composition (a) $x_{\mathrm{HS,tot}} = 0$, (b) $x_{\mathrm{HS,tot}} = 0.2$, and (c) $x_{\mathrm{HS,tot}} = 0.5$ exhibiting smectic monolayer at surfaces. The configurations are viewed in a direction perpendicular to the hard surface (perpendicular to the xy plane)on the left, and a direction parallel to the surface (xy plane)on the right. The colours denote the orientation of the HSC particles relative to the frame of the simulation box.

Chapter 8

Concluding remarks

The main aim of the work presented in this thesis has been on understanding and describing liquid crystalline phase behaviour by using both theory and computer simulation. In the first part of the work including Chapters 2-4, we develop a generic equation of state for isotropic and nematic phases of hard oblate disc-like particles. The effect of attractive interactions on the LC phase behaviour is explored in Chapters 3 and 4 based on these reference hard-core anisotropic particle models. The focus of the work turns to computer simulation of LC mixtures in the second part of the thesis (Chapters 5-7). The isotropic-nematic phase diagram of rods-sphere mixtures and a detailed study of the surface behaviour of the system in contact with impenetrable walls is presented. Various ordering transitions and the competing adsorbing between rods and spheres on the surface is investigated.

In Chapter 2, our efforts are devoted to an improvement and extension of Onsager-Parson-Lee theory for the isotropic and nematic phases of hard disc particles. Simulation results [87] show the higher-order virial coefficients of very thin hard disc (cut sphere of $L/D < 0.1$) exhibit negative values. However, the Parsons-Lee approach adopts an effective hard-sphere fluid as the reference system in which the virial coefficients are always positive. The negative higher-order virial coefficients are incorporated by using an extra parameter and a Vega-Lago scaling relation, a generic equation of state for disc-like particles is developed, which provides a more accurate description than with the Parsons-Lee approach. Combined with the extended cell theory for the columnar phase [92, 94], the complete phase diagram of hard cut spheres is presented. The incorporation of negative virial coefficients is shown to improve the description of both the isotropic-nematic and nematic-columnar transitions.

Hard anisotropic fluids are reasonable models for lyotropic LCs, while for thermotropic LCs, the effects of both density and temperature should be considered on an equal footing. In Chapter 3, we propose an attractive cylindrical disc (ACD) for thermotropic LCs of disc-like partciles. Based on a hard-disc model, anisotropic attractions are placed on the centre of the particle. The free energy for ACD systems is constructed using a perturbation theory and the Onsager trial function is adopted to represent the orientational order in the nematic phase. The theory is used to describe the fluid phase behaviour of ACD particles, including vapour-(isotropic)liquid, isotropic-nematic and nematic-nematic coexistence. It is worth noting that the coexistence between two nematic phases of different orientational order is exhibited by ACD model for large values of the aspect ratio. We also study the effects of anisotropy in the attractive interactions and the range of attractions on the phase behaviour of ACD particles.

In Chapter 4, the perturbation theory is extended to the attractive hard-spherocylinders (AHSC) model which is used to represent the thermotropic LCs of rod-like shape. Since the aspect ratio of real colloidal or polymeric rod-like LC systems can be very large, we focus on the LC phase behaviour of the rods of $L/D > 50$ and the effect of the anisotropic attractions. The most salient feature of rods with large aspect ratio is the appearance of nematic-nematic phase separation. A low-density (gas-like) nematic phase of lower orientational order is found to coexist with a high-density (lqiuid-like) nematic phase of higher orientational order and the two nematic phases become indistinguishable at the critical point of the nematic-nematic coexistence. The AHSC model is then successfully applied to the descriptions of liquid crystalline phases of solutions of the polypeptide, poly-(γ-benzyl-L-glutamate) in dimethylformamide (DMF) and a quantitative agreement can be obtained between the theoretical description using the AHSC model and experimental data [19].

In the second part of the thesis corresponding to Chapters 5-7, our focus is shifted to simulating the bulk isotropic-nematic phase behaviour of a binary mixture of hard spero-cylinders (HSCs) and hard spheres (HSs) and thier the LC ordering behaviour on a hard structureless surface.

In Chapter 5, the bulk phase diagram of HSC-HS mixture is simulated in the constant normal-pressure ensemble. In order to study the bulk region in the simulation cell and overcome the problem of the size-dependence of the orientational order parameter, we di-vide the simulation cell into three equally-size bins: two surface regions close the hard walls

and one large bulk region in the central part of the cell. We first examine the effect of the hard surface on the bulk phase transition in the system of pure HSC of $L/D = 5$. For the size size and geometry studied, the hard walls are not found to have a significant effect on isotropic-nematic phase behaviour in the bulk region compared with the results obtained with conventional NPT-MC of the fully periodic systems [45]. This allows for a detailed study of the bulk isotropic-nematic phase behaviour of HSC-HS mixture. Due the presence of the walls, the composition in the bulk region varies with the imposed pressure. The coexisting phases of different compositions are simulated in the constant normal-pressure ensemble rather than using Gibbs ensemble which is more computationally expensive. The simulation results are further compared with the predictions of the one-fluid version of the Parsons-Lee theory and a two-fluid approach and previous NPT-MC simulation results.

The binary mixture of HSCs and HSs exhibits rich surface behaviour due to the presence of the impenetrable walls in the z-axis of the simulation cell. In Chapter 6, we present a detailed MC simulation of pure HSC and equal-molar HSC-HS mixture ($x_{\mathrm{HS}} = 0.5$). For the system of pure HSC, we observe surface drying by the rods in the low-density regime which is indicated by peaks of density profiles located at a distance of half of the length of the rods away from the hard wall. As the pressure is increased, the rods wet the wall with a homogeneous planar anchoring configuration and the surface nematization of HSCs appears prior to the formation of the bulk nematic phase. Our simulation results are in line with previous observations of experiments [273, 274] and computer simulation [74,243,244,256]. The effect of hard spheres on the surface behaviour of HSC-HS mixture is then studied. The interplay between rods, spheres and the hard walls leads to various types of surface phase behaviour. In very low-density regime we observe a competing adsorption of the rods and spheres with respect to the hard wall. The competing adsorption is quantified by the surface adsorption curves of rods and spheres. The crossover of the surface adsorption curves of the HSC and HS particles as the pressure is increased indicates the rods are more favoured by the hard wall in the intermediate to high density region. The simulation results for the HSC-HS mixture show that the addition of spheres in the mixture destabilizes the orientational ordering both on the surface and in the bulk region.

It is well known that the HSC rods exhibits nematic-smectic transition at high densities. In Chapter 7, we report the formation of smectic monolayers of hard rods at hard surfaces in the states with sufficiently high normal pressures. The surface transition between nematic ordering and smectic layer is studied in detail in the pure rod system and for the

equimolar HSC-HS mixture. We show that the surface transition between the nematic layer and smectic layer results in a change in the average orientation of the rods with respect to the wall. As illustrated in Chapter 6, the HSCs adopt a planer anchoring configuration in the nematic layer while it is observed that rods are in the homoetropic alignment in the smectic monolayer (with the molecules perpendicular to the plane of the surface). The formation of smectic monolayer results in a discontinuous change in the surface adsorption. Since the hard spheres are pushed into the centre of the simulation cell, there is no obvious impact of the hard spheres on the smectic ordering of rods on the wall but the hard spheres still destabilizes the bulk ordered states. We find that the pressure for the formation of the smectic layer depends linearly on the composition of hard spheres. The system size is found to have a weak impact on the formation of smectic layer on the surface.

As illustrated in the preceding chapters, both theoretical approaches and computer simulation methods are powerful tools in helping to understanding LC phases exhibited in various systems ranging from the basic physical models (hard rods, hard discs) to the biomacromolecular systems such as the polypeptide solution. It is hoped that some of the work presented in this thesis will help to inspire future research in some way, and to show that the study of liquid crystals phase behaviour is an interesting and dynamic field which is full of challenges and unsolved mysteries. Finally, the author would like to thank you for reading the thesis.

Bibliography

[1] P. J. Collings. *Introduction to Liquid Crystals: Chemistry and Physics*. Taylor & Francis, London, 1982.

[2] S. Chandrasekhar. *Liquid Crystals*. Cambridge University Press, Cambridge, 2nd ed. edition, 1992.

[3] P. G. de Gennes and J. Prost. *The Physics of Liquid Crystals*. Oxford University Press,Oxford, 2nd ed. edition, 1993.

[4] F. Reinitzer. Contributions to the understanding of cholesterol(Beitrge zur Kenntiss des Cholesterins). *Monatshefte für Chemie (Wien)*, 9:421–441, 1888.

[5] J. M. Jung and R. Mezzenga. Liquid crystalline phase behavior of protein fibers in water: experiments versus theory. *Langmuir*, 26:504–514, 2010.

[6] R. Mezzenga, J. M. Jung, and J. Adamcik. Effects of charge double layer and colloidal aggregation on the isotropic-nematic transition of protein fibers in water. *Langmuir*, 26:10401–10405, 2010.

[7] F. C. Bawden, N. W. Pirie, J. D. Bernal, and I. Fankuchen. Liquid crystalline substances from virus-infected plants. *Nature*, 138:1051–1052, 1936.

[8] V. A. Parsegian and S. L. Brenner. The role of long range forces in ordered arrays of tobacco mosaic virus. *Nature*, 259:632–635, 1976.

[9] Z. Dogic and S. Fraden. Smectic phase in a colloidal suspension of semiflexible virus particles. *Physcial Review Letters*, 78:2417–2420, 1997.

[10] Z. Dogic and S. Fraden. Cholesteric phase in virus suspensions. *Langmuir*, 16:7820–7824, 2000.

[11] E. Grelet and S. Fraden. What is the origin of chirality in the cholesteric phase of virus suspensions? *Physical Review Letters*, 90:198302, 2003.

[12] K. R. Purdy, S. Varga, A. Galindo, G. Jackson, and S. Fraden. Nematic phase transitions in mixtures of thin and thick colloidal rods. *Physcial Review Letters*, 94:057801, 2005.

[13] S. Varga, K. Purdy, A. Galindo, S. Fraden, and G. Jackson. Nematic-nematic phase separation in binary mixtures of thick and thin hard rods: Results from Onsager-like theories. *Physical Review E*, 72:051704, 2005.

[14] Z. Dogic and S. Fraden. Ordered phases of filamentous viruses. *Current Opinion in Colloid & Interface Science*, 11:47–55, 2006.

[15] F. Livolant and A. Leforestier. Condensed phases of DNA: Structures and phase transitions. *Progress in Polymer Science*, 21:1115–1164, 1996.

[16] M. Nakata, G. Zanchetta, B. D. Chapman, C. D. Jones, J. O. Cross, R. Pindak, T. Bellini, and N. A. Clark. End-to-end stacking and liquid crystal condensation of 6to 20base pair DNA duplexes. *Science*, 318:1276–1279, 2007.

[17] C. Robinson. Liquid-crystalline structures in polypeptide solutions. *Tetrahedron*, 13:219–234, 1961.

[18] H. Fujita, A. Teramoto, K. Okita, T. Yamashita, and S. Ikeda. Solution properties of synthetic polypeptides. I. Light scattering and osmometry of Poly-γ-benzyl-L-glutamate in helicogenic solvents. *Biopolymers*, 4:769–779, 1966.

[19] W. G. Miller, Chia Chuan Wu, Elizabeth L. Wee, G. L. Santee, J. H. Rai, and K. G. Goebel. Thermodynamics and dynamics of polypeptide liquid crystals. *Pure and Applied Chemistry*, 38:37–58, 1974.

[20] P. S. Russo and W. G. Miller. On the nature of the poly(γ-benzyl glutamate)-dimethylformamide "complex phase". *Macromolecules*, 17:1324–1331, 1984.

[21] P. S. Russo and W. G. Miller. Coexistence of liquid crystalline phases in poly(γ-benzyl alpha,L-glutamate)-dimethylformamide. *Macromolecules*, 16:1690–1693, 1983.

[22] D. L. Tipton and P. S. Russo. Thermoreversible gelation of a rodlike polymer. *Macromolecules*, 29:7402–7411, 1996.

[23] J. C. Horton, A. M. Donald, and A. Hill. Coexistence of two liquid crystalline phases in poly(γ-benzyl-α, L-glutamate) solutions. *Nature*, 346:44–45, 1990.

[24] B. M. Ginzburg and A. A. Shepelevskii. Construction of the full phase diagram for the system of poly(γ-benzyl-L-glutamate)/dimethylformamide on the basis of the complex of literature data. *Journal of Macromolecular Science, Part B: Physics*, B42:1–56, 2003.

[25] L. Onsager. The effects of shape on the interaction of colloidal particles. *Annals of the New York Academy of Sciences*, 51:627–659, 1949.

[26] A. B. D. Brown, S. M. Clarke, and A. R. Rennie. Ordered phase of platelike particles in concentrated dispersions. *Langmuir*, 14:31293132, 1998.

[27] F. M. van der Kooij and H. N. W. Lekkerkerker. Formation of nematic liquid crystals in suspensions of hard colloidal platelets. *Journal of Physical Chemistry B*, 102:78297832, 1998.

[28] F. M. van der Kooij, K. Kassapidou, and H. N. W. Lekkerkerker. Liquid crystal phase transitions in suspensions of polydisperse plate-like particles. *Nature*, 406:868, 2000.

[29] F. M. van der Kooij, D. van der Beek, and H. N. W. Lekkerkerker. Isotropic-nematic phase separation in suspensions of polydisperse colloidal platelets. *Journal of Physical Chemistry B*, 105:16961700, 2001.

[30] S. Liu, J. Zhang, N. Wang, W. Liu, C. Zhang, and D. Sun. Liquid-crystalline phases of colloidal dispersions of layered double hydroxides. *Chemistry of Materials*, 15:32403241, 2003.

[31] J. O. Fossum, E. Gudding, D. d. M. Fonseca, Y. Meheust, E. DiMasi, T. Gog, and C. Venkataraman. Observations of orientational ordering in aqueous suspensions of a nano-layered silicate. *Energy*, 30:873883, 2005.

[32] L. J. Michot, I. Bihannic, S. Maddi, S. S. Funari, C. Baravian, P. Levitz, and P. Davidson. Liquid-crystalline aqueous clay suspensions. *Proceedings of the National Academy of Sciences*, 103:16101–16104, 2006.

[33] Henk N. W. Lekkerkerker and Remco Tuiner. *Colloids and the Depletion Interaction*. Springer, Heidelberg, 2011.

[34] P. G. de Gennes. Short-range order effects in the isotropic phase of nematics and cholesterics. *Molecular Crystals and Liquid Crystals*, 12:193–214, 1971.

[35] M. Born. *Sits. Phys. Maths.*, 25:614, 1916.

[36] M. Born. *Ann. Phys.*, 55:221, 1918.

[37] Wilhelm Maier and Alfred Saupe. Eine einfache molekulare Theorie des nematischen kristall in flüssigen Zustandes. *Zeitschrift für Naturforschung A*, 13:564–566, 1958.

[38] Wilhelm Maier and Alfred Saupe. Eine einfache molekularstatistische Theorie der nematischen kristall in flüssigen phase. Teil I. *Zeitschrift für Naturforschung A*, 14:882–889, 1959.

[39] W. Maier and A. Saupe. Eine einfache molekularstatistische Theorie der nematischen kristall in flüsign phase. Teil II. *Zeitschrift für Naturforschung A*, 15:287–292, 1960.

[40] G. R. Luckhurst and C. Zannoni. Why is the Maier-Saupe theory of nematic liquid crystals so successful? *Nature*, 267:412–414, 1977.

[41] P. A. Lebwohl and G. Lasher. Nernatic-liquid-crystal order-A Monte Carlo calculation. *Physcial Review A*, 6:426–429, 1972.

[42] M. P. Allen, G. T. Evans, D. Frenkel, and B. M. Mulder. Hard convex body fluids. *Advances in Chemical Physics*, 86:1–166, 1993.

[43] D. Frenkel. Computer simulation of hard-core models for liquid-crystals. *Molecular Physics*, 60:1–20, 1987.

[44] C. Vega and D. Frenkel. Monte-Carlo study of rod-like molecules-a test of perturbation-theory for the Kihara model. *Molecular Physics*, 67:633–650, 1989.

[45] S. C. McGrother, D. C. Williamson, and G. Jackson. A re-examination of the phase diagram of hard spherocylinders. *Journal of Chemical Physics*, 104:6755–6771, 1996.

[46] R. Eppenga and D Frenkel. Monte-carlo study of the isotropic and nematic phases of infinitely thin hard platelets. *Molecular Physics*, 52:1303–1334, 1984.

[47] J. A. C. Veerman and D. Frenkel. Phase-behavior of disk-like hard-core mesogens. *Physical Review A*, 45:5632–5648, 1992.

[48] D. van der Beek, T. Schilling, and H. N. W. Lekkerkerker. Gravity-induced liquid crystal phase transitions of colloidal platelets. *Journal of Chemical Physics*, 121:5423–5426, 2004.

[49] M. A. Bates and D Frenkel. Infinitely thin disks exhibit a first order nematic-columnar phase transition. *Physical Review E*, 57:4824–4826, 1998.

[50] J.-P. Hansen and I. R. McDonald. *Theory of Simple Liquids*. Academic Press, New York, 3rd ed. edition, 2006.

[51] M. Franco-Melgar, A. J. Haslam, and G. Jackson. A generalisation of the onsager trial-function approach: describing nematic liquid crystals with an algebraic equation of state. *Molecular Physics*, 106:649–678, 2008.

[52] G. J. Vroege and H. N. W. Lekkerkerker. Phase-transition in lyotropic colloidal and polymer liquid-crystals. *Reports on Progress in Physics*, 55:1241–1309, 1992.

[53] T. Odijk and H. N. W. Lekkerkerker. Theory of the isotropic-liquid crystal phase separation for a solution of bidisperse rodlike macromolecules. *Journal of Phyiscal Chemistry*, 89:2090–2096, 1985.

[54] N. Metropolis, A. W. Rosenbluth, M. N. Rosenbluth, A. H. Teller, and E. Teller. Equation of state calculations by fast computing machines. *Journal of Chemical Physics*, 21:1087–1092, 1953.

[55] B. J. Alder and T. E. Wainwright. Phase transition in elastic disks. *Physcial Review*, 127:359–361, 1962.

[56] W. G. Hoover and B. J. Alder. Studies in molecular dynamics. IV. the pressure, collision rate, and their number dependence for hard disks. *Journal of Chemical Physics*, 46:686–691, 1967.

[57] W. W. Wood. Monte carlo calculations for hard disks in the isothermal-isobaric ensemble. *Journal of Chemical Physics*, 48:415–434, 1968.

[58] Jacques Vieillard-Baron. Phase transition of the classical hard ellipse system. *Journal of Chemical Physics*, 56:4729–4744, 1972.

[59] J. Vieillard-Baron. The equation of state of a system of hard spherocylinders. *Molecular Physics*, 28:808–818, 1974.

[60] D. Frenkel and B. M. Mulder. The hard ellipsoid-of-revolution fluid I. Monte Carlo simulations. *Molecular Physics*, 55:1171–1192, 1985.

[61] A. Stroobants, H. N. W. Lekkerkerker, and D. Frenkel. Evidence for smectic order in a fluid of hard parallel spherocylinders. *Physcial Review Letters*, 57:1452–1455, 1986.

[62] D. Frenkel, H. N. W. Lekkerkerker, and A. Stroobants. Thermodynamic stability of a smectic phase in a system of hard rods. *Nature*, 332:822–823, 1988.

[63] P. G. Bolhuis and D Frenkel. Tracing the phase boundaries of hard spherocylinders. *Journal of Chemical Physics*, 106:666–687, 1997.

[64] W. G. Hoover and F. H. Ree. Melting transition and communal entropy for hard spheres. *Journal of Chemical Physics*, 49:3609–3617, 1968.

[65] P. N. Pusey and W. van Megen. Phase behaviour of concentrated suspensions of nenear hard colloidal spheres. *Nature*, 320:340–342, 1986.

[66] Z. Cheng, P. M. Chaikin, W. B. Russel, W. V. Meyer, J. Zhu, R. B. Rogers, and R. H. Ottewill. Phase diagram of hard spheres. *Materials and Design*, 22:529–534, 2001.

[67] P. G. Bolhuis and D. Frenkel. Numerical study of the phase diagram of a mixture of spherical and rodlike colloids. *Journal of Chemical Physics*, 101:9869–9875, 1994.

[68] G. A. Vliegenthart and H. N. W. Lekkerkerker. Phase behavior of colloidal rod-sphere mixtures. *Journal of Chemical Physics*, 111:4153–4157, 1999.

[69] R. Roth, J. M. Brader, and M. Schmidt. Entropic wetting of a colloidal rod-sphere mixture. *Europhysics Letter*, 63:549–555, 2003.

[70] Matthias Schmidt and Joseph M. Brader. Hards phere fluids in random fiber networks. *Journal of Chemical Physics*, 119:3495–3500, 2003.

[71] N. Urakami and M. Imai. Dependence on sphere size of the phase behavior of mixtures of rods and spheres. *Journal of Chemical Physics*, 119:2463–2470, 2003.

[72] S. Lago, A. Cuetos, B. Martínez-Haya, and L. F. Rull. Crowding effects in binary mixtures of rod-like and spherical particles. *Journal of Molecular Recognition*, 17:417–425, 2004.

[73] A. Cuetos, B. Martínez-Haya, S. Lago, and L. F. Rull. Use of parsons-lee and onsager theories to predict nematic and demixing behavior in binary mixtures of hard rods and hard spheres. *Physcial Review E*, 75:061701, 2007.

[74] P. E. Brumby. *Modelling and understanding confinement and chirality in liquid-crystalline systems*. PhD thesis, Imperial College London, 2010.

[75] L. Onsager. *Physcial Review*, 62:558–559, 1942.

[76] C. Vega and S. Lago. Isotropic-nematic transition of hard polar and nonpolar molecules. *Journal of Chemical Physics*, 100:6727–6737, 1994.

[77] A. Stroobants and H. N. W. Lekkerkerker. Liquid-crystal phase-transitions in a solution of rodlike and disclike particles. *Journal of Physical Chemistry*, 88:3669–3674, 1984.

[78] A. Stroobants, H. N. W. Lekkerkerker, and D. Frenkel. Evidence for one-, two-, and three-dimensional order in a system of hard parallel spherocylinders. *Physcial Review A*, 36:2929–2945, 1987.

[79] P. D. Duncan, M. Dennison, A. J. Masters, and M. R. Wilson. Theory and computer simulation for the cubatic phase of cut spheres. *Physical Review E*, 79:031702, 2009.

[80] R. Evans. The nature of the liquid-vapour interface and other topics in the statistical mechanics of non-uniform, classical fluids. *Advances in Physics*, 28:143–200, 1979.

[81] J. Z. Wu and Z. D. Li. Density-functional theory for complex fluids. *Annual Review of Physical Chemistry*, 58:85–112, 2007.

[82] L. Harnau. Structure and thermodynamics of platelet dispersions. *Molecular Physics*, 106:1975–2000, 2008.

[83] D. L. Cheung, L. Anton, M. P. Allen, and A. J. Masters. Structure of molecular liquids: Cavity and bridge functions of the hard spheroid fluid. *Physical Review E*, 73:061204, 2006.

[84] D. L. Cheung, L. Anton, M. P. Allen, A. J. Masters, J. Phillips, and M. Schmidt. Structure and stability of isotropic states of hard platelet fluids. *Physical Review E*, 78:041201, 2008.

[85] A. Esztermann, H. Reich, and M. Schmidt. Density functional theory for colloidal mixtures of hard platelets, rods, and spheres. *Physical Review E*, 73:011409, 2006.

[86] H. Hansen-Goos and K. Mecke. Fundamental measure theory for inhomogeneous fluids of nonspherical hard particles. *Physical Review Letters*, 102(1):018302, 2009.

[87] X. M. You, A. Y. Vlasov, and A. J. Masters. The equation of state of isotropic fluids of hard convex bodies from a high-level virial expansion. *Journal of Chemical Physics*, 123:034510, 2005.

[88] A. J. Masters. Virial expansions. *Journal of Physics: Condensed Matter*, 20:283102, 2008.

[89] J. D. Parsons. Nematic ordering in system of rods. *Physical Review A*, 19:1225–1230, 1979.

[90] S. D. Lee. The Onsager-type theory for nematic ordering of finite-length hard ellipsoids. *Journal of Chemical Physics*, 89:7036–7037, 1988.

[91] S. D. Lee. A numerical investigation of nematic ordering based on a simple hard-rod model. *Journal of Chemical Physics*, 87:4972–4974, 1987.

[92] H. H. Wensink and H. N. W. Lekkerkerker. Phase diagram of hard colloidal platelets: a theoretical account. *Molecular Physics*, 107:2111–2118, 2009.

[93] A. A. Verhoeff, H. H. Wensink, M. Vis, G. Jackson, and H. N. W. Lekkerkerker. Liquid crystal phase transitions in systems of colloidal platelets with bimodal shape distribution. *Journal of Physical Chemistry B*, 113:13476–13484, 2009.

[94] H. H. Wensink. Equation of state of a dense columnar liquid crystal. *Physical Review Letters*, 93:157801, 2004.

[95] N. F. Carnahan and K. E. Starling. Equation of state for nonattracting rigid spheres. *Journal of Chemical Physics*, 51:635–636, 1969.

[96] J. Herzfeld, A. E. Berger, and J. W. Wingate. A highly convergent algorithm for computing the orientation distribution functions of rodlike particles. *Macromolecules*, 17:1718–1723, 1984.

[97] D. C. Williamson and G. Jackson. Monte-Carlo annealing technique for the minimization of the Onsager free-energy functional. *Molecular Physics*, 83:603–611, 1994.

[98] M. Franco-Melgar. *Developing a molecular-based equation of state for engineering applications of fluid-phase equilibria and orientational ordering in liquid crystal systems.* PhD thesis, Imperial College London, 2006.

[99] N. Ibarra-Avalos, A. Gil-Villegas, and A. Martinez Richa. Excluded volume of hard cylinders of variable aspect ratio. *Molecular Simulation*, 33:505–515, 2007.

[100] R. W. D. Nickalls. A new approach to solving the cubic: cardan's solution revealed. *The Mathematical Gazette*, 77:354–359, 1993.

[101] S. D. Zhang, P. A. Reynolds, and J. S. van Duijneveldt. Phase behavior of mixtures of colloidal platelets and nonadsorbing polymers. *Journal of Chemical Physics*, 117:9947–9958, 2002.

[102] M. Marechal, A. Cuetos, B. Martinez-Haya, and M. Dijkstra. Phase behavior of hard colloidal platelets using free energy calculations. *Journal of Chemical Physics*, 134:094501, 2011.

[103] D. C. Williamson and G. Jackson. Liquid crystalline phase behavior in systems of hard-sphere chains. *Journal of Chemical Physics*, 108:10294–10302, 1998.

[104] Angel Mulero, editor. *Theory and simulation of hard-sphere and related systems.* Springer-Verlag,Berlin, 2008.

[105] W. H. Press, S. A. Teukolsky, W. T. Vetterling, and B. P. Flannery. *Numerical Recipes in FORTRAN: the art of scientific computing, 2nd ed.* Cambridge University Press, Cambridge, 1992.

[106] A. Cuetos and B. Martinez-Haya. Columnar phases of discotic spherocylinders. *Journal of Chemical Physics*, 129:214706, 2008.

[107] Bruno Martínez-Haya and Alejandro Cuetos. Simulation study of discotic molecules in the vicinity of the isotropic-liquid crystal transition. *Molecular Simulation*, 35:1077–1083, 2009.

[108] Bruno Martínez-Haya and Alejandro Cuetos. Columnar phases of discotics with orientation-dependent interactions. *Journal of Chemical Physics*, 131:074901, 2009.

[109] F. Gámez, P. J. Merkling, and S. Lago. Parsons-lee approach for oblate hard spherocylinders. *Chemical Physics Letter*, 494:45–49, 2010.

[110] B. M. Mulder. The excluded volume of hard-zonotopes. *Molecular Physics*, 103:1411–1424, 2005.

[111] N. F. Carnahan and E. A. Müller. Shape factors in equations of state part ii. repulsion phenomena in multicomponent chain fluids. *Physical Chemistry Chemical Physics*, 8:2619, 2006.

[112] A. Malijevský, G. Jackson, and S. Varga. Many-fluid Onsager density functional theories for orientational ordering in mixtures of anisotropic hard-body fluids. *Journal of Chemical Physics*, 129:144504, 2008.

[113] R. Alben. Liquid-crystal phase-transitions in mixtures of rodlike and platelike molecules. *Journal of Chemical Physics*, 59:4299–4304, 1973.

[114] P. J. Camp, M. P. Allen, P. G. Bolhuis, and D. Frenkel. Demixing in hard ellipsoid rod-plate mixtures. *Journal of Chemical Physics*, 106:9270–9275, 1997.

[115] S. Varga, A. Galindo, and G. Jackson. Ordering transitions, biaxiality, and demixing in the symmetric binary mixture of rod and plate molecules described with the onsager theory. *Physcial Review E*, 66:011707, 2002.

[116] H. H. Wensink, G. J. Vroege, and H. N. W. Lekkerkerker. Biaxial versus uniaxial nematic stability in asymmetric rod-plate mixtures. *Physical Review E*, 66:041704, 2002.

[117] A. Galindo, A. J. Haslam, S. Varga, G. Jackson, A. G. Vanakaras, D. J. Photinos, and D. A. Dunmur. The phase behavior of a binary mixture of rodlike and disclike mesogens: Monte Carlo simulation, theory, and experiment. *Journal of Chemical Physics*, 119:5216–5225, 2003.

[118] M. Franco-Melgar, A. J. Haslam, and G. Jackson. Advances in generalised van der waals approaches for the isotropic-nematic fluid phase equilibria of thermotropic liquid crystals-an algebraic equation of state for attractive anisotropic particles with the onsager trial function. *Molecular Physics*, 107:2329–2358, 2009.

[119] A. Gil-Villegas, S. C. McGrother, and G. Jackson. Chain and ring structures in smectic phases of molecules with transverse dipoles. *Chemical Physics Letters*, 269:441–447, 1997.

[120] M. Houssa, A. Oualid, and L. F. Rull. Reaction field and ewald summation study of mesophase formation in dipolar Gay-Berne model . *Molecular Physics*, 94:439–446, 1998.

[121] S. C. McGrother, A. Gil-Villegas, and G. Jackson. The effect of dipolar interactions on the liquid crystalline phase transitions of hard spherocylinders with central longitudinal dipoles. *Molecular Physics*, 95:657–673, 1998.

[122] R. Berardi, S. Orlandi, and C. Zannoni. Columnar phases and field induced biaxiality of a gay-berne discotic liquid crystal. *Physical Chemistry Chemical Physics*, 2:2933–2942, 2000.

[123] J. S. van Duijneveldt, A. Gil-Villegas, G. Jackson, and M. P. Allen. Simulation study of the phase behavior of a primitive model for thermotropic liquid crystals: Rodlike molecules with terminal dipoles and flexible tails. *Journal of Chemical Physics*, 112:9092–9104, 2000.

[124] A. G. Vanakaras, S. C. McGrother, G. Jackson, and D. J. Photinos. Hydrogen-bonding and phase biaxiality in nematic rod-plate mixtures. *Molecular Crystals and Liquid Crystals*, 323:199–209, 1998.

[125] D.A. Dunmur, A. Fukuda, and G. R. Luckhurst, editors. *Physical properties of liquid crystals: nematics (EMIS Datareviews Series No. 25)*. INSPEC, London, 2001.

[126] Peter J. Collings. *Liquid Crystals: Nature's Delicate Phase of Matter (2nd ed.)*. Princeton University Press, Princeton, NJ,, 2002.

[127] D. Guillon, B. Donnio, D. W. Bruce, F. D. Cukiernik, and M. Rusjan. Columnar mesomorphic order in thermotropic liquid crystals. *Molecular Crystals and Liquid Crystals*, 396:141–154, 2003.

[128] J. G. Speight. *The Chemistry and Technology of Petroleum, Fourth Edition (Chemical Industries)*. Marcel Dekker (New York), 1999.

[129] M. Shishido, H. Inomata, K. Arai, and S. Saito. Application of liquid crystal theory to the estimation of mesophase pitch phase-transition behavior. *Carbon*, 35:797–799, 1997.

[130] R. H. Hurt and Y. Hu. Thermodynamics of carbonaceous mesophase. *Carbon*, 37:281292, 1999.

[131] B. Aguilera-Mercado, C. Herdes, J. Murgich, and E. A. Müller. Mesoscopic simulation of aggregation of asphaltene and resin molecules in crude oils. *Energy & Fuels*, 20:327–338, 2006.

[132] Ward A. Burgess, Mark S. Zhuang, Ying Hu, Robert H. Hurt, and Mark C. Thies. SAFT-LC: An equation of state for predicting liquid-crystalline phase behavior in carbonaceous pitches. *Industrial & Engineering Chemistry Research*, 46:7018–7026, 2007.

[133] P. A. Artola, F. E. Pereira, C. S. Adjiman, A. Galindo, E. A. Müller, G. Jackson, and A. J. Haslam. Understanding the fluid phase behaviour of crude oil: Asphaltene precipitation. *Fluid Phase Equilibria*, 306:129136, 2011.

[134] A. Samborski, G. T. Evans, C. P. Mason, and M. P. Allen. The isotropic to nematic liquid crystal transition for hard ellipsoids: An Onsager-like theory and computer simulations. *Molecular Physics*, 81:263–276, 1994.

[135] D. van der Beek, H. Reich, P. van der Schoot, M. Dijkstra, T. Schilling, R. Vink, M. Schmidt, R. van Roij, and H. N. W. Lekkerkerker. Isotropic-nematic interface and wetting in suspensions of colloidal platelets. *Physical Review Letters*, 97:087801, 2006.

[136] H. Reich, M. Dijkstra, R. van Roij, and M. Schmidt. Entropic wetting and the free isotropic-nematic interface of hard colloidal platelets. *Journal of Physical Chemistry B*, 111:78257835, 2007.

[137] H. Reich and M/ Schmidt. Capillary nematization of hard colloidal platelets confined between two parallel hard walls. *Journal of Physics: Condensed Matter*, 19:326103, 2007.

[138] Ludger Harnau, David Rowan, and J. P. Hansen. Thermodynamics and phase behavior of the lamellar Zwanzig model. *Journal of Chemical Physics*, 117:11359, 2002.

[139] M. Bier, L. Harnau, and S. Dietrich. Bulk and interfacial properties of binary hard-platelet fluids. *Physcial Review E*, 69:021506, 2004.

[140] D. Costa, J. P. Hansen, and L. Harnau. Structure and equation of state of interaction site models for disc-shaped lamellar colloids. *Molecular Physics*, 103:1917–1927, 2005.

[141] L. Wu, H. H. Wensink, G. Jackson, and E. A. Müller. A generic equation of state for liquid crystalline phases of hard-oblate particles. *Molecular Physics*, 110:1269–1288, 2012.

[142] M. M. Piñeiro, A. Galindo, and A. O. Parry. Surface ordering and capillary phenomena of confined hard cut-sphere particles. *Soft Matter*, 3:768–778, 2007.

[143] D. Chandler, J. D. Weeks, and H. C. Andersen. Van der waas picture of liquids, solids, and phase transformations. *Science*, 220:787–794, 1983.

[144] H. Kimura. Nematic ordering of rod-like molecules interacting via anisotropic dispersion forces as weII as rigid-body repulsions. *Journal of the Physical Society of Japan*, 36:1280–1287, 1974.

[145] M. A. Cotter. Hard spherocylinders in an anisotropic mean field: A simple model for a nematic liquid crystal. *Journal of Chemical Physics*, 66:1098–1106, 1977.

[146] M. A. Cotter. Generalized van der Waals theory of nematic liquid crystals: Requirements for self-consistency. *Journal of Chemical Physics*, 67:4268–4270, 1977.

[147] M. A. Cotter. Generalized van der Waals theory of nematic liquid crystals: An alternative formulation. *Journal of Chemical Physics*, 66:4710–4711, 1977.

[148] W. M. Gelbart and B. A. Baron. Generalized van der waals theory of the isotropic-nematic phase transition. *Journal of Chemical Physics*, 66:207–213, 1977.

[149] W. M. Gelbart and Barboy B. A van der waals picture of the isotropic-nematic liquid crystal phase transition. *Accounts of Chemical Research*, 13:290–296, 1980.

[150] P. G. Bolhuis, A. Stroobants, D. Frenkel, and H. N. W. Lekkerkerker. Numerical study of the phase behavior of rodlike colloids with attractive interactions. *Journal of Chemical Physics*, 107:1551–1564, 1997.

[151] D. C. Williamson. The convex peg model: the long range approximation. *Molecular Physics*, 95:319–329, 1998.

[152] P. I. C. Teixeira. A thermotropic nematic of slightly non-spherical molecules: generalized van der waals theory. *Molecular Physics*, 96:805–811, 1999.

[153] E. Garcia, D. C. Williamson, and A Martinez-Richa. Effects of molecular geometry on liquid crystalline phase behaviour: isotropic-nematic transition. *Molecular Physics*, 98:179–192, 2000.

[154] E. García-Sanchez, A. Martínez-Richa, J. A. Villegas-Gasca, L. H. Mendoza-Huizar, and A. Gil-Villegas. Predicting the phase diagram of a liquid crystal using the convex peg model and the semiempirical PM3 method . *Journal of Physical Chemistry A*, 106:10342–10349, 2002.

[155] D. C. Williamson and F. del Rio. The isotropicnematic phase transition in a fluid of square well spherocylinders. *Journal of Chemical Physics*, 109:4675–4686, 1998.

[156] D. C. Williamson and Y. Guevara. Deviation from corresponding states for a fluid of square well spherocylinders. *Journal of Physical Chemistry B*, 103:7522–7530, 1999.

[157] E. M. del Río, A. Galindo, and E. de Miguel. Density functional theory and simulation of the columnar phase of a system of parallel hard ellipsoids with attractive interactions. *Physical Review E*, 72:051707, 2005.

[158] F. Gámez, S. Lago, B. Garzón, P. J. Merkling, and C. Vega. Vapour-liquid equilibrium of fluids composed by oblate molecules. *Molecular Physics*, 106:13311339, 2008.

[159] S. C. McGrother, A. Gil-Villegas, and G. Jackson. The liquid-crystalline phase behaviour of hard spherocylinders with terminal point dipoles. *Journal of Physics: Condensed Matter*, 8:9649–9655, 1996.

[160] B. Groh and S. Dietrich. Orientational order in dipolar fluids consisting of nonspherical hard particles. *Physical Review E*, 55:2892–2901, 1997.

[161] S. Varga, I. Szalai, J. Liszi, and G. Jackson. A study of orientational ordering in a fluid of dipolar GayBerne molecules using density-functional theory. *Journal of Chemical Physics*, 116:9107–0119, 2002.

[162] D. C. Williamson, N. A. Thacker, and S. R. Williams. Effects of intramolecular dipolar coupling on the isotropic-nematic phase transition of a hard spherocylinder fluid. *Physical Review E*, 71:021702, 2005.

[163] S. Varga and G Jackson. Study of the pitch of fluids of electrostatically chiral anisotropic molecules: mean-field theory and simulation. *Molecular Physics*, 104:3681–3691, 2006.

[164] H. H. Wensink and G. Jackson. Generalized van der waals theory for the twist elastic modulus and helical pitch of cholesterics. *Journal of Chemical Physics*, 130:234911, 2009.

[165] H. H. Wensink and G. Jackson. Cholesteric order in systems of helical yukawa rods. *Journal of Physics: Condensed Matter*, 23:194107, 2011.

[166] AJ Stone. *The Theory of Intermolecular Forces*. Clarendon Press, 1996.

[167] R. W. Zwanzig. High-temperature equation of state by a perturbation method. I. nonpolar gases. *Journal of Chemical Physics*, 22:1420–1426, 1954.

[168] Leonid V. Yelash, Thomas Kraska, E. A. Müller, and Norman F. Carnahan. Simplified equation of state for non-spherical hard particles : an optimized shape factor approach. *Physical Chemistry Chemical Physics*, 1:4919–4924, 1999.

[169] G. R. Luckhurst and G. W. Gray, editors. *The Molecular Physics of Liquid Crystals*. Academic Press, London, 1979.

[170] E. Meneses-Juáres, S. Varga, P. Orea, and G. Odriozola. Towards understanding the empty liquid of colloidal platelets: vapourliquid phase coexistence of square-well oblate ellipsoids. *Soft Matter*, 9:5277, 2013.

[171] D. Vijayaraghavan and Sandeep Kumar. Effect of slow cooling on a discotic nematic liquid crystal: evidences for nematicnematic transitions. *Molecular Crystals and Liquid Crystals*, 452:11–26, 2006.

[172] P. J. Flory. Phase equilibria in solutions of rod-like particles. *Proceedings of the Royal Society of London. Series A, Mathematical and Physical Sciences*, 234:73–89, 1956.

[173] Mark Warner and P. J. Flory. The phase equilibria in thermotropic liquid crystalline systems. *Journal of Chemical Physics*, 73:6327–6332, 1980.

[174] A. R. Khokhlov and A. N. Semenov. On the theory of liquid-crystalline ordering of polymer chains with limited fexibility. *Journal of Statistical Physics*, 38:161–182, 1985.

[175] S. Varga, D. C. Williamson, and I. Szalai. Square-well fluid based decoupling approximation for system of hard non-spherical particles with spherical square-wells. *Molecular Physics*, 96:1695–1703, 1999.

[176] M. H. J. Hagen and D. Frenkel. Determination of phase diagrams for the hard-core attractive yukawa system. *Journal of Chemical Physics*, 101:4093–4097, 1994.

[177] P. G. Bolhuis, M. H. J. Hagen, and D. Frenkel. Isostructural solid-solid transition in crystalline systems with short-ranged interaction. *Physcial Review E*, 50:48804890, 1994.

[178] A. Gil-Villegas, A. Galindo, P. J. Whitehead, S. J. Mills, G. Jackson, and A. N. Burgess. Statistical associating fluid theory for chain molecules with attractive potentials of variable range. *Journal of Chemical Physics*, 106:4168–4186, 1997.

[179] E. A. Müller and K. E. Gubbins. Molecular-based equations of state for associating fluids: A review of SAFT and related approaches. *Industrial & Engineering Chemistry Research*, 40:2193–2211, 2001.

[180] A. Lymperiadis, C. S. Adjiman, A. Galindo, and G. Jackson. A group contribution method for associating chain molecules based on the statistical associating fluid theory (SAFT-γ). *Journal of Chemical Physics*, 127:234903, 2007.

[181] A. Lymperiadis, C. S. Adjiman, G. Jackson, and A. Galindo. A generalisation of the SAFT-γ group contribution method for groups comprising multiple spherical segments. *Fluid Phase Equilibria*, 274:85–104, 2008.

[182] C. Avendaño, T. Lafitte, A. Galindo, C. S. Adjiman, G. Jackson, and E. A. Müller. SAFT-γ force field for the simulation of molecular fluids.1. A single-site coarse grained model of carbon dioxide. *Journal of Physical Chemistry B*, 115:11154–11169, 2012.

[183] T. Lafitte, C. Avendaño, V. Papaioannou, A. Galindo, C. S. Adjiman, G. Jackson, and E. A. Müller. SAFT-γ force field for the simulation of molecular fluids: 3. Coarse-grained models of benzene and hetero-group models of n-decylbenzene. *Molecular Physics*, 110:1189–1203, 2012.

[184] C. Avendaño, T. Lafitte, C. S. Adjiman, A. Galindo, E. A. Müller, and G. Jackson. SAFT-γ force field for the simulation of molecular fluids: 2. Coarse-grained models of greenhouse gases, refrigerants, and long alkanes. *Journal of Physical Chemistry B*, 117:2717–2733, 2013.

[185] T. Sato and A. Teramoto. Concentrated solutions of liquid-crystalline polymers. *Advances in Polymer Science*, 126:85–161, 1996.

[186] R. S. Werbowj and D. G. Gray. Liquid crystalline structure in aqueous hydroxypropyl cellulose solutions. *Molecular Crystals and Liquid Crystals*, 34:97–103, 1976.

[187] A. F. Miller and A. M. Donald. Imaging of anisotropic cellulose suspensions using environmental scanning electron microscopy. *Biomacromolecules*, 4:510–517, 2003.

[188] D. B. DuPré and R. W. Duke. Temperature, concentration, and molecular weight dependence of the twist elastic constant of cholesteric poly-benzyl-L-glutamate. *Journal of Chemical Physics*, 63:143–148, 1975.

[189] V. T. Rajan and C. Woo. Liquid-crystalline properties and reentrance phenomena in PBLG solutions. *Physical Review A*, 21:990–997, 1980.

[190] J. M. Zimmel, C. C. Wu, W. G. Miller, and R. P. Mason. Rotational motion of rodllke poly(benzyl glutamate). *Journal of Physical Chemistry*, 87:5435–5443, 1983.

[191] H. Yamakawa. Stiff-chain macromolecules. *Annual Review of Physical Chemistry*, 35:23–47, 1984.

[192] I. Uematsu and Y. Uematsu. Polypeptide liquid crystals. *Advances in Polymer Science*, 59:37–73, 1984.

[193] T.J. McMaster, H.C.M.J. Miles, and V.J. Morris. Polypeptide structures imaged by the scanning tunneling microscope. *Journal of Vaccum Science and Technology A*, 8:648–651, 1990.

[194] M. A. Tracy and R. Pecora. Dynamics of rigid and semirigid rodlike polymers. *Annual Review of Physical Chemistry*, 43:525–557, 1992.

[195] N. Mori and S. Itou. Coexistence of two cholesteric phases in poly(gamma-benzyl-l-glutamate) liquid crystals. *Chemistry Letters*, pages 2203–2206, 1994.

[196] J. Lin, A. Abe, H. Furuya, and S. Okamoto. Liquid crystal formation coupled with the coil-helix transition in the ternary system poly(γ-benzyl L-glutamate)/dichloroacetic acid/dichloroethane. *Macromolecules*, 29:2584–2589, 1996.

[197] C. Yen, S. Edo, H. Oka, M. Tokita, and J. Watanabe. Phase diagram for solutions of alpha-helical poly(L-glutamate)s in m-cresol including isotropic, cholesteric, and columnar phases. *Macromolecules*, 41:3727–3733, 2008.

[198] J. A. Barker and D. Henderson. What is "liquid"? Understanding the states of matter. *Review of Modern Physics*, 48:587–671, 1976.

[199] S. Varga and G. Jackson. Simulation of the macroscopic pitch of a chiral nematic phase of a model chiral mesogen. *Chemical Physics Letters*, 377:6–12, 2003.

[200] T. Odijk. Theory of lyotropic polymer liquid crystals. *Macromolecules*, 19:2313–2329, 1986.

[201] G. J. Vroege and T. Odijk. Induced chain rigidity, splay modulus, and other properties of nematic polymer liquid crystals. *Macromolecules*, 21:2848–2858, 1988.

[202] Z. Y. Chen. Nematic ordering in semiflexible polymer chains. *Macromolecules*, 26:3419–3423, 1993.

[203] D. B. DuPré and S. Yang. Liquid crystalline properties of solutions of persistent polymer chains. *Journal of Chemical Physics*, 94:7466–7477, 1991.

[204] M. Dijkstra and D. Frenkel. Simulation study of the isotropic-to-nematic transitions of semifiexible polymers. *Physical Review E*, 51:5891–5898, 1995.

[205] T. Hino and J. M. Prausnitz. A perturbed hard-sphere-chain equation of statefor nematic liquid crystals and their mixtureswith polymers. *Liquid Crystals*, 22:317–326, 1997.

[206] S. C. McGrother, R. P. Sear, and G. Jackson. The liquid crystalline phase behavior of dimerizing hard spherocylinders. *Journal of Chemical Physics*, 106:7315–7330, 1997.

[207] T. Hino and J. M. Prausnitz. Hard-sphere-chain equations of state for lyotropic polymer liquid crystals. *Polymer*, 40:1241–1250, 1999.

[208] P. P. F. Wessels and B. M. Mulder. isotropic-nematic transition liquid-crystalline heteropolymers: I. formalism and main-chain liquid-crystalline polymers. *Journal of Physics: Condensed Matter*, 18:9335–9357, 2006.

[209] Y. Jiang and J. Z. Y. Chen. Isotropic-nematic interface in a lyotropic system of wormlike chains with the Onsager interaction. *Macromolecules*, 43:10668–10678, 2010.

[210] Y. X. Zheng, Y. X. Yu, and Y. F. Li. An equation of state for the isotropic-nematic phase transition of semifiexible polymers. *Industrial & Engineering Chemistry Research*, 50:6460–6469, 2011.

[211] M. Dennison, M. Dijkstra, and R. van Roij. Phase diagram and effective shape of semifiexible colloidal rods and biopolymers. *Physical Review Letters*, 106:208302, 2011.

[212] M. Dennison, M. Dijkstra, and R. van Roij. The effects of shape and fexibility on bio-engineered fd-virus suspensions. *Journal of Chemical Physics*, 135:144106, 2011.

[213] P. J. Flory. Statistical thermodynamics of semi-flexiblel chain molecules. *Proceedings of the Royal Society of London. Series A, Mathematical and Physical Sciences*, 234:60–73, 1956.

[214] L. M. DeLong and P. S. Russo. Thermodynamic and dynamic behavior of semiflexible polymers in the isotropic phase. *Macromolecules*, 24:6139–6155, 1991.

[215] K. Inomata, H. Shimizu, and T. Nose. Phase equilibrium studies on rod/solvent and rod/coil/solvent systems containing poly(α,L-glutamate) having oligo(ethylene glycol) side chains. *Journal of Polymer Science: Part B: Polymer Physics*, 38:1331–1340, 2000.

[216] E. Frezza, A. Ferrarini, H. B. Kolli, A. Giacometti, and G. Cinacchi. The isotropic-to-nematic phase transition in hard helices: Theory and simulation. *Journal of Chemical Physics*, 138:164906, 2013.

[217] P. B. Warren. Depletion effect in a model lyotropic liquid crystal theory. *J. Phys. I France*, 4:2, 1994.

[218] R. P. Sear and G. Jackson. Theory for the phase behavior of a mixture of a rodlike colloid and a rodlike polymer. *Journal of Chemical Physics*, 103:8684–8693, 1995.

[219] P. Paricaud, S. Varga, and G. Jackson. Study of the demixing transition in model athermal mixtures of colloids and flexible self-excluding polymers using the thermodynamic perturbation theory of Wertheim. *Journal of Chemical Physics*, 118:8525–8536, 2003.

[220] W. G. Chapman, K. E. Gubbins, G. Jackson, and M. Radosz. New reference equation of state for associating liquids. *Industrial & Engineering Chemistry Research*, 29:1709–1721, 1990.

[221] C. McCabe and A. Galindo. *"SAFT Associating Fluids and Fluid Mixtures" in Applied Thermodynamics of Fluids*. Royal Society of Chemistry, London, 2010.

[222] H. Zocher. *Z. Anorg. Chem.*, 147:91, 1925.

[223] M. Bravo-Sanchez, T. J. Simmons, and M. A. Vidal. Liquid crystal behavior of single wall carbon nanotubes. *Carbon*, 48:3531–3542, 2010.

[224] J. A. C. Veerman and D. Frenkel. Phase diagram of a system of hard spherocylinders by computer simulation. *Physcial Review A*, 41:3237–3244, 1990.

[225] F. M. van der Kooij and H. N. W. Lekkerkerker. Liquid-crystalline phase behavior of a colloidal rod-plate mixture. *Physcial Review Letters*, 84:781–784, 2000.

[226] A. Cuetos, A. Galindo, and G. Jackson. Thermotropic biaxial liquid crystalline phases in a mixture of attractive uniaxial rod and disk particles. *Physical Review Letters*, 101:237802, 2008.

[227] M. Adams, Z. Dogic, S. Keller, and S. Fraden. Entropically driven microphase transitions in mixtures of colloidal rods and spheres. *Nature*, 393:349–352, 1998.

[228] D. Frenkel. Onsager's spherocylinders revisited. *Journal of Phyiscal Chemistry*, 91:4912–4916, 1987.

[229] H. Hansen-Goos and K. Mecke. Tensorial density functional theory for non-spherical hard-body fluids. *Journal of Physics: Condensed Matter*, 22:364107, 2010.

[230] T. Koda, M. Numajiri, and S. Ikeda. Smectic-A phase of bidisperse system of parallel hard rods and hard shperes. *Journal of the Physical Society of Japan*, 65:3551–3556, 1996.

[231] S. D. Peroukidis, A. G. Vanakaras, and D. J. Photinos. Liquid crystalline phases and demixing in binary mixtures of shape-anisometric colloidals. *Journal of Materials Chemistry*, 20:10495–10502, 2010.

[232] P. E. Brumby, A. J. Haslam, E. de Miguel, and G. Jackson. Subtleties in the calculation of the pressure and pressure tensor of anisotropic particles from volume-perturbation methods and the apparent asymmetry of the compressive and expansive contributions. *Molecular Physics*, 109:169–189, 2011.

[233] Tomáš Boublík. Hard-sphere equation of state. *Journal of Chemical Physics*, 53:471, 1970.

[234] M. P. Allen and D. J. Tildesley. *Computer Simulation of Liquids*. Clarendon Press, 1989.

[235] Daan Frenkel and Berend Smit. *Understanding Molecular Simulation: From Algorithms to Applications, 2nd edition*. Academic Press, 2001.

[236] C. A. Croxton and R. P. Ferrier. Statistical mechanical calculation of surface properties of simple liquids: IV Molecular dynamics . *Journal of Physics C*, 4:2447–2456, 1971.

[237] H. J. Leamy, G. H. Gilmer, K. A. Jackson, and P. Bennema. Lattice-gas interface structure: a Monte Carlo simulation. *Physical Review Letters*, 30:601–603, 1973.

[238] Enrique de Miguel and G. Jackson. Detailed examination of the calculation of the pressure in simulations of systems with discontinuous interactions from the mechanical and thermodynamic perspectives. *Molecular Physics*, 104:3717–3734, 2006.

[239] M. Dijkstra and R. van Roij. Entropy-driven demixing in binary hard-core mixtures: From hard spherocylinders towards hard spheres. *Physical Review E*, 56:5594–5602, 1997.

[240] A. Richter and T. Gruhn. Structure formation and fractionation in systems of polydisperse attractive rods. *Journal of Chemical Physics*, 125:064908, 2006.

[241] D. Frenkel. Structure of hard-core models for liquid crystals. *Journal of Physical Chemistry*, 92:3280–3284, 1988.

[242] J. A. C. Veerman and D. Frenkel. Relative stability of columnar and crystalline phases in a system of parallel hard spherocylinders. *Physcial Review A*, 43:43344343, 1991.

[243] Y. Mao, P. Bladon, H. N. W. Lekkerkerker, and M. E. Cates. Density profiles and thermodynamics of rod-like particles between parallel walls. *Molecular Physics*, 92:151–159, 1997.

[244] M. Dijkstra, R. van Roij, and R. Evans. Wetting and capillary nematization of a hard-rod fluid: A simulation study. *Physcial Review E*, 63:051703, 2001.

[245] R. Evans, U. Marini Bettolo Marconi, and P. Tarazona. Fluids in narrow pores: Adsorption, capillary condensation, and critical points. *Journal of Chemical Physics*, 84:2376, 1986.

[246] Blandine Jérôme. Surface effects and anchoring in liquid crystals. *Reports on Progress in Physics*, 54:391–451, 1991.

[247] T. J. Sluckin. Anchoring transitions at liquid crystal surfaces. *Physica A*, 213:105–109, 1995.

[248] Ping Sheng. Phase transition in surface-aligned nematic films. *Physical Review Letters*, 37:1059–1062, 1976.

[249] M. M. Telo da Gama. The interfacial properties of a model of a nematic liquid crystal I. The nematic-isotropic and the nematic-vapour interfaces. *Molecular Physics*, 52:585–610, 1984.

[250] M. M. Telo da Gama. The interfacial properties of a model of a nematic liquid crystal II. Induced orientational order and wetting transitions at a solid-fluid interface. *Molecular Physics*, 52:611–630, 1984.

[251] M. M. Telo da Gama, P. Tarazona, M. P. Allen, and R. Evans. The effect of confinement on the isotropic-nematic transition. *Molecular Physics*, 71:801–821, 1990.

[252] A. Poniewierski and T. J. Sluckin. Statistical mechanics of a simple model of the nematic liquid crystal-wall interface. *Molecular Crystals and Liquid Crystals*, 111:373–386, 1984.

[253] A. Poniewierski and T. J. Sluckin. Theory of the nematic-isotropic transition in a restricted geometry. *Liquid Crystals*, 2:281–311, 1987.

[254] A. Poniewierski and R. Holyst. Nematic alignment at a solid substrate: The model of hard spherocylinders near a hard wall. *Physcial Review A*, 38:37213727, 1988.

[255] A. Poniewierski. Ordering of hard needles at a hard wall. *Physical Review E*, 47:3396, 1993.

[256] R. van Roij, M. Dijkstra, and R. Evans. Interfaces, wetting, and capillary nematization of a hard-rod fluid: Theory for Zwanzig model. *Journal of Chemical Physics*, 113:7689–7701, 2000.

[257] L. Harnau and S. Dietrich. Fluids of platelike particles near a hard wall. *Physcial Review E*, 65:021505, 2002.

[258] A. Malijevský and S. Varga. Phase behaviour of parallel hard rods in confinement: an Onsager theory study. *Journal of Physics: Condensed Matter*, 22:175002, 2010.

[259] Y. Mao, M. E. Cates, and H. N. W. Lekkerkerker. Theory of the depletion force due to rodlike polymer. *Journal of Chemical Physics*, 106:3721–3729, 1997.

[260] D. de las Heras, E. Velasco, and L. Mederos. Effects of wetting and anchoring on capillary phenomena in a confined liquid crystal. *Journal of Chemical Physics*, 120:4949–4957, 2004.

[261] M. Dijkstra and R. van Roij. Entropic wetting in colloidal particles. *Journal of Physics: Condensed Matter*, 17:S3507–S3514, 2005.

[262] M. P. Allen. Molecular simulation and theory of liquid crystal surface anchoring. *Molecular Physics*, 96:1391–1397, 1999.

[263] M. P. Allen. Molecular simulation and theory of the isotropic-nematic interface. *Journal of Chemical Physics*, 112:5547–5453, 2000.

[264] F. Barmes and D. J. Cleaver. Computer simulation of a liquid-crystal anchoring transition. *Physcial Review E*, 69:061705, 2004.

[265] Thomas Gruhn and Martin Schoen. Substrate-induced order in confined nematic liquid-crystal films. *Journal of Chemical Physics*, 108:9124–9136, 1998.

[266] E. A. Müller, I. Rodríguez-Ponce, A. Oualid, J. M. Romero-Enrique, and L. F. Rull. Wetting of planar surfaces by a gay-berne liquid crystal,. *Molecular Simulation*, 29:385–391, 2003.

[267] L. F. Rull, J. M. Romero-Enrique, and E. A. Müller. Observation of surface nematization at the solid-liquid crystal interface via molecular simulation. *Journal of Phyiscal Chemistry C*, 111:15998–16005, 2007.

[268] Qing Ji, R. Lefort, and D. Morineau. Influence of pore shape on the structure of a nanoconfined GayBerne liquid crystal. *Chemical Physics Letter*, 478:161–165, 2009.

[269] M. Greschek and M. Schoen. Orientational prewetting of planar solid substrates by a model liquid crystal. *Journal of Chemical Physics*, 135:204702, 2011.

[270] D. L. Cheung and F. Schmid. Monte carlo simulations of liquid crystals near rough walls. *Journal of Chemical Physics*, 122:074902, 2005.

[271] Haiko Steuer, Siegfried Hess, and Martin Schoen. Phase behavior of liquid crystals confined by smooth walls. *Physcial Review E*, 69:031708, 2004.

[272] Yu. Trukhina and T. Schilling. Computer simulation study of a liquid crystal confined to a spherical cavity. *Physcial Review E*, 77:011701, 2008.

[273] J. Galanis, D. Harries, D. L. Sackett, W. Losert, and R. Nossal. Spontaneous patterning of confined granular rods. *Physical Review Letters*, 96:028002, 2006.

[274] A. Kuijk, D. V. Byelov, A. V. Petukhov, A. van Blaaderen, and A. Imhof. Phase behavior of colloidal silica rods. *Faraday Discussions*, 159:181–199, 2012.

[275] H. N. W. Lekkerkerker, Coulon P., R. van der Haegen, and R. Deblieck. On the isotropic liquid crystal phase separation in a solution of rodlike particles of different lengths. *Journal of Chemical Physics*, 80:3427–3433, 1984.

[276] R. van Roij and B. Mulder. Absence of high-density consolute point in nematic hard rod mixtures. *Journal of Chemical Physics*, 105:11237–11245, 1996.

[277] G. H. Koenderink, G. A. Vliegenthart, S. G. J. M. Kluijtmans, A. van Blaaderen, A. P. Philipse, and H. N. W. Lekkerkerker. Depletion-induced crystallization in colloidal rod-sphere mixtures. *Langmuir*, 15:4693–4696, 1999.

[278] G. Cinacchi and Luca De Gaetani. Diffusion in the lamellar phase of a rod-sphere mixture. *Journal of Chemical Physics*, 131:104908, 2009.

[279] A. Galindo, G. Jackson, and D. J. Photinos. Computer simulation of the interface between two liquid crystalline phases in rod-plate binary mixtures. *Chemical Physics Letters*, 325:631–638, 2000.

[280] H. H. Wensink, G. J. Vroege, and H. N. W. Lekkerkerker. Isotropic-nematic density inversion in a binary mixture of thin and thick hard platelets. *Journal of Physical Chemistry B*, 105:10610–10618, 2001.

[281] F. Gámez, R. D. Acemel, and A. Cuetos. Demixing and nematic behaviour of oblate hard spherocylinders and hard spheres mixtures: Monte Carlo simulation and Parsons-Lee theory. *Molecular Physics*, 2013.

[282] J. R. Henderson and F. van Swol. On the interface between a fluid and a planar wall: Theory and simulations of a hard sphere fluid at a hard wall. *Molecular Physics*, 51:991–1010, 1984.

[283] J. R. Henderson and F. van Swol. Grand potential densities of wallliquid interfaces approaching complete drying . *Journal of Chemical Physics*, 89:5010–5014, 1988.

[284] Frank van Swol and J. R. Henderson. Wetting and drying transitions at a fluid-wall interface: Density-functional theory versus computer simulation. *Physical Review A*, 40:25672578, 1989.

[285] N. A. Clark, T. Bellini, R. M. Malzbender, B. N. Thomas, A. G. Rappaport, C. D. Muzny, D. W. Schaefer, and L. Hrubesh. X-ray scattering study of smectic ordering in a silica aerogel. *Physical Review Letters*, 71:3505–3508, 1993.

[286] G. S. Iannacchione, J. T. Mang, S. Kumar, and D. Finotello. Surface-induced discrete smectic order in the isotropic phase of 12CB in cylindrical pores. *Physcial Review Letters*, 73:2708–2711, 1994.

[287] M. Fukuto, O. Gang, K. J. Alvine, B. M. Ocko, and P. S. Pershan. Wetting of liquid-crystal surfaces and induced smectic layering at a nematic-liquid interface: An x-ray reflectivity study. *Physcial Review E*, 77:031607, 2008.

[288] L. Wu, B. Zhou, C. W. Garland, T. Bellini, and D. W. Schaefer. Heat-capacity study of nematic-isotropic and nematic-smectic-A transitions for octylcyanobiphenyl in silica aerogels. *Physcial Review E*, 51:2157–2165, 1995.

[289] Z. Kutnjak, S. Kralj, G. Lahajnar, and S. Žumer. Calorimetric study of octylcyanobiphenyl liquid crystal confined to a controlled-pore glass. *Physcial Review E*, 68:021705, 2003.

[290] Z. Kutnjak, S. Kralj, G. Lahajnar, and S. Žumer. Influence of finite size and wetting on nematic and smectic phase behavior of liquid crystal confined to controlled-pore matrices. *Physcial Review E*, 70:051703, 2004.

[291] L. Moreau, P. Richetti, and P. Barois. Direct measurement of the interaction between two ordering surfaces confining a presmectic film. *Physcial Review Letters*, 73:3556–3559, 1994.

[292] K. Kočevar, A. Borštnik, I. Muševič, and S. Žumer. Capillary condensation of a nematic liquid crystal observed by force spectroscopy. *Physcial Review Letters*, 86:5914–5917, 2001.

[293] K. Kočevar and I. Muševič. Surface-induced nematic and smectic order at a liquid-crystal-silanated-glass interface observed by atomic force spectroscopy and brewster angle ellipsometry. *Physcial Review E*, 65:021703, 2002.

[294] Z. Pawlowska, T. J. Sluckin, and G. F. Kventsel. Systematics of wetting and layering phenomena in smectic materials. *Physcial Review A*, 38:5342–5351, 1988.

[295] P. G. de Gennes. Interactions between solid surfaces in a presmectic fluid. *Langmuir*, 6:1448–1450, 1990.

[296] G. Navascués and P. Tarazona. A model for capillary crystallization and the capillary triple point. *Molecular Physics*, 62:497–507, 1987.

[297] P. C. Ball and R. Evans. Structure and adsorption at gas-solid interfaces: Layering transitions from a continuum theory. *Journal of Chemical Physics*, 89:4412–4423, 1988.

[298] D. de las Heras, L. Mederos, and E. Velasco. Wetting properties of a hard-spherocylinder fluid on a substrate. *Physcial Review E*, 68:031709, 2003.

[299] D. de las Heras, E. Velasco, and L. Mederos. Capillary smectization and layering in a confined liquid crystal. *Physical Review Letters*, 94:017801, 2005.

[300] D. de las Heras, E. Velasco, and L. Mederos. Capillary effects in a confined smectic phase of hard spherocylinders: Influence of particle elongation. *Physcial Review E*, 74:011709, 2006.

[301] Daniel de las Heras, Yuri Martínez-Ratón, and Enrique Velasco. Surface and smectic layering transitions in binary mixtures of parallel hard rods. *Physcial Review E*, 81:021706, 2010.

[302] S. Dhakal, F. J. Solis, and M. O. de la Cruz. Nematic liquid crystals on spherical surfaces: Control of defect configuration by temperature, density, and rod shape. *Physical Review E*, 86:011709, 2012.

[303] B. Mulder. Density-functional approach to smectic order in an aligned hard-rod fluid. *Physical Review A*, 35:3095–3101, 1987.

[304] R. P. Sear and G. Jackson. Stability of the nematic phase of a mixture of aligned cylinders with respect to the smectic and columnar phases. *Journal of Chemical Physics*, 102:2622–2627, 1995.

Appendix A

Appendix Bifurcation analysis

A bifurcation analysis is applied to locating of the nematic-columnar transition of hard-disc particles. The method is initially used to test the stability of smectic phase against the nematic state by truncating the free energy at the level of second virial coefficient [303,304]. The work in [303] studies the effect of higher-order terms in the density expansion on the bifurcation point. Here, we incorporate the higher-order virial coefficients using Parsons-Lee scaling approximation:

$$\frac{A_{\mathrm{PL}}}{NkT} = \frac{A^{\mathrm{id}}}{NkT} + \frac{4\eta - 3\eta^2}{(1-\eta)^2}\frac{B_2}{B_{2,\mathrm{hs}}}. \tag{A.1}$$

The integral of the ideal contribution to free energy and second virial coefficient can be evaluated by using the cylindrical symmetry of the particle and the translational invariance along the z axis. the Equation (A.1) can be expanded to second order in ϵ:

$$\frac{A_{\mathrm{PL}}}{NkT} = \ln \rho\mathcal{V} - 1 + \frac{\epsilon^2}{4} + \frac{4\eta - 3\eta^2}{(1-\eta)^2}\left[1 + \frac{\epsilon^2}{2} j_0\left(q_z L\right) J_{1'}\left(q_r D\right)\right], \tag{A.2}$$

where $j_0\left(q_z L\right) = \sin\left(q_z L\right) / \left(q_z L\right)$, $J_{1'}\left(q_r D\right)$ is defined as

$$J_{1'}\left(q_r D\right) = \frac{J_1\left(q_r D\right)}{1/2\left(q_r D\right)} \tag{A.3}$$

and J_1 is the first Bessel function. Since we focus on the columnar order, the zeroth-order Bessel function corresponds to the unity. Taking the derivative of free energy with respect to the wave vector in xy plane ($q_r D$) and ϵ, the bifurcation point can be determined from

$$1 + \frac{2(4\eta - 3\eta^2)}{(1-\eta)^2} J_{1'}\left(q_r D\right) = 0 \tag{A.4}$$

When the isotropic fluid phase is used as the reference system for the anisotropic phase (Vega-Lago scaling approximation), we have

$$B_n = \frac{B_2}{B_2^{\mathrm{iso}}} B_n^{\mathrm{iso}} \tag{A.5}$$

Using the generic algebraic EoS for isotropic hard cut-sphere fluid, cf. Equation (2.41), the expressions for free energy, chemical potential and pressure can be derived in the similar way to Parsons-Lee method:

$$\frac{A_{\mathrm{VL}}}{NkT} = \ln \rho\mathcal{V} - 1 + \frac{\epsilon^2}{4} + G(\eta)\left[4 + 2\epsilon^2 j_0\left(q_z L\right) J_{1'}\left(q_r D\right)\right] \tag{A.6}$$

where the density dependent factors $G(\eta)$ and $G'(\eta)$ are given in Equation (2.45) and (2.48), respectively. The equation determining the location of bifurcation point is then obtained in the similar form to Equation (A.4):

$$1 + 8G(\eta)J_{1'}\left(q_r D\right) = 0. \tag{A.7}$$